Apprentissage de la Complexité du Corps-Cerveau en Robotique Bio-Inspirée

Alexandre Alex Pitti

Université de Cergy-Pontoise

Habilitation à Diriger la Recherche

présentée et soutenue publiquement pour obtenir l'habilitation à diriger la recherche en Robotique et Sciences Cognitives, Section 61, Discipline Robotique

---

APPRENTISSAGE DE LA COMPLEXITÉ DU CORPS-CERVEAU EN ROBOTIQUE BIO-INSPIRÉE

---

par

Alexandre PITTI

laboratoire ETIS - Université Paris-Seine / CNRS UMR 8051 / Université de Cergy-Pontoise / ENSEA

Soutenue le 30 Novembre 2017, devant le jury composé de :

RAJA CHATILA,	Directeur de recherche UPMC	Rapporteur
TONY PRESCOTT,	Professeur des universités Sheffield	Rapporteur
PETER FORD DOMINEY,	Directeur de recherche INSERM Lyon	Rapporteur
PIERRE-YVES OUDEYER,	Directeur de Recherche INRIA Bordeaux	Examinateur
JACQUELINE FAGARD,	Chercheuse CNRS Université Paris Descartes	Examinatrice
PHILIPPE GAUSSIER,	Professeur des universités UCP	Garant
MATHIAS QUOY,	Professeur des universités UCP	Référent

Remerciements

Mes pensées vont vers mes frères, Gérard et Lionel, mes parents et ma femme, Rié, même si je vous le dis trop rarement.
Je remercie aussi tous mes mentors qui m'ont fait progresser, mes amis et collègues avec qui j'ai travaillé et mes étudiants à qui j'ai transmis et qui m'ont appris.

Synopsis

Comprendre le lien entre la sensorialité et l'acte moteur est à la fois un point de départ et un point d'arrivé pour comprendre la cognition humaine. Le robot est par là-même l'outil idéal pour étudier ces différents aspects. Cela nécessite à la fois de comprendre le niveau microscopique et macroscopique des modèles neuronaux et cérébraux, comprendre la biomécanique du corps et le traitement de l'information fait par les cellules sensorielles et musculaires, ainsi que toute la chaîne de processus pour apprendre, s'adapter dynamiquement face à l'imprévu. Ces questions rebouclent sans cesse dans ma recherche pour définir les mécanismes de l'Intelligence Encorporée.

J'y explore trois axes de recherche qui sont la génération du mouvement, le développement cognitif, l'apprentissage sensorimoteur. Il s'agit de comprendre comment le corps est constitué, quelle est sa structure bio-mécanique, comment un système agissant peut apprendre sur le long-terme et arrive à apprendre à apprendre de ses propres actions. Ce qui lie mes recherches est une vision complexe et encorporée de l'intelligence, transversale, dont les mots-clefs sont les processus itératifs, émergents, auto-associatifs, génératifs.

Table des matières

Introduction

Motivation and Objective

For the last decade, the perspective to make robots based on a new AI, embodied, enactive and bio-inspired, has been the central motivation of my research activity. I attempted to deepen my understanding in search of the very general principles of intelligent autonomous systems from the micro-scale of the neurons, of the muscles, to the macro-scale of learning and development. Such interdisciplinary research faces the problem of complexity and requires a systemic approach to model interaction at all levels in order to have a system capable to learn as an infant does and capable to deal with the unexpected as most mahines fail to do.

The new fields of cognitive and bio-inspired robotics aligned with cognitive researchers, neuroscientics urge to find design principles explaining cognitive development, autonomous behavior, learning and to replicate them in robots. These are complex scientific objects, bio-inspiration may unveil some findings capable to be replicated in robots but also to understand from a developmental aspect, neural architectures capable to explain and replicate human normal as well as abnormal cognition development from birth.

My research aims at answering these questions from various angles in order to find from the most general to the most specific design principles on AI, Physics and Biology. I try to look at how cognitive and motor development of infants perception arise and human biological organization of the musculo-skeletal system and of the brain structures is made for intelligent behaviors.

In this area, from a complex system approach of intelligent systems, my research work has mainly focused for the last 9 years on three main tracks :

1. Complex system approach to Motor Synergies and Soft Robotics
2. Neural mechanisms for Multimodal Integration and Embodied Cognition
3. Cognitive Architectures for a Working Memory

I try to follow these three directions. To do so, I modeled different brain areas and neural mechanisms involved in multimodal integration toward the learning and development of a body image in robots.

Première partie

Part I Overview

CHAPITRE 1

CURRICULUM VITAE

Administrative data

First name Alexandre

Last name Pitti

Date/Place of Birth january 1st 1977, Paris, France

Marital Status Maried

Current Position Maître de Conférences (Associate Professor) university of Cergy-Pontoise

Professional Address ETIS Lab, UMR 8051, ENSEA, University of Cergy-Pontoise, CNRS, 2 av. Adolphe Chauvin, 95302, Cergy-Pontoise

email alexandre.pitti@u-cergy.fr / alexandre.pitti@ensea.fr

homepage http://perso-etis.ensea.fr/alexpitt/

Diploma, Qualification and Others

2011-2016 CNRS-UCP Chaire d'Excellence on Cognitive Robotics.

2012 French Universities CNU Qualification section 61.

2004-2007 Doctor of Engineering in Mechanical and Computer Science Tokyo University, dept. Mech. and Comp. Science, Tokyo, Japan.

- **Title** : Phase Synchronization Between Internal and Body Dynamics for Exploration, Memory, and Control of Embodied Behavior
- **Supervisor** : Professor Yasuo Kuniyoshi
- **Jury member** : Aihara, Nakamura, Harada, Kanzaki

2001-2002 Master of Science in AI and Pattern Recognition (Diplôme d'Enseignement Avancé), Artificielle et Reconnaissance des Formes Appliquées (DEA IARFA), Université Pierre et Marie Curie, Paris, France.

1998-2002 Master of Engineering, Ingénieur Généraliste, (spec. in Computer Science) Engineer School ESME Sudria, Paris, France.

Professional Experience

from 2011 Maître de Conférence (associate professor)/ CNRS Chaire d'Excellence Robotique Cognitive Dept. Computer Sciences, ETIS laboratory, Cergy-Pontoise University, CNRS UMR 8051, ENSEA, Cergy-Pontoise, France.

2007-2011 Researcher, JST (Japan Science and Technology), Tokyo University, Tokyo, Japan.

2004-2007 PhD student (funded by Japanese Government), Tokyo University, Tokyo, Japan.

2002-2003 "Moniteur" (Contractual Lecturer), University Paris XIII, Villetaneuse, France.

Scientific Activity

Extended Abstract

Scientific Production

H-index= 8, i10=6, 173 citations (Google Scholar) 13 Journal Articles, 14 Proc. of International Conferences, 2 book chapters, 2 books.

Scientific Supervision

Ph.D. Students

During the period 2011–2017, I co-supervise two doctoral students, Raphael Braud et Ganna Pugach, on the emergence of tool-use and on on the prototyping of an artificial skin for self-perception in a robot. From april 2017, I co-supervise the thesis of Kevin Hoang (funding Thalès) on the neuronal control of an event-based camera. From october 2017, I will co-supervise the thesis of Julien Abrossimof on motor sequence incremental learning, and another thesis on neural modeling of the human mechano-receptors (no candidate yet, funding Valeo Peugeot).

2012 – 2016 (70% co-supervision with P. Gaussier)
Raphaël Braud, Subject : "From Objects to Tools : Emergence of Tool-use in Robots",
ETIS laboratory, Dept. Computer Sciences, Cergy-Pontoise University, France.
Bourse ED-SI de l'université de Cergy-Pontoise.

2013 – 2016 (70% co-supervision with P. Gaussier)
Anna Pugach, Subject : "Artificial Skin Conception for Tactile Perception in Robots"
ETIS laboratory, Dept. Computer Sciences, Cergy-Pontoise University, France.
Bourse Agence Universitaire Française.

2017 – 2020 (50% co-supervision with P. Gaussier)
Kevin Hoang, Subject : "Neural Controller for an Event-based Camera"
ETIS laboratory, Dept. Computer Sciences, Cergy-Pontoise University, France.
Thèse CIFRE Thalès.

2017 – 2020 (50% co-supervision with P. Gaussier)
Julien Abrossimoff, Subject : "Apprentissage Neuronal de la Représentation Corporelle et de la Sélection de l'Action Pour des Tâches de Préhension Chez un Robot"
ETIS laboratory, Dept. Computer Sciences, Cergy-Pontoise University, France.
Bourse Ecole Doctorale.

2017 – 2020 (50% co-supervision with O. Romain)
no candidate yet, Subject : "Neural Modeling of the Human Mechano-Receptors"
ETIS laboratory, Dept. Computer Sciences, Cergy-Pontoise University, France.
Bourse institut VEDECOM, financed by Peugeot and Valeo.

M.Sc. Students

On the period 2007–2011, in ISI Kuniyoshi's laboratory, University of Tokyo, I have unofficially helped in daily day a dizain of students from License to Doctoral Students on some papers correction, helped on algorithms or on analysis, or on setting up of some experiences as I was the most graded in a place slightly isolated from the rest of the lab, on developmental robotics and on bio-robotics.

stages de master 2

avr- 2017 sep 2017 stage de master 2 Julien Abrossimov, Intégration visuo-motrice-tactile par l'utilisation de neurones gain-fields pour une tâche de préhension d'objets.
Suivi : écriture d'un papier pour conférence Humanoids 2017, sélection en Thèse ETIS bourse école doctorale.

sep- 2016 dec 2016 stage de master 2 Ihor Kuras, Neural Control of a Tensegrity-based Modeling of a Soft Spinal Cord System.
Suivi : écriture d'un papier pour conférence AMAM accepté et papier Frontiers in Neurorobotics non accepté, Thèse à EPFL.

avr- 2016 sep 2016 stage de master 2 Meryem Slimani, joint attention from audio-visual integration

avr- 2016 sep 2016 stage de master 2 Jiamin Xian, speech recognition and production in a head robot with deep networks.
Suivi : CDD start-up en IA et Deep Learning

avr- 2015 sep 2015 stage de master 2 Oriane Dermy, joint attention and audiovisual speech gesture recognition in a head robot.
Suivi : écriture d'un papier pour conférence ROMAN 2015 (non accepté), meilleure note de stage master, thèse robotique au LORIA, Nancy.

sept- 2014 feb 2015 stage de master 2 Anton Zdhanov, exploiting gain-fields neurons for the visuo-motor representation of an arm robot in reaching and grasping tasks

apr- 2014 aug. 2014 stage de master 2 Kemo Adrian, Apprentissage et sélection de règles par un modèle de cortex préfrontal lors d'une tâche de manipulation d'objet.
Suivi : écriture d'un papier en cours, meilleure note de stage master, thèse en IA à Barcelone.

sept. 2013 feb 2014 stage de master 2 Igor Kuksin, utilisation des signaux électriques de phase pour la mesure de pression d'un prototype de peau artificielle

apr- 2013 aug. 2013 stage de master 2 Sylvain Mahé, Coordination visuo-motrice par l'utilisation de neurones gain-fields pour une tâche de préhension d'objet.
Suivi : écriture d'un papier Neural Networks, meilleure note de stage master, thèse CIFRE robotique à Montpellier.

sept. 2012 feb 2013 stage de master 2 Anna Pugach, utilisation d'un réseau de neurone pour la reconstruction de la tomographie d'impédance électrique d'une peau artificielle.
Suivi : écriture d'un papier conférence ElNano, meilleure note de stage master, thèse à ETIS.

apr- 2012 aug. 2012 stage de master 1 Mathieu Cardinaux, Contrôle et coordination audio-visuelle d'une tête robotique par modélisation des neurones audio-moteurs pariétaux.
Suivi : écriture d'un papier Humanoids, CDI start-up robotique et vision.

Collaborations and Projects

2011– Participation au projet national Equipex Robotex au niveau de l'équipe ETIS.

2011–2012 Participation au projet ANR INTERACT laboratoire ETIS, ENSEA, UCP, CNRS. Participation formelle à ce projet en cours.

2007–2011 Participation au projet JST-ERATO Synergistic Intelligence entre les laboratoires de l'université de Tokyo, Osaka et Kyoto. Professeurs Minoru Asada, Hiroshi Ishiguro, Yasuo Kuniyoshi, Toshio Inui, Koh Hosada.

Ecriture de 6 papiers dans des revues internationales avec comité de lecture [JOUR01 - JOUR07] et de trois papiers dans des conférences internationales [CONG04-CONF06].

2010 Marie Curie International Reintegration Grants Call : FP7-PEOPLE-2010-RG
Projet CogPlexity, accepté, mais refusé volontairement pour obtenir la chaire d'excellence CNRS-UCP.

Fellowships and Awards

2011-2016 Chaire d'Excellence Univ. Cergy-Pontoise-CNRS, international-level competition, France.

2004–2007 PhD Scholarship (Monbusho Kagakusho), highly-selective competition (5 scholarships per year in physics, engineering and maths), Japanese Ministry of Education, Japan.

Scientific Evaluations

2016 évaluation scientifique de l'agence française de recherche CNRS : A (note max)

2014 évaluation scientifique de l'agence française de recherche CNRS : A (note max)

2011 évaluation scientifique de l'agence japonaise de recherche JST : A+ (note max)

2009 évaluation scientifique de l'agence japonaise de recherche JST : B

Teaching Activity

Teaching

J'effectue mon activité d'enseignement à l'université de Cergy-Pontoise, au département des sciences informatiques. La Chaire d'Excellence Scientifique du CNRS me déroge 64h de service par an entre 2011 et 2016.

Depuis 2011, je donne des cours d'introduction aux réseaux de neurones au M1 du Master Système Intelligents et Communicants (SIC), des cours sur les techniques avancées d'IHMs pour les M2 Pro et les M2 Recherche. Depuis 2014 je donne des cours en robotique bio-inspirée pour les M2 Recherche. J'ai donné entre 2011 et 2013 des cours d'introduction à la robotique et à Arduino pour les L3. En 2015, j'ai donné des cours d'Optimisation Algorithmiques et des cours d'Intelligence Artificielle pour les M2 Recherche.

from 2011 :
Artificial Intelligence, Neural Networks, 2nd cycle, Master 1, 22.5 hours eq. TD
Advances in Human-Machine Interface, 2nd cycle, Master 2, 18 hours eq. TD
Introduction to Robotique ad Arduino 1st cycle, Licence 3 24 hours eq. TD
2011 – 2012 : 111 hours
2012 – 2013 : 101 hours
2013 – 2014 : 67.5 hours

from 2015 :
Artificial Intelligence, 2nd cycle, Master 2 Recherche 15 hours eq. TD
Machine Learning, 2nd cycle, Master 2 Recherche 15 hours eq. TD
2015 – 2016 : 100 heures

from 2016 :
Introduction au Langage C, 1st cycle, 50 hours eq. TD
Robotics, 2nd cycle, Master 2 Recherche 20 hours eq. CM
AI Specialization, 2nd cycle, Master 1 37 hours eq. CM

from 2011 – Associate Professor, University of Cergy-Pontoise, France
M2 level– Advances in HMI, 24 hours (50 % courses 50 % practical works)
M1 level– Introduction to AI & Neural Networks, 12 hours per year (100 % courses)
L3 level– Introduction to Robotics and Arduino, 24 hours (20 % courses 80 % tutorial)

Administrative Responsabilities

from 2013 membre du comité scientifique d'ETIS, Univ. Cergy-Pontoise, France

from 2014 co-responsable "Parcours IA et Robotique", Master 2 Recherche, Univ. de Cergy-Pontoise.

2015-2016 co-responsable du Master 2 Recherche I&ISC, Univ. de Cergy-Pontoise.

2015-2016 chef d'équipe de l'équipe neurocybernétique, laboratoire ETIS.

from 2016 responsable "Parcours IA et Robotique", Master 2 Recherche, Univ. de Cergy-Pontoise.

Scientific Animation

from 2014 co-animateur du Groupe De Recherche en Robotique (GDR) Groupe de Travail (GT) 8 du CNRS "Robotique Cognitive et Neuroscience", France Invitation de personnalités de la communauté pour faire échanger des idées et faire rencontrer les scientifiques entre eux et insérer les doctorants post-doctorants.

13 june 2017 "Journée Robotique Cognitive et Neuroscience", Cergy-Pontoise, France.

17 nov. 2016 "Journée Robotique Cognitive et Neuroscience", Bordeaux, France. 40 participants

may 2016 "Journée Robotique Cognitive et Neuroscience", Toulouse, France. 40 participants

04 nov. 2015 "Journée Robotique Cognitive et Neuroscience", Cergy, France. 40 participants

17 jul. 2015 "Journée Robotique Cognitive et Neuroscience", Paris, France. 30 participants

27 nov. 2014 "Journée Robotique Cognitive et Neuroscience", Paris, France. 30 participants

2017-2018 Publicity chair – IEEE Int. Conf. on ICDL EPIROB 2018, Tokyo, Japan.

6 dec. 2016 Organizer and chairman – Workshop "Touch for Brains, Bodies and Babies", Cergy-Pontoise, France.
7 invited researchers on tactile perception in robotics
https://docs.google.com/forms/d/1hB6rM1y60b8SwxKVSRhqm1ylRMPmDAHO1_JyudFXMeU/edit

19 sep. 2016 Program chair – IEEE Int. Conf. on ICDL EPIROB, Cergy, France.
Supervisor of the associate editors and reviewer of 70 papers.

Été-automne Organizer – semestre thématique 2016 U. de Cergy-Pontoise « Robotique Bio-Inspirée »

9 dec. 2013 Workshop "The Robotics and the Living", Cergy-Pontoise, France.
Organizer and chairman, 7 invited international researchers on bio-inspired robotics, neurocomp. 70 participants [& 140 followers on internet]
http://perso-etis.ensea.fr/alexpitt/LaRobotiqueEtLeVivant_en.html

april 2013 Organizer of a Special Issue in the journal Frontiers in NeuroRobotics in the topic of « Social Behaviour and Neural Control ».http://www.frontiersin.org/Neurorobotics/researchtopics/Social_Behaviour_and_Neural_Co/1302, 9 articles. [nearly 20.000 views]

9 sep. 2012 Workshop on "Developmental and bio-inspired approaches for social cognitive robotics" at Ro-Man 2012, 21st IEEE Int. Symp. on Robot and Human Interactive Comm., France.
Main organizer and chairman, 6 invited renowned researchers on cognitive science, dev. psy., social robotics, 60 participants.
http://www-etis.ensea.fr/WorkshopRoMan2012/Home.html

july 2011 Workshop on Coordination Dynamics and Social Robotics at Dynamic Brain Forum @ICCN conference, Hokkaido, Japan.
Co-organizer & chairman, reviewer of the workshop' papers. 20 participants

Invited Talks

Sept 2017 Selected Talk, Workshop on Development of Self, IEEE Conference on ICDL EPIROB, Lisbon.

July 2017 Invited Talk, Waseda University, Tokyo, Japan.

Jun 2017 Conférence Human Brain Project "Soft Bodies for Brains, Soft Brains for Bodies", Université de Genève, Suisse.

Mars 2017 Conférence UNESCO "Machines Ethiques et Morales", Université de Laval, Québec, Canada.

Dec 2016 Auto-invitation Workshop Touch for Brains, Body, and Babies, Cergy-Pontoise.

May 2016 Conférence Débat "Machines Morales", UNESCO, Paris.

Apr 2016 Invited Talk, Centre Recherche Inter-disciplinaire, Paris, France.

Mar 2016 Invited Talk, "Etique des Nouvelles Technologies", CHU Reims, Reims, France.

Feb 2016 TedX, Arts&Metiers ParisTech, Lille

Jan 2016 Invited Talk, BabyLab, Nanterre University, Nanterre, France.

July 2015 Invited Talk ASSC Workshop on Sensorimotor Theory, Paris.

July 2015 Invited Talk, Journées NeuroSTIC, Paris

Jan 2015 Frontiers of Science CNRS-JSPS joint symposium, Kyoto [general scientist]

Jan 2015 Invited Talk, Asada Laboratory, Osaka University, Osaka, Japon.

June 2014 Invited Keynote Talk, part of IPAC seminars, LORIA, Nancy, France. (http://ipac.loria.fr)

May 2014 Keynote on Embodiment, Spring School "Robots and Social Cognition", Landes, France.

Mar 2014 Invited Talk special session for M2H Seminar, EuroMov Center, Montpellier, France.

2012 Invited Talk, Dynamic Brain Forum, Carmona, Spain, "spatial mapping in parietal cortex"

2010 Invited presentation to LPP Laboratory university Paris Descartes, on "Developmental Robotics"

2009 Invited seminar for ShanghAI Lectures, at ETH Zurich on "Cognitive Robotics"

2009 Keynote oral presentation, workshop NeuroComputing (NC2009), University of Sapporo

Vulgarisation Scientifique

March, 2017 interview for "Machine Morale", radio Canada.

January, 2017 Student interview for Bio-inspired Robots, radio France.

Dec, 2016 - March 2017 CNRS Fresque BioInspired Robotics, Métro Montparnasse, Paris.

October, 2016 interview for webTV, "Esprit Sorcier", Fete de la Science, Cité de la Science, la Villette, Paris.

April, 2015 interview for regional magazine "Onze comme Une".

June 2015 National Event on NewTech, Futur-en-Seine, Cergy-Pontoise. [200 persons]

April 2015 2 pages Interview for the popular science magazine « Thinkovery » (number #3, may/june 2015) on the new Artificial Intelligence and Bio-Inspired Robotics.

October 2014 National Scientific Event "Fête de la science", Polytechnique, Palaiseau. [présentation orale devant 4 classes de lycéens et de collégiens].

May 2013 Forum des sciences cognitives, École de médecine, Paris.

June 2012 #MQRF Mais que Re-faire, au 104, le Cent-Quatre, Paris. [1000 persons]

May 2012 Forum des sciences cognitives, École de médecine, Paris.

May 2011 Forum des sciences cognitives, École de médecine, Paris.

2012 Rolf Pfeifer et A. Pitti. La révolution de l'intelligence du corps. Manuella Editions 2012, 196 pages.

2009 Audio Interview for ROBOT PODCAST website on "Chaos Control and Bio-inspired Robots"

Scientific Expertize

December 2017 Rapporteur (PhD Evaluator), Université Paris-Orsay, Orsay, France.

February 2017 Examinateur (PhD Evaluator), ENSTA, Palaiseau, France.

January 2016 Examinateur (PhD Evaluator), Ecole Centrale de Nantes, France.

July 2014 Examinateur (PhD Evaluator), LIRMM, Montpellier, France.

March 2014 Project Grant reviewer, ANR, France. Reviewer of the scientific content of a 5-year project.

February 2014 Project Grant reviewer, NWO div. Earth and Life Sciences, Netherlands. Reviewer of the scientific content of a 3-year project.

Januray 2014 Review Panel Member, Human Brain Project, Sc. of Pharmacy, UK. Evaluation of 50 european projects.

December 2013 Examinateur (PhD Evaluator), University of Versailles, France.

Reviewer

Conferences CogSci 2015 / IEEE ICDL-EPIROB 2011, 2012, 2013, 2014, 2015 / IROS 2012, 2013 / IJCNN 2012

Journals 2015 Bio-signal / 2015 Frontiers in Psychology / 2012 IEEE Trends in Autonomous Mental Developmental / 2012 & 2013 Frontiers in NeuroRobotics / 2011 RSTI - RIA

Associate editor for conferences and journals Frontiers in Psychology & in NeuroRobotics / Conférence IEEE ICDL-EPIROB 2013, 2014, 2015, 2016/ Conférence IEEE SII 2015

Collaborations and Projects

Local Collaborations

from 2016 Spectral Methods for Tactile Devices, Olivier Romain, ENSEA. [Joint PhD Thesis in 2017, financed by VEDECOM Consortium]

from 2016 project on AI tools for Learning in ASD infants, Institut Medico Educatif de Cergy-Pontoise. [création d'une application éducative basée sur une IA pour enfants avec handicap]

National Collaborations

from 2016 Neuromorphic computing, IRCICA, Université de Lille. [ANR 2017 submitted]

from 2016 Multimodal Integration in Robots and Babies, Université de Nanterre. [Fondation de France Grant 2016, ANR 2017 submitted]

international Collaborations

2016-2017 Generative Adversal Networks for Robot Control, Hiroki Mori, Osaka University Assistant Professor. [Invited Professor, stayed one year at Cergy-Pontoise]

from 2016 Touch and Grasping in Robots and Babies, University of Tenesse, Daniella Corbetta. [Joint Robotic and Developmental research]

from 2014 Rubber-hand Illusion and Self-Perception Modeling, Sotaro Shimada, University of Meiji. [invitation in 2015, one paper in Scientific reports 2017 JOUR11]

Projects

from 2016 Multimodal Integration in Robots and Babies, Université de Nanterre. [Fondation de France Grant 2016, 2 stages de M2 Recherche]

2011–2012 Participation au projet ANR INTERACT laboratoire ETIS, ENSEA, UCP, CNRS.

2007–2011 Participation au projet JST-ERATO Synergistic Intelligence entre les laboratoires de l'université de Tokyo, Osaka et Kyoto. Professeurs Minoru Asada, Hiroshi Ishiguro, Yasuo Kuniyoshi, Toshio Inui, Koh Hosada.

2010 Marie Curie International Reintegration Grants Call : FP7-PEOPLE-2010-RG
Le Projet CogPlexity a accepté avec l'unviversité Pierre et Marie Curie mais je l'ai refusé volontairement pour obtenir la chaire d'excellence
CNRS-UCP.

Full List of Publications (2005-2017)

Book

BOOK03 Frontiers in NeuroRobotics, Research Topic of « Body Representations, Peripersonal Space, and the Self : Humans, Animals, Robots », (2018, *to appear*).
http://journal.frontiersin.org/researchtopic/6865/ body-representations-peripersonal-space-and-the-self-humans-animals-robots

BOOK02 Frontiers in NeuroRobotics, topic of « Social Behaviour and Neural Control », (2012).
http://www.frontiersin.org/Neurorobotics/researchtopics/Social_Behaviour_and_Neural_Co/1302, 9 articles. [nearly 20.000 views]

BOOK01 Rolf Pfeifer & Alex Pitti, (2012), "la Révolution de l'Intelligence du Corps", Manuella Editions. 196 pages A popular science book on design principles for new AI and Embodied Robotics, Cognitive Science, Material Science, Complex Systems, Biomechanics, Developmental Psychology and Neuroscience.

Journal Articles

(13 publications, asterisk * : 2 publications are co-authored under PhD supervision, underlined : 4 publications are co-authored with my students)

JOUR13 Braud, R. Pitti, A. Gaussier, P. (2017). A modular Dynamic Sensorimotor Model for affordances learning, sequences planning and tool-use. IEEE Trends in Cognitive and Developmental Systems (previously IEEE TAMD [IF 2.17]). (to appear)

JOUR12 Pitti A., Gaussier P. & Quoy M. (2017) Incremental Free-Energy Optimization for Recurrent Neural Networks (INFERNO). PLoS ONE. 12(3) : e0173684

JOUR11 Pitti, A., Pugach, G., Gaussier, P., and Shimada, S. (2017). Spatio-temporal tolerance of visuo-tactile illusions in artificial skin by recurrent neural network with spike-timing-dependent plasticity. Scientific Reports, 7 :41056.

Novel EIT topographic map reconstruction of a tactile skin based on self-organizing neural networks.

JOUR10 Pugach G., Pitti A. & Gaussier P. (2015), Neural Learning of the Topographic Tactile Sensory Information of an Artificial Skin through a Self-Organizing Map, Journal of Advanced Robotics, Oct 2015, vol.29, no. 21, pp.1393-1409. Special Issue on Artificial Skins in Robotics. [IF 0.5]

Robotic design principles applied to explain infant learning motor skills and neonate imitation.

JOUR09 Mahé S., Braud R., Quoy M., Gaussier P & Pitti A. (2015), Exploiting the gain-modulation mechanism in parieto-motor neurons : Application to visuomotor transformations and embodied simulation. Neural Networks, 62 :102–111. J'ai supervisé la recherche, l'analyse des résultats et sa rédaction, je suis le correspondant pour ce manuscript.

JOUR08 Pitti A., Braud R., Mahé S., Quoy M. & Gaussier P. (2013) Neural Model for Learning-to-Learn of Novel Task Sets in the Motor Domain. Frontiers in Psychology, 4 :771, 1–14. [IF 2.4]

JOUR07 Pitti A., Kuniyoshi Y., Quoy M. & Gaussier P. (2013) Modeling the Minimal Newborn's Intersubjective Mind : The Visuotopic-Somatotopic Alignment Hypothesis in the Superior Colliculus. PLoS ONE, 8 :7, e69474.

Chaotic controllers applied toward the control of motor synergies and central pattern generators.

JOUR06 Pitti A., Niiyama R. & Kuniyoshi Y. (2010) Creating and modulating rhythms by controlling the physics of the body. Autonomous Robots, 28 :3, 317-329.

JOUR05 Pitti A., Lungarella M. & Kuniyoshi Y. (2009) Generating Spatiotemporal Joint Torque Patterns from Dynamical Synchronization of Distributed Pattern Generators. Frontiers in NeuroRobotics, 3 :2, 1-14.

Spiking neural networks applied to multimodal integration modelling the Mirror Neurons system

JOUR04 Pitti A., Mori H., Kouzuma S. & Kuniyoshi Y. (2009) Contingency Perception and Agency Measure in Visuo-Motor Spiking Neural Networks. IEEE Trans. on Autonomous Mental Development, 1 :1, 86-97. [IF : 2.17]

JOUR03 Pitti A., Alirezaei H. & Kuniyoshi Y. (2009) Cross-modal and scale-free action representations through enaction. Neural Networks. Special issue "What it means to communicate", 22 :2, 144-154. [IF : 2.70]

We modeled an original scale-based causality measure for the study of complex systems

JOUR02 *Pitti A., Lungarella M. & Kuniyoshi Y. (2008) Metastability and functional integration in anisotropically coupled map lattices. Eur. Phys. J. B, 63, 239-243. [IF : 1.28]

JOUR01 *Lungarella M., Pitti A. & Kuniyoshi Y. (2007) Information transfer at multiple scales. Physical Review E, 76, 056117. [IF : 2.31]

Selection of Proceedings of International Conferences with Peer Reviews

(10 publications, 3 publications are co-authored under PhD supervision, 4 publications are co-authored with my students)

CONF10 Pugach, Melnyk, Tolochko, Pitti, & Gaussier. (2016) Touch-Based Admittance Control of a Robotic Arm Using Neural Learning of an Artificial Skin, IEEE IROS 2016, 3374-3380.

CONF09 Pugach G., Khomenko V., Pitti A., Melnyk A., Henaff P. & Gaussier P. (2013) Electronic hardware design of a low cost tactile sensor device for physical Human-Robot Interactions. IEEE XXXIII Inter. Conference on Electronics and NanoTechnology, Kiev : Ukraine, 1-6.

A neural model of the gain-field mechanism applied for multi-modal integration in robots

CONF08 Pitti A., Blanchard A., Cardinaux, M. & Gaussier P. (2012) Gain-Field Modulation Mechanism in Multimodal Networks for Spatial Perception. IEEE HUMANOIDS Conf., 297-302.

CONF07 Pitti A., Blanchard A., Cardinaux, M. & Gaussier P. (2012) Distinct Mechanisms for Multi-modal integration and unimodal representation in spatial development. IEEE ICDL-EPIROB, 1-6.

Model of hippocampal memory development triggered by the neuromodulator Acetylcholine

CONF06 Pitti A. & Kuniyoshi Y. (2011) Modeling the Cholinergic Innervation in the Infant Cortico-Hippocampal System and its Contribution to Early Memory Development and Attention. Proc. of the Int. Joint Conference on Neural Networks IJCNN 2011, 1409-1416.

CONF05 Pitti A. & Kuniyoshi Y. (2011) Contribution of the Cholinergic Innervation to Early Memory Development in the Neonate Para-Hippocampal System. Proc. of the 3rd Int. Conf. on Cognitive Neurodynamics ICCN 2011, 1-8. **[Poster Award, 5% selection out of 100 papers]**

Model of the Mirror Neurons Systems development for spatial skills in multi-DOF infant-like robot

CONF04 Pitti A., Mori H., Yamada Y. & Kuniyoshi Y. (2010) A Model of Spatial Development from Parieto-Hippocampal Learning of Body-Place Associations. Proc. of the 10th Int. workshop on Epigenetic Robotics, pp.89-96.

Design central pattern generators & motor synergies for locomotion and control of multi-DOF robots

CONF03 *Pitti A., Lungarella M. & Kuniyoshi Y. (2006) Synchronization : adaptive mechanism linking internal and external dynamics. Proc. 5th Int. Work. on Epigenetics Rob., 127-134.

CONF02 *Pitti A., Lungarella M. & Kuniyoshi Y. (2006) Exploration of natural dynamics through resonance and chaos. Proc. 9th Int. Conf. on Intell. Autonomous Systems, 558-565.

CONF01 *Pitti A., Lungarella M. & Kuniyoshi Y. (2005) Quantification of emergent behaviors induced by feedback resonance of chaos. Recent Advances in Artificial Life : Advances in Natural Computation, vol.3, chap.15, 199-213.

Book Chapters

CHAP05 Pitti A. (2017) the Alignment Hypothesis for Modeling the Self. The Development of Self Workshop. *to appear*

CHAP04 Pitti A. (2017) Ideas from Developmental Robotics and Embodied AI on the Questions of Ethics in Robots. Report for UNESCO Symposium, Marie-Hélène Parizeau. *to appear*

CHAP03 Pitti A. & Gaussier P. (2017) Reaching and Grasping : what we can learn from psychology and robotics. Book Chapter, Editors Daniella Corbetta. *to appear*

review chapters on my research to model the Mirror Neurons System

CHAP02 Pitti A. & Kuniyoshi Y. (2012) Neural Models For Social Development In Shared Parieto-Motor Circuits. Book Chapter 11 in "Horizons in Neuroscience Research. Volume 6", Nova Science Publishers, 247-282.

CHAP01 Pitti A., Alirezaei H. & Kuniyoshi Y. (2008) Mirroring Maps and Action Representation through Embodied Interactions. Book Chapter in Connectionist Models of Behaviour and Cognition II, World Scientific, 27-37.

CHAPITRE 2

Summary of My Research Activities (2007-2016)

Introduction

Recalls on my PhD work

I have started my Ph.D. research in computational neuroscience and bio-inspired robotics on the modelling of the motor synergies and the motor control at the spinal cords level. The motor control was made by the neuromodulation of chaotic oscillators that phase synchronize their activities to the body dynamics toward emergence of rhythmical motion patterns. I have exploited various embodied morphologies with quadruped, biped, or highly redundant robot architectures, in simulation as well as in real with muscle-like McKibben pneumatic actuators. I follow this research toward achieving low-cost, ecological, bio-inspired, soft and multi-articulated robotic designs.

The aim of my thesis was to propose a constructive approach to study the mechanisms underlying the intelligent processes arising between the body, its internal dynamics, with the environment. The body and nervous system are inseparable interacting constituents of an organism, and it is a mistake to think of the former passively obeying the commands of the latter : they operate in complex and subtle harmony.

Our claim is that synchronization may provide a coherent and unified framework to model how people learn, control their body, interact and develop themselves. More precisely, I contributed to a methodology to explore, quantify and categorize the natural dynamics of a given robotic system by exploiting the property in nonlinear oscillators to match (to synchronize) the resonant frequencies of any driving force (feedback resonance) ; see Fig 2.1.

The mechanism of phase synchronization in dynamical systems may be exploited to control the system's global dynamics, and can be applied to high dimensional system and to the "tuning" of its material property and morphology. At reverse, the design of the robot's body requires to have some constrains on its geometry, its material properties in order to process *morphological computations* Pfeifer et al. [2007a]; Pfeifer and Pitti [2012].

We pursue further the idea of a network of chaotic units used as a model for exploration of body dynamics. One of the core features of our model is that it allows to switch between

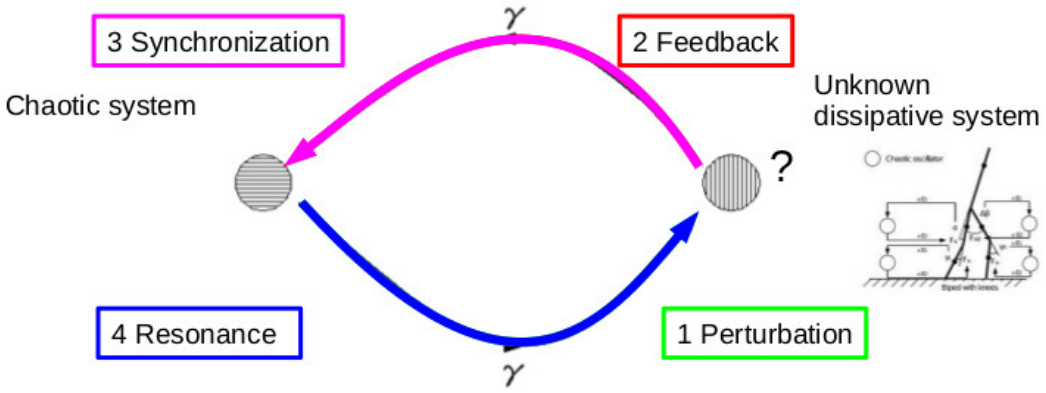

FIGURE 2.1 – Presentation of the chaos control framework for modeling central pattern generators in robots. Chaotic systems are returning maps with an infinite frequencies. For certain coupling parameters with a passive or under-actuated system, it can perturb and triggers its resonant frequencies through feedback. Chaotic oscillators are prety much like 'energy' pumps that move one system ack and forth along homoclinic lines for one amount of energy furnished. We propose that chaos control is similar to energy-shaping control of under-actuated systems toward the discovery of stable/unstable equilibrium points as well as dynamical regimes near homoclinic energy lines.

different attractors while maintaining adaptation. In the following section, we will present the three pillars on which our augmented model rests : (a) dynamical systems approach, in particular the notions of global dynamics and interaction dynamics ; (b) mechanism of feedback resonance thanks to which the neural system tunes into the natural frequencies of the intrinsic dynamics of the mechanical system ; and (c) concept of coupled chaotic fields which is responsible for exploration of the neural dynamics.

Neural Models and Physical Design for Motor Synergies in Robots

Traditionally, motion control strategies have revolved around trajectory planning, inverse kinematics and inverse dynamics modeling, or adaptive methodologies such as reinforcement learning or genetic algorithms. Alas, if movements are generated by some fixed control structure or by optimization of some evaluation function it is not clear how the system can adapt to unpredicted dynamic changes. Rather than on control or optimization, we suggest that the emphasis should be put on exploiting the coherent patterns of motor activity which emerge from the interaction dynamics between brain, body, and environment. Nikolaus Bernstein was probably the first to address in a systematic way the question of how humans purposefully exploit the interaction between neural and body-environment dynamics to solve the complex equations of motion involved in the coordination of the large number of mechanical degrees of freedom of our bodies. In the last decade or so, Bernstein's degrees of freedom problem has been tackled many times through the framework of dynamical systems. Such research has three important implications which are relevant in this part. First, movements are dynamically soft-assembled by the continuous and mutual interaction between the neural and the body-environment dynamics. Second, embodiment and task dynamics impose consistent and invariant (i.e. learnable) structure on sensorimotor patterns. Third, when the neural dynamics of a system is coupled with

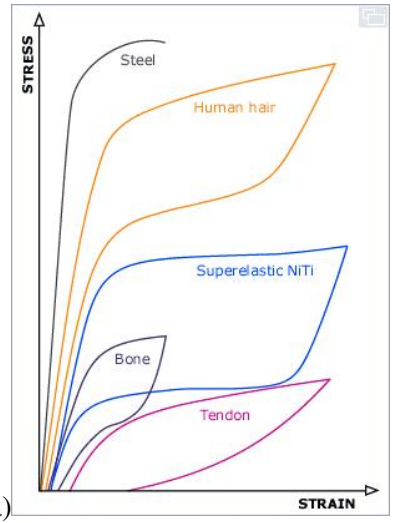

a)

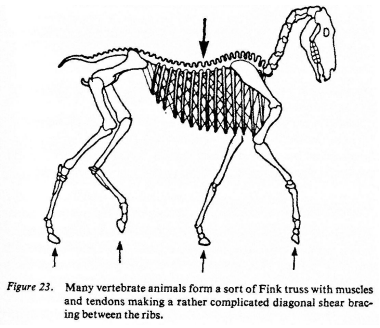

Figure 23. Many vertebrate animals form a sort of Fink truss with muscles and tendons making a rather complicated diagonal shear bracing between the ribs.

b)

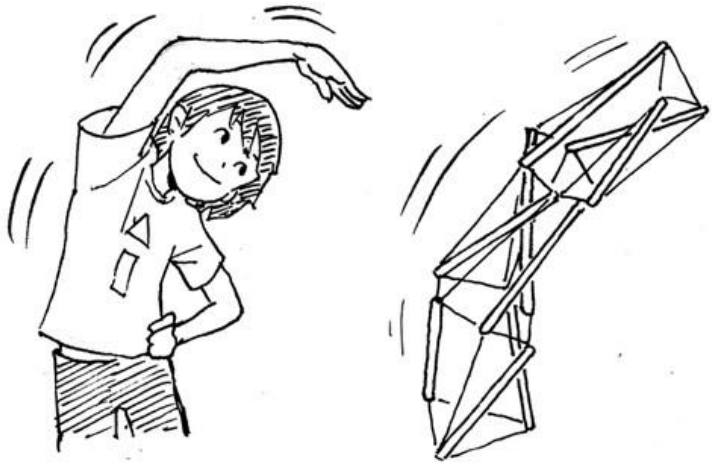

c)

FIGURE 2.2 – The structure of the body helps a lot for morphological computation and postural control. the necessary files to compile. Wh(a) Elasticity of tendons and muscles serve for energy saving and release durng dynamical motion. (b) posture serves for tension distribution thanks to the geometry features of its morphology. (c) tensegrity principle to understand the compliance of the body based on muscles prestress and bones compression.

its natural intrinsic dynamics, even a complicated body can exhibit very robust and flexible behavior, mainly as a result of mutual entrainment (e.g. neural oscillator based biped walking and pendulation).

Feedback Resonance of Chaos for Discovering Motor Synergies

Related papers :

- Pitti A., Lungarella M. & Kuniyoshi Y. (2005). Quantification of emergent behaviors induced by feedback resonance and chaos. Recent Advances in Artificial Life : Advances in

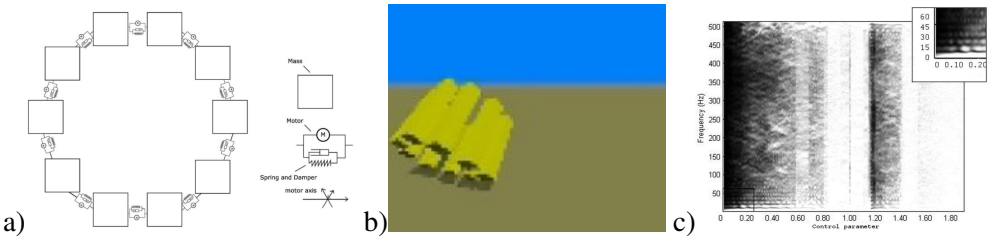

FIGURE 2.3 – Ring-shape mass-spring structure driven by a network of coupled chaotic pattern generators (called coupled chaotic fields). b) Spectral Bifurcation Diagram. Inset shows spectral peaks for low values of neural chaoticity. The control parameter is α. (Arrow) second harmonics.

Natural Computation, vol.3, chap.15, 199-213.

- Pitti A., Lungarella M. & Kuniyoshi Y. (2006) Exploration of natural dynamics through resonance and chaos. Proc. 9th Int. Conf. on Intell. Autonomous Systems, 558-565.

- Pitti A., Lungarella M. & Kuniyoshi Y. (2006) Synchronization : adaptive mechanism linking internal and external dynamics. Proc. 5th Int. Work. on Epigenetics Rob., 127-134.

We address the issue of how an embodied system can autonomously explore and discover the action possibilities inherent to its body. Our basic assumption is that the intrinsic dynamics of a system can be explored by perturbing the system through small but well-timed feedback actions and by exploiting a mechanism of feedback resonance. We hypothesize that such perturbations, if appropriately chosen, can favor the transitions from one stable attractor to another, and the discovery of stable postural configurations. To test our ideas, we realize an experimental system consisting of a ring-shaped mass-spring structure driven by a network of coupled chaotic pattern generators (called coupled chaotic fields), see Fig. 2.3. We study the role played by the chaoticity of the neural system as the control parameter governing phase transitions in movement space. Through a frequency-domain analysis of the emergent behavioral patterns, we show that the system discovers regions of its state space exhibiting notable properties.

Our analysis was mainly focused on understanding how the body dynamics evolution in time is related to the chaoticity of the neural units that is varied. The initial value of α is zero. For this value the output of the neural system is a constant, and the system doesn't move. The "ring" starts to vibrate almost unperceivably at a very small spatial scale by increasing by a small amount the chaoticity of the neural units ($\alpha \in]0.0, 0.1]$). After a certain amount of time, the seemingly random movements converge to a slow rhythmical rocking movement, that is, the system's dynamics have found a stable attractor.

Up to a very specific level of chaoticity ($\alpha = 0.097477$), the system strikes a perfectly poised balanced posture, and does not have sufficient energy to start rolling. By slightly increasing the control parameter ($\alpha = 0.1$), a phase transition occurs, and the system starts to roll. Interestingly, for values of $\alpha < 0.15$, the system oscillates quite unpredictably between rolling and balancing. The corresponding phase diagrams suggest that the emergence of particular movement patterns depends on the presence or absence of entrainment between neural and body-environment dynamics because coupled logistic maps for these particularly weak values of the control parameter α cannot produce a state transition (the first period doubling occurs at $\alpha = 0.4$).

For levels of neural chaoticity $\alpha \in [0.15\,;\,0.4]$, novel behaviors and patterns of locomotion emerges. The neural system seems to exploit the natural dynamics of the ring-shaped body to balance, rock, roll, accelerate and decelerate, and in rare occasions, even to jump. The instability of the movement patterns are mainly caused by micro-scale perturbations acting on the neural dynamics with a consequent disruption of the entrainment between neural and body-environment dynamics and the emergence of new locomotion patterns (relying on evidences that we will explain in the next section).

The Spectral Bifurcation Diagram for varying levels of chaoticity in the chaotic units is reproduced in Figure 2.3 c). Low levels of chaoticity at the output of the chaotic units ($\alpha < 0.05$) are characterized by sharp peaks in the power spectral density of the force sensors located in the joints, and given a particular value of α the resonance response is close to the one of a damped oscillator. The low frequency component around 2 Hz dominates the interaction dynamics between the neural system and the ring. This frequency corresponds to the fundamental mode of the coupled system, that is, its eigen-frequency. For this frequency, the joints are highly synchronized and the system displays a high degree of coordination. A minimal amount of energy is required to move the system and to transfer energy to the different parts of the body.

When the chaoticity increases higher harmonics appear introducing discontinuities in the resonance response. The main resonance persists for all values of but we observe abrupt changes and bifurcations in the magnitude of other peaks. The new harmonic peaks are located at integer and fractional multiples of the first eigen-frequency. The latter peaks are caused by small damped actions of the chaotic system and affect the joint properties, in the sense that a change of chaoticity of the neural system can induce a change in the stiffness of the springs in the joints. As a result the system is able to generate a large variety of patterns (stable, weakly stable, and unstable).

When the amplitude of the harmonics is too large, it negatively affects the groups formed in different regions of the body generating decoherence and destroying stable activity patterns. Note that the harmonic states are intrinsic to the coupling between neural, body, and environmental dynamics, and even if the spectral patterns seem complex, they should not be considered to be the outcome of yet another kind of neural noise.

We have previously suggested that behavioral changes are a complex function of the coupling between neural and body-environment dynamics. By using the Spectral Bifurcation Diagram we can now shed light on the patterns of neural activity leading to such changes. For example for a level of chaoticity α = 0.097477 (that is, when the ring starts to roll) the power spectrum has a second harmonic (arrow) which disappears in the interval [0.1, 0.13] (that is, when the system presents difficulties to roll again). The more harmonics there are, the more complex the behavior, despite preservation of coherence of behavior.

Similar results are found for a dog-like 2D robot with two actuators on the hip joints and passive dynamics at the knee-joints, see Fig. 2.4. Below a threshold for the coupling parameter $\alpha < 1.0$, no synchronization occurs between the internal logistic maps and the body dynamics and very random motions are seen as a vibrating mode. From the value $\alpha = 1.0$, small hops are triggered as the coupling between internal and external dynamics starts, see Fig. 2.4 top a). This corresponds to the fundamental resonant mode of the dog-like musculo-skeletal system. Above this value, more harmonics are found and the robot is capable to perform higher bumps and hops till the forces kick higher the robot The higher the harmonics, the faster the strokes on the body dynamics while the motor controllability looses precision to make higher jumps but

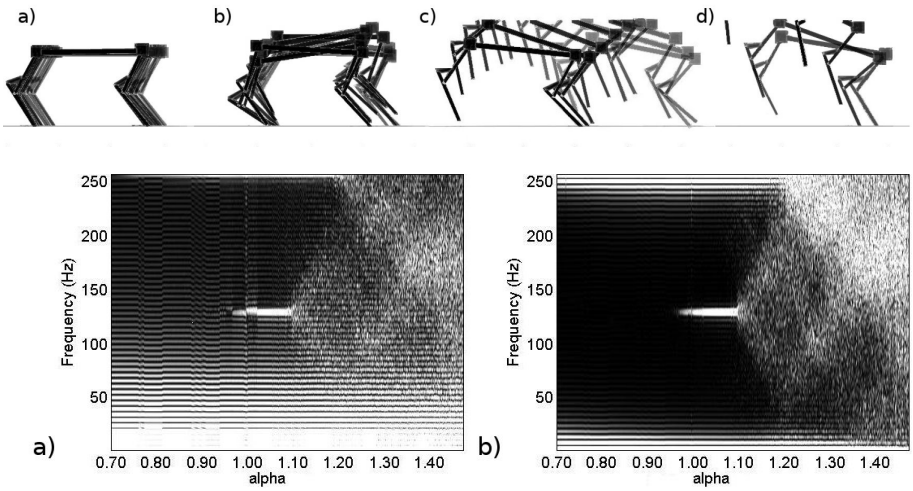

FIGURE 2.4 – Chaos control on a Quadruped underactuated robot. Experiments are based on energy-shaping with chaotic controllers for which we control the coupling parameters to the torques. Energy injected and synchronized to the body dynamics thanks to the phase synchronisation, permits to generate many dynamical behaviors corresponding to various regimes in the phase space and in the sprectal space.

less controllable.

Emergence of Rhythmical Patterns of McKibben Pneumatic Actuators

Related papers :

- Pitti A., Niiyama R. & Kuniyoshi Y. (2010). Creating and modulating rhythms by controlling the physics of the body. Autonomous Robots, 28 :3, 317-329.
- Pitti A., Lungarella M. & Kuniyoshi Y. (2009) Generating Spatiotemporal Joint Torque Patterns from Dynamical Synchronization of Distributed Pattern Generators. Frontiers in NeuroRobotics, 3 :2, 1-14.

The motion behaviors of vertebrates require the correct coordination of the muscles and of the body limbs even for the most stereotyped ones like the rhythmical patterns. It means that the neural circuits have to share some part of the control with the material properties and the body morphology in order to rise any of these motor synergies. To this respect, the chemical downward neuromodulators that supervise the pattern generators in the spinal cord create the conditions to merge (or to disrupt) them by matching the phase of the neural controllers to the body dynamics. In this paper, we replicate this control based on phase synchronization to implement neuromodulators and investigate the interplay between control, morphology and material. We employ this mechanism to control three robotic setups of gradual complexity and actuated by McKibben type air muscles : a single air muscle, an elbow-like system and a frog leg-like articulation, see Fig. 2.5. We show that for specific values, the control parameters modulate the internal dynamics to match those of the body and of the material physics to either the rhythmical and non-rhythmical gait patterns.

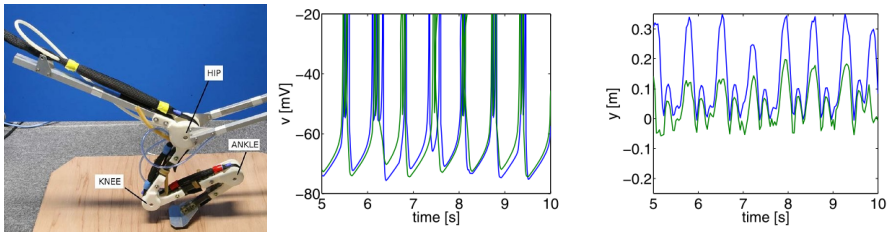

FIGURE 2.5 – Frog-like robot with co-articulated muscles. For certain coupling regimes, the McKibben air muscles are co-activated synchronously with the good amount of pressure in the valves for generating energy efficient hops.

Multimodal Integration and Sensory-motor Predictive Coding

After my PhD, I then expanded my field of scientific research as a Research Fellow extending it to multimodal integration by the modeling of the parieto-motor neurons at the cortical level with the so-called mirro-neurons and by modeling of the superior colliculus at subcortical level. These structures encode useful multimodal information (tactile, visual, proprioceptive and sound) however differently and for different purposes. While the cortical layer is found important for spatial perception and for the generation of purposeful actions, the more primitive subcortical layer is found crucial for rapid reactions stimulus-response rules. The cortical layer represents the physical space occupied by the body and objects nearby (i.e., the peri-personal space) and the possible actions to be performed depending on the context (i.e. affordances). The multimodal information is encoded with associative neurons recurrently connected in parallelized networks that bind information based on contingency prediction only in a unified fashion rather than separatedly. The parieto-motor network is sensitive to timing and robust to some points to prediction errors at the order of hundred of milliseconds, see section 2.4.1. The subcortical layer instead is a more reactive structure that has to be faster and represents unimodal information in layers organized topologically, whereas multimodal binding is done in an intemediate layer with no recursive feedback to each modality, see section 3.1 in section 3. Multimodal integration is important for the development of social cognition in babies, and similarly important for the future of social robotics.

Considering the modeling part, most of my models are based on discharge pulse models or spiking neurons because they exploit timing integration to shape the functional organization of complex networks such as small-world networks, see Fig. 2.6. Timing integration based on Spike Timing-Dependent Plasticty is useful for detecting the spatial and temporal contingency in multimodal signals, see section 2.4.1. I am currently pursuing this research to the advent of body-awared robots for social and physical interactions, with the development of an artificial skin for tactile perception and the study of audition and langage also, see section 2.4.2.

Cross-modal and Scale-free action representation in Spiking Neural Networks

Related papers :

- Pitti A., Alirezai H. & Kuniyoshi Y. (2009). Cross-modal and Scale-free action representation through enaction. Neural Networks, vol.22 (2), 144-154.

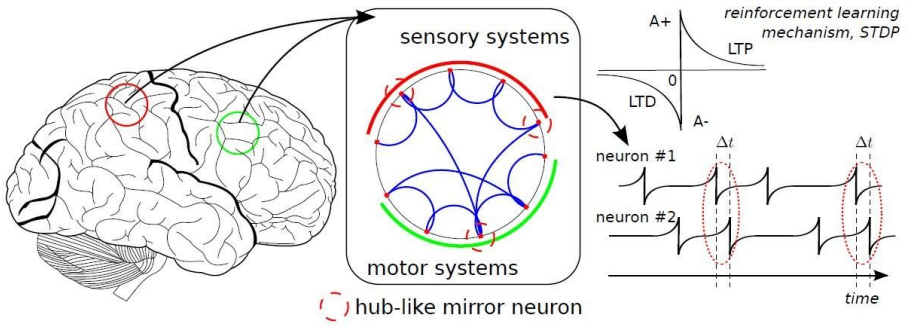

FIGURE 2.6 – A scale-free model of multimodal integration in the cortex for emergence of mirror-like neurons ased on timing contingency learning.

- Pitti A., Mori H., Kouzuma S. & Kuniyoshi Y. (2009) Contingency Perception and Agency Measure in Visuo-Motor Spiking Neural Networks. IEEE Trans. on Autonomous Mental Development, 1 :1, 86-97.

- Pitti A., Mori H., Yamada Y. & Kuniyoshi Y. (2010) A Model of Spatial Development from Parieto-Hippocampal Learning of Body-Place Associations. Proc. of the 10th Int. workshop on Epigenetic Robotics, pp.89-96.

Embodied action representation and action understanding are the first steps to understand what it means to communicate. We present a biologically plausible mechanism to the representation and the recognition of actions in a neural network with spiking neurons based on the learning mechanism of spike-timing-dependent plasticity (STDP). We show how grasping is represented through the multi-modal integration between the vision and tactile maps across multiple temporal scales. The network evolves into a small-world network.

We reproduce the experimental series conducted by Rizzolatti et al. (1996) illustrating the qualitative aspects of mirror neurons and of canonical neurons : inter-modal binding, action representation and action understanding with temporal constraint, see Fig. 2.7. These neurons combine visuo-motor properties to represent one action sequence and to fire at precise timing. In our experiments, we investigate the conditions for such situation to arise in a network of spiking neurons that would lead from the temporal linkage between the visuo-tactile maps to actions representation. We count, to this end, on the regulating roles of STDP and of the body (embodiment) to coordinate the neuron dynamics to the timing integration among the maps.

In the first part, we conduct some repeated experiences of visually perceived acts (i.e., seeing and touching one object) to be mapped in the neural system in the form of linked visuo-tactile representations (encoding both vision and tactile information).

Over time, the network acquires the direct matching from behaviors to neural dynamics. As the representation of physical actions is fetched into the network as multi-modal patterns, it is possible then to access one modality from the activation of the other, see Fig. 2.8. The functional integration within the network permits to access one missing modality from the activation of another one for instance to the understanding of actions performed by others, when no tactile information is received.

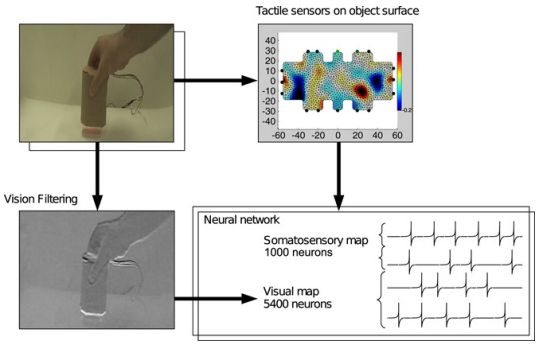

FIGURE 2.7 – STDP-based visuo-tactile integration with spiking recurrent neural networks. a) The experiencing of co-occurrent visuo-tactile perception during grasping (in the upper-left corner) by the network (bottom-right corner) is done by receiving the incoming information from the camera and from the pressure sensitive device. b) Neural dynamics of the visuo-tactile maps during physical interactions. In red (resp. in cyan) the synaptic activation from the neurons of the vision map (resp. the tactile map). At time-to-contact (t = t 1), the retina anticipates only the temporal changes about the hand motion in the direction of the cup : the spatial information about the cup is filtered. When grasping the object (t = t 2), joint detection of hand motion contingent to the cup motion and the haptic activity corresponding to a coordination in the neural dynamics (synchronization among the maps). Temporal rules about the sequential order of the event are then associated to a neural representation into the network. (For interpretation of the references to colour in this figure legend, the reader is referred to the web version of this article.)

Neural Modeling of Tactile Perception for Body Image

Related papers :

- Pugach G., Khomenko V., Pitti A., Melnyk A., Henaff P. & Gaussier P. (2013) Electronic hardware design of a low cost tactile sensor device for physical Human-Robot Interactions. IEEE XXXIII Inter. Conference on Electronics and NanoTechnology, Kiev : Ukraine, 1-6.

- Pugach G. , Pitti A. & Gaussier P. (2015), Neural Learning of the Topographic Tactile Sensory Information of an Artificial Skin through a Self-Organizing Map, Adv. Robotics. Oct 2015, vol.29, no. 21, pp.1393-1409. Special Issue on Artificial Skins in Robotics.

- Pugach G., Melnyk A., Pitti A., Tolochko, O. & Gaussier P. (2016) Touch-based Admittance Control of a Robotic Arm using Neural Learning of an Artificial Skin. Touch-Based Admittance Control of a Robotic Arm Using Neural Learning of an Artificial Skin IEEE/RSJ International Conference on Intelligent Robots and Systems (IROS), Daejeon, 2016, 3374 – 3380.

- Pitti A., Pugach G., Gaussier P. & Shimada, S. (2017) Visuo-Tactile Illusions in Artificial Skin from Fake Synchronization of Spiking Neurons. Scientific Reports (7) :41056

Touch perception is an important sense to model in humanoid robots to interact physically and socially with humans. These years, we have developed an artificial skin based on a large area piezoresistive tactile device (ungridded) that changes its electrical properties in the presence of the contact. The localization of contact force on its surface is based on inverse transform of

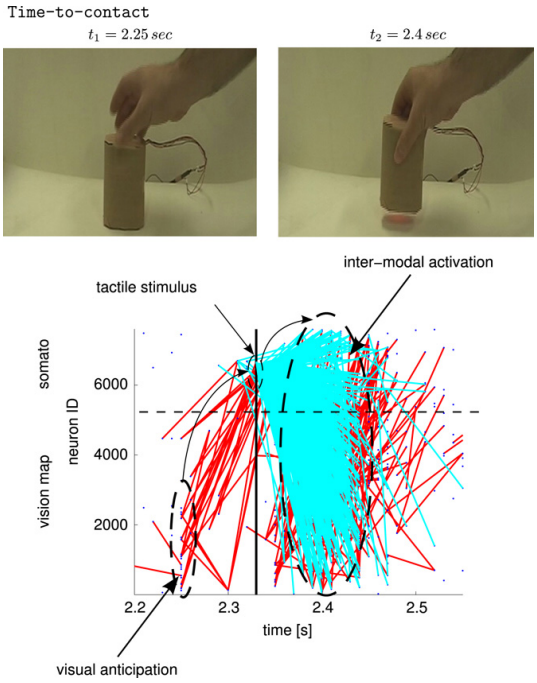

FIGURE 2.8 – Neural dynamics of the visuo-tactile maps during physical interactions. In red (resp. in cyan) the synaptic activation from the neurons of the vision map (resp. the tactile map). At time-to-contact (t = t_1), the retina anticipates only the temporal changes about the hand motion in the direction of the cup : the spatial information about the cup is filtered. When grasping the object (t = t_2), joint detection of hand motion contingent to the cup motion and the haptic activity corresponding to a coordination in the neural dynamics (synchronization among the maps). Temporal rules about the sequential order of the event are then associated to a neural representation into the network. (For interpretation of the references to colour in this figure legend, the reader is referred to the web version of this article.).

the Electrical Impedance Tomography (EIT), which is a well-known technic used in medical application for non-invasive signal detection.

Despite to be classic, this technic is interesting combined with machine learning algorithms as it generates lot of raw sensory data that Neural Networks and AI methods can exploit to learn new information such as the topology of the surface, the precision of contact force, see Fig. 2.9. Furthermore, once the learning process is done, the pattern reconstruction of the signal can be done in a very fast manner. We made several robotic experiments using self-organizing maps for learning the topology of the tactile map used alone. By doing so, each neuron of the self-organizing map learns a tactile receptive field sensitive to localization and pressure, which is similar to the slow adaptive Merkel cells in human skin, see Fig. 2.9.

Put in a robotic arm, a neural controller can adapt its compliance in four directions of its 2 DOFs using as input the tactile information taken from an artificial skin and as output the estimated torque for admittance control-loop reference. This adaption is done in a self-organized fashion with a neural system that learns first the topology of the tactile map when we touch it and associates a torque vector to move the arm in the corresponding direction. The neural system associates each tactile receptive field with one direction and the correct force. These methods can be used in the future for humanoid adaptive interaction with a human partner.

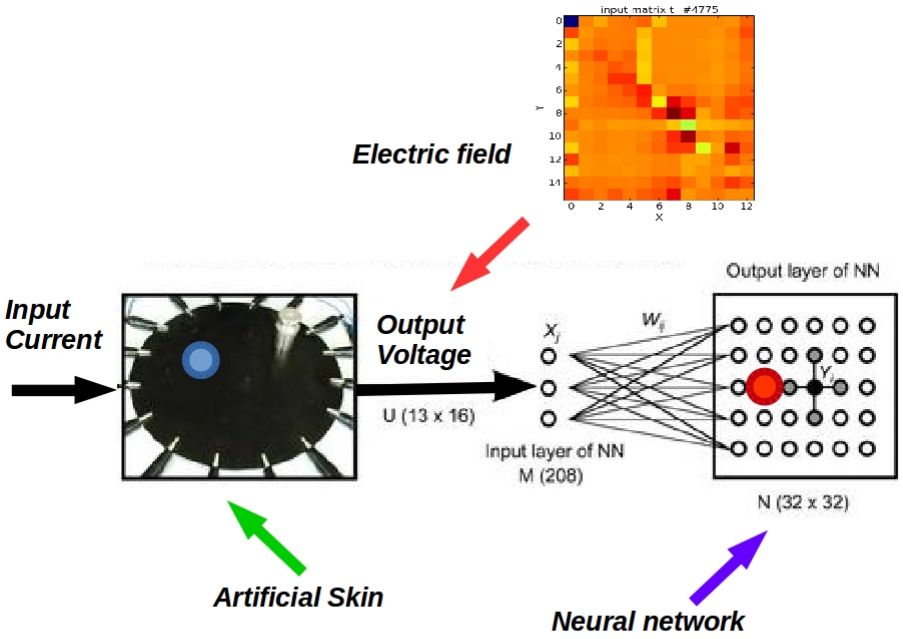

[Pugach, 2013, 2015]

FIGURE 2.9 – Schematic diagram to estimate the resistivity distribution on the tactile sheet by a Kohonen map based on the EIT method. The input current **I** is injected at 16 different locations, which give the voltage matrix **U**, the input of the Kohonen map of 32 × 32 units.

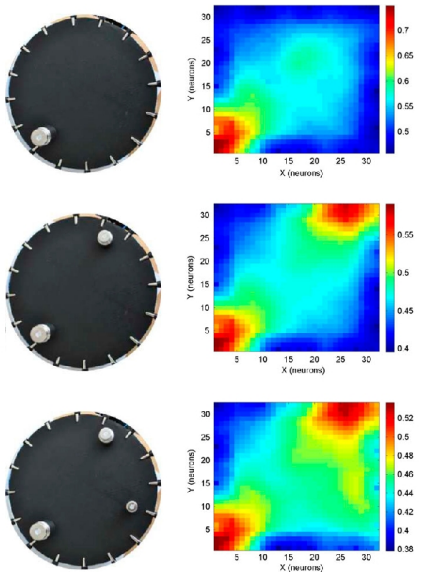

FIGURE 2.10 – Neural activity of the Kohonen map for multi-touch task for one, two or three weights of 100, 50 and 20 g ; resp (a), (b) and (c). The neurons are able to estimate correctly and simultaneously the objects of different location and weights.

Deuxième partie

Part II Research Activities in Details

CHAPITRE 3

Contributions to Multimodal Integration and Sensorimotor Predictive Coding

Action and perception are so deeply intertwined in the brain that the sensory and motor systems are continuously learning from each other an expectation of their complementary activity. We introduce here our modeling on multimodal integration considering neural mechanisms that may be involved during birth and early infancy and that we implement in robots. I have particularly studied developmental trajectory of multimodal integration based on temporal integration mechanisms like spike timing-dependent plasticity, found over the whole cortex and particularly in the Post Parietal Cortex (PPC), or other mechanisms based on topolographically organized maps as found in the Superior Colliculus (SC). Multimodal integration is found important for the spatial representation of the body and for the learning of sensorimotor rules in order to locate objects in space and to reach them. Although the SC is more attuned to ego-centred representations of each modality anchored on the head, the PPC is more complex spatio-temporal transformations toward body-centered maps (shoulder-, hand-, eye-, objects, etc...).

We present first in section 3.1 a development hypothesis of neonatal imitation, its neural mechanism involved at birth and during the feotal stage. Based on anatomical studies on the different brain areas that mature at birth and on the behavioral studies ofon this period, we focused our attention on the interesting structure of the superior colliculus, to give rise at birth to automatic social abilities, like facial preferences or imitation.

In second we present in section 3.2 some robotic works on the mechanism of *gain-modulation* found in parietal neurons for head-, arm-centered transformation that we used for body representation as well as reaching and grasping. We investigated largely on these bio-inspired mechanisms to serve on Audio - Motor - Visual - Tactile integration. We ommit on ppurpose our works on multimodal integration using spiking neurons due to space, although we beleive they are an important aspect for describing in details contingency detection.

Although not mentionned specifically, these different models of multimodal integration aimed at understanding the underlying the construction of the Mirror Neurons System, the development of social cognition and of sensorimotor predictive coding.

Sensory Alignments in Superior Colliculus

A growing number of developmental studies raise that the newborn infant is prepared, evolutionarily and physiologically, to be born intersubjective Nagy [2010]; Porges and Furman [2010]; Trevarthen [2010]. Here, social cognition is thought to start at the very beginning of infant development Rochat [2011], Reddy [2008], Johnson [2005], instead of at its achievement as Piaget proposed it Piaget [1954]. The unmatured brain of the fetus is argued to be socially prepared to recognize human faces at birth, to make eye contact with others Rigato et al. [2010], to respond emotionally to biological motion and to imitate others with limited abilities. In this nature versus nurture debate, we propose to investigate what could be the minimal neural core responsible for the development of the neonate social brain. This work pursues some other investigations in which we modeled different aspects of fetal and infant development features with computer simulations Kuniyoshi et al. [2003]; Kuniyoshi and Sangawa [2006]; Mori and Kuniyoshi [2007]; Kinjo et al. [2008]; Mori and Kuniyoshi [2010]; Yamada et al. [2010]; Pitti et al. [2010]; Boucenna et al. [2010].

Perhaps the most famous experiment in favor of neonate social engagement is the one conducted by Meltzoff, who showed that newborns are capable of imitating facial gestures off-the-shelf Meltzoff and Moore [1977].

Although still under debate, neonate imitation suggests that the bonding of human newborns is either innate or acquired from an early imprinting of the body image. Whether these neural circuits are pre-wired or not, they necessarily influence the normal cognitive development of neonates to guide the spontaneous interactions in the physical world and in the social world. Meltzoff suggests that neonates interact with others because they are capable of goal-directed actions and because they recognize this genuine characteristic in others. He summarized this idea in his "like-me" theory Meltzoff [2007b] where he proposes that this mirroring mechanism between self and others could be based on a supra-modal representation of the body constructed from intra-uterine motor babbling experiences. Accordingly, this supramodal body image is supposed to identify organs and their configural relations that will serve him later for the cross-modal equivalence underlying imitation Meltzoff [1997]. The successful replicating of neonatal imitation in monkeys by Ferrari argues further for the commonality of an early recognition mechanism in mammals' development, which may be based on "mouth mirror neurons" for facial and ingestive actions Ferrari et al. [2009]; Lepage and Théoret [2007] . Although the visual and motor cortices seem mature enough to support such system at birth, a subcortical scenario is more probable Valenza et al. [1996]; Simion et al. [1998], in which the subcortical units shape the cerebral cortex. This scenario may explain how a primitive body image could be accessible at an early age for sensorimotor coordination.

Consequently, the early functioning of the subcortical structures from the fetal stage appears very important for cortical development and therefore for the development of the social brain de Haan et al. [2002]; Johnson [2005, 2007]. Considering further the case of neonate face recognition, Johnson argues that the visual cortex is not mature enough before two months to support this function Senju and Johnson [2009]. He proposes that a fasttrack modulation model that includes the superior colliculus (SC), the pulvinar and the amygdala is at work in newborns for face detection, mood recognition and eye contact. He suggests also that this midbrain structure –dubbed as the CONSPEC model–includes an innate face-like visual pattern, nonplastic, that influences gradually the learning of a separate plastic cortical system, dubbed as the

CONLERN model Morton and Johnson [1991]; Johnson et al. [1991] ; a variant of this model has been given by de Schonen and Mathivet [1989]; Acerra et al. [2002].

In so far, despite their appealling layouts, Meltzoff's and Johnson's models have been criticized for lacking evidence that (i) the visual motor pathway has feature detectors that would cause faces to be attractive Nelson [2001]; Turati [2004] and that (ii) motor outputs look actually the same from a third party perspective Heyes [2003], which refers to the so-called correspondence problem Brass and Heyes [2005]; Ray and Heyes [2011]. We propose nonetheless that a framework consistent with both viewpoints can be drawn based on the neural functioning of the SC. More precisely, the SC presents three relevant features that are potentially determinant for the building of a social brain Johnson [2005].

First, SC supports unisensory processing in the visual, auditory and somatosensory domains accessible in a topographically- ordered representation to orient the animal to the source of sensory stimuli. Just as visual cues orient the eyes for tracking behaviors Kalesnykas and Sparks [1996], somatosensory cues extend the motor repertoire for full-body representation, including the neck and the face Stein and Meredith [1993]; Ferrell [1996]; Crish et al. [2006] ; the SC is coextensive with the pons, which is concerned with facial sensation, movement and vibroacoustic sensation Joseph [2000] and the face is represented in a magnified fashion with receptive fields Stein and Meredith [1993]. Although the SC is a structure late to mature, the somatosensory modality is the first modality to be mapped in the third trimester of pregnancy B.E. et al. [2009], followed by vision with observations of occular saccades behaviors Stanojevic and Kurjak [2008]. These aspects are important since some developmental studies attribute to SC a role in fetal learning using some form of vibro-acoustic stimulation to explain how the fetus is capable to sense and to learn through the body skin James [2010] and that SC is well-known as an important pathway for gaze shifting and saccade control Groh and Sparks [1996]; Moschovakis [1996]. Second, the SC supports sensory alignment of each topographic layer. That is, the somatotopic organization (in the deeper layers) is not only topographic but also follows the design of the visual map (in the superficial layers) Stein and Meredith [1993]; Stein et al. [1975]; Dräger and Hubel [1976]; King [2004]. Third, the intermediate layers exhibit 'multisensory facilitation' to converging inputs from different sensory modalities within the same region in space. As expressed by King, "multisensory facilitation is likely to be extremely useful for aiding localization of biologically important events, such as potential predators and prey, (...) and to a number of behavioral phenomena" King [2004]. Stein and colleagues underline also the importance of the multimodal alignment between visuotopic and the somatotopic organizations for seizing or manipulating a prey and for adjusting the body Stein et al. [1975].

Collectively, these aligned colliculus layers suggest that the sensorimotor space of the animal is represented in ego-centered coordinates Ferrell [1996] as it has been proposed by Stein and Meredith Stein and Meredith [1993] [38] and others Dominey et al. [1995] ; the SC is made up not of separate visual, auditory, and somatosensory maps, but rather of a single integrated multisensory map. Although comparative research in cats indicate that multimodal integration in SC is protracted during postnatal periods after considerable sensory experiences Stein [1984]; Wallace [2004]; Stein et al. [2010b], multisensory integration is present at birth in the rhesus monkey Wallace and Stein [2001] and has been suggested to play a role for neonatal orientation behaviors in humans. Moreover, while the difficulty to compare human development with other species has been acknowledged, "some human infant studies suggest a developmental pattern wherein some low-level multisensory capabilities appear to be present at birth or emerge shortly

thereafter" Stein et al. [2010a].

Considering these points about SC functionalities and develop- mental observations, we make the hypothesis that SC supports some neonatal social behaviors like facial preference and simple facial mimicry as a multimodal experience between the visual and somatosensory modalities, not just as a simple visual processing experience as it is commonly understood (see Fig. 3.1. We argue that, in comparison to standard visual stimuli, face-like visual patterns could correspond to unique types of stimuli as they overlap almost perfectly the same region in the visual topographic map and in the somatotopic topographic map. We propose therefore that the alignment of the external face-like stimuli in the SC visual map (some others' face) with the internal facial representation in the somatotopic map (one's own face) may accelerate and intensify multisensory binding between the visual and the somatosensory maps. Occular saccades to the correct stimulus may furtherly facilitate the fine tuning of the sensory alignment between the maps.

Moreover, in comparison with unimodal models of facial orientation, which support a phylogenetic ground of social development Ray and Heyes [2011]; Bednar and Miikulainen [2003]; Balas [2010], this scenario would have the advantage to explain from a constructivist viewpoint why neonates may prefer to look at configurational patterns of eyes and mouth rather than other types of stimuli Johnson [2005]; Pascalis et al. [2002] [25,58]. Stated like this, the ego-centric and multimodal representation in the SC has many similarities with Meltzoff's suggestion of an inter- but not supra-modal representation of the body responsible for neonate imitation. In this paper, we model the perinatal period starting from the maturation of unisensory layers to multisensory integration in the SC. This corresponds to the fetal maturation of the deep layers (somatosensory only) and of the superficial layer (vision only) at first, then to the post-natal visuo-somatosensory integration in the intermediate layers when the neonate perceives face-like patterns. Nonetheless, we make the note to the reader that we do not model the map formation in SC at the molecular level although there is some evidence that activity-independent mechanisms are used to establish topographic alignment between modalities such as the molecular gradient-matching mechanism studied in Triplett et al. [2012]. Instead, we focus at the epigenetic level, on the experience-driven formation of the neural maps during sensorimotor learning, in which we model the adaptation mechanisms in multisensory integration that occurs when there is a close spatial and temporal proximity between stimuli from different senses Benedetti [1995]; Perrault Jr et al. [2005]; Benedetti [2006]; Wallace and Stein [2000, 2007]. In computer simulations with realistic physiological properties of a fetus face, we simulate how somatosensory experiences resulting from distortions of the soft tissues (e.g., during the motion of the mouth or the contraction of the eyes' muscles) contribute to the construction of a facial representation. We use, to this end, an original implementation of feed-forward spiking neural networks to model the topological formation that may occur in neural tissues. Its learning mechanism is based on the rank order coding algorithm proposed by Thorpe and colleagues Van Rullen et al. [1998]; Thorpe et al. [2001], which transforms one input's amplitude into an ordered temporal code. We take advantage of this biologically-plausible mechanism to preserve the input's temporal structure on the one hand and to transpose it into its corresponding spatial topology on the other hand.

In comparison to other topological algorithms Kohonen [1982]; Sirosh and Miikulainen [1994]; Casey and Pavlou [2008]; Pavlou and Casey [2010]; Glasër and Joublin [2010], the synaptic weights of each neuron inform about the vicinity to other neurons based on their rank

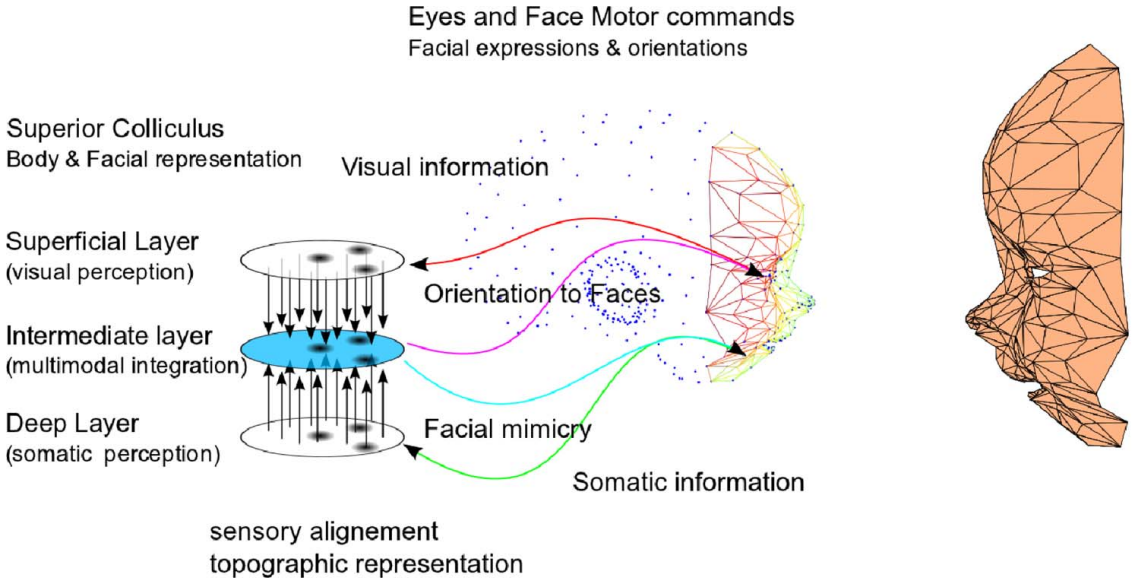

FIGURE 3.1 – Proposal for a minimal network in SC for an inter-subjective mind. In comparison to normal stimuli, we propose that faces are particular patterns because the visual and somatic maps in the superior colliculus are perfectly aligned topologically in the intermediate layer. We suggest that the spatial distribution of the neurons in the somatotopic map is preserved in the intermediate map, which makes the multimodal neurons salient to visual patterns with a similar spatial configuration of eyes and mouth. We hypothesize that this feature potentially influence the social skills in neonates, for detecting faces and reproducing facial movements.

order : that is, neurons with similar rank codes are spatially near. First, we study how the sensory inputs shape the sensory mapping and how multimodal integration occurs between the two maps within an intermediate layer that learns information from both. We propose that the registration of the somatosensory neural image aligned with the visual coordi- nates, as it could occur in the SC at birth, may give an easy solution to the correspondence problem, for instance, to recognize and to mimic the raw configuration of other people's facial expressions at birth. This scenario is in line with Boucenna and colleagues who showed how social referencing can emerge from simple sensorimotor systems Boucenna et al. [2010].

Methods

Face Modeling

In order to simulate the somatosensory information on the skin, we use a physical simulation that verifies the average character- istics of a 7–9 months-old fetus' face. In our experiments, the whole face can move freely so that its motion can generate weak displacements at the skin surface and strong amplitude forces during contact. The face tissue is modeled as a mass-spring network and local stretches are calculated with the Hook's spring law (see below) representing the forces that a spring exerts on two points. The resulting forces on each node of the mesh simulate tactile receptors like the Meissner's corpuscles, which detect facial vibro-acoustic pressures and distortions during facial actions Tsunozaki and Bautista [2009], see Fig.. 3.2.

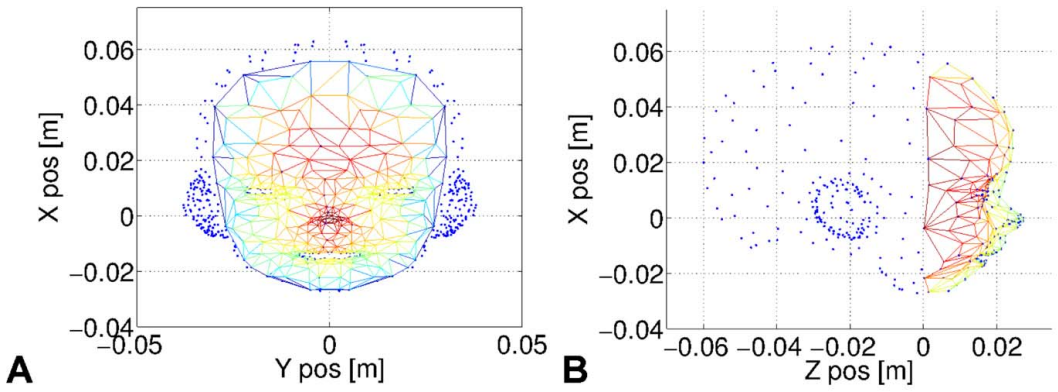

FIGURE 3.2 – Face mesh of the fetus model. The distorsion of the facial tissue is simulated as a mass-spring network of 354 tactile points and 1039 springs. Stress and displacement of the facial tissue are rendered by the actions of group muscles around the mouth and the eyes. In A, the front view of the face, the warm colors indicate the position of the segments in depth. The plot in B, the profile view, indicate the action limits of the face mesh in Z axis.

The facial tissue is modeled with 354 vertices and 1039 edges, and the mouth and the eyes apertures represent concave sets forming non-contiguous ensembles. The collision detection between two points or two springs is activated depending on the relative distance between the nodes and whether they are connected or not. On the one hand, for the case of contiguous points –that is, for the points connected with a spring– force collision is proportionnal to the local spring stiffness, to which no ad hoc force is added ; this physical model corresponds to the behavior of the Meissner's corpuscles.

On the other hand, for the case of non-contiguous points –that is, unconnected points– virtual springs are added at the contact points to model the softness of the tissue material jonction and the stress in the radial direction ; this physical model corresponds to the behavior of the Merkel cells, which are tactile receptors that detect pressure at localized points Boot et al. [1992]. The radial force is added when the nodes' spatial location is below a certain minimal distance d equals to 1mm.

For the sake of simplicity, we model the mouth motor activity and the eyes motor activity with virtual springs on the two lips of the mouth and on the two lids of the eyes. The contractions of these fictuous links control either the closure or the opening of the aperture of the mouth or of the eyes. In addition, we define as a prior choice that the two eyes move together (no eye blinking).

Results

Development of Unisensory Maps

Our experiments with our fetus face simulation were done as follows. We make the muscles from the eyelids and from the mouth to move at random periods of time, alternating rapid and slow periods of contraction and relaxation. The face model simulates the tension lines, which propagate across the whole facial tissue, producing characteristic strain patterns mostly localized around the organ contours, see Fig. 3.3. Here, the stress induced by the mouth's displacement is distributed to all the neighbouring regions. During the learning process, the nodes from each

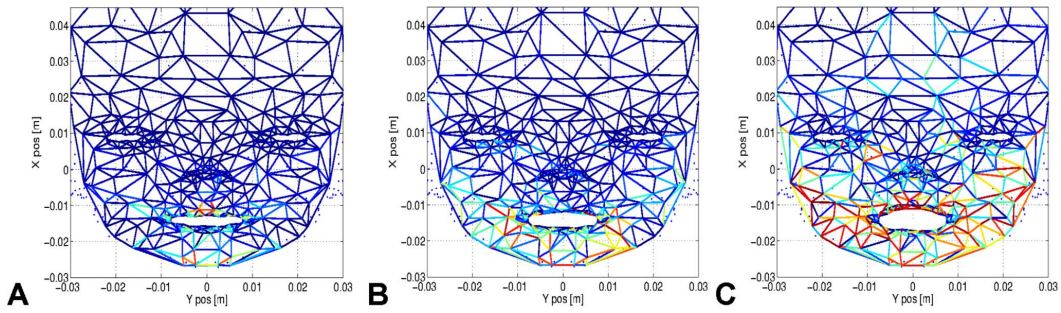

FIGURE 3.3 – Strain/stress evolution of the facial tissue during the opening and the closing of the mouth. The figures highlight the propagation of the strain/stress lines on the facial tissue around the mouth during its opening. The color intensity indicates the variation on each edge of the relative stress, which is propagated from neighbouring points to neighbouring points. The tension lines permits to draw the functional connectivity of each region on the facial tissue.

map encode one specific temporal pattern and the most frequent patterns get over-represented with new nodes added.

We reconstruct in Figures 3.4 and 3.5 the final configuration of the visuotopic and somatopic maps using the Fruchterman-Reingold (FR) layout algorithm Fruchterman and Reingold [1991], which is a force-directed graph based on the a measure distance between the nodes. Although very caricatural, the FR algorithm has been used for molecular placement simulations and can serve here to some extent to simulate the competition within the SC maps during ontogeny. We compute the euclidean distance between the weights distribution to evaluate the nodes' similarity and the attraction/ repulsion forces between them. The color code used for plotting the visual neurons follows a uniform density distribution displayed in Fig. 3.4. Here, the units deploy in a retinotopic manner with more units encoding the center of the image than the periphery. Hence, the FR algorithm models well the logarithmic transformation found in the visual inputs.

Parallely, the topology of the face is well reconstructed by the somatic map as it preserves well the location of the Merkel cells, see Fig. 3.4. The neurons' position respects the neighbouring relation between the tactile cells and the characteristic regions like the mouth, the nose and the eyes : for instance, the neurons colored in green and blue are encoding the upper-part of the face, and are well separated from the neurons colored in pink, red and orange tags corresponding to the mouth region. Moreover, the map is also differentiated in the vertical plan, with the green/yellow regions for the left side of the face, and the blue/red regions for its right side.

Multisensory Integration

The unisensory maps have learnt somatosensory and visual receptive fields in their respective frame of reference. However, these two layers are not in spatial register. According to Groh Groh and Sparks [1996], the spatial registration between two neural maps occur when one receptive field (e.g., somatosensory) lands within the other (e.g., vision). Moreover, cells in true registry have to respond to the same visuo-tactile stimuli's spatial locations. Regarding how spatial registration is done in the SC, clinical studies and meta-analysis indicate that multimodal integration is done (1) in the intermediate layers, and (2) later in development after unimodal maturation Stein et al. [2010b].

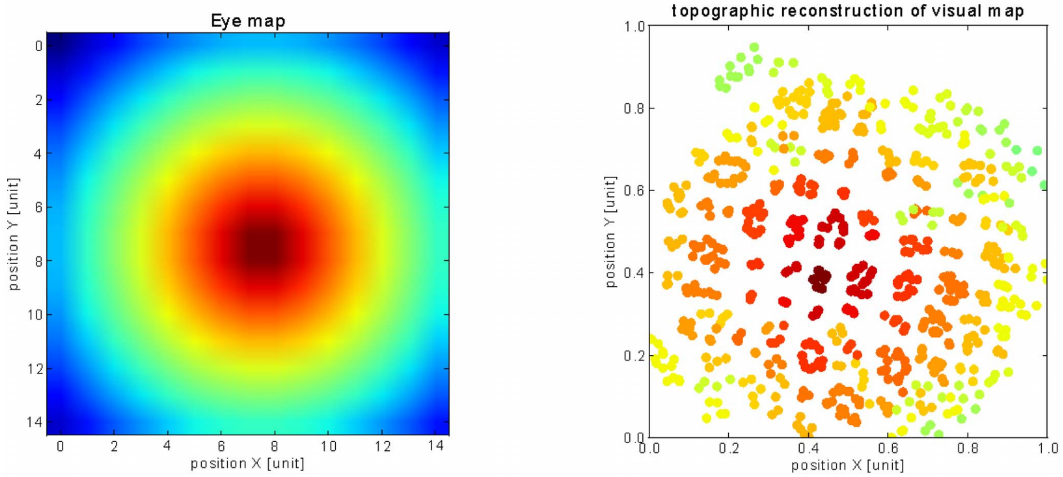

FIGURE 3.4 – Visuotopic reconstruction using the Fruchterman-Reingold layout algorithm. This graphic layout (right) displays spatially in a 2D map the distance between neurons computed in the weights space on the principle of attraction/repulsion forces. The layout models grossely the molecular mechanisms of map formation. The graph shows that the visual neural network represents well the fovea-centered distribution of its visual input represented on the left with the same color code.

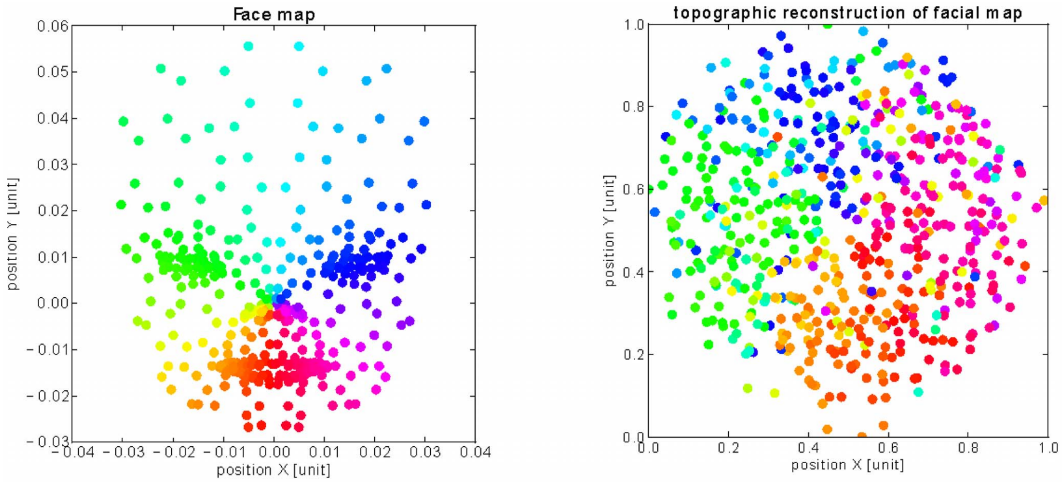

FIGURE 3.5 – Somatopic reconstruction using the Fruchterman-Reingold layout algorithm. As in the previous figure, the Fruchterman- Reingold graphic layout (right) displays spatially in a 2D map the distance between neurons computed in the weights space for the tactile neurons, based on the principle of attracting and repelling forces. In accordance with the previous figure, the graph shows that the tactile neural network respects quite well the topology of the face (left) with the same color code for the neurons connected to their respective somatic area : the neural clusters respects the vertical and horizontal symmetries of the face with the orange-red-pink regions corresponding to the lower part of the face, the green-cyan-blue regions to the higher part of the face, the green and orange regions to left-side of the face and the blue-pink regions to the right- side of the face.

To simulate the transition that occurs in cognitive development, we introduce a third map that models this intermediate layer for the somatic and visual registration between the superficial

and the deep-layers in SC ; see Figs. 3.1 and 3.6. We want to obtain through learning a relative spatial bijection or one-to-one correspondence between the neurons from the visual map and those from the somatopic map. Its neurons receive synaptic inputs from the two unimodal maps and are defined with the rank-order coding algorithm as for the previous maps. Furthermore, this new map follows a similar maturational process with at the beginning 30 neurons initialized with a uniform distribution, the map containing at the end one hundred neurons.

We present in Fig. 3.7 the raster plots for the three maps during tactual-visual stimulation when the hand skims over the face, in our case the hand is replaced by a ball moving over the face. One can observe that the spiking rates between the vision map and the tactile map are different, which shows that there is not a one-to-one relationship between the two maps and that the multimodal map has to combine partially their respective topology. The bimodal neurons learn over time the contingent visual and somatosensory activity and we hypothesize that they associate the common spatial locations between a eye-centered reference frame and the face-centered reference frame. To study this situation, we plot a connectivity diagram in Fig. 3.8 A constructed from the learnt synaptic weights between the three maps. For clarity purpose, the connectivity diagram is created from the most robust visual and tactile links. We observe from this graph some hub-like nodes in the bimodal map (the blue segment), which correspond to converging neurons from the two unimodal maps. Here, the intermediate neurons binds the two modalities. As an example, we color four links from the visual and tactile maps (resp. cyan, green and magenta, red segments) converging to two neurons from the bimodal map. We transcribe the associated visual and tactile patterns location at the top figures with the same color code. In these figures, on the left, the green dots in the visual map (resp. cyan and blue) indicate where the neurons trigger in visual coordinates and on the right, the red dots in the tactile map (resp. magenta and blue) indicate where the neurons trigger in tactile coordinates. Thus, the congruent spatial locations are mostly in registration from each others, and the bimodal map matches up with the two topologies.

In B, we reproduce the histogram distribution of the inter-modal connection weights taken from the tactile and visual maps to the bimodal map. The weights are uniformly distributed for the two modalities in blue and green with in average an equal number of weak connections (low values) and of strong connections (high values). However, for the neurons having necessarily strong links from both modalities (the red histogram), their number dramat- ically diminishes. For these neurons, only 18% of the neurons population (i.e., eighteen neurons) have their synaptic weights above 0 :4 from the two unimodal populations. For neurons having their synaptic weights above 0 :5, their number decreases to 8% of the neurons population (i.e., eight neurons). Although the global nework is not fully recurrent, the probability distribution describes a log-curve distribution very similar to small-world and to complex networks Sporns and Honey [2006]. Complex networks are well-known structures for efficient information processing, locally within the sub-parts and globally over the whole system Pitti et al. [2008].

The histogram in C draws a similar probability distribution for the spatial congruence between the visual mapping and the tactile mapping. This histogram displays the spatial error between the associated receptive fields taken from their respective barycentre (e.g., Fig. 3.8) and normalized. It shows that the unimodal receptive fields linked by the intermediate neurons overlap mostly their spatial location with 10% error only. Besides, the spatial distance decreases drastically above this value. As a result, most of the neurons from the two maps (90%) are in spatial registry.

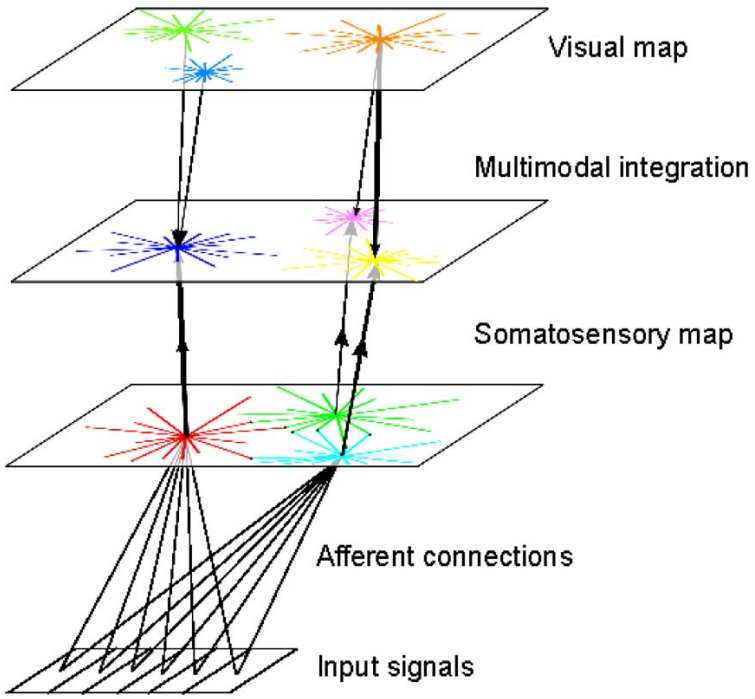

FIGURE 3.6 – Multimodal integration schema in SC between vision and tactile information. Integration is done as follows, the visual signals in the superfical layer and the somatosensory signals in the deep layer converge to the intermediate multimodal map (no reentrance) in which bimodal neurons align pair-wise visuo-tactile associations. In certain cases, the synaptic links from different neurons in the unisensory maps converge to the same bimodal neurons whereas in other cases the synaptic links from the same neurons in the unisensory maps diverge to different bimodal neurons.

Sensitivity to Configuration of Eyes and Mouth

In order to investigate the functional properties of the global network, we replicate the three dots experiment tested on the newborns by Mark Johnson Rigato et al. [2010]; Johnson [2005]. This test aims at demonstrating facial imitation and facial perception in newborns.

We analyze the networks' activity response for different configurations of an iconified face-like pattern exemplified by three large dots corresponding to the two eyes and the mouth, see the framed figure in Fig. 3.9 on the top-left.

For this, we rotate this pattern between [0,2pi] and collect the neural activation responses from the vision map (in blue) and from the intermediate map (in red). When the pattern is modulated by 2pi/3 radians (120°), we can observe a strong response activation taken from the visual map as the face-like stimuli is well-aligned with the visual neurons, which have encoded this spatial distribution. Concerning the multimodal map, its neural response presents a similar activity pattern but two time stronger and shifted by pi/6 radians (30°). This slight difference in response between the two maps indicates that they share some common features in their respective receptive fields but do not completely overlap from each other. Although visual and somatosensory maps are not organized in the same manner due to the skin-based or retinotopic reference frames.

Furthermore, we can observe cross-modal enhancement as the activity in the multimodal

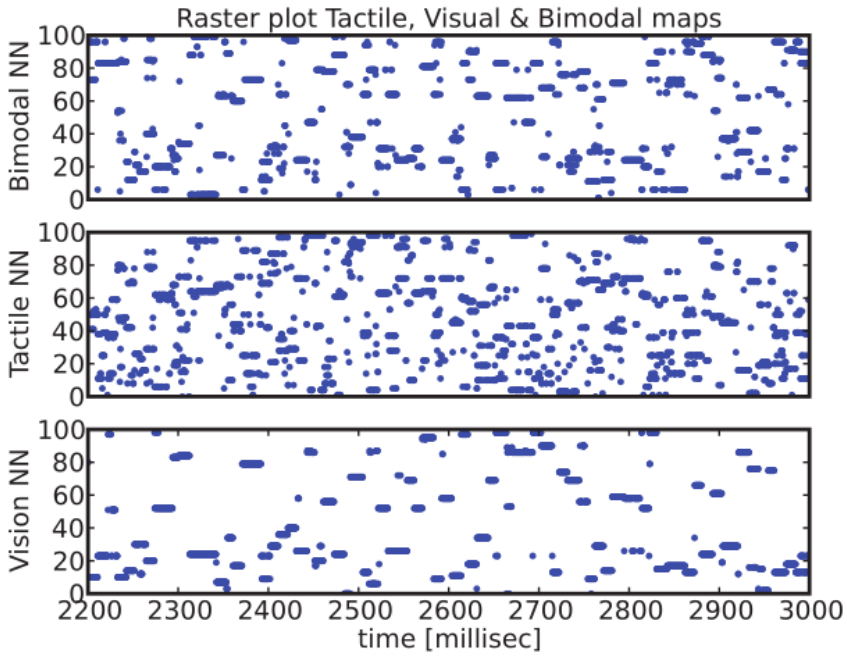

FIGURE 3.7 – Raster plots from the visual, the tactile and the bimodal maps, during visuo-tactual stimulation when the hand skims over the face. The activity of the visual, tactile and bimodal maps is drawn respectively at the bottom, the middle and at the top frame. At a given time, the spikes contingency across the neurons in the three different maps creates the conditions for reinforcing their synaptic links from the neurons of the unisensory maps to the neurons of the bimodal map. The difference of spiking rates between the maps show that there is not a bijective connection between the neurons and that some bimodal neurons may associate groups of visual neurons to groups of tactile neurons.

map is higher than from its visual input. The face-like stimulation pattern boosts the neurons activity when they are presented in the correct orientation coinciding with the facial topology. Thus, activity in the intermediate layer is stronger despite it does not receive any information from the tactile map. That is, thanks to the sensory alignment between the two modalities, the intermediate layer is able to simulate the neural activity of the tactile map.

Detection of Mouth and Eyes Movements

Our next experiment studied the influence of facial expressions on the multimodal system. A sequence of facial expression images, which alternated stare and smile, is presented to the visual map at regular timing period. First, the images were pre-processed with a motion detection filter, which simply subtracts two consecutive images, see Fig. 3.10 on the top. As a result, the static regions between the two consecutive images are filtered (e.g., the background and the cheeks) whereas its dynamical parts (i.e., the eyelids, the eyes, the nose and the mouth) are strongly emphasized when a strong facial expression is established. In this situation, the salient regions match well the three dots icon in Fig. 3.9.

At the network level, not all the neurons are active but some are very receptive to certain

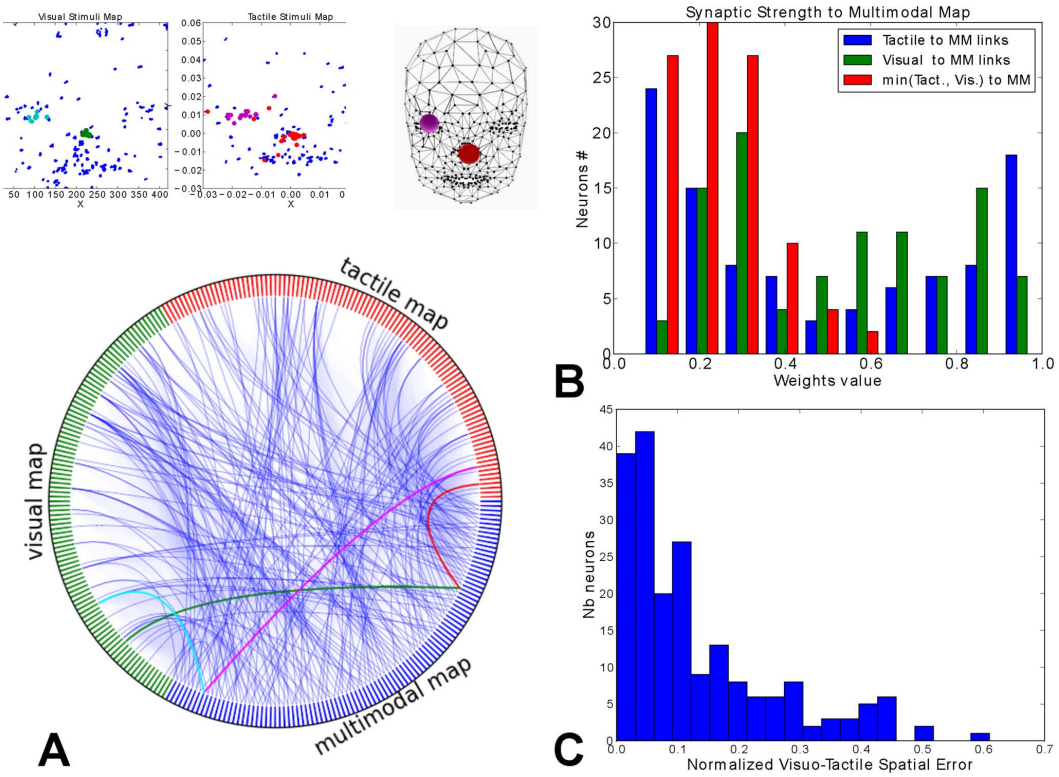

FIGURE 3.8 – Networks analysis of visuo-tactile integration and connectivity. A Connectivity circle linking the visual and tactile maps (resp. green and red) to the bimodal map (blue). The graph describes the dense connectivity of synaptic links starting from the visual and tactile maps and converging to the multimodal map. The colored links correspond to localized visuo-tactile stimuli on the nose (green/red links) and on the right eye (cyan/magenta links), see the patterns on the upper figure. The links show the correct spatial correspondance between the neurons of the two maps. B Weights density distribution from the visual and tactile maps to the bimodal map relative to their strength. These histograms show that the neurons from both modalities have only few strong connections from each others. This suggest a bijection between the neurons of each map. C Normalized distance error between linked visual and tactile neurons. When looking at the pairwise neurons of the two maps (red histogram in B for weights w0 :5), the spatial distortion between the neurons from the two maps is weak : vision neurons coding one location on the eyes receptive fields are strongly linked to the tactile neurons coding the same region on the face.

facial expressions and to the dynamic activation of certain spatial regions. We display a neuron dynamics in Fig. 3.10 for different facial expressions presented at periodic time from staring to surprise, and then from surprise to staring.

Here, the visuo-tactile neuron in the intermediate map is visually highly receptive to the regions that characterize the face because of sensory alignment and that its distribution is correlated to the tactile distribution of its own face. Therefore, whenever a transition occurs in facial expression, the neuron fires. One can imagine then that if the intermediate cells feed-forward this activity to the corresponding facial motor activity, then imitation will occur.

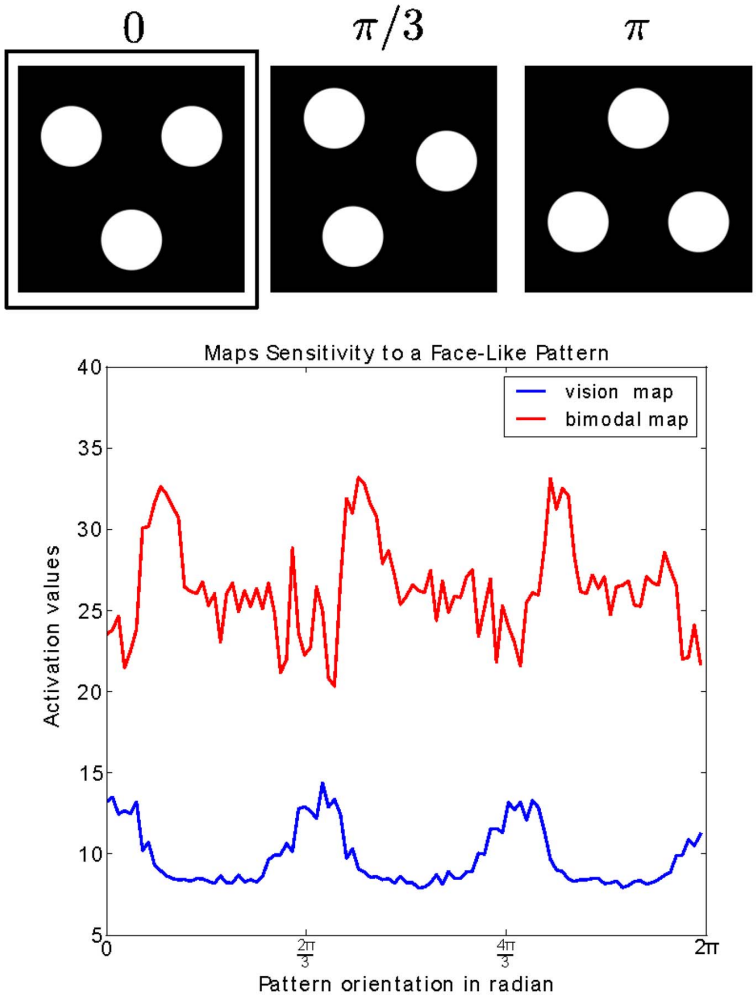

FIGURE 3.9 – Sensitivity to face-like patterns for certain orientations. This plot presents the sensitivity of the neural network to face-like patterns, with an experimental setup similar to the three-dots test done in newborns Johnson et al. [1991]. When rotating the three dots pattern centered on the eye, the neural activity within the visual map and the bimodal map gets higher only to certain orientations, 0 and p=6, when the three dots align correctly to the caricatural eyes and mouth configurational topology.

Discussion

We have introduced a developmental model of SC starting from the fetal stage in the context of social primitive behaviors. In comparison to normal stimuli, we propose that faces are particular patterns as the visual and somatic maps in SC are perfectly aligned topologically. We suggest that multimodal alignment may influence neonates for social skills, to recognize faces and to generate mimicry. The model consists of two unisensory layers, receiving the raw tactile information from the facial mechano- receptors simulated with a mass-spring mesh network and the raw visual information from the not-yet matured eyes. We make the note that the SC is comprised of two hemispheres and a unilateral SC lesion produces contralateral sensory (visual, somatosensory and auditory) deficits Sprague and Meikle [1965]. Although we could have modeled only one

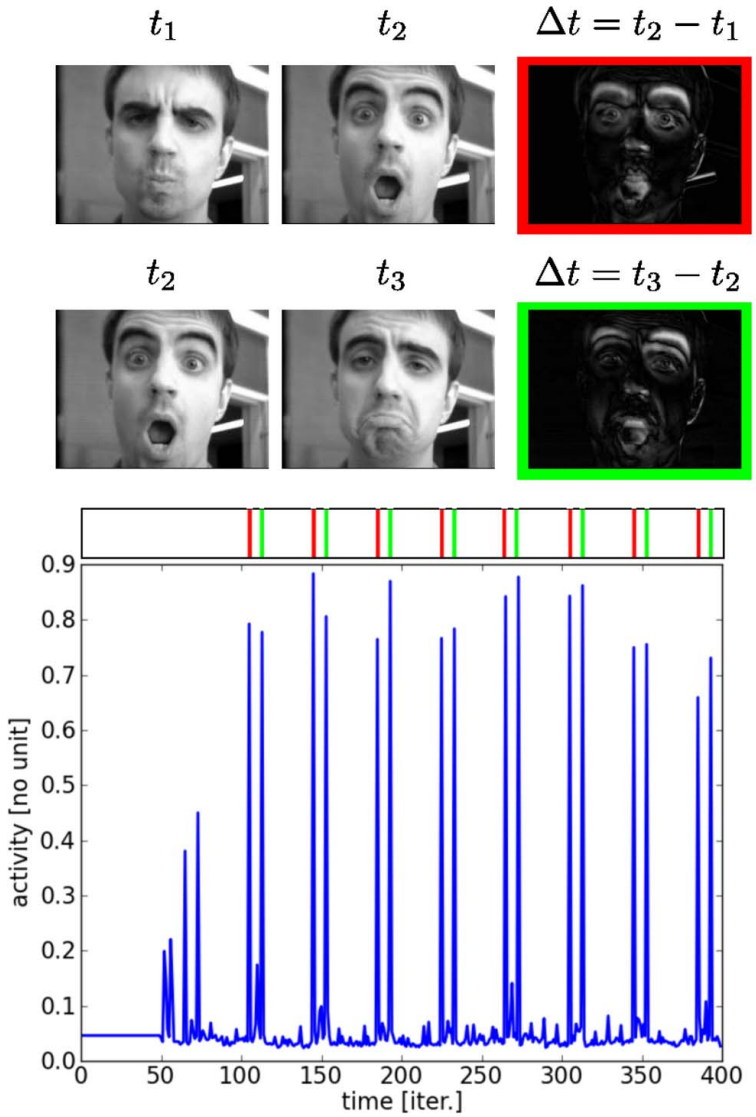

FIGURE 3.10 – Neural activity taken from the intermediate visuo-tactile map during observation of a facial expression : surprise (red frame) and stare (green frame). We present a sequence of facial expressions from surprise to stare and vice-versa. The selected bimodal neuron taken from the intermediate map triggers to the characteristic visual configurational patterns of the face during rapid changes, which permits to detect the mouth and eyes movements. This behavior is due to the sensory alignment and of the high correlation with the tactile distribution of its own face. Note : the subject has given written informed consent to publication of his photograph.

hemisphere and given to the system only half of the contralateral sensory information, we think our system would have learnt the same. The two circuits are initialized in a primitive stage starting with few neurons with randomized synaptic connections. We simulate the developmental aspects of the map formations during the third trimester of pregrancy through the mechanisms of activity-dependent neural growth Pellegrini et al. [2007] and synaptic plasticity. Over time, the two maps evolve into topographic networks and a third map is introduced, which corresponds

to the intermediate layer in SC that aligns the visual and tactile sensory modalities from each other. The neurons are modeled with the rank-order coding algorithm proposed by Thorpe and colleagues Thorpe et al. [2001] [66], which defines a fast integrate-and-fire neuron model that learns the discrete phasic information of the input vector.

The major finding of our model is that minimal social features, like the sensitivy to configuration of eyes and mouth, can emerge from the multimodal integration operated between the topo- graphic maps built from structured sensory information Lungarella and Sporns [2005, 2006]. A result in line with the plastic formation of the neural maps built from sensorimotor experiences Benedetti [2006]; Wallace and Stein [2000, 2007]. We acknowledge however that this model does not account for the fine-tuned discrimination of different mouth actions and imitation of the same action. We believe that this can be done only to some extent due to the limitation of our experimental setup. In our predictions, however, we believe that a more accurate facial model which includes the gustative motor system can account to represent the somatopic map with more fine-tuned discrimination of mouth movements with throat-jaws and tongue motions (tongue protrusion) against jaw and cheeks actions (mouth opening). Moreover, our model of the visual system is rudimentary and does not show sensitivity in the three dots experiments of dark components against light background as observed in infants Farroni et al. [2005]. A more accurate model integrating the retina and V1 area may better fit this behavior.

Although it is not clear whether the human system possesses inborn predisposition for social stimuli, we think our model could provide a consistent computational framework on the inner mechanisms supporting that hypothesis. This model may explain also some psychological findings in newborns like the preference to face-like patterns, contrast sensitivity to facial patterns and the detection of mouth and eyes movements, which are the premise for facial mimicry. Furthermore, our model is also consistent with fetal behavioral and cranial anatomical observations showing on the one hand the control of eye movements and facial behaviors during the third trimester Kurjak et al. [2005], and on the other hand the maturation of specific sub-cortical areas ; e.g. the substantia nigra, the inferior-auditory and superior-visual colliculi, responsible for these behaviors Stanojevic and Kurjak [2008].

Although neonate imitation is only a marker that disappears after 2–3 months in human, we propose that the SC is at the root of this behavior for enabling automatic social interactions. This hypothesis has been also suggested by Nagy [2010]; Neil et al. [2006]; Salihagic Kadic et al. [2008] who emphasized the central place that occupies the SC for fusioning the senses with respect to other brain regions not yet matured. Anatomical studies on collicular cells show that the eye neurons go forward to the deep layers without recurrent synaptic connections, which has to confer to SC a strong computational power due to alignment ; e.g., the easy and rapid construction of a primitive body image. This primitive body image may correspond to the first-stage of Piaget's spatial and motor development landscape characterized by an egocentric representation and sensorimotor coordination before the apparition of a more complex spatial representation of the body in allocentric metric Piaget [1954]; Bremner et al. [2008], mapped into the cortex. The multimodal cells in SC, along with the other forebrain structures such as the hippocampus and the amygdala, may help the construction of such body schema in the parieto-motor cortices.

Learning Multimodal Co-Variation Rules with Gain-Field Neurons

We propose in this section some models based on gain-modulation of the parietal neurons for sensorimotor *transformation* between reference frames centered on the eye-, head- or arm- spatial locations. Gain-modulation is a neural mechanism found in the network organization of parietal areas based on multiplicative neurons. Its properties are interesting as it combines aspects of radial-basis functions, sigma-pi networks and the recently proposed gated networks. We develop our study of this mechanism on three different transformations realizing eye-to-arm transformation for reaching and grasping based on visuo-motor integration, see section 3.2.1, audio- and visual integration for eye-to-head integration, resp. section 3.2.2 and visuo-tactile integration for body representation, see section 3.2.3.

Spatial Perception in Multimodal Co-Variation Rules with Gain-Field Neurons

Perceiving objects in space is one of the first tasks babies have to deal with during infancy. It is a rather difficult problem since infants have to represent one object with multiple sensory modalities (vision, sound, tactile) encoded in different reference frames (e.g., eye-centered, head-centered or hand-centered). This curse of dimensionality corresponds to the so-called binding problem across the modalities and requires at least to construct one amodal and unified reference frame relying on coordinates transformation between the senses *or* to form a network of partially inter-connected reference frames to represent one stimulus in each modality Heed et al. [2015]. Our aim in this review is to present some underlying neuro-computational mechanisms that can serve for such multimodal integration in infants in order to reach and grasp objects.

According to Bremner, the way infants perceive the space around them (i.e., infants' spatial representation) relies on two different mechanisms that mature separately during the first year Bremner et al. [2008]. One is ego-centric and achieves a spatial correspondence of the default body parts and the other is allocentric and helps to localize dynamically the position of the limbs. For instance, infants find hard to locate their own hands when their arms are crossed.

It is assumed that the infant brain exploits strongly Hebbian learning to acquire those spatial maps Del Giudice et al. [2009]; Heyes [2010]; Keysers et al. [2014]. Hebbian learning can provide to neurons the ability to correlate the contingent events, even across multiple modalities. For instance, infants even at birth can connect the modulation of a sound (from low pitch to high pitch) with the modulation of a light intensity (from low brightness to high luminosity Lewkowicz and Turkewitz [1980]), they can relate the contingency between their legs motion and their visual location displayed on a TV monitor Rochat [1998]; Shimada et al. [2005] or between the texture of a pacifier on mouth and its visual shape Meltzoff and Borton [1979].

Tenants of the embodied system approach suggest that infants learn the regularities in the structure of sensorimotor information to shape the neural activity in the brain. In this line, sensorimotor neurons become sensitive to the geometrical features of objects in space (their position, their orientation) relative to their bodily gestures and postures ; what we call sensorimotor primitives. In return, these neurons would guide and constrain the baby behaviours toward its affordances on the environment ; e.g., to orient oneself in the environment or to grasp one object in the correct orientation relative to the body.

All-in-all, we propose that the contingency found across the body signals during sensorymotor exploration –, coming from the arms muscles spindles, the joint angles from the shoulder-elbow-wrist system, the tactile information from the hand, the sound of a noisy object in the

hand and the eye's vision cells as well as their orientation,– may organize the cortical memory into a map of "reachable regions" cells via Hebbian learning. Following this, we can propose that the parietal cortex –, which is acknowledged as the center for multi-modal integration and body representation,– learns body-place associations by creating parieto-motor "reaching cells" for manipulation tasks Graziano and Cooke [2006] in a similar fashion the hippocampus learns "place cells" for navigation purpose Gaussier et al. [2007], see Fig. 3.11 respectively a) and b).

Visual and Motor Integration with Gain-Field Neurons for Arm Control

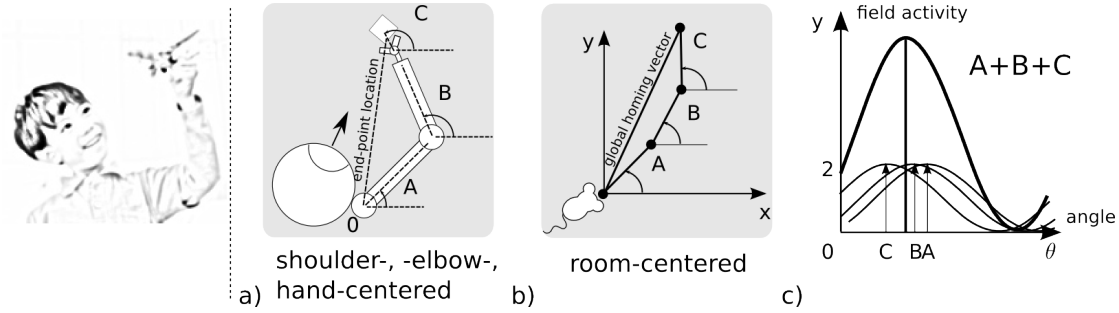

FIGURE 3.11 – Infant holding a toy in his hand. Reaching, grasping and holding objects are non trivial tasks. In a), they require to coordinate one's own actions relative to the objects' relative spatial location and orientation in eye-, hand-, or body-centered reference frames. In b), Reaching and grasping with the hand are similar in essence to a navigation task in a third-person perspective toward a place. In c), it requires to integrate information through time to perform homing Gaussier et al. [2007].

We suppose that the learning of *reach cells* is presumably done by discovering the correct binding that relates each stimulus in its correct reference frame with others in different reference frames ; for example this would help for locating the hand in eye coordinates (self-recognition), one object in hand-centered coordinates (relative distance) or one object in shoulder-centered coordinates (body-centered distance).

Those reach cells require to combine contextually or conditionally different sensory signals to represent one location, even if they change dynamically ; e.g., if an object is placed at a relative distance of the arm independent of the arm location. For instance, tactile information is dependent on the fingers in the hands, but also on the wirst orientation and arm location, see Fig. 3.12 a) and b). The visual information is dependent of the eye angle in its orbit (eye-centered) *and* to the head orientation (body-centered), for which the later is only valid for auditory signals.

Considering the neural mechanisms involved in the construction of reach cells, visuomotor neurons have been found to encode the Preferential visual movement Direction (PD) in extrinsic coordinates (likely shoulder-centered) in 3D space Blohm et al. [2008]; Blohm and Crawford [2012]. Kakei and colleagues for instance found some muscle-like neurons based on the composition of cosine functions tuned to visual PD and modulated monotically with the limb posture, see the neuron's activity in Fig. 3.12 a). When the wrist rotates, the extrinsic neurons discharge proportionally to the preferred visual direction in order to compensate the muscles displacement Kakei et al. [2003]. Other researchers like Scherberger and colleagues found some hand-centered cells whose activity depends both on the object features like the size and the orien-

tation and on the grip type (pronation or suppination) Gail et al. [2009]; Fluet et al. [2010], see Fig. 3.12 b). These reach neurons are multimodal and context-dependent. They compute *where* an object is located with respect to the hand position and *how* it is oriented with respect to the hand posture. They are called also in the literature Gain-Field neurons (GF), because their gain-level or amplitude is varying depending on multiple inputs to represent the current object-body relation Salinas and Thier [2000]; Salinas and Sejnowski [2001] as shown in Fig. 3.12.

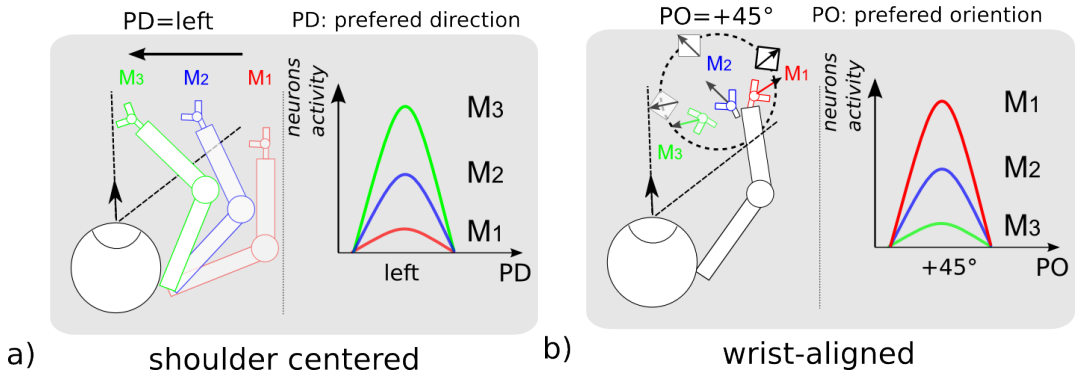

FIGURE 3.12 – Principle of gain-modulation in parieto-motor neurons (gain-field neurons) for the arm reaching and orientation. Gain-field neurons combine visuo-motor features to encode one prefered direction (PD) or one prefered orientation (PO). In a), exemplar activity of one GF neuron with visual PD *and* when the arm moves on the left. In b), exemplar activity of one GF neuron with some visual PO *and* when the wirst is on pronation.

The gain-field modulation mechanism describes the phenomenon where the motor and the sensor signals (resp. A and B) mutually influence the amplitude activity of their afferent parietal neurons (resp. C) Andersen and Mountcastle [1983]; Andersen et al. [1985]. As an example, one possible modulation is the multiplicative effect across the unimodal neurons, A and B, so that the afferent multimodal neuron C possesses the activity $C = A \times B$. Following this, these neurons encode stimulus location simultaneously in more than one reference frame using basis function or 'gain fields' Pouget and Snyder [1997, 2000]. For instance, there is a non-linear dependency on eye position for certain visual neurons in posterior parietal neurons (PPNs) whose reference frame is centered on the head, whilst others are found to be influenced more by the coding of somatic information into hand/arm-centered reference frame. The same is found for audio-visual signals integration Deneve and Pouget [2004]; Pitti et al. [2012].

Gain modulation contributes therefore as a major computational mechanism for coordinates transformation and for the compensating of distortions caused by movements Salinas and Sejnowski [2001]. Its role is even broader as PPNs are found also important for reaching targets, goal-directed movements Chang et al. [2009] and even for intentional acts Cui and Andersen [2009]. Pouget and Deneve suggest that the parietal neurons behave as a population of basis functions that are continuously adapting their dynamics to the current coordinate frame relative to the task Pouget and Snyder [1997]; Deneve et al. [2002].

Kakei's and colleagues Kakei et al. [2003] proposed a three stages architecture to explain the extrinsic-to-intrinsic transformation necessary for hand reaching using visual directional cells. It is inspired from the model of directional motor cells discovered by Georgopoulos Georgopoulos et al. [1982]; A.P. et al. [2007]. Its schematic is plotted in Figure 3.13 and can be explained as

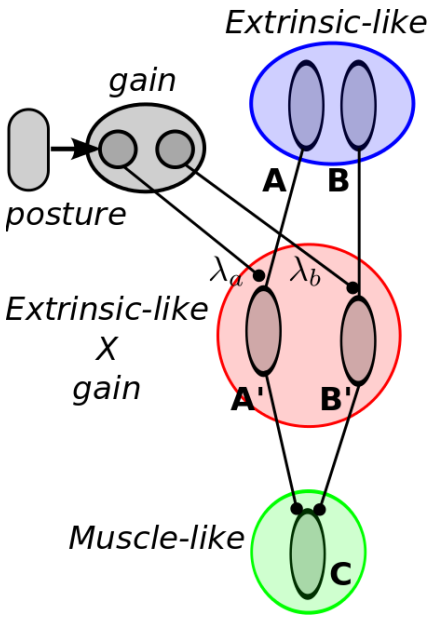

FIGURE 3.13 – A simple model that derives muscles-like shifts in PD C from activity of two types of extrinsic-like neurons A and B, replicated from Kakei et al. [2003]. The neurons A' and B' is the product between gain posture λ_a and λ_b with the extrinsic-like neurons. This model can be used for ebow-shoulder co-ordination, wrist-object relative position and alignment.

follows.

At the first stage, extrinsic-like neurons A and B encode some preferred directions (PD) of the movement orientation toward θ_A and θ_B respectively for the neuron A and B in the form of cosine-like functions : $A = \cos(\theta - \theta_A)$, $B = \cos(\theta - \theta_B)$.

At a second stage, the gain levels λ_A and λ_B receive incoming signals from various modalities (e.g., visual, somatopic, proprioceptive or auditory) and modulate the amplitude of the extrinsic neurons proportionally to it, so that we have the gain-modulated extrinsic neurons A' and B' equal to : $A' = \lambda_A \cos(\theta - \theta_A)$, $B' = \lambda_B \cos(\theta - \theta_B)$.

At the third stage, the gain-modulated extrinsic-like eurons A' and B' are combined linearly to produce the generation of muscle-like neurons C and the encoding of the motor angle into $C = A' + B'$.

In this motor scheme, the input activity of the gain-levels λ_A and λ_B are connected to the preferred direction in the visual space toward objects so that the motor responses of these neurons are linked to the goal-directed actions toward these objects. The muscle response C, will be either (1) the shoulder-elbow-hand articular system in the reaching task, (2) the wrist muscle in the close reaching posture of the hand, or (3) the wrist muscle in the close wrist/object relative orientation task Mahe et al. [2015].

Shoulder-elbow co-ordination – visuomotor directional cells

Our first experiment corresponds to the modeling of the shoulder-elbow co-variation for which Georgopoulos discovered that a majority of cells demonstrated gain changes across posture following a cosine function Georgopoulos et al. [1993]; Ajemian et al. [2001]. Cosine neurons are

defined as the preferred direction of motion of the hand w_{PD} computed from the shoulder and elbow joint angles, resp. φ_1 and φ_2. An M1 cell's directional tuning curve, as derived from the standard center-out task Georgopoulos et al. [1982] relates the average movement-related cell activity to the hand movement direction :

$$\begin{aligned} V &= r_H \cos(w_H - w_{PD}), \\ w_H &= \varphi_1 + \varphi_2, \\ r_H &= RMS(X_O, X_H), \end{aligned} \tag{3.1}$$

where w_H is the current direction of the hand calculated as the sum of the shoulder and elbow angles, r_H the relative euclidean distance of the hand position X_H to the shoulder X_0 so that the the neural activity at the population-level corresponds to a vector that possesses a magnitude in addition to a direction, r_H, which scales the directional component of a cell activity Ajemian et al. [2001]. As explained by Ajemian, the direction of a spatial pd vector represents the direction to which a cell is tuned and the magnitude of a spatial pd vector represents the degree to which the cell is tuned. A cell's gain at any given posture is directly proportional to the magnitude of the spatial pd vector at that posture. The spatial PD and the vector magnitude cell modulation *scales* with the biomechanical advantage of the 'action' controlled by the cell.

For instance, for 20 directional neurons with *PD* equally distributed, we have the following neural activity plotted in Fig. 3.14 when the arm is exploring fully its working space for various elbow configurations, back and forth starting from concentric semi-circles trajectories and finishing by excentric semi-circles trajectories, between the two static points A and B. In Fig. 3.14 at the top chart, we plot the activity level of the neural population on a timeline for which the color code indicates the amplitude of the neurons ; see Fig. 3.14 the subplot in the middle. The 2D plot of the arm trajectory is displayed in Fig. 3.14 on the bottom chart on which we superimposed the color of the most activated neurons, which corresponds to the tuning of each neuron depending on their location.

The circular motion patterns of the arm trajectory in these plots permit to understand better the function of the gain-field neurons. In this plot, each GF neuron encodes a stable pseudo-radial distribution relative to the location on the shoulder reference frame during the arm's motion – i.e, the prefered orientation of the hand, which is stable,– whereas at the two static points A and B, the various GF neurons contribute altogether to encode the different possible orientions to reach them. That is, the sensitivity of each GF neuron to the end-effector orientation during motion reduces the complexity of the control of the hand's trajectory, which corresponds to a stable neural field or a motor synergy (top chart). Instead, the encoding of one specific location requires the correct combination of many GF neurons. Seen at the unit level or at the population level, GF neurons can provide information about position and velocity at the same time Hwang et al. [2003].

For instance, Fig. 3.15 plots the basis function for 4 gain-modulated neurons with respect to the joint angle variables φ_1 and φ_2. The functions are nonlinear and depend on both variables. Moreover, each GF neuron is sensitive to one prefered direction, the φ_2 angle, which corresponds to the elbow joint, whereas φ_1 modulates almost linearly the gain level relative to it. Thus, GF neurons encode an information specific about the neural architecture's embodiment.

Using these motor GF neurons, it is possible then to learn a desired motor command for a reaching task similar to Baraduc et al. [2001]. The desired motor command corresponds to a motor synergy, which is the weight product of a posture with a desired visual activity. After a

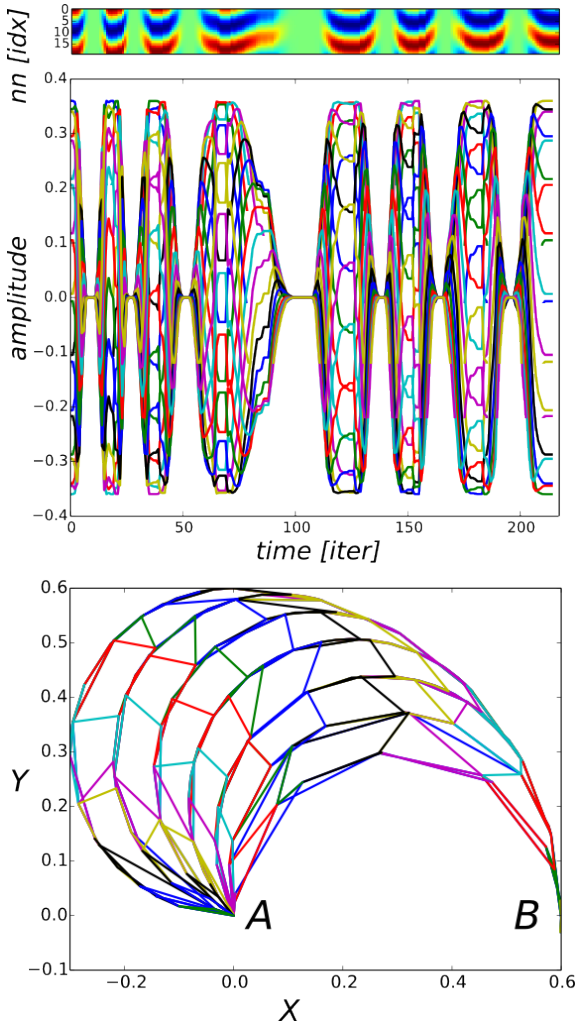

FIGURE 3.14 – Simulation of the gain-field neurons activity during full exploration of a two-link arm. (top) Raster plot of the gain-fields neural population during hand motion and amplitude level (middle). Plot of the arm trajectory on which we super-imposed the location of the most active gain-field neurons (bottom).

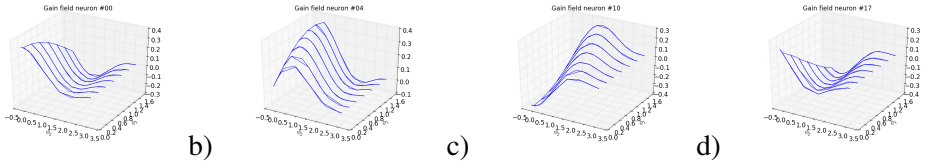

FIGURE 3.15 – Plots of four gain-fields basis functions. The X-Y axis are the shoulder and elbow variables, φ_1 and φ_2 and the Z axis the amplitude level of the neurons. These graphs show the support functions are bi-dimensional although they are more sensistive to one prefered direction with respect the shoulder-elbow co-variation.

learning stage, for a reaching task from the position A to the ending position B, it is possible to

select the desired visual component that will trigger the correct motor primitives using the gain-modulated network, see Figs. 3.16 a-c). The selection of the currently best motor primitive for the planning strategy is seen in Figs. 3.16 b-d) in the bottom chart, which changes with respect to the visual direction and current posture. The quadratic error to the targetted goal is plotted in the upper chart, which shows a linear decreasing when the motor synergy is continuously selected.

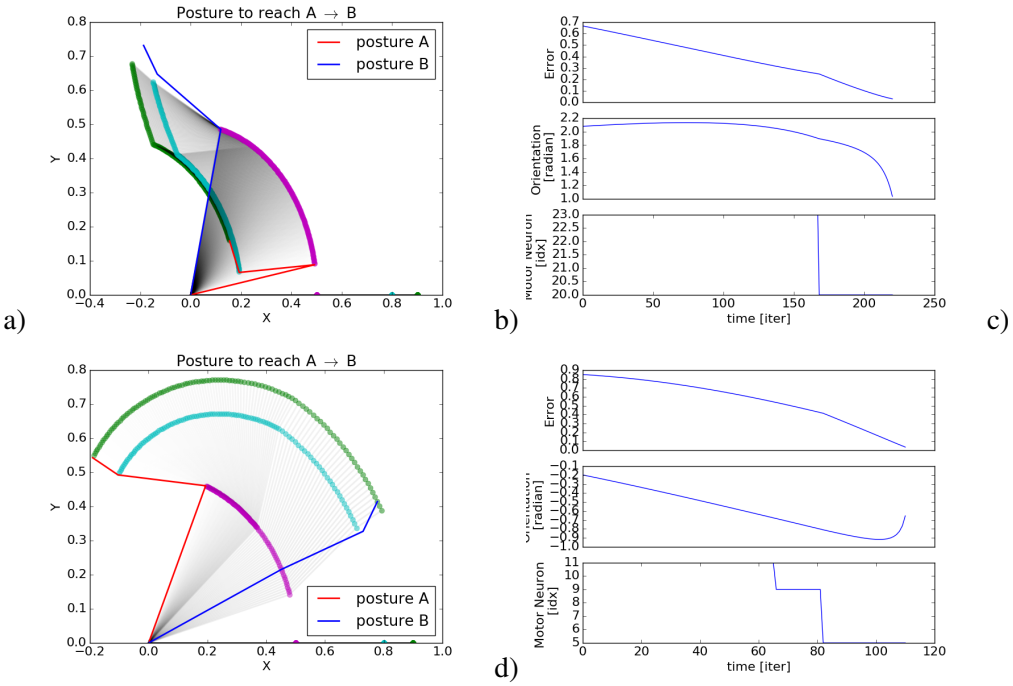

FIGURE 3.16 – Motor control for a reaching task from posture A to posture B using a GF network combining Posture X desired Visual Direction to provide a desired Motor Command.

Hand Orientation based on the Shape of the Object – visuomotor directional cells

Using the visuo-motor framework presented before, it is possible to learn the *alignment* between the robotic hand with the visual features of an object (e.g., its shape, its orientation) using the same neural framework exposed above with multiplicative neurons for different forearm muscle configurations.

Here, the wrist muscle activity is multiplied with the density probability of the four orientations found in the image, which means four Gabor cells aligned to $0°$, $45°$, $90°$ and $135°$. The product activity is then feeded to one LMS regression model that learns to predict the object relative orientation with respect to the wrist angle ; see Fig. 3.13.

To understand better how the gain-field neurons intervene in the control, we display in Fig. 3.17 a) the LMS neural activity for five particular wrist motor angles in abscisse with the LMS activity colored with respect to the global visual orientation of the stick (colormap hsv, resp. $0°$ to $180°$). This graph shows how the LMS neuron amplitude modulates its activity level depending on the wrist orientation (intrinsic coordinates) *and* to the stick orientation (extrinsic coordinates) ; it corresponds to a muscle-like neural activity that makes the transformation

from intrinsic to extrinsic coordinates. The shift in PO of the neuron corresponds to te graded contribution fo the GF neurons.

Fig. 3.17 b) presents the same data of the neural activity but this time the color code (colormap jet) corresponds to different angles of the motor activity and we plot in the abscisse the global orientation of the stick in radian. The oblique graded lines shifted with respect to the visual orientation shows the visuomotor transformation that the output neuron is capable to perform. The graded activity of the neuron is salient for each motor angle to one visual orientation. It indicates a linear relationship between the wrist and the object orientation that the LMS learned.

By extension, we believe that we can learn the inter-dependence between elbow and wrist orientations. Therefore, the forearm has a PO with respect to the wrist posture ; for wrist values under 0.5, we have the prefered orientation of the forearm in its pronation mode (red dots) whereas for wrist values above 0.7, the forearm's prefered orientation is at its suppination posture (blue dots). For a wrist angle around 0.6, in between, the forearm is at its intermediate mode (green dots).

During the test phase, the experimenter removes the stick and moves it in front of the robot vision eye-field by varying the stick orientation from $0°$ to $125°$.

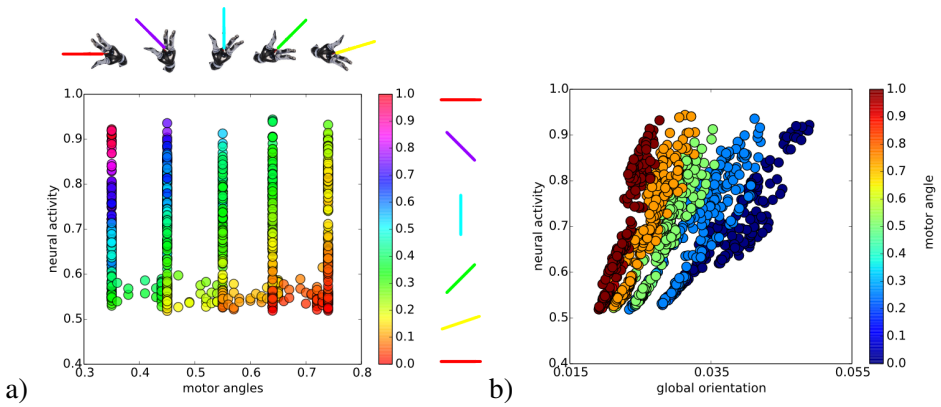

FIGURE 3.17 – Gain-modulation of one visuomotor neuron with respect to Object Visual Direction and Wrist Motor Orientation. After a learning phase, the GF neuron aligns its activity level to the visual direction of the object with the motor angle of the wrist so that for each Orientation of the robotic Wrist, the neuron is selective to one specfic Object Direction.

Hand-centered relative position – visuomotor directional cells

This experiment aims at reproducing Kakei's observation of hand-centered cells sensitive to the relative position of an object with respect to the hand. The activity level of these cells depends both on the hand posture (proprioceptive feedback) and the object location in the eye-field, as presented in Fig. 3.12 a). Again, the underlying mechanism observed in parietal neurons is based on multiplicative activity of GF neurons exposed earlier in Fig. 3.13.

First, the extrinsic input is the object position O, resp. (X_O, Y_O), in eye-centered coordinate, which uses the color detection in the image. The location of the object on the image is translated into log-polar coordinates with a particular angle φ_O projected into four receptive fields as in eq. **??**, which are four extrinsic-like Gabor neurons $\{A, B, C, D\}$ respectively $0°$, $45°$, $90°$,

$135°$ sensitive to four different orientations $\varphi_* = \{\varphi_A, \varphi_B, \varphi_C, \varphi_D\} : \cos(\varphi_O - \varphi_*)$.

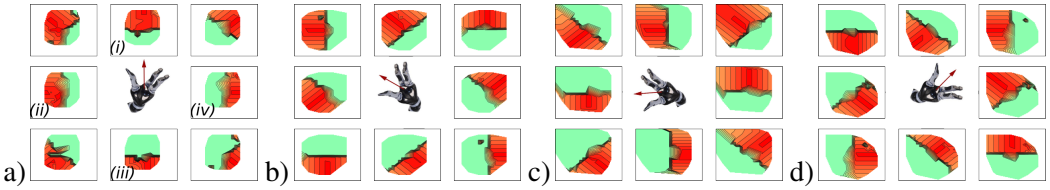

FIGURE 3.18 – Gain-field neurons' activity (eight neurons) in their respective receptive fields for different Hand-Object alignments when the robot wrist has the angles $0°$, $45°$, $90°$, $135°$ in the eight directions around the hand, resp. a-d). The experiment reproduces the results of Scherberger and colleagues on gain-field neurons that are sensitive to wrist posture and object orientation. Depending on the object orientation and the pronation or suppination of the robot wrist, the neurons dynamically update their alignment.

Second, the intrinsic input is the postural command of the hand, resp. (M_{hand}), which moves the forearm on its axis of rotation with the motor angle θ_*, replacing the antagonist and protagonist muscles. The gain-field neurons multiply these two variables to encode a PD modulated by the motor activity.

Finally, these GF neurons are used to interpolate a hand-centered representation : eight output cells encode the relative position vector $(X_{OH}, Y_{OH}) = (X_O - X_H, Y_O - Y_H)$ in hand-centered coordinates. These cells compute the linear combination of the GF neurons weighted by coefficients ω to be learned :

$$O_{k\in[0,\ldots,7]} = \sum_{i=0} \omega_{ij}[cos(\varphi - \varphi_*) * cos(\theta - \theta_*)], \tag{3.2}$$

which corresponds to a coordinate transform. For optimal ω, each output neuron can represent a particular location relative to the hand. They represent the extrinsic-like neurons from Kakei's model, see Fig. 3.13.

Their synaptic weights have been learned during a babbling period in a supervised manner in which we move the robot wrist in front of the eye-field with the object in the hand (centered-location), and on the eight locations described above. We plot the result of the learning process with the neural activity of these eight output neurons in Fig. 3.18 a-d), when an object is moved around the hand for different orientation of the hand : respectively when the hand is at its central posture, in pronation on the left-side, in suppination on the right-side or at its maximum rotation angle on the left-side. The red color corresponds to a high activity of the neurons and the green color corresponds to a low activity of the neurons. The X-Y axis represent the position of the object in front of the eye-field.

For example, in the situation of Fig. 3.18 a), the output neuron located at the top corresponds to the case where the object is presented in front of the hand. In this situation, the neuron will be the more active. However, when the hand moves, say by $45°$ on the left as in Fig. 3.18 b), the neural activity will shift to another perceived receptive field with neurons on the left-side of the arm, which is the most active for this particular configuration.

When the wrist is rotated again by $45°$ to the left as in Fig. 3.18 c), we observe one more time the shifting patterns of the cell's activity : the cell in the top center of the figure triggers the most for a position of the object in the upper-left visual field. Thus, the cell still has its maximum activity for a position of the object that is located in front of the hand whereas the other cells

show an adjusted activity in the same way. During a grasping task, we will privilege the GF neuron *(i)* plotted in Fig. 3.18 a) for motor control in order to have centered objects in front of the hand. See for a relative spatial representation the plots in Fig. 3.19.

The synaptic weights have learned a trigonometric function so that the wrist orientation modulated by the object position produces a rotation-like transformation independent to the hand orientation. As in the previous experiment, the output cells are only perceptual and serve to maintain a stable internal representation of the body relative to dynamical changes in its environment Wolpert et al. [1998]. It is possible then to add an inverse kinematic model to it for moving the hand in the desired orientation Wolpert and Kawato [1998].

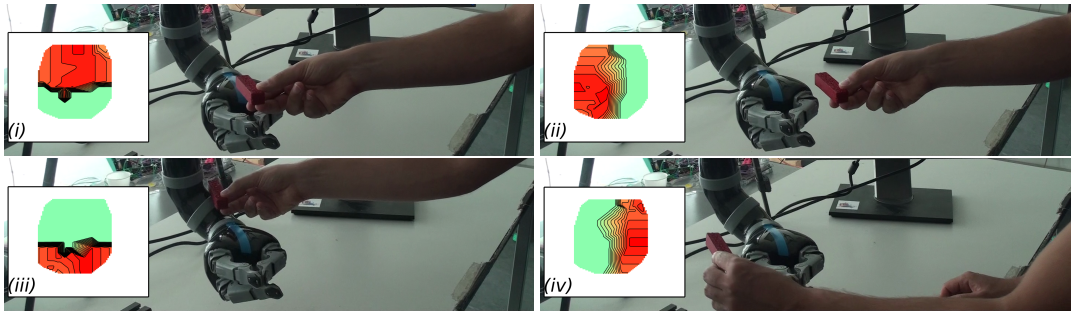

FIGURE 3.19 – Output cells encode a relative position centered on the hand (reach cells). This behaviour is learned from multiplicative neurons combining the wrist motion (intrinsic activity) with the direction of motion in the eye-field (extrinsic activity) and replicate the reach cells circuit proposed by Kakei Kakei et al. [2001].

Audio-Visual Integration for Head-Centered Representation

In this section, we study the eye-to-head spatial transformation based on audio-visual integration using gain-field neurons. For this purpose, we use a robot-head with a unique eye and two bionic ears to model visual, audio and proprioceptive integration for objects spatial localization and coordinate transformation. This work pursues several models of the parieto-motor system on which we studied the contributions of motor and spatial development to social cognition Pitti et al. [2009c].

In this previous research, we emphasized the role of contingency with the use of spiking neural networks for the detection and learning of synchrony based on the mechanism of spike timing-dependent plasticity, either in robotic experiments or in computer simulations. Here we focus more on the mechanism for spatial transformation across different modalities.

Our robot head locates visual and audio stimuli relative to their respective reference frame, even during motion. The objective is to replicate the gain-field effect of parietal neurons for different spatial locations from audio, visual and proprioceptive pairings. Using a re-entrant mechanism, the processed information is then fed back to the unisensory maps. It follows that the assembled audio-visual signal can then estimate back the position of a stimulus in each modality. We can observe then phenomena such as multimodal enhancement of spatial perception, which can serve for audio-visual speech perception ; i.e., correlations between dynamical face and acoustic cues.

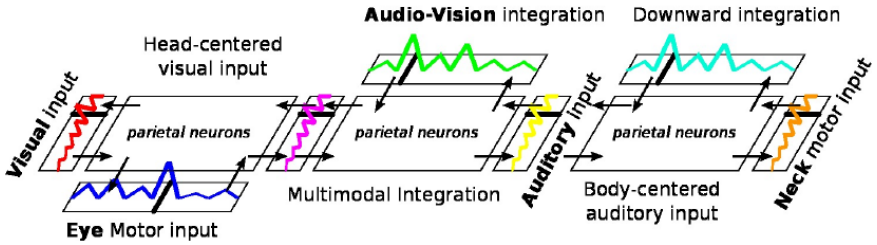

FIGURE 3.20 – Overall framework based on the gain-field modulation of parietal neurons for coordinate transform and multimodal integration ; adapted from Pouget et al. **?**. Parietal neurons translate and coordinate the stimuli information from the visual, the auditory and the proprioceptive signals in eye-, head-, body-reference frame, by varying their gain levels.

Modeling Gain-Field Modulation

Gain-field neurons receive the activity-dependent information from two neural population by multiplying unit by unit their value to each other, see Fig.3.21 (blue lines). The multiplication between afferent sensory signals from the two population codes, N1 and N2 , generates the signal activity η to the n gain-field neurons, n $\in$ N1 x N2 : $\eta = v_{n1} \times v_{n2}$.

As expressed in the previous sections, the key information here is the specific amplitude modulation between the two neurons. Note that this is a little more subtle than Hebb's law or spiking-or-not activity where neurons are selected only when they have both a high value above a certain threshold. Then, downward efferent neurons can learn the neural activity from the gain-field neurons. By doing so, they realize the encoding of a bimodal information based on the two unisensory signals. The computed mutual information is used next to re-estimate the unisensory

signals through a reentry processing stage ; see Fig.3.21 (red lines). The reentry mechanism is as follows. The triggered pre- synaptic gain-field neurons reinforce their links with the post-synaptic downward neurons ; their activity is updated in consequence to have $\eta = v_{n1} \times v_{n2} + v_n$. This reentry mechanism is similar to the one proposed by Roelfsema and van Ooyen [2005] for mutimodal integration, which can serve then for coordinates transform from one reference frame to another ; e.g., auditory or tactile information in eye- or head-centered reference frame.

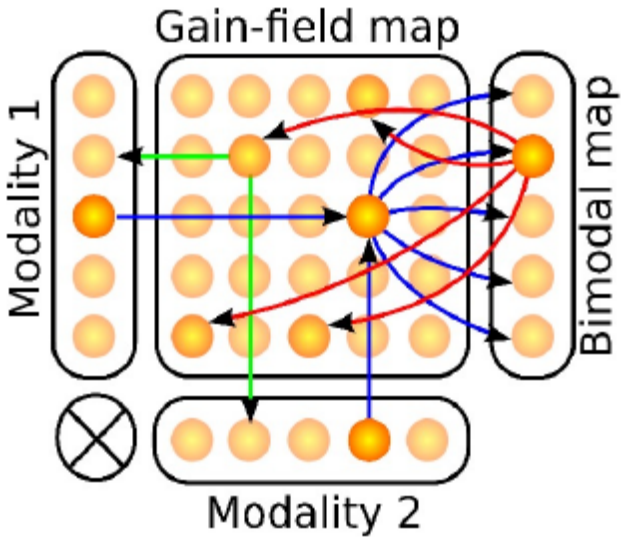

FIGURE 3.21 – Reentrant mechanism. The unimodal neurons fed univocal sensory signals to the gain-field neurons and to the downward neurons, and receive back the multimodal response.

Hardware and Experimental Setup

Our head-robot consists of a box-shaped device mounted on a servo-motor, the neck turns on the sagittal plane and a camera, which is fixed on its eye axis, rolls on the horizontal plane. We plug on the device two bionic ears on which microphones are attached on the eardrums, see Fig.. Although the whole system has only two degrees of freedom, the sensory-motor information flow that it can generate (with

visual and auditory signals) is already complex enough for modeling difficult coordinate transform problems. The bionic ears have been designed with a 3D-printer based on a 3D model of a human-ear in order to replicate its bio-mechanical characteristics. The microphones can receive an audio signal in the range $[200Hz; 30kHz]$. Moreover, the box-like shape of the head has also a function, it creates a sound shadow that eases the discriminating between the left and the right ear. The auditory channel conveys a bank-filter of 40 frequencies selected in the interval $[300Hz; 20kHz]$ following a logarithmic scale to respect the auditory discrimination. Considering the visual inputs, we chose an analogic cam- era to transmit the video signal with a pixels' resolution reduced to $[40 \times 30]$. The motors are moving within the interval $[60; +60]$, and their resolution is discretized to correspond to a 20 bins vector so that each index is associated to one motor angle with a linear scale. Finally, learning is done online in an unsupervised manner with no offline training data.

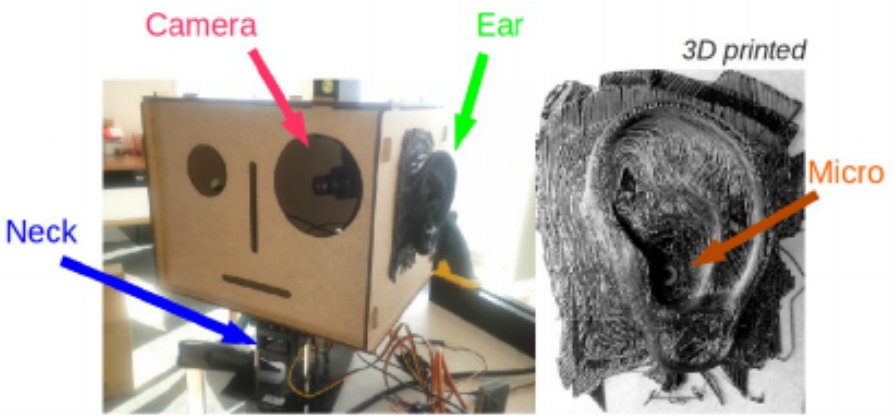

FIGURE 3.22 – Our head-robot consists of a head-neck-eye device with ears. The head rotates on its neck and the eye on its axis (left). The 3D-printed bionic ears replicate the shape of human's ears for mimicking human-like spatial localization of audio sources and a similar bandwith filtering of sound's envelope (right).

Experiments – Saccadic Eye-Movement

Our first experiment consists of modeling the visuomotor features of parietal neurons to encode retinal coordinates into a head-centered reference frame using the eye motor signal.

In this setup, we take into account the eye motion only with the visual information, which means that we purposefully ommit the neck and the auditory inputs. The neural population dedicated to the motor-eye signal has respectively 20 neurons (e.g., modality 1 in Fig.3.21) and the neural population dedicated to the retina signal has 50 neurons (e.g., modality 2 in Fig.3.21) receiving the pixels' activity from the camera. The parietal neurons count therefore 20$\times$ 50 = 1000 units (see the gain-field map in Fig.3.21). We add an efferent downward network of 150 units that learns the visuo-motor associations from the afferent parietal neurons activity. Furthermore, each map is initialized with random connections so that all the neurons are at the beginning unspecific to any stimuli.

During the learning stage, at each iteration, the winner neuron of each map (the most salient neuron) sees its synap- tic weights updated to shape the receptive field salient to the current entry code. Over time, the neural nets self-organize themselves to map the retina and the eye motor signals. Figure 3.23 shows the activity of an eye-motor neuron during motion. The neuron's activity describes its selectivity to a specific eye angle, and the firing events occur when the motor response reach a posture close to the neuron's receptive field. At the population level, the neurons responsive to similar visuo-motor signals produce identified activity patterns in the three maps while the cross-product of the visual and motor neural patterns feeds the posterior head-centered neurons, see the snapshots activity in Figures 3.24. The gain-field effect is observed in Figure 3.25 for one downward neuron only.

The visual receptive fields #69 encodes one retina coordinate in head-centered reference frame so that its position in space is independent of where the eye is fixating (the color index is assigned to one particular motor angle). The neuron is tuned to position pixel 190 and motor angle 20 . Its amplitude combines therefore two information at once ; a code response similar

to ventral intraparietal (VIP) neurons. The linear combination of the downward neurons can be used for tracking behaviours (e.g., for correcting the distance to the eye center) or for translation purpose with other modalities.

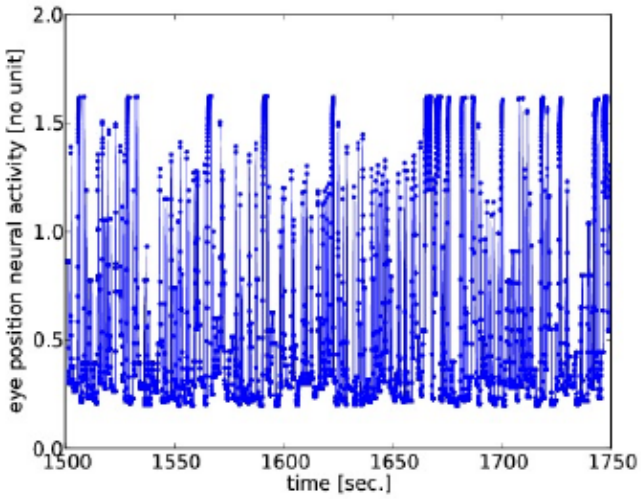

FIGURE 3.23 – Neural activity of one eye motor neuron for 250 seconds. Over time, each neuron learns to be selective to one specific motor angle, whose sensitivity is translated as a gain-modulated activity.

Auditory Mapping in Head and Body Reference Frames

Although sound information is naturally mapped into a head coordinate system, a consistent proportion of auditory neurons in the parietal cortex exhibits eye-centered and body- centered remapping. That is, the magnitude of the responses for these neurons is modulated respectively by the eye position and the neck movement. For instance, some observations showed that an intended eye movement influences the mapping of the auditory space, and reversely, a perceived sound can influence where to foveate. It is suggested that these behaviours exploit transformation mechanisms such as the one modeled in the previous part.

The neural population of the auditory map receives the vector signal of 2×40 frequencies. Then, the sound shadow produced by the head permits the rapid self-organizing of the auditory neurons to two distinct receptive fields that discriminate accurately the left and right sides relative to the head horizontal plan, their appropriate reference frame ; see the neural activity in Fig. 3.26 a). The remapping of the auditory signals into a body-centered coordinate system is computed as for the retina/eye-motor transformation in the previous section : here, the auditory signals and the neck-motor signals modulate a gain-field map that computes the spatial estimation of the sound localization, and this estimation is irrespective to the head motion, see the gain-field effect for one downward neuron in Fig. 3.26 b). As we can observe, the neuron's gain level correlates almost linearly with the sound location. The result is that the referential for sounds is now changed into body-centered coordinates. The neuron is now tuned to a fixed position 40 on the left side of the head. Moreover, in comparison to the head-centered profiles in Fig. 3.26 a), the neural fields in body-centered coordinates are now enhanced with sharper sound profiles.

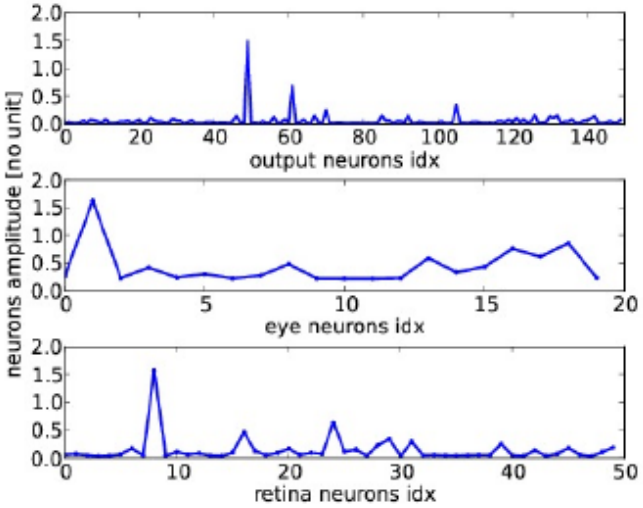

FIGURE 3.24 – Snapshot of the vision, eye-motor neural fields and the visuo- motor parietal neurons. A specific parietal neuron (top) is selective to one particular visuo-motor neural pair. Here, the most salient downward parietal neuron (top) is tuned to a motor angle and retina position, resp. the most active motor (middle) and vision neurons (bottom).

Audio-Visual Speech Perception

Using the reentry mechanism, mutimodal information can leverage the perceptual processing of unimodal maps in their respective frame of reference to infer spatial location of noisy signals. In our framework, audio-visual information in head-centered reference frame can be transferred back into retinal coordinates within the proper eye-centered reference

frame for the visual input, in retinal coordinates. We plot in Figure 3.27 a) and b) the perceptual processing for audio-visual temporal coherence in retinal coordinates, for facial gestures and acoustic cues. The tuning across the modalities can serve then for locating salient onset and offset signals such as for speech processing in different sensory modalities. In comparison to visuomotor only receptive fields in Fig. 3.25, and audio only neural fields in Fig. 3.26, audio- visual mapping takes a position in-between, mixing both information : the center and the variance of the tuning curves.

In a), multimodal information is exploited to estimate the position of the unitary visual stimulus. Here, we super- impose the audiovisual receptive fields in the same abscisse coordinates of the image with a color set 'jet', from the most salient one in red to lowest in blue. The black line indicates the visual stimulus. We observe that the reddest neural fields, whose bubbles are centered on retinal location X = 10 in a), are well aligned with the person's face location. In b), during the person's vocalization in a different location relative to the robot's head, the later receives audiovisual stimuli, which are combined to produce a spatial decision. In this situation, the probability distribution of the neural fields are grossly centered on the person.The perceptual system combines each modality in a common shared space to estimate the speech information. By doing so, it shifts the attentional focus to multimodal stimuli, which are understood to be part of the same entity.

We perform statistical analysis from ten minutes data ; 10.000 samples. The visual and audio-

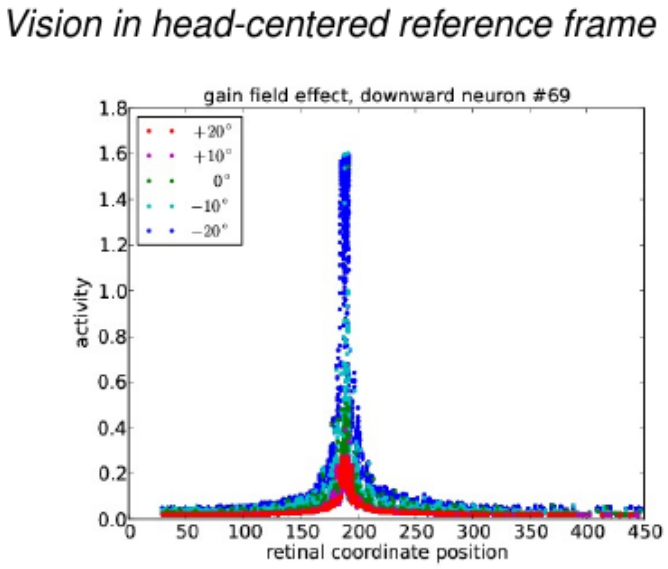

FIGURE 3.25 – Gain-field effect relative to visual stimuli localization on the retina for downward neurons #69 (a) and #127 (b). The downward neurons are tuned to certain retinal coordinates, their amplitude is modulated by the motor angles.

visual receptive fields overlap for mostly 80% of the time when a visual stimulus is seen in front of the eye field. Thus, we can strictly measure the performance of the system only when the two neural maps differ their estimations. When there is a conflict between the two maps to locate audio-visual stimuli, we observe that audio-visual receptive fields perform two third time better than the visual population, the ratio is 68.75% versus 31.25%. Having audio-visual receptive fields, the performance level of correct location is globally increased by 10% in comparison to the sole retina system with visual receptive fields.

Discussion

Seeing engages all our senses. Perceiving one object in space requires to compute its distance relative to our gaze, to our head, or to our hand from multiple sensory types that are not in the same reference frame. Neurobiological observations locate the superior colliculus and the parietal area as the two brain regions where this unified conception of the world could be built.

Accordingly, it is interesting to note that these two regions exploit both the same neural mechanism of gain-field modu- lation. In gain fields, various kinds of combinations of multimodal sensors are represented. In order to organize a reference frame, it is theoretically necessary to bind all possible singleton from all modalities by a multiplicative function. However, only certain combinations of retina and motor are learned, but they are sufficient enough to map the most pertinent sensorimotor experiences.

The gain-field effect is hypothesized to serve for trans- lating the unisensory signals to whichever reference frame, possibly making each modality aligned to another. Thus, the gain-field modulatory mechanism may give some hints on the organizational principle for optimal sensory arrangement ; e.g., for compensating the relative motion from the body posture to targets. For instance, it may serve for the construction of the peripersonal space as it is found for the VIP

mirror neurons, which integrate many modalities. Although its implication to infant social tasks has not been proposed yet, it may furnish a framework for a coordinate transform mechanism to retranscribe one's body posture to someone else postural configuration, which is a possible link to imitation.

Our robotic experiments are preliminary results and we propose to search for more robust solutions within our framework. Also, we will investigate its impact in more complex robot tasks using this time a robot torso with an arm.

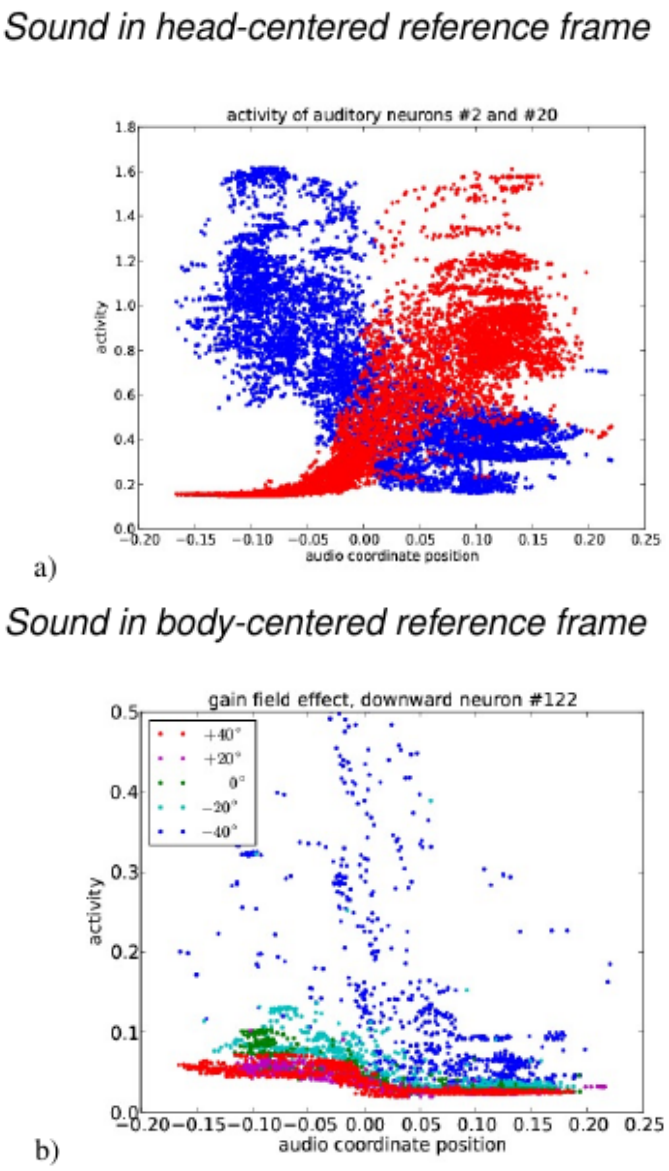

FIGURE 3.26 – Sound localization in head- and body-centered reference frames. In a), sounds are naturally mapped into the head-centered reference frame, neurons easily discriminate left and right sides from sound energy intensity. In b), gain-field effect for a downward neuron relative to the neck-motor signals. The auditory stimuli localization from the left and right ears are modulated by the head amplitude signals.

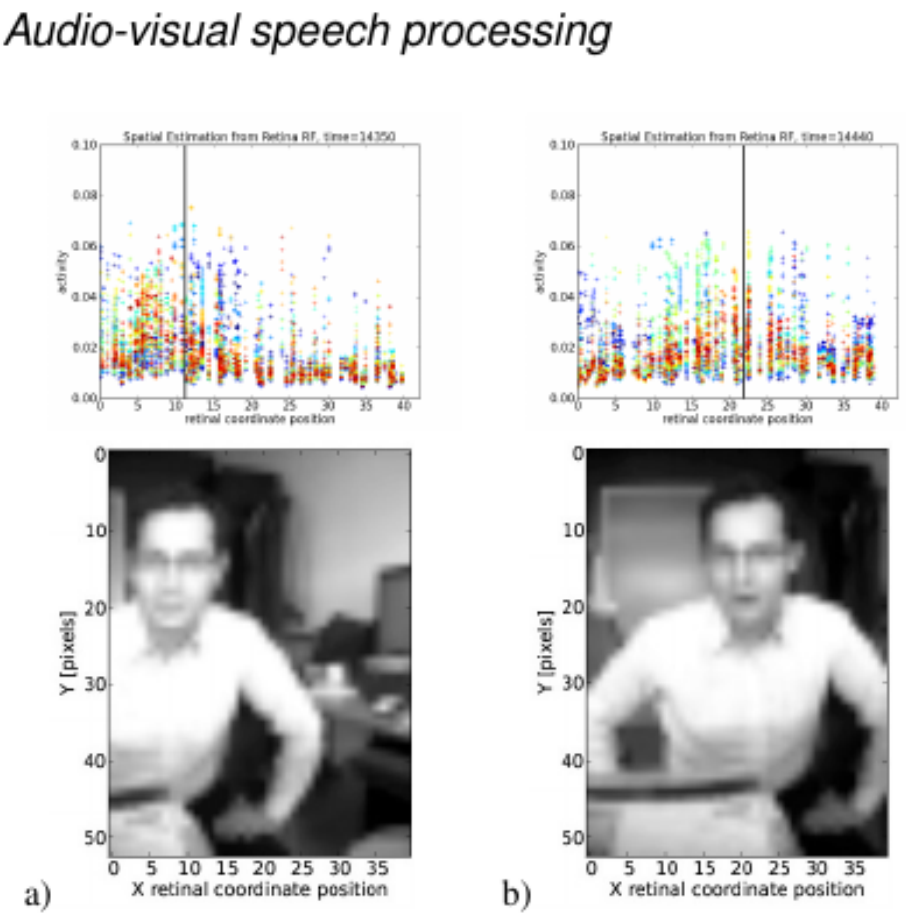

FIGURE 3.27 – Super-imposed audio-visual receptive fields in eye-centered coordi- nates from reentrant signals. The most salient receptive fields are aligned on the top of the camera image ; the reddest dots represent the most active retina neurons. In a), the visual information only provides enough information for locating the face correctly. In b), speech vocalization drives the reestimating of the location of the stimulus in space using audio-visual information.

Tactile-Proprioceptive Integration for Body-Centered Representation

Touch is often neglected when we consider reaching and grasping tasks. However, these actions are goal-directed toward manipulating objects. Although tactile information is acquired at the very end of these tasks, it has an influence on the whole action sequence from the beginning till its end, by *anticipating* the orientation of the hand with respect to the object to be manipulated and touched. The predictive coding done by the somatosensory neurons, combined with other senses (vision, proprioception), may give rise to the emerging capabilities of the so-called mirror neurons, invisible to the eyes like body image Maravita et al. [2003]; Rizzolatti and Craighero [2004]; Caggiano et al. [2009]; Pitti et al. [2013b], anticipatory touch Keysers [2004]; Pitti et al. [2008], action observation Keysers et al. [2014], social cognition Keysers et al. [2010] as well as tool-use Maravita and Iriki [2004] and language Rizzolatti and Arbib [1998].

Touching objects permits to discover the physical limits of the body and to construct its spatial representation with the use of vision and proprioception Pitti et al. [2017]; Braud et al. [2017]. This spatial representation is however non-linear, the same tactile stimulus can correspond to different visuo-motor pairs. However, the tactile stimuli can serve to learn the relative locations of these different visuo-motor pairs with respect to the hand motion as in Fig. 3.11. Over time, the tactile cells can develop extended visual receptive fields with anticipatory effect Graziano et al. [1997]; Graziano and Cooke [2006]; Pitti et al. [2009a], see Fig. 3.28 right graph. These effects have been attributed also to the so-called mirror neurons in the premotor area that integrate multisensory information for action purposes Rizzolatti and Gallese [1997]; Keysers [2004]; Caggiano et al. [2009].

These visuo-tactile receptive fields can be learned from the same gain-modulation mechanism introduced in the previous sections. The output motor neuron C, which combines visuo-motor information for hand position/orientation, is here replaced by the tactile neuron T anchored in one location on the skin and relative to the arm posture. An example of the body schema-like representation done by visuomotor neurons anchored to the tactile map of a robotic arm following the GF network described above is shown in Fig. 3.29.

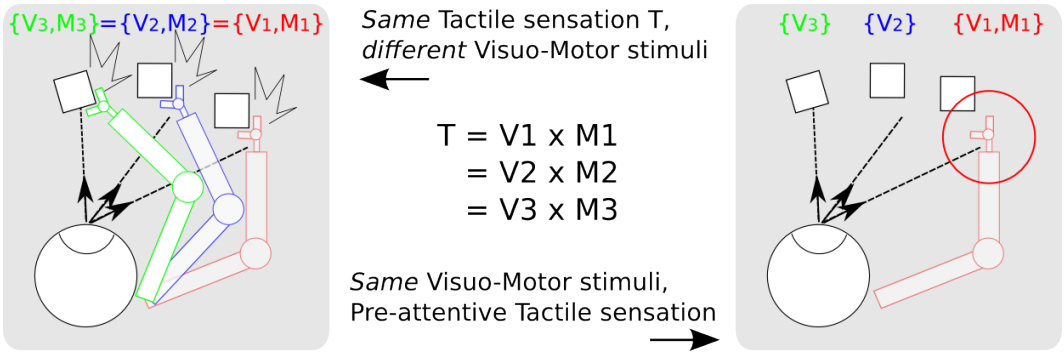

FIGURE 3.28 – Tactile information is important for calibrating and anticipating spatial locations for reaching and grasping tasks. On the left, one task that reach cells have to resolve is to link the same tactile cell with different visuo-motor pairs. On the right, when spatial locations have been learned by reach cells with the mechanisms of multimodal integration explained above, they can serve for anticipating visually one touch ; acquisition of body image.

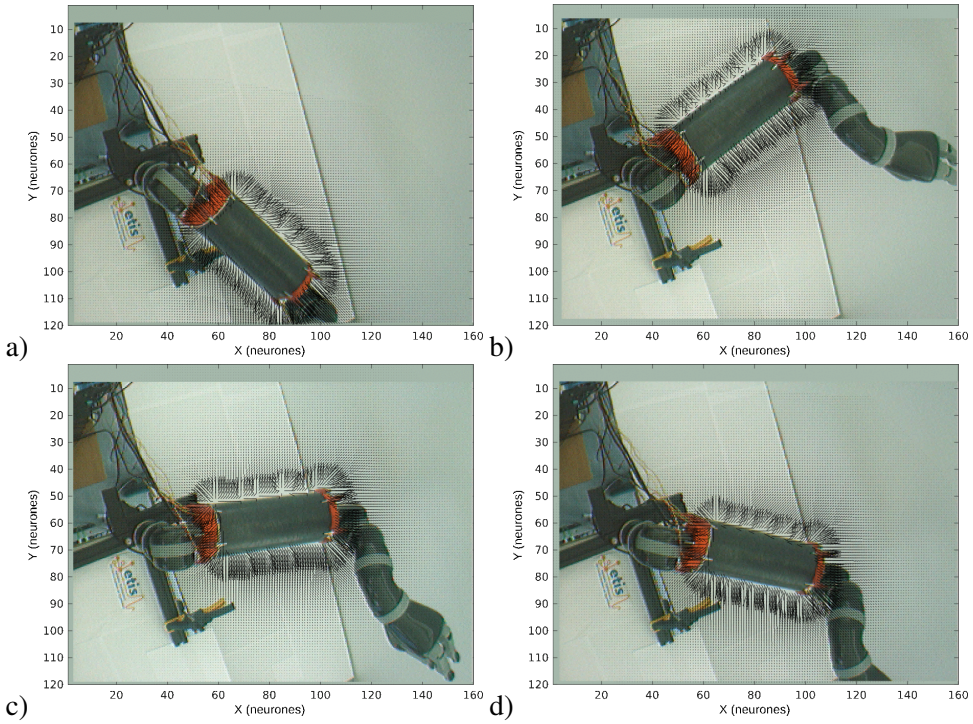

FIGURE 3.29 – visuotactile neurons anchored in arm-centered reference frame toward body schema.

CHAPITRE 4

Contributions to Neural Architectures for Cognitive Development and Working Memory

After my PhD, I started working on computational theories based on the theory of dynamical systems on the normal or abnormal cognitive development in children, cognitive architectures on learning and brain development. This work led me to study the role of acetylcholine in the neuro-modulator in the development of memory and its influence in the functional structure of the hippocampus and cortex enthorinal, the pre-natal stage to stage post native. I have started then to design other neural models that behave like working memories to learn internal models and to plan action sequences based on reinforcement learning. One of the goals that I pursue with these models is to understand better normal and abnormal developmental mechanisms for the scientific community and to design for robotics new neuromorphic architectures that mimick the plasticity of human cognition.

Infant cognition starts before birth with the developing of the neocortex and of its subcortical areas. The neonate behaviors are mostly reactive at this period and it is only at the end of the first year that working memories are mostly blown for more adaptive behaviors. The prefrontal cortex along with the parietal cortex is one of these working memories. The hippocampal prefrontal coupled structure also as well as the cortico-basal coupling. Each of these working memories develop at different periods depending on their maturation, the level of neuromodulator receptors, the synaptic plasticity, the number of neurons.

WMs are involved in manipulating old and new information for memory consolidation or novelty detection, problem solving under uncertainties, and the generation of neural chains for actions or for processes.

In this line, the development of the hippocampus is interesting because it is a structure that is rapid to develop but long to mature due to changes in proportion of chemical receptors, like the neuromodulator acetylcholine (ACh), changing its functional properties during the first year from a responsive associative memory to a working memory, salient to novelty, and growing in complexity. Following observations done in the neonates rat on the developping of learning capabilities, we propose that the dynamical change in distribution of two species of chemical receptors of acetylcholine necessary for reinforcement learning on the one hand and for detecting

novelty on the other hand changes the functional structure of the hippocampus very early in life. As emerging behavior, our hipppocampal model attempts to learn new things while not to forget old ones, which induce some complex patterns of organization, synchronous activity, with a increase of the complexity of the model. The hippocampal memory is hypothesized to serve for cnsolidated the new memory and is therefore associated to novelty or curiosity-driven behaviors as it is found that HP is very active during new episodes. At reverse, its dysfunctioning may underly the shift found in certain developmental trajectories for loss of memory consolidation in abnormal developments. We will explain its neural modeling in sec. 4.1 based on dynamical systems approach and attractor learning.

This coupled mechanism between excitation and inhibition, absorption dissipation,precision-generalization, is a hallmark of self-organized systems in evolution and development d'Arcy [1917]; Nicolis and Prigogine [1977]. It characterizes some general principles of WMs with links to complex networks Strogatz [2003], dissipative systems, as well as chaos and attractors Tsuda [2015], or the free-energy principle Friston et al. [2009].

This last decade has seen the development of new neural networks, such as Echo-State Networks, Dynamic Neural Fields, Deep Networks, Long-Short Terms Memories, Neural Turing Machines Graves [2016] or Coupled Adversial Networks. These breakthroughs have achieved to surpass conventional neural networks in supervised learning and are capable to deal with a huge amount of data to refine their learning.

Nonetheless, most of these models still lack the capabilities of working memories to deal with uncertainties, to be attentional, to learn multiple tasks set or to produce long temporal signals. Differently said, they are still missing the capability of open systems to self-organize themselves in an open manner, to be self-directed, curiosity-driven.

Although the design principles for creating neural machines capable of *learning-to-learn* are not fully understood, specific concepts and techniques have been characterized such as artificial curiosity Kaplan and Oudeyer [2007], goal-directed behaviors Chersi et al. [2013], reinforcement learning Barto and Sutton [1997], active inference or predictive coding Pezzulo et al. [2014]; Pezzulo and Cisek [2016]. These concepts presented in section 4.2 put forward the idea that instead of learning model categories of the sensory inputs from raw data, the brain learns to predict the probability distribution of those that he can generate. The brain is seen here as an inference machine that can compare predicted signals with the real ones that in turn elicit or favorish one category among others as seen in the activity level of the neurons. Instead of learning solely the sensory patterns, the active motor neurons learn the underlying causes that diminish the error prediction of these data. Relative error is then a salient information tramsitted to the higher level brain structures to be processed.

This viewpoint can be seen as a brain theory of embodied causation based on Bayesian theory because the causes are infering to which class the samples of the sensory distribution are belonging with. This Bayesian hypothesis of the brain has become highly popular this decade by reknown scientists like Schultz et al. [1997]; Schultz [2000]; Friston [2009] with neural models of Bolztman machines, auto-encoders, free-energy based neural processes. Predictive coding is also a theory of enaction popularized by authors in cognitive science like Clark [2015]; Pezzulo and Cisek [2016] in which affordances – the capability to select one action based on sensory information– and active inference – estimating sensory input from one motor activity (throbbing the finger on a texture, eye-saccades or the processing of the visual receptor fields)– are a byproduct of it. We develop this idea in section 4.3 in which we present a working memory

for recurrent neural networks based on the free-energy principle and predictive coding. Furthermore, cognitive development appears to be marked also by Bayesian processes early in life as it is supported by Gopnik et al. [2000, 2004]; Meltzoff [2007a]; Tenenbaum et al. [2011] who showed how infants develop very rapidly statistical abilities to infer qualitative and structured information from sensorimotor information. We present our attempts to deal with such behaviors with the modeling of different cognitive architectures.

Hippocampal Model for Incremental Learning

Among the principal neuromodulators, acetylcholine (ACh) plays a particular role on the human developing brain and thus, on the acquisition of cognitive capabilities. During early postnatal development, ACh regulates critical aspects of maturation and plasticity of the neocortex, hippocampus and cerebellum for memory and learning Lauder and Schambra [1999]; Descarries et al. [2004]; Hasselmo [2006].

For instance, prenatal choline suppletion, which is a precursor of acetylcholine, causes long-lasting improvements in spatial memory whereas choline deficiency is associated with poor performance in certain cognitive tasks Matsukawa et al. [1997]; Meck et al. [1989]. Although the mechanism by which choline influences learning and memory remains unclear, converging evidences attribute a developmental role to ACh and suggest that it may involve changes to the hippocampal cholinergic system. In this section, we propose that ACh operates as a kind of "order parameter" for memory development that reorganizes functionally the cortico-hippocampal system into a working memory.

The cholinergic system is composed of two chemical families with different genes expressions that have high affinity either with nicotine or muscarine via nicotinic acetylcholine receptors (nAChRs) and muscarinic acetylcholine receptors (mAChRs). Current researches in pharmacology focus their attention especially on nAChRs because of its high sensitivity with nicotine which can exert neurotoxic effects on development Dwyer et al. [2009]. Prenatal and early postnatal exposures to tobacco smoke can result in altered morphological features in the developing hippocampus and cortex that can impact long-term cognitive deficits Court et al. [1993]. This is particularly detrimental because acetylcholine modulates brain development during critical periods when brain maturation is most sensitive to perturbation.

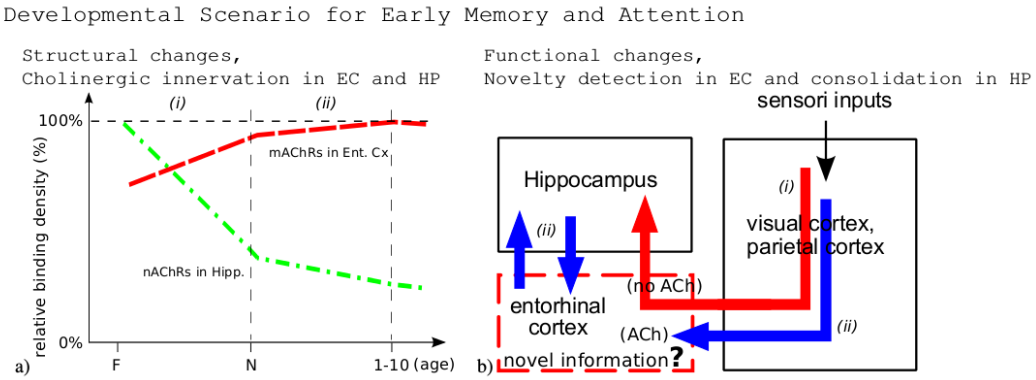

FIGURE 4.1 – Structural and functional changes in the hippocampal system and its contribution for early memory development and attention. The graph a) retranscribes the cholinergic changes in the entorhinal cortex and in the hippocampus (CA3 and CA1), adapted from Court and al. [1997]. Figure b) presents our hypothesis on the functional activation of the hippocampal structure after maturation of the cholinergic system during the first year, period (ii).

Innervation of nicotinic receptors nAChRs in the cerebral cortex and hippocampus is very early and rapid as it falls within the first six months of life Hasselmo and Stern [2006]; Court and al. [1997]; Dwyer et al. [2009]. Their roles however are found important as they regulate synaptic transmission and plasticity Gold [2003]. Besides, abnormalities in nicotinic acetylcholine

receptors may relate to disruptions in cerebral circuitry development while their genetic dysfunctions have been implicated as a major feature in the neurochemical pathology of autism Dwyer et al. [2009]. In contrast, the binding of muscarinic acetylcholine receptors mAChRs tends to rise significantly after birth till the first year and particularly in the entorhinal cortex – which is the gating pathway to hippocampus– to reach 80% density corresponding to the childhood period Hasselmo and Stern [2006]; Court and al. [1997]. Their roles differ from nAChRs but are equally important since mAChRs regulate the maturing entorhinal system to detect and to support the encoding of novel signals into the hippocampus Doya [2002]. Taken together, these findings suggest that the understanding of the innervation timeline of the cholinergic system into the various brain regions, more marked in the hippocampal system, can provide us a better comprehension of the developmental changes occurring during the first year.

From a cognitive viewpoint, the cholinergic system is known to regulate the balance between memory storage and renewal depending on its concentration level and the brain regions where it is released. In the cerebral cortex, ACh modulates the synaptic plasticity by enhancing long-term potentiation depending on its concentrate rate Hasselmo and McGaughy [2004]. In the hippocampal system, ACh acts as a working memory for novel information Hasselmo [2006]; Doya [2002] ; high concentration level of ACh sets the circuit dynamics for attention and encoding of new memory whereas low level of ACh regulates the consolidation of older memories Knight [1996]. More precisely, mAChRs are involved in the persistent firing of individual entorhinal neurons for the maintenance of novel information Klink and Alonso [1997]; Kumaran and Maguire [2009]; Adolph and Joh [2009] and nAChRs are involved in synaptic plasticity of the hippocampal cells for learning memory patterns.

Interestingly, the period of cholinergic maturation in the hippocampal system coincides with the period when infants enrich their motor repertoire with novel actions Smith and Samuelson [1997], categorize novel objects into new classes Quinn et al. [2006]; Newcombe and Huttenlocher [2006], shift from an egocentric represention of space to an allocentric one [20] which are all features attributed to hippocampal processing. Furthermore, this chronology agrees with Nelson's proposal and others that the brain systems responsible for adult-like explicit memory, including the hippocampus and surrounding cortex, do not come online until the second half of the first year of life Yu and Dayan [2002] and that infants rely on different types of learning systems during the first year Piaget [1954]; Smith and Samuelson [1997]. One might envision therefore the cholinergic system to activate rapidly the learning capabilities of the hippocampal system (i.e., fast nAChRs binding) while it regulates slowly the filtering capabilities of the entorhinal system for novelty detection (i.e., slow mAChRs binding), see Fig. 4.1. We think that these two parallel processes change the functionality of the hippocampus into an efficient working memory dealing with novelty, which is not at birth.

The section is organized as follows. In the first part we define the networks architecture of the para-hippocampal system and the neuromodulatory mechanism of the cholinergic system that regulates learning and attention. The good balance between these rules controls the overall stability and plasticity of the system to maintain top-down hippocampal signals and to sustain the novel ones coming from the entorhinal system (i.e., novelty detection and support of bottom-up signals). It follows that, without ACh, the cortico-hippocampal system behaves as a classical associative memory that extracts the statistical features from the inputs ; e.g., a probabilistic network based on statistical learning. In contrast, the gradual activation of ACh changes the cortico-hippocampal system into a self-organizing map that rewards the novel signals over

the familiar patterns ; e.g., a hierarchical memory map such as a Bayesian tree. The new system acquires the emerging functionalities of a working memory dealing with novelty by categorizing the novel patterns and by maintaining them active during encoding. Hasselmo suggests that this feature could underlie the intrinsic mechanism for delayed-response tasks for novel stimuli in the para-hippocampal cortices even over 810 sec whereas other brain regions seem to be sufficient for normal delayed matching function with small numbers of highly familiar stimuli Doya [2002].

Neuromodulators and neural circuits models

We describe in this section the models defined for the hippocampus and the entorhinal cortex with their respective networks architecture and regulatory mechanisms.

Stellate Cells of Entorhinal Neurons

In comparison with the most common types of neurons in the neo-cortex, the stellate cells of entorhinal neurons possess some specific internal currents, cholinergic-dependent, which permit them to sustain long-lasting bursting even if inputs fade away Kumaran and Maguire [2009]; Cuevas and Bell [2011]. Moreover, the entorhinal neurons possess very few recurrent connections so that the entorhinal cortex can be modeled as a segregated network of isolated neurons with no synaptic connections between them. According to Hasselmo, it is the muscarinic cholinergic receptors that enable persistent spiking to continue after the sample stimulus Hasselmo [2006]; Doya [2002]. We formalize them with the neuron model proposed by Izhikevich Izhikevich [2003, 2007] which is a resonator cell whose bursting frequency increases depending on the input current I :

$$Cv' = k(v - v_r)(v - v_t) - u + I \tag{4.1}$$

$$u' = ab(v - v_r) - u \tag{4.2}$$

where I is the external input bound in the interval $[0; 2000\mu A]$, v represents the membrane potential of the neuron and u represents a membrane recovery variable (c.f. Diamond [1985]; Munakata [1998]) ; v' and u' their temporal derivate. The voltage threshold level v_t is set to $-45\,mV$ and the resetting voltage level V_r to $-60\,mV$. We set also the constants $C = 2.000$ and $k = 0.75$. The after-spike resetting is done with

$$if\, v \geq +v_{peak},\, then \tag{4.3}$$

$$v \leftarrow c \tag{4.4}$$

$$u \leftarrow u + d \tag{4.5}$$

with $v_{peak} = 30mV$. The variables set $\{a, b, c, d\}$ defines the neurons attributes $(a; b) = (0.01; 15.0)$ and $(c; d) = (-50; 200)$.

Hippocampal Neurons

We define the hippocampal neurons with the model proposed by Colliaux Colliaux et al. [2009] that realizes a up- and down-states where up-states are associated with firings and down-states with silences. Up- and down-states occur at each theta cycle – which is the natural rhythm of the hippocampal neurons betwen 610 Hz– and the up-state firings trigger in advance or in retard to it. The phasic (temporal) information from all the neurons represent then one memory pattern. The model consists of two coupled variables, S and φ, such that an oscillation component $\cos\varphi$ produces the intrinsic oscillation of the membrane potential S for which the phase φ depends on its level of depolarization. In a network of N units, the state of the cell i is defined by $\{S_i, \varphi_i\} \in R \times [0, 2\pi[$, for $(i \in [1, N])$ and evolves according to the dynamics :

$$S'_i = -S_i + \frac{1}{N}\sum_{j=1}^{N} W_{ij} R(S_j) + \gamma(\Phi_i) + I_i \tag{4.6}$$

$$\Phi'_i = \omega + (\beta - \Delta(S_i)) sin\Phi_i \tag{4.7}$$

with w_{ij} , the synaptic weight between cells i and j. $R(S_j)$ is the spike density of the cell j and I_i represents the driving stimulus which enables to selectively activate a cell. In the second equation, ω and β are respectively the frequency and the stabilization coefficient of the internal oscillation. The spike density is defined by a sigmoid function :

$$R(x) = \frac{1}{2}(\tanh(g(x - 0.5)) + 1). \tag{4.8}$$

The coupling between the two equations, γ and Δ appear as follows :

$$\gamma(\Phi_i) = \sigma(\cos\Phi_i - \cos\Phi_0)\Delta(S_i) = \rho S_i \tag{4.9}$$

where ρ and σ modulates the coupling between the internal oscillation and the membrane potential, and φ_0 is the equilibrium phase obtained when all cells are silent ($S_i = 0$) ; i.e., $\varphi_0 = \arcsin(-\omega/\beta)$. We used the following parameters in our experiments : $\omega = 1$, $\beta = 1.2$ and $g = 10$. Accordingly, $\cos\varphi \approx -0.55$. ρ, σ are adjusted respectively to 1 and 0.96, and external voltages I are normalized below 0.1 to not saturate the hippocampal dynamics.

The coupling to the entorhinal system is done as follows. The entorhinal neurons receive the membrane voltage S from their respective hippocampal neurons, which is originally comprised between $[-0.5V; 1.5V]$ and renormalized to $[0\,mA; 2000\,mA]$, such that any up-state oscillation entrains the entorhinal neuron to increase its firing rate. The system behaves as follows. For a hippocampal network of eighty units ($N = 80$) regrouped into ten clusters with initial synaptic weights, the system transits freely from one pattern to another without external inputs, see the raster plot in Fig. 4.2 ; same conditions as in Smith and Samuelson [1997]. The small perturbations pull up one pattern (up-state) and pull down the others (down state) at each theta cycle. Under these conditions, the coupled system has a poor stability-plasticity trade-off as it can recall rapidly its already learnt patterns but cannot maintain easily the new ones.

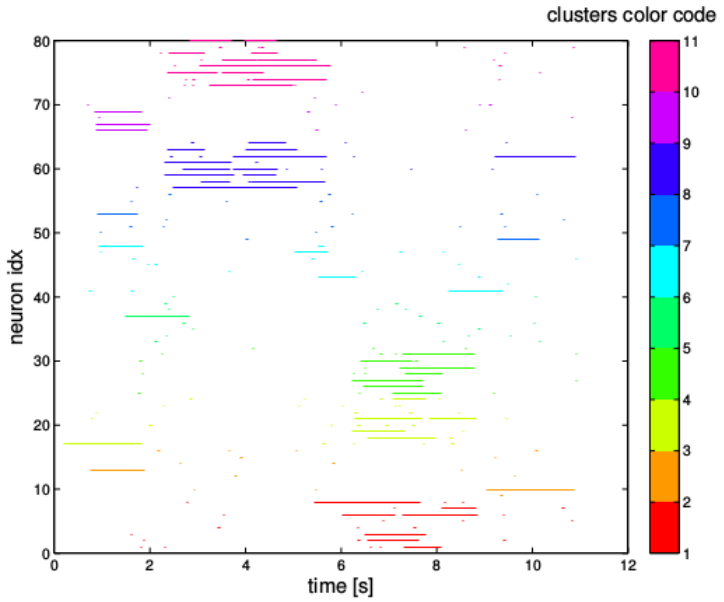

FIGURE 4.2 – Raster plot of the hippocampal dynamics without external drive. The network dynamics stabilize or switch from one cluster to another at each theta cycle.

Hebbian Learning

Memory patterns in the hippocampal system are associated with the respective up-state of the active cells, see Fig. 4.2. The robustness of one particular neural pattern depends then on the strength of the neurons' synaptic weights. The regulation of these weights are done by the classical hebbian rule that strengthens the links of two contingent neurons i and j by a small fraction δw (long-term potentiation) computed by

$$\Delta w \epsilon I_i I_j, \tag{4.10}$$

with learning rate $\epsilon = 10^{-5}$. The weights' updating rule is then :

$$w_{ij}(t+1) = w_{ij}(t) + \Delta w. \tag{4.11}$$

The hippocampal system behaves as a classical associative memory which follows the probability distribution of the imposed external inputs. The exposure to random inputs –e.g., a Poisson distribution of 1 spike per millisecond– will drive slowly the hippocampal weights from their initial configurations to follow the inputs' probability distribution (not plotted here). Hence, without any attentional mechanism to sustain novel information, the network is too weak to learn novel inputs in one-shot exposure but it is robust enough to persevere to familiar dynamics

Cholinergic Neuromodulation

Acetylcholine levels control the balance between memory storage and memory update at both the cellular and circuits levels Doya [2002]. In the hippocampus, nAChRs modulate the synap-

ses' plasticity at the circuit level whereas mAChRs modulate the neurons firing at the cells level in the entorhinal cortex : on the one hand, when a novel input is exposed, high cholinergic levels make the entorhinal cells to generate spikes and favor hippocampal plasticity ; i.e., plasticity to afferent input, on the other hand, when a familiar input is exposed, low cholinergic levels unaffect the entorhinal cells and consolidate the hippocampal network ; i.e., robustness against afferent input. This mechanism could be very important for maintaining responsiveness to sensory input in attentional tasks and for encoding new memories. The concentration level of ACh can be defined then as the relative novelty index of one input pattern I to the embedded hippocampal patterns. The novelty distance can be computed from the hippocampal weights w of dimension N^2 ($w_{i,j} \in [1,..,N] \times [1,...,N]$). For an input I of N elements ($I_{i\in[1,...,N]}$), the novelty index ACh_level is defined as :

$$Ach\_level = 1 - \frac{1}{N(N-1)\sum_i \sum_j I_i.W_{ij}},\ for\, i \neq j. \tag{4.12}$$

with ACh_level comprised between $[0, 1]$ for which a low value corresponds to a familiar pattern and a high value corresponds to a novel one. Its action on the networks is as follows. In the entorhinal network, input currents are sustained for any concentration rates above a specified level $novelty\_threshold$. One simple rule to relate the entorhinal neurons' resonance to ACh_level is : if $ACh\_level > novelty\_threshold$, then sustain input current intensity I.

This condition applies for the first time the input is above the threshold and its value stays fixed during the whole period when $ACh\_level > novelty\_threshold$. In the hippocampal network, the plasticity of the hippocampal weights is adjusted proportionally to ACh_level which functions as a variable learning rate Klink and Alonso [1997]. The updating rule in eq. 4.11 is changed in : $w_{ij}(t+1) = w_{ij}(t)$+ $ACh\_level\ \Delta w$.

To understand better the effect of neuromodulation on the networks, we reconduct a priming task experiment when the networks EC-HP are exposed to a novel input, see Fig. 4.3. The physiological mechanism responsible for the recognition of novelty and stabilization of input pattern in EC has been identified as the ACh dependent's intracellular Alonso current Doya [2002]. We simulate its effect on the HP-EC networks. We recall that HP and EC have eigthy units each with intramap connections for HP (not for EC) and that EC units have unidirectional connections to their respective HP units.

The presentation of a novel input to the entorhinal cortex at $t = 186.25\,s$ (see Fig. 4.3 b) automatically rises ACh_level to a high value (see the blue crosses in Fig.4.3 a). ACh's increasing has for net effect to keep the entorhinal neurons firing for several seconds and to enhance the hippocampal encoding of the novel memory with respect to eq. 4.12, see the black line in Fig. 4.3 a). Therefore, the more novel a pattern is, the higher ACh_level (ascending phase). In return, the hippocampus strengthens more its synaptic links to the novel pattern, which makes it less novel and reduces accordingly $< \delta w >$ and ACh_level (descending phase).

Thus, this process produces a temporal cost that depends on the variables ACh_level, $novelty\_threshold$, δw and I. In other words, it plays the role of a retainer that can be used further for attentional purposes, either for learning one novel memory or assessing one old memory. The cholinergically-enhanced network operates therefore very differently from its normal regime showed in Section II-C.

We think that the neural development of acetylcholine into the hippocampal system is related

to the cognitive development in memory and categorization tasks observed during the postnatal period.

Experiments

Develpomental timeline of cholinergic innervation

In the previous section, we presented how the hippocampal network behaves with and without cholinergic neuromodulation. Here we design the progressive cholinergic innervation into the hippocampal system. Muscarinic binding in the entorhinal cortex –responsible for sustaining novel signals– is slow to mature and reaches its highest level at one year-old period Court and al. [1997]. Besides, nicotinic binding in the hippocampus –responsible for reinforcement learning– is very fast to mature as it drastically falls with age during the fetal and post-natal period Court and al. [1997]; Court et al. [1993]. We model the gradual mAChRs binding in EC with the variable activation ratio that grows continuously within the range $[0, 1]$: $activ.\_ratio = 0$ corresponds to the fetal period when there is no muscarinic binding and $activ.\_ratio = 1$ corresponds roughly to the period when the infant reaches its first year.

To simplify our experimental setup, the growing parameter is set to augment linearly with a step of 10^{-4} per iteration (1 ms), starting at $t = 50\,sec$. The variables ACh_level and $novelty\_threshold$ are weighted to it so that they reach progressively their maximal value when $activation\_ratio = 1$. The initial level of $novelty\_threshold$ is set to 0.85 to filter as much as possible novel signals in the beginning. During the transitory period, we decrease its value to allow more novel signals to pass. This is the unique ad hoc rule that we impose to the system to simulate the functional acceleration observed during cholinergic innervation. The equations set for the cholinergic activation is then :

$$Ach\_level(t+1) = activ\_ratio \times ACh\_level(t) \tag{4.13}$$

$$novelty\_threshold(t+1) = activ\_ratio \times (0.85 - 0.25 activ\_ratio), \tag{4.14}$$

where $activ.\_ratio$ stands for activation ratio. We present in Fig. 4.4 the results of this developmental scenario when the hippocampal system is exposed to random inputs, starting at $t = 50\,sec$, when activ. ratio increases linearly to 1.

Fig. 4.4 a) plots the weights modification $< \delta w >$ averaged over all the weights at each time step, Fig. 4.4 b) plots the evolution of ACh_level during cholinergic activation and Fig. 4.4 c) displays the overall complexity inside the hippocampal network computed from the synaptic weight matrix. The complexity measure $C(w)$ of the system's weight matrix w is defined as the difference between the integration level $I(w)$ considered as a whole and the average integration for small subsets within, following : $C_N(w) = \sum_{k=1}^{n}[(k/n)I(w) - < I(w_j^k) >]$. Low complexity levels reflect a poorly organized network with low memory capacity (a uniform distribution) whereas high levels reflect functional connectivity within the network and higher memory capacity.

The situation before ACh activation when $activ.\_ratio = 0$ ($t < 50\,sec$) corresponds to the case described in Section II-C when the learning system encodes continuously the external inputs and converges to its probabilistic distribution. The weights rapidly stabilize themselves within a minimal fluctuation regime and the system behaves as a classical associative memory.

Parallely, the complexity measure decreases continuously indicating the hippocampal structure always adapt itself to the novel inputs but do not retain them for a long period.

At contrary, the activation of the cholinergic variables when $activ.\_ratio > 0$ at $t = 50\,sec$ reverses the process and generates a phase transition within the neural dynamics. Here, the variable ACh_level starts to oscillate between low and high states with bigger amplitudes as activ. ratio augments : the learning system becomes more and more sensitive to the inputs' novelty and scaffolds its memory capacity by embedding one at a time a novel input. The ascending phases (i.e., the crests) correspond to the encoding periods and the descending phases (i.e., the troughs) correspond to the consolidation periods.

Moreover, the capability to detect and to encode novel inputs creates some new emergent functionalities within the system. For instance, since the new patterns do not overlap with the old memories, the hippocampal system tends to be sparsely organized, which rise in fine its complexity level. In line with Hasselmo's proposal Hasselmo and McGaughy [2004], this mechanism could prevent interference from previously stored patterns during the learning of new patterns. In other words, it enables the hippocampal system to categorize on the fly new memories while preserving the old ones. The result is the emergence of a 'working memory' that scaffolds over time, the memory organization is kept motivated for novelty and reaches a high complexity level.

When the learning system reaches its fullest capacity (i.e., its highest complexity level), it attains the so-called plasticity/stability limit where it cannot embed new memories without erasing old ones. Despite this unavoidable trade-off, ACh mechanism slows down memory decays in comparison to the situation without, see Fig. 4.5. From a system theory viewpoint, ACh acts therefore as a kind of low-pass filter that retains information.

Moreover, ACh plays a similar function during memory encoding as it slows down the scattering of one novel pattern by sustaining its trace in EC ; the memory retention of one novel signal depends then indirectly on activ. ratio, see Fig. 4.6. The time duration for holding one novel pattern augments with activation ratio to reach 6 or 7 seconds when ACh is fully active. As a result, these two mechanisms permit to create a working memory (i.e., an attentional system) that can serve advantegeously when the system is dealing with delays or with unexpected events ; e.g., to sustain object continuity during objects' rotation and occlusion.

Memory retention, transfer and consolidation into the neo-cortex

ACh creates the conditions for the rapid formation of memory traces in the hippocampus and allows the retention of specific episodes while preventing as much as possible interferences. However, in order to avoid memory decay, the hippocampus has to reinstantiate the short-term memories into the neo-cortical maps, which are performing at a slower learning rate Piaget [1954]. When the later structures finish to consolidate the memory patterns, they can start manipulate them ad libitum without the need of the hippocampus. The role of acetyholine is however not impotent in this scheme. For instance, Peinado demonstrated that ACh mediates the propagation of slow waves of electrical activity in the developing neocortex Izhikevich [2003]. We propose to model the memory remapping from short-term hippocampal memories to long-term cortical memories. Cortical maps are commonly defined as networks with recurrent connections. We use as neuron model a variant of the stellate cell defined in eq. 4.5, also proposed by Izhikevich [2003] :

$$v' = 0.004v^2 + 5v + 140 - u + I \tag{4.15}$$

$$u' = a(bv - u) \tag{4.16}$$

where I is the external input. The auxiliary after-spike resetting equation is the same as eq. 4.5 with $v_{peak} = 30\,mV$ such as the variables v and u represent also the membrane potential of the neuron and the membrane recovery variable. The variables set a, b, c, d defines the neurons attributes whether excitatory $(a; b) = (0.02; 0.2)$ and $(c; d) = (65; 8)$, or inhibitory ; $(a; b) = (0.02; 0.25)$ and $(c; d) = (65; 2)$.

The hebbian learning is based on the mechanism of spike timing-dependent plasticity introduced in Izhikevich [2006] and each neuron receives the external current I from their respective entorhinal neurons I_{ent} ($I_{ent} = 20\,mA$ when the neuron fires) and pre-synaptic neurons i : $I = \sum_{i \in pre} I_i.w_i + I_{ent}$. The cortical map is composed of 800 excitatory neurons and 200 inhibitory neurons with a coupling probability distribution of 0.1 (10 connections per neuron) for all the neurons. Therefore, the cortical map is ten time bigger than the entorhinal system –which has only eighty neurons– and each entorhinal cell is exactly connected to only one excitatory cortical neuron with index corresponding to the entorhinal neuron index multiplied by 10. The other cortical neurons are therefore inter-neurons that receive indirect signals from their recurrent connections.

During memory consolidation, we evaluate the rate of cortical encoding with the Victor-Purpura metric distance (VP) that quantifies the similarity between two spike trains Victor and Purpura [1997] ; e.g., the signal/noise ratio of one pattern. We use this measure because probabilistic methods are more approximative as they require to average the signals into spike rates. The VP distance computes the minimal cost D_V of transforming x to x' using two basic operations : the event insertion or deletion with a cost equals 1 and the event movement for which the cost is proportional to the distance (constance C_V) ; the time constant is defined as $\tau_V = 1/C_V$; here $C_V = 1$. In the case that the two spike trains are identical, then we will have $D_V = 0$.

We define the memory retention inside the cortical map as the inverse of D V renormalized between 0 to 100%, calculated from the hippocampal and the cortical dynamics. Under this condition, the more the cortico-hippocampal spike trains are synchronous, the more the cortical map is accurate and the higher is the memory retention.

We present in Fig. 4.7 the retention score of the cortical map when exposed to hippocampal dynamics and a raster plot of cortico-hippocampal synchronization during memory consolidation/retrieval in Fig. 4.8. In comparison with the performance of the hippocampus for learning one memory in one-shot and very rapidly [see Fig. 4.3 a)], the cortical map is much slower for encoding one memory pattern as it takes one hundred seconds to converge (10 5 iterations). Moreover, the cortical map performs worse than HP as it reaches 70 75% retention score whereas the hippocampus can learn a very precise pattern without interference. The reason for this behavior comes from the recurrent connections that amplify the neural activity inside the cortical map, which performs then as an associative memory. Moreover, memory consolidation generates the theta/gamma rhythm synchronization : the rhythmic activity corresponds here to the formation of coherent clusters that can be used for memory retrieval or for other tasks such as memory association and/or anticipation.

The temporal durations of hippocampal decay (Fig. 4.5) and cortical encoding (Fig. 4.7) are therefore critical as they delineate the interval length during which a memory pattern in

the hippocampus is available for cortical encoding, before being lost permanently. Like for the hippocampus, the cortical map has a trade-off in terms of plasticity and stability for consolidating the short-term memories into long-term memories that depends on the learning rates of both systems.

Discussion

In this section, we proposed to model the cholinergic system innervation in the hippocampal system and its influence for learning, attention and memory development. Acetylcholine is involved in the structural and functional adjustments of the hippocampus, transforming it into an attentional system ; i.e., a working memory for novel information. Under its action, the entorhinal cortex sustains and facilitates the learning of novel stimuli relative to the old patterns already present in the hippocampus. We show in our experiments how this dual mechanism may generate simply some emergent properties necessary for cognitive development. For instance, it limits the interference between memories which has for effect to scaffold the memory organization and to discretize the memory space into separated categories in the same time.

Our cholinergic hypothesis may give some partial answers to the paradoxes that pose the hippocampus and other subcortical structures that appear to function at birth but show some evidence of slow development and/or functional reorganization. Here, we propose that the neurotransmitter acetylcholine may play the role of a "catalyst" that activates the functional organization of the cortico-hippocampal system (i.e., detecting and holding stimuli, preserving and acquiring memories).

Although ACh is generally known to regulate the structural maturation of the central nervous system Lauder and Schambra [1999]– e.g., the growth, differentiation, and plasticity of the neurons– the precise timing of cholinergic innervation to the cortex appears to be crucial also for the normal development of cognitive functions. Its action is even broader since ACh has been identified for mediating the propagation of slow waves of electrical activity in the developing neocortex Descarries et al. [2004]; Izhikevich [2003], which are associated with long-term memory and categorization performances Quinn et al. [2006]; Newcombe and Huttenlocher [2006]. In our model, we show how theta waves could slowly shape the neocortical maps into coherent patterns (rhythmical theta/gamma activity). Hence, the modeling of the cholinergic system in the para-hippocampal system is not only critical for understanding development during the first year but also for understanding memory transfer, attention processes and retrieval task Hasselmo [2006].

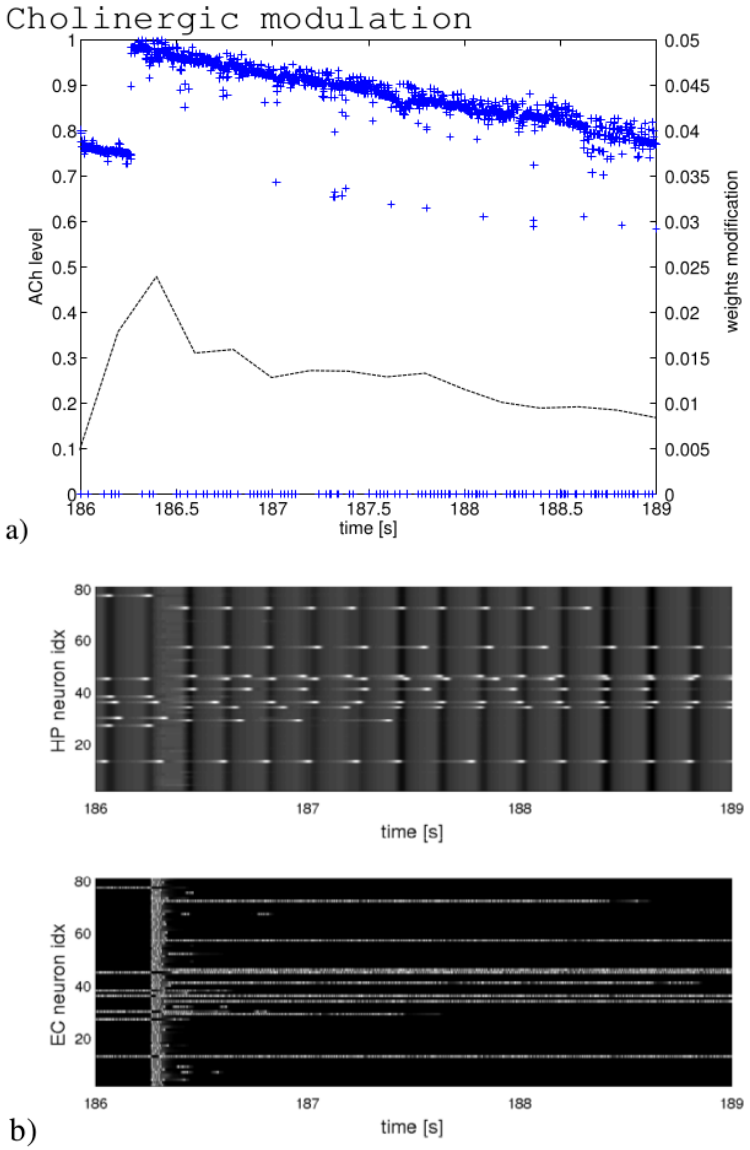

FIGURE 4.3 – Effect of cholinergic activation on the hippocampal and entorhinal dynamics after presentation of a novel input. The exposure of a novel input rises ACh_level to its highest value [blue crosses in a)], which contributes to sustain the dynamics in both networks and to enhance its learning. While the pattern is being learnt, ACh_level slowly decreases as a counter-effect.

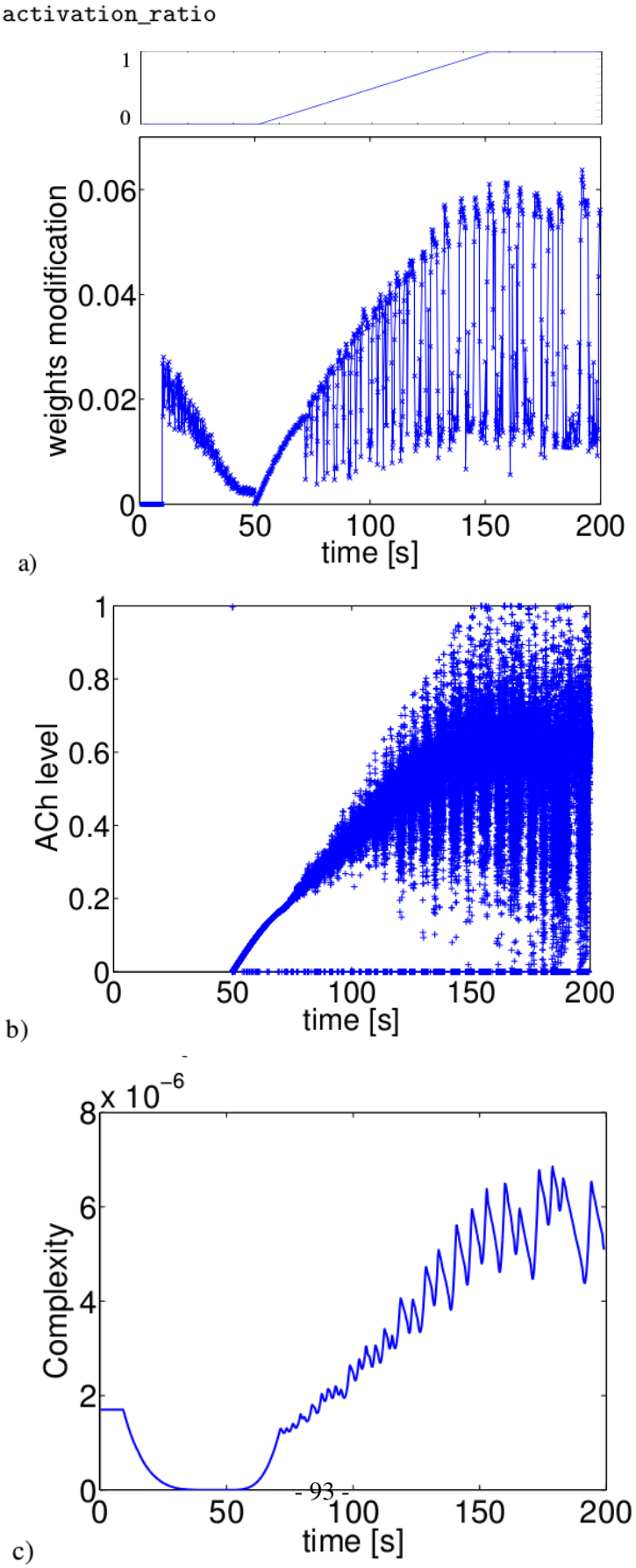

FIGURE 4.4 – Weight modication for Hebbian learning with gradual activation of ACh modulation starting at t = 50 sec resp. a) and b). Complexity measures computed from the connection matrix of the hippocampal network relative to cholinergic activation rate (c).

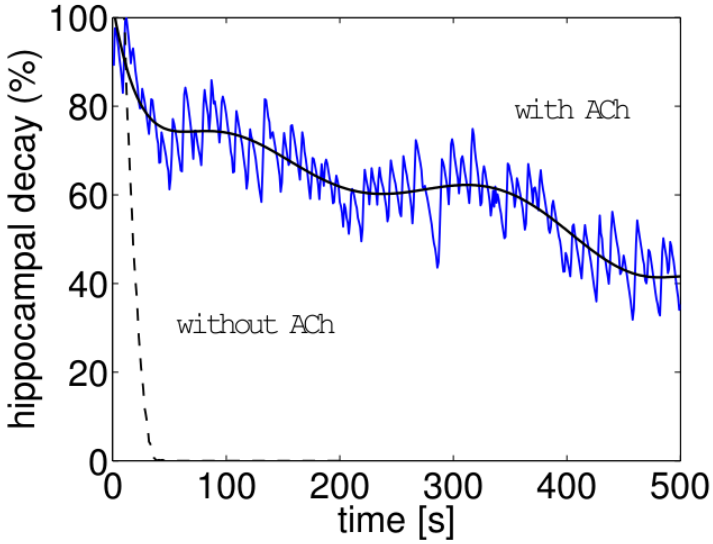

FIGURE 4.5 – Hippocampal memory retention and decay. Without cholinergic activation, the newly acquired memories in the hippocampus vanish asymptotically and are replaced by other memories whereas the ACh mechanism augments the retention time with a slow decay.

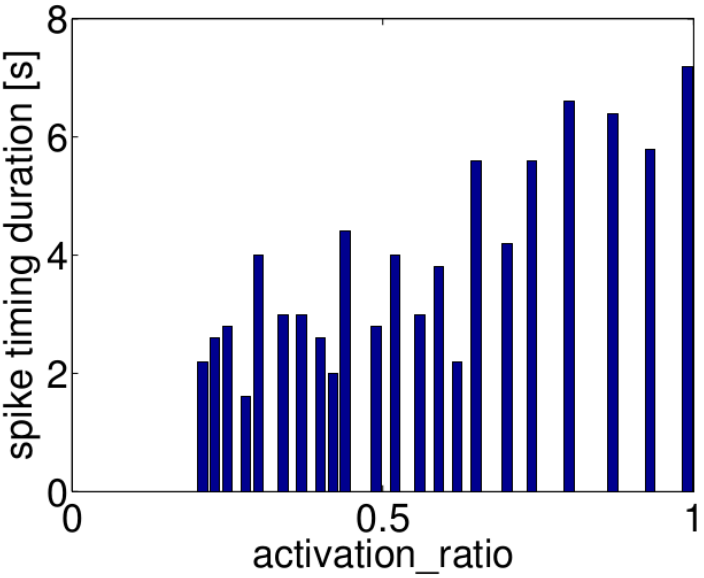

FIGURE 4.6 – Time duration relative to activation ratio. It shows the performance of the working memory in terms of time duration to hold novel information. The spike duration correlates almost linearly with the values of the activation parameter.

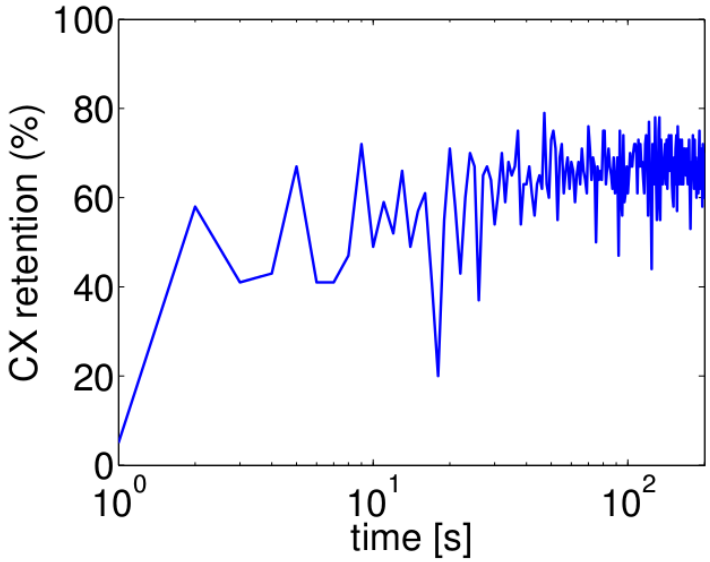

FIGURE 4.7 – Memory consolidation in the cortical map. Memory retention is estimated from the signal per noise ratio between the hippocampal items and the cortical map activity with the Victor and Purpura distance between two spike trains Victor and Purpura [1997]. The cortical map learns the hippocampal patterns at a very slow rate compared with the hippocampus.

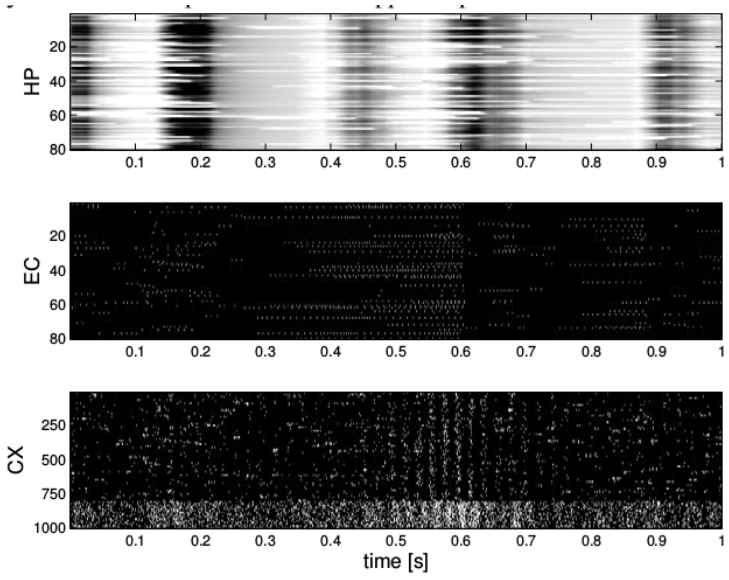

FIGURE 4.8 – Cortico-hippocampal synchronization. The raster plots of the cortico-hippocampal maps present the /-bands synchronization of the cortical neurons to the hippocampal rhythm for a familiar pattern, the gamma waves enhance selectivity to the input patterns.

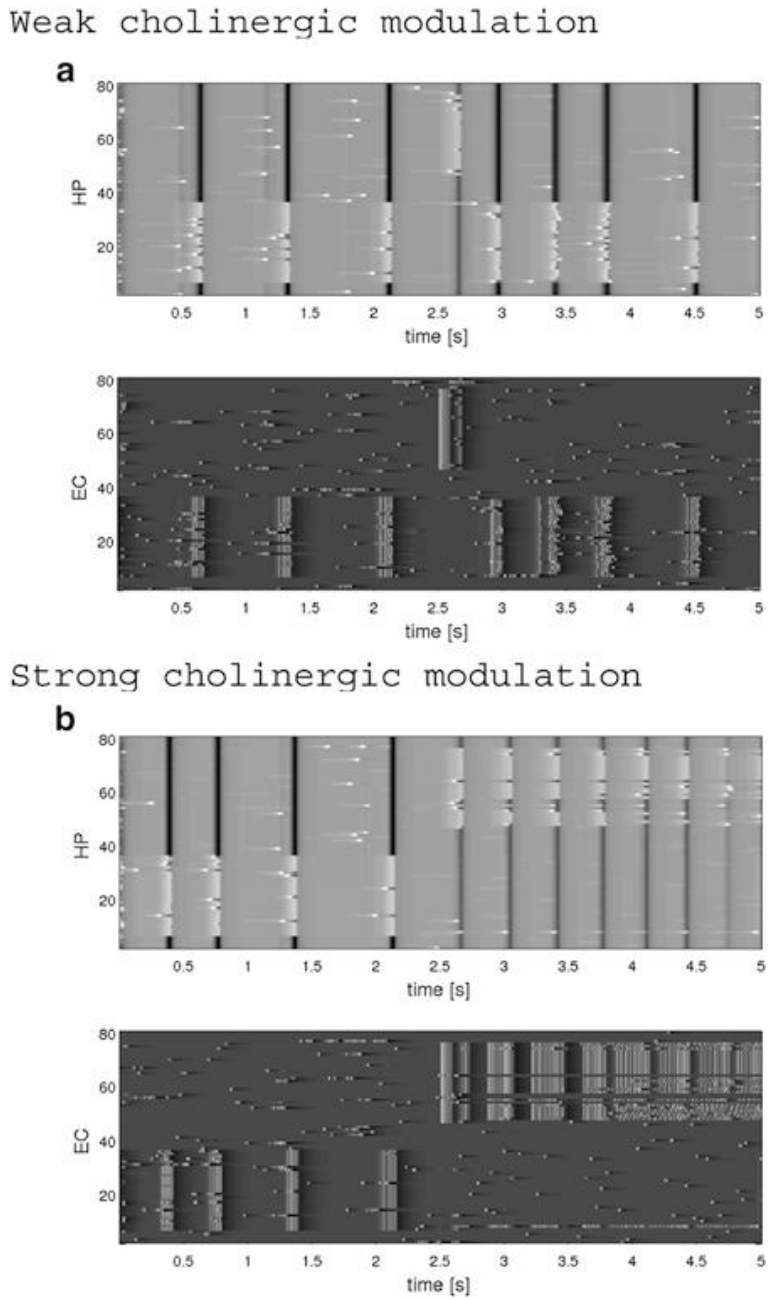

FIGURE 4.9 – A-not-B experiment with a protocol similar to **?**. The localized peaks of activation in the neural system respect the spatial topology of the environment such that location A is represented by neurons of low-ranked indices and location B by those of high rank.

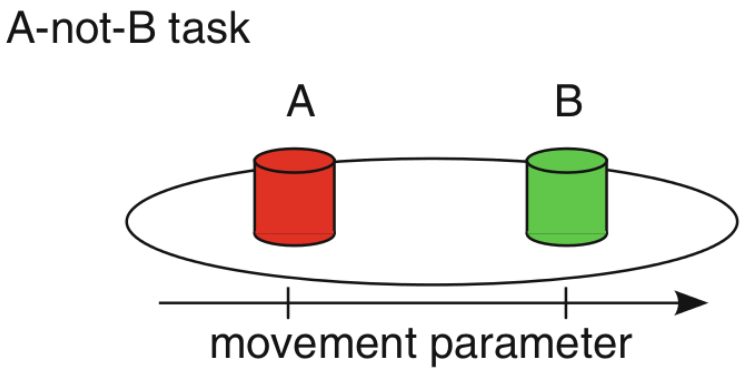

FIGURE 4.10 – A-not-B task before and after cholinergic activation, resp. (a) and (b). Without cholinergic neuromodulation, the short exposure of an object placed at a novel location B for several hundreds of milliseconds does not influence the dynamics of the entorhino-hippocampal system whereas the novel pattern is sustained for several seconds for the situation with cholinergic activation **?**.

ACC Negative Reward for Cortical Task-Set Selection and Learning

The design of a multi-tasks robot that can cope with novelty and evolve in an open-ended manner is still an open challenge for robotics. It is however an important goal (1) for conceiving per- sonal assistive robots that are adaptive (e.g., to infants, the elderly and to the handicapped people) and (2) for studying from an inter-disciplinary viewpoint the intrinsic mechanisms underlying decision making, goal-setting and the ability to respond on the fly and adaptively to novel problems. For instance, robots cannot yet reach the level of infants for exploring alternative ways to surmount an obstacle, searching for a hidden toy in a new environment, finding themselves the proper way to use a tool, or solving a jigsaw puzzle. All these tasks require to be solved within boundaries of their given problem space, with- out exploring it entirely. Thus, robots lack this ability to detect and explore new behaviors and action sequences oriented toward a goal ; i.e., what is called a task set Harlow [1949]; Collins and Koechlin [2012]. The ability to manipulate dynamically task sets is however a fundamental aspect of cognitive development. Early in infancy, infants are capable to perform flexible decision- making and dynamic executive control even at a simple level in order to deal with the unexpected Tenenbaum et al. [2011]. Later on, when they are more mature, they learn to explore the tasks space, to select goals and to focus progressively on tasks of increasing complexity. One example in motor development is the learning of different postural configurations. Karen Adolph explains for instance how infants progressively differentiate their motor behaviors into task sets (i.e., the motor repertoire) and explore thoroughly the boundaries of each postural behavior till becoming expert on what they discover Adolph and Joh [2005, 2009]. Adolph further argues that the building of a motor repertoire is not preprogrammed with a specific developmental timeline but that each postural behavior can be learned indepen- dently as separated tasks without pre-ordered dependencies to the other ones (crawling, sitting, or standing). This viewpoint is also shared by neurobiologists who conceive the motor system to structure the actions repertoire into "internal models" for each goal to achieve. Each novel contextual cue (e.g., handling a novel object) promotes the acquisition and the use of a dis- tinct internal model that does not modify the existing neural representations used to control the limb on its own. Moreover, each task set is evaluated depending on the current dynamics and on the current goal we want to perform Orban and Wolpert [2011]. For instance, we switch dynamically from different motor strategies to the most appropriate one depending on the context ; e.g., tilting the racket to the correct angle in order to give the desired effect on the ball, or for executing the proper handling of objets with respect to their estimated masses Cothros et al. [2006]. From a developmental viewpoint, the capability for flexible decision-making gradually improves in 18 months-old infants Tenenbaum et al. [2011]. Decision-making endows infants to evaluate the different alternatives they have for achieving one goal with respect to the ongoing sequence and to select the correct one(s) among different alternatives. It owes them also the possibility to inhibit some previously learned strategies in order to explore new ones never seen before Yokoyama et al. [2005]. IN AI, this craving to explore, to test and to embed new behaviors is known as intrinsic motivation Kaplan and Oudeyer [2007].

In Kaplan and Oudeyer's words : "The idea is that a robot (...) would be able to autonomously explore its environment not to fulfill predefined tasks but driven by some form of intrinsic motivation that pushes it to search for situations where learning happens efficiently". In this section, we focus more on the idea that the rewards are self-generated by the machine it-

self Singh et al. [2010] and that the function of intrinsic motivation is mainly to regulate the exploration/exploitation problem, driving exploratory behavior and looking for different successful behaviors in pursuing a goal. In that context, we propose that the ability to choose whether or not to follow the same plan or to create a novel one out of nothing—in regard to the current situation—is an intrinsic motivation. We studied for instance the role of the neuromodulator acetylcholine in the hippocampus for novelty detection and memory formation Pitti and Kuniyoshi [2011b].

Meanwhile, the capability to make decision and to select between many options is one important aspect of intrinsic motivation because otherwise the system would be only passive and would not be able to select or encourage one particular behavior. Taking decisions in deadlock situations requires therefore some problem-solving capabilities like means-end reasoning Koechlin et al. [2003] and error-based learning capabilities Adolph and Joh [2009]. For instance, means-end reasoning and error-based learning are involved in some major psychological tests such as the Piagetian "A-not-B error test" Diamond [1985], Harlow's learning set test Harlow [1949] and tool-use.

The A-not-B error test describes a decision-making problem where a 9-month old infant still pertains to select an automatic wrong response (e.g., the location A) and cannot switch dynamically from this erronous situation to the correct one (e.g., the location B). Above this age, however, infants do not make the error and switch rapidly to the right location. A similar observation is found in Harlow's experiments on higher learning Harlow [1949] where Rhesus monkeys and humans have to catch the pattern of the experiment in a series of learning experiences. Persons and monkeys demonstrate that they learn to respond faster when facing a novel and similar situation by switching to the correct strategy, by catching the pattern to stop making the error : they show therefore that they do not master isolated tasks but, instead, they grasp the relation between the events. In one situation, if the animal guessed wrong on the first trial, then it should switch directly to the other solution. In another situation, if it guessed right on the first trial, then it should continue. This performance seems to require that the monkey, the baby or the person use an abstract rule and solve the problem with an apparent inductive reasoning Tenenbaum et al. [2011]. In line with these observations on the development of flexible behaviors, researchers focused on tool-use : when infants start to use an object as a means to an end, they serialize their actions toward a specific goal, as for example reaching a toy with a stick.

Tool-use requires also finding patterns like the shape of grasping, order and sequentiality of patterns Cothros et al. [2006]. Considering the mechanisms it may involve, Karen Adolph emphasizes the ability of learning-to-learn Adolph and Joh [2005], a process akin to Harlow [1949]. Harlow coined the expression to distinguish the means for finding solutions to novel problems from simple associative learning and stimulus generalization Adolph [2008].

Adolph reinterprets this proposal and suggests that two different kinds of thinking and learning are at work in the infant brain, governing the aspects of exploration and of generalization Adolph and Joh [2009]. On the one hand, one learning system is devoted to the learning of task sets from simple stimulus-response associations. For instance, when an infant recognizes the context, he selects his most familiar strategy and reinforces it within his delimiting parameter ranges. On the other hand, a second learning is devoted to detect a new situation as is and to find a solution dynamically in a series of steps. Here, the acceptance of uncertainty gradually leads for making choices and decisions in situation never seen before. However, which brain regions and which neural mechanisms this framework underlies ?

Among the different brain regions, we emphasize that the post-parietal cortex (PPC) and the pre-frontal cortex (PFC) are found important (1) for learning context-dependent behavior and (2) for evaluating and selecting these behaviors relative to their uncertainty and error prediction. Regarding the PPC, different sensorimotor maps co-exist to represent structured information like spatial information or the reaching of a target, built on coordinate transform mechanisms. Furthermore, recent studies acknowledge the existence of context-specific neurons in the parieto-motor system for different grasp movements. Regarding the PFC, Johnson identifies the early development of the pre-frontal cortex as an important component for enabling executive functions Johnson [2012] while other studies have demonstrated difficulty in learning set formation following extensive damage of the prefrontal cortex.

The PFC manipulates information on the basis of the current plan, and it is active when new rules need to be learned and other ones rejected. Besides, its behavior is strongly modulated by the anterior cingulate cortex (ACC) which plays an active role for evaluating task sets and for detecting errors during the current episode. If we look now at the functional organization of these brain structures, many authors emphasize the interplay between an associative memory of action selection in the temporal and parietal cortices (i.e., an integrative model) and a working memory for actions prediction and decision making in the frontal area (i.e., a serial model). All-in-all, these considerations permit us to draw a scenario based on a two complementary learning systems. More precisely, we propose to model a dual system based on (1) the learning of task sets and on (2) the evaluation of these task sets relative to their uncertainty, and error prediction. Accordingly, we design a two-level based neural system for context-dependent behavior (PPC) and task exploration and prediction (ACC and PFC) ; see Fig. 4.11.

In our model, the task sets are learned separately by reinforcement learning in the post parietal cortex after their evaluation and selection in the prefrontal cortex and anterior cyngulate cortex. On the one hand, the learner or agent stores and exploits its familiar knowledge through a reinforcement learning algorithm into contextual patterns called and collected from all its different modalities. On the other hand, the learner evaluates and compares the way it learns, and selects the useful strategies while it discards others or tests new ones on the fly if no relevant strategy is found. We perform two different experimental setups to show the sensorimotor mapping and switching between tasks, one in a neural simulation for modeling cognitive tasks and another with an arm-robot for motor task learning and switching. We use neural networks to learn simple sensorimotor mapping for different tasks and compute their variance and error for estimating the sensorimotor prediction. Above a certain threshold, the error signal is used to select and to valuate the current strategy. If no strategy is found pertinent for the current situation, this corresponds to a novel motor schema that is learned independently by a different map. In a cognitive experiment similar to Diamond [1990], we employ this neural structure to learn multiple spatio-temporal sequences and switch between different strategies if an error has occurred or if a reward has been received (error-learning). In a psycho-physic experiment similar to Wolpert and Flanagan [2010], we show how a robotic arm learns the visuomotor strategies for stabilizing the end-point of its own arm when it moves it alone and when it is holding a long stick. Here, the uncertainty on the spatial location of the end-point triggers the decision-making from the two strategies by selecting the best one given the proprioceptive and visual feedback and the error signal delivered.

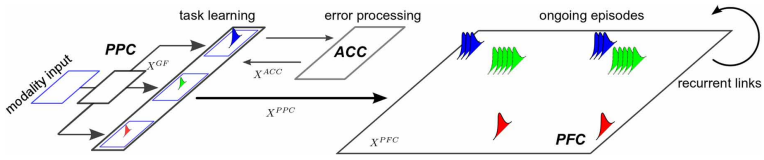

FIGURE 4.11 – Framework for task set selection. The whole system is composed of three distinct neural networks, inspired from Khamassi et al. [2011]. The PPC network conforms to an associative network. It binds the afferent sensory inputs from each other and map them to different motor outputs with respect to a task set. The ACC system is a error-based working memory that processes the incoming PPC signals and feeds back an error to them with respect to current task. This modulated signal is used to tune the population of neurons in PPC by reinforcement learning, it is also conveyed to the PFC map, which is a recurrent network that learns dynamically the spatio-temporal patterns of the ongoing episodes with respect to the task.

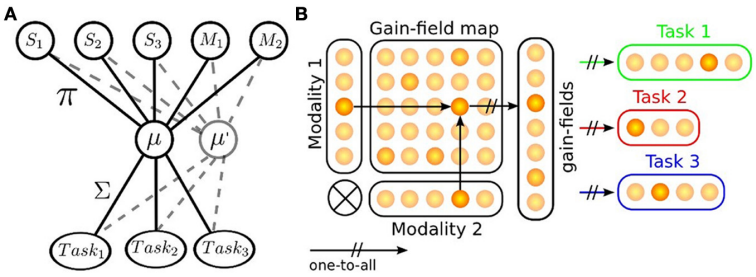

FIGURE 4.12 – Task sets mapping, the mechanism of gain-fields. (A) Gain-fields neurons are units used for sensorimotor transformation. They transform the input activity into another base, which is then fed forward to various outputs with respect to their task. Gain-fields can be seen as meta-parameters that decrease the complexity of the sensory-motor problem into a linear one. (B) example of GF neurons sensorimotor transformation for two modalities projecting to three different task sets ; each GF neuron contributes to one particular feature of the tasks Pouget and Snyder [2000]; Orban and Wolpert [2011].

Materials and Methods

In this section, we present the neural architecture and the mechanisms that govern the dynamics of the neurons, of reinforcement learning and of decision-making. We describe first the bio-inspired mechanism of rank-order coding from which we derive the activity of the parietal and of the pre-frontal neurons. In second, we describe the reinforcement learning algorithm, the error prediction reward and the decision-making rules.

PPC—Gain-Field Modulation And Sensorimotor Mapping

We employ the rank-order coding neurons to model the sensorimotor mapping between input and output signals with an architecture that we have used in a previous research Pitti et al. [2012]. This architecture implements multiplicative neurons, called gain-field neurons, that multiply unit by unit the value of two or more incoming neural populations, see Fig. 4.12. Its organization is interesting because it transforms the incoming signals into a basis functions' representation that could be used to simultaneously represent stimuli in various reference frames Salinas and Thier [2000]. The multiplication between afferent sensory signals in this case from two population codes, X_{m_1} and X_{m_2}, $\{m_1 , m_2 \in M_1, M_2 \}$, produces the signal activity X_n to the n gain-field

neurons, $n \in N$:

$$X^{GF} = X^{M_1} \times X^{M_2} \tag{4.17}$$

The key idea here is that the gain-field neurons encode two information at once and that the amplitude of the gain-field neurons relates the values of one modality conditionally to the other ; see Fig. 4.12 A. The task is therefore encoded into a space of lower dimension Braun et al. [2009, 2010]. We exploit this feature to model the parietal circuits for different contextual cues and internal models, which means that, after the encoding, the output layers learn the receptive fields of the gain-field map and translates this information into various gain levels. In Fig. 4.12 B, we give a concrete example of one implementation, here delineated to two modalities, with N gain-fields projecting to three different tasks set of different size. We explain thereinafter (1) how the gain fields neurons learn the associations between various modalities and (2) how the neurons of the output map learn from the gain fields neurons for each desired task.

Rank-Order Coding Algorithm

We implement a hebbian-like learning algorithm proposed by Van Rullen et al. [1998] called the Rank-Order Coding (ROC) algorithm. The ROC algorithm has been proposed as a discrete and faster model of the derivative integrate-and-fire neuron Van Rullen and Thorpe [2002]. ROC neurons are sensitive to the sequential order of the incoming signals ; that is, its rank code, see Fig. 4.13 A. The distance similarity to this code is transformed into an amplitude value. A scalar product between the input's rank code with the synaptic weights furnishes then a distance measure and the activity level of the neuron. More precisely, the ordinal rank code can be obtained by sorting the signals' vector relative to their amplitude levels or to their temporal order in a sequence. We use this property respectively for modeling the signal's amplitude for the parietal neurons and the spatio-temporal patterns for the prefrontal neurons. If the rank code of the input signal matches perfectly the one of the synaptic weights, then the neuron fully integrates this activity over time and fires, see Fig. 4.13 A. At contrary, if the rank order of the signal vector does not match properly the ordinal sequence of the synaptic weights, then integration is weak and the neuron discharges proportionally to it, see Fig. 4.13 B.

The neurons' output X is computed by multiplying the rank order of the sensory signal vector I, $rank(I)$, by the synaptic weights w ; $w \in [0, 1]$. For a vector signal of dimension M and for a population of N neurons (M afferent synapses), we have for the GF neurons and for the output PPC neurons :

EQ2

$$X_n^{GF} = \sum_{m \in M} \frac{1}{rank(I_m)} w_{n,m}^{GF-Modality} \tag{4.18}$$

$$X_n^{PPC} = \sum_{m \in M} \frac{1}{rank(I_m)} w_{n,m}^{PPC-Modality} \tag{4.19}$$

The updating rule of the neurons' weights is similar to the winner-takes-all learning algorithm of Kohonen's self-organizing maps Kohonen [1982]. For the best neuron $s \in N$ and for all afferent signals $m \in M$, we have for the neurons of the output layer :

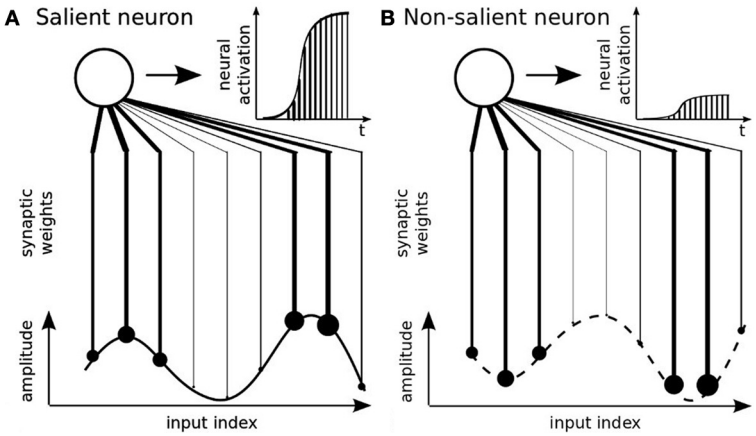

FIGURE 4.13 – Rank-Order Coding principle Thorpe et al. [2001]. This type of neuron encodes the rank code of an input signal. Its amplitude is translated into an ordered sequence and the neuron's synaptic weights are associated to this sequence. The neural activity is salient to this particular order only, see (A), and otherwise not, see (B).

EQ3

$$w_{s,m}^{PPC-GF} = w_{s,m}^{PPC-GF} + \Delta w_{s,m}^{PPC-GF} \tag{4.20}$$

$$\Delta w_{s,m}^{PPC-GF} = \frac{1}{rank(I_m)} - w_{s,m}^{PPC-GF} \tag{4.21}$$

the equations are the same for GF neurons (not reproduced here). We make the note that the synaptic weights follow a power-scale density distribution that makes the rank-order coding neurons similar to basis functions. This attribute permits to use them as receptive fields so that the more distant the input signal is to the receptive field, the lower is its activity level ; e.g., Fig. 4.13 B.

Reinforcement Learning And Error Reward Processing

The use of the rank-order coding algorithm provides an easy framework for reinforcement learning and error-based learningBarto [1995]. For instance, the adaptation of the weights in Equation 3 can be modified simply with a variable $\alpha \in [0, 1]$ that can ponder w ; see Equation 4. If $\alpha = 0$, then the weights are not reinforced : $W_{t+1} = W_t$. If $\alpha = 1$, then the weights are reinforced in the direction of W : $W_{t+1} = W_t + \alpha W$. In addition, conditional learning can be made simply by summing an external bias β to the neurons output X. By changing the amplitude of the neurons, we change also the rank-order to be learned and influence therefore the long-term the overall organization of the network ; see Equation 5.

EQ 4 5

$$\Delta w \leftarrow \alpha \Delta w,\ \alpha \in [0, 1] \tag{4.22}$$

$$X \leftarrow X + \beta,\ \beta \in [= 1, +1] \tag{4.23}$$

$$\tag{4.24}$$

Cortical Plasticity in PPC

For modeling the cortical plasticity in the PPC output maps, we implement an experience-driven plasticity mechanism. Observations done in rats show that during the learning of novel motor skills the synapses rapidly spread in the neocortex immediately as the animal learns a new task. Rougier and Boniface proposed a dynamic learning rule in self-organizing maps to combine both the stability of the synapses' population to familiar inputs and the plasticity of the synapses' population to novel patterns Rougier and Boniface [2011]. In order to model this feature in our PPC map, we redefine the coefficient in Equation 5 and we rearrange the formula proposed by Rougier and Boniface :

EQ 6

$$\alpha = e^{1/\eta^2/||max(X^{PPC})-X_S^{PPC}||} \in [0,1] \tag{4.25}$$

where η is the elasticity or plasticity parameter that we set to 1 and $max(X_{PPC})$ is the upper bound of the neural activity, its maximal value, whereas $max(X_{PPC})$ is the current maximum value within the neural population, with $\alpha = 0$ when $X_{s_{PPC}} = max(X_{PPC})$. In this equation, the winner neuron learns the data according to its own distance to the data. If the winner neuron is close enough to it, it converges slowly to represent the data. At contrary, if the winner neuron is far from the data, it converges rapidly to it.

Error-reward function in ACC

For modeling ACC, we implement an error-reward function similar to Khamassi et al. [2011] and to Q-learning based algorithms. The neurons' value is updated afterwards only when an error occurs, then a ihnibitory feedback error signal is sent to the winning neuron to diminish its activity X_{win} : $ACC(X_{win}) = 1$; the neurons equation X is updated as follows :

EQ7

$$X^{PPC} = \sum_{m \in M} \frac{1}{rank(I_m)} w_{n,m} + ACC(X_n^{PPC}). \tag{4.26}$$

The neurons activity in ACC is cleared everytime the system responds correctly or provides a good answer. ACC can be seen then as a contextual working memory, a saliency buffer extracted from the current context when errors occur inhibiting the wrong actions performed. Its activity may permit to establish an exploration-based type of learning by trial and errors and an attentional switch signal from automatic responses, in order to deal with the unexpected when a novel situation occurs.

PFC—Spatio-Temporal Learning In a Recurrent Network

We can employ the rank-order coding for modeling spike-based recurrent neural network in which the amplitude values of the incoming input signals are replaced by its past spatio-temporal activity pattern. Although the rank-order coding algorithm has been used at first to model the fast processing of the feed-forward neurons in V1, its action has been demonstrated to replicate also the hebbian learning mechanism of Spike Timing-Dependent Plasticity (STDP) in cortical neurons Bi and Poo [1998]; Abbott and Nelson [2000]; Izhikevich et al. [2004]. For a population of N neurons, we arbitrarily choose to connect each neuron to a buffer of size $20 \times N$ so that

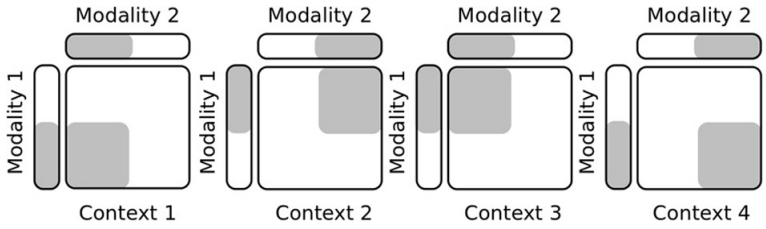

FIGURE 4.14 – Protocol setup in task sets learning. This simple protocol explains how the experimental setup is done for acquiring different contexts incrementally and for selecting them.

they encode the rank code of the neurons amplitude value over the past 20 iterations. At each iteration, this buffer is shifted to accept the new values of the neurons.

EQ 8

$$X_n^{PFC} = \sum_{m \in M} \frac{1}{rank(buffer_m)} w_{n,m} + X_n^{PPC}. \tag{4.27}$$

Recurrent networks can generate novel patterns on the fly based on their previous activity pattern while, at each iteration, a winning neuron gets its links reinforced. Over time, the system regulates its own activity whereas coordinated dynamics can be observed. These behaviors can be used for anticipation and predictive control.

Results

We propose to study the overall behavior of each neural system during the learning of task sets and the dynamics of the ensemble working together. The first three experiments are performed in a computer simulation only. They describe the behavior of the PPC maps working solely, working along the ACC system and working along the ACC and PFC systems for learning and selecting context-dependent task set.

Experiment 1—Plasticity vs Stability In Learning Task Sets

In this first experiment, we test the capabilities of our network to learn incrementally novel contexts without forgetting the older ones, which corresponds to the so-called plasticity/stability dilemma of a memory system to retain the familiar inputs as well as to incorporate flexibly the novel ones. Our protocol follows the diagram in Fig. 4.14 in which we show gradually four different contexts for two input modalities with vectors of ten indices. The input patterns are randomly selected from an area in the current context chosen randomly and for a period of time also variable. In this experiment, the PPC output map has 50 neurons that receive the activity of twenty gain-fields neurons, see Fig. 4.12 B.

We display in Fig. 4.15 A the raster plot of the PPC neurons' dynamics with distinct colors with respect to the context. Contexts are given gradually, one at a time, so that some neurons have to unlearn their previous cluster first in order to fit the new context. It is important to note that categorization is unsupervised and decided due to the experience-driven plasticity rule in Equation 6. In order to demonstrate the plasticity of the PPC network during the presentation of a new context, we present the context number four, plotted in magenta and never seen before, at t = 11500. Here, the new cluster is rapidly formed and stable over time due again to the cortical

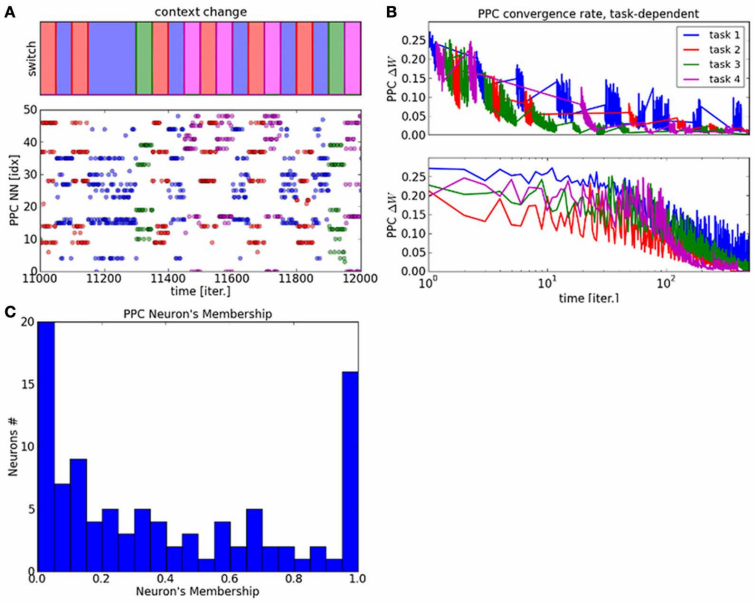

FIGURE 4.15 – Raster plot of the PPC output map and plasticity vs. stability within the map. (A) the graph displays the neural dynamics during task switch among four different contexts. (B) Convergence rate of the PPC network with respect to each task. (C) The degree of plasticity and stability within the PPC output map is represented as the probability distribution of the neurons membership to the cluster relative to a context. This histogram shows two behaviors within the system. On the one hand, one third of the neurons present very stable dynamics with membership to one context only. On the other hand, two third of the neurons are part of different clusters and therefore to different contexts. The later neurons follow a power law distribution showing very plastic dynamics.

plasticity mechanism from Equation 6. The graph displays therefore not only the plasticity of the clusters in the PPC network but also their robustness.

This property is also shown in Fig. 4.15 B where the convergence rates of the PPC weights vary differently for each task. This result explains how the PPC self-organizes itself into different clusters that specialize flexibly with respect to the task. The ratio between stability and plasticity in shown in Fig. 4.15 C within the network with the histogram of the neuron's membership over a certain time interval. The stability of one neuron is computed as its probability distribution relative to each context. The higher values correspond to very stable neurons, which are set to one context only and do not deviate from it, whereas the lower values correspond to very flexible neurons that change frequently context from one to another.

The histogram shows two probability distributions within the system and therefore two behaviors. For the neurons corresponding to values near the strong peak at 1.0, their activity is very stable and strongly identified to one context. This shows that for one third of the neurons, the behavior of the neural population is very stable. At reverse, the power law curve centered on 0.0 shows the high variability of certain neurons, which are very dynamic for one third of the neural population.

We study now the neurons' activity during a task switch in Fig. 4.16. In graph (A), the blue lines correspond to the neurons' dynamic belonging to the context before the switch and the red lines correspond to the neurons' dynamic belonging to the context after the switch. The activity

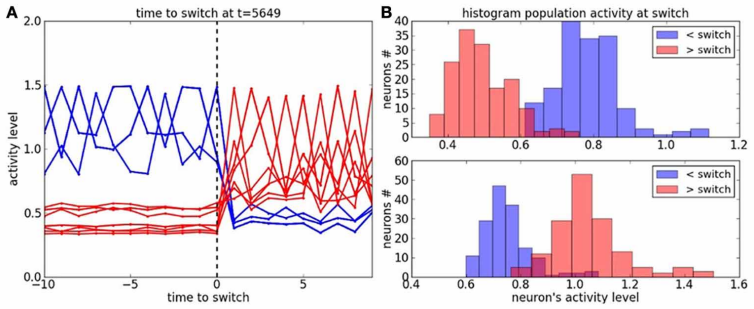

FIGURE 4.16 – Cluster dynamics at the time to switch. (A) Neural dynamics of the active clusters before and after the switch ; resp. in blue and in red. (B) Histogram of the neural population at the time to switch with respect to the active clusters before and after the switch.

level in each cluster is very salient for each context. The probability distribution of the neurons' dynamic, with respect to each context is plotted in Fig. 4.16 B. It shows a small overlap between the contexts before and after the switch.

Experiment 2 — Learning Task Sets with a Reinforcement Signal

In this second experiment, we reproduce a decision-making problem similar to those done in monkeys and humans with multiple choices and rewards Churchland and Ditterich [2012]. The rules are not given in advance and the tasks switch randomly after a certain period of time with no regular pattern. The goal of the experiment is to catch the input-output correspondence pattern to stop making the error. The patterns are learned dynamically by reinforcement learning within each map and should ideally be done without interference from each other. The error signal indicates when an input-output association is erronous with respect to a hidden policy, however, we make the note that it does not provide any hint about how to minimize the error. To understand how the whole system works, we focus our experiment on the PPC network with the ACC error processing system first, then with the PFC network. We choose to perform a two-choices experiment, with two output PPC maps initialized with random connections from the PPC map. The PPC network consists therefore of the gain-field architecture with the two output maps for modeling the two contexts. The two maps are then bidirectionally linked to the ACC system ; the input signals for modality 1 and 2 are projected to the PPC input vectors of twenty units each ; map1 has twelve output units and map2 has thirteen output units and project to ACC of dimension twenty-five units.

The hidden context we want the PPC maps to learn is to have output signals activated for specific interval range of the inputs signals, namely, the first output map has to be activated when input neurons of indices below ten are activated, and reciprocally, the second output map has to be activated when input neurons of indices above ten are activated—this corresponds to the two first contexts in Fig. 4.14. The error prediction signal is updated anytime a mistake has been done on the interval range to learn. As expressed in the previous section, the ACC error signal resets always its activity when the PPC maps start to behave correctly.

We analyze the performance of the PPC-ACC system in the following. We display in Fig. 4.17 A,B the raster plots of the PPC and ACC dynamics with respect to the context changes for different periods of time. The chart on the top displays the timing for context switch, the chart on

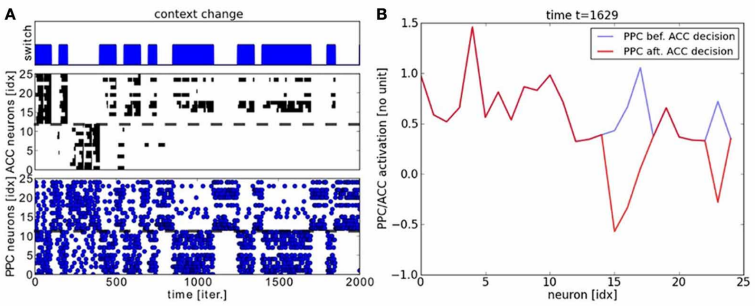

FIGURE 4.17 – Experiment on two-choices decision making and task switching. (A) Neural dynamics of PPC neurons and ACC error system during task switch. We plot in the chart in the top the temporal interval for each task. Below the, neural dynamics of the PPC maps and in the middle, its erronous activity retranscribed in the ACC system. ACC works as a working memory that keep tracks of the erronous outputs, which is used during the learning stage. ACC is reset each time the PPC system gives a correct answer. Through reinforcement learning, the PPC maps converge gradually to the correct probability distribution. (B) Snapshot of the PPC maps in blue modulated negatively by ACC in red.

the middle plots the ACC system working memory and the chart below plots the output of the PPC units. The Fig. 4.17 A is focusing on the beginning of the learning phase and the Fig. 4.14 B when the system has converged. We observe from these graphs that the units of the output maps self-organize very rapidly to avoid the error. ACC modulates negatively the PPC signals. We make the note that the error signal does not explicitly inhibit one map or the other but only the wrongly actived neuron of the map. As it can be observed, over time, each map specializes to its task. As a result, learning is not homogenous and depends also to the dimension of the context ; that is, each map learns with a different convergence rate. ACC error rapidly reduces its overall activity for the learning of task1 with respect to map1, although the error persists for the learning of task2 with respect to map2 where some neurons still fires wrongly.

We propose to study the convergence of the two maps and the confidence level of the overall system for the two tasks. We define a confidence level index as the difference of amplitude between the most active neurons in map1 and map2. We plot its graph in Fig. 4.18 where the blue color corresponds to the confidence level for task1 with v_{s_map1} v_{s_map2} and the color red corresponds to the confidence level for task2 with v_{s_map2} v_{s_map1} during the learning phase. The dynamics reproduce similar trends from Fig. 4.17 where the confidence level constantly progresses till convergence to a stable performance rate, with a threshold around 0.4 above which a contextual state is recognized or not. Before 1000 iterations, the maps are very plastic so the confidence level fluctuates rapidly and continuously between different values but at the end of the learning phase, the maps are more static so the confidence level appears more discrete.

This state is clearly observable from the histogram of the confidence level plotted on the right in Fig. 4.18 B for the case where the ACC error signal is injected to the associative network. The graph presents a probability distribution with two bell-shaped centred on 0.1 and 0.7, which corresponds to the cases of recognition or not of the task space. In comparison, the probability distribution for the associative learning without error-feedback is uniform, irrespective to the task ; see Fig. 4.18 B in blue.

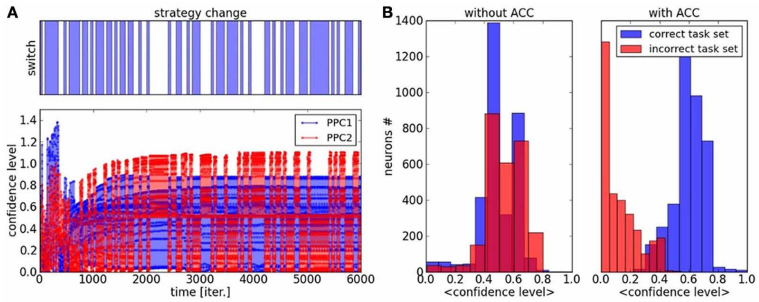

FIGURE 4.18 – Confidence Level of PPC maps during task switch, dynamics and histogram. (A) The confidence level is the difference between the amplitude of most activated neuron and the second one within each map. After one thousand iterations, the two maps rapidly specialize their dynamics to its associated task. This behavior is due to the ACC error-based learning. (B) histogram of the probability distribution of the confidence level with and without ACC. With ACC, we observe a clear separation in two distributions, which correspond to a decrease of uncertainty with respect to the task. In comparison, the confidence level in an associative network without an error feedback gives a uniform distribution.

Experiment 3—Adaptive Learning On a Temporal Sequence Based On Error Prediction Reward

We attempt to replicate now Harlow's experiments on adaptive learning, but, in comparison to the previous experiments, it is the temporal sequence of task sets that is taken into account for the reward. We employ our neural system in a cognitive experiment first to learn multiple spatio-temporal sequences and then to predict when a change of strategy has occurred based on the error or on the reward received. With respect to the previous section also, we add the PFC-like recurrent neural network to learn the temporal sequence from the PPC and ACC signals, see Fig. 4.11. The experiment is similar to the previous two-choices decision-making task, expect that the inputs follow now a temporal sequence within each map. When the inputs reach a particular point in the sequence–, a point to switch,– we proceed to a random choice between one or the two trajectories. As in the previous section, the learning phase for the PPC rapidly converges to the specialization of the two maps thanks to the ACC error-learning processing. Meanwhile, the PFC learns the temporal organization of the PPC outputs based on their sequential order, Fig. 4.19 A. We do not give to the PFC any information about length, the number of patterns or the order of the sequence. Besides, each firing neuron reinforces its links with the current pre-synaptic neurons ; see the raster plot in Fig. 4.19 B. After the learning phase, each PFC neuron has learned to predict some portion of the sequence based on the past and current PFC activity.

Their saliency to the current sequence is retranscribed in their amplitude level. We plot the activity level of the neurons #10 and #14 respectively in black and red in the second chart. This graph shows that their activity level gradually increases for period intervals of at least ten iterations till their firing. The points to switch are also learned by the network and they are observable when the variance of the neurons' activity level becomes low, which is also seen when the confidence level goes under 0.4 ; which corresponds to the dashed black line in the first chart. For instance, we plot the dynamics of the PPC neurons and of the PFC neurons during such situation in Fig. 4.20 A at time $t = 1653$. The neural dynamics of each map display different patterns and therefore, different decisions. The PPC activates more the neurons of the first map (the neurons with indices below thirteen in blue) whereas the PFC activates more

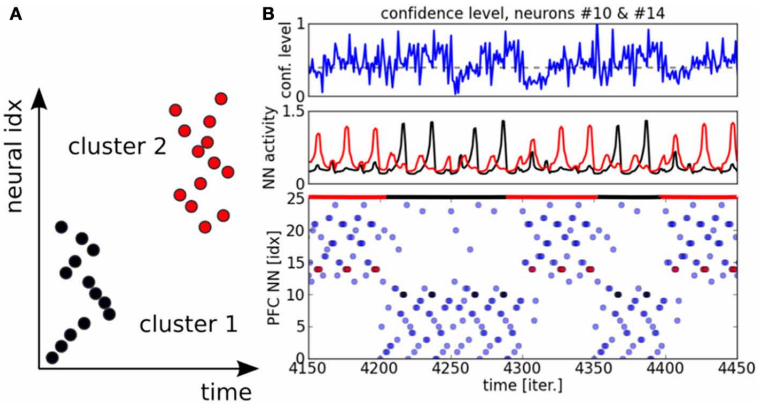

FIGURE 4.19

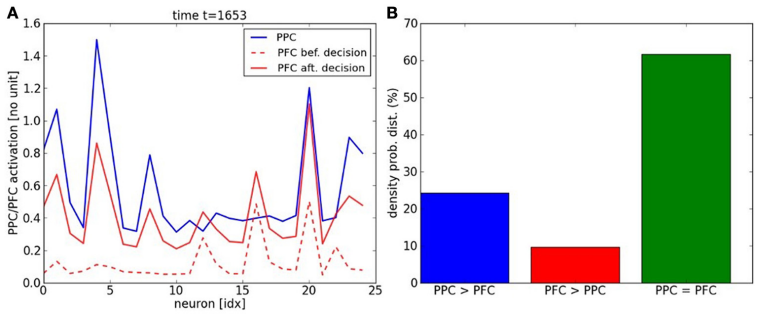

FIGURE 4.20 – Raster plot for PFC neurons. In (A), the PFC learns the particular temporal sequence from PPC outputs and it is sensitive to the temporal order of each unit in the sequence. In (B) on the top chart, the confidence level on the incoming signals from the PPC is plotted. The char in the middle displays the neural activity for two neurons from the two distinct clusters. The neuron #10 in black (resp. cluster #1) and the neuron #14 in red (resp. cluster #2). The raster plot of the whole system is plotted in the chart below.

the neurons of the second map (the neurons with indices above thirteen in dashed red). This shows that the PFC is not a purely passive system driven by the current activity in PPC/ACC. Besides, it learns also to predict the future events based on its past activity. The PFC fuses the two systems in its dynamics, and this is why it generates here a noisy output distribution due to the conflicting signals. We plot in Fig. 4.20 B the influence of PPC on the PFC dynamics. In 60% of the cases, the two systems agree to predict the current dynamics. This corresponds to the case of an automatic response when familiar dynamics are predicted. During conflicts, a prediction error is done by one of the two systems and in more cases the PPC dynamics, modulated by ACC, overwrite the values of the PFC units (blue bar). This situation occurs during a task switch for instance. At reverse, when PFC elicites its own values with respect to PPC (red bar), this situation occurs more when there is ambiguous sensory information that can be overpassed.

In order to understand better the decision-making process within the PFC map, we display in Fig. 4.21 A,B the temporal integration done dynamically at each iteration within the network. Temporal integration means the process of summing the weights in Equation 2 at each iteration with respect to the current order. If the sequence order is well recognized, then the neuron's va-

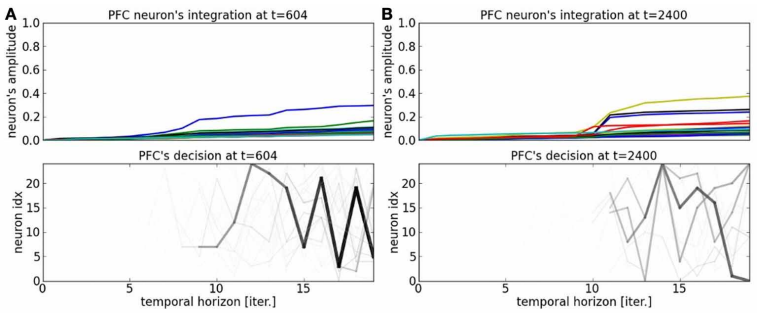

FIGURE 4.21 – PFC neuron's integration at time $t = 604$ and $t = 2400$. (A) Depending on the current situation, a neuron will be more selective to one part of the sequence or to another. The earlier a sequence is detected, the farther the prediction of the trajectory. (B) At bifurcation points, the trajectories are fuzzier and several patterns are elicited.

lue goes high very rapidly, otherwise its value remains to a low value. As we explained it in the previous paragraph, each neuron is sensitive to certain patterns in the current sequence based on the synaptic links within the recurrent network. This is translated in the graph by the integration of bigger values. The spatio-temporal sequences they correspond to are darkened proportionally to their activation level. The higher is the activation level integration during the integration period, the faster is the anticipation of the sequence. We present the cases for a unambiguous pattern in Fig. 4.21 A and for an ambiguous sequence activity in Fig. 4.21 B. The case for a salient sequence recognition in Fig. 4.21 A indicates that the current part of the sequence is well estimated by at least one neuron, the winning neuron, which predicts well the sequence over twenty steps in advance, see the chart below. In comparison, the dynamics in Fig. 4.21 B show a more uniform probability distribution. This situation arises when a bifurcation point is near in the sequence, it indicates that the system cannot predict correctly the next steps of the sequence. Considering the decision-making process per se, there is not a strict competition between the neurons, however, each neuron promotes one spatio-temporal sequence and one probability distribution. Therefore, we have within the system 25 spatio-temporal trajectories embedded. Based on the current situation, some neurons will detect better one portion of the sequence than others and the probability distribution will be updated in consequence to chain the actions sequentially, whereas other portions will collapse. The decision-making looks therefore similar to a self-organization process. At this point, no inhibitory system has been implemented directly in PFC that would avoid a conflict in the sequence order. Instead, the PFC integrates the PPC signals with the ACC error signals. The temporal sequences done in the PPC to avoid the errors at the next moves are learned little by little by reinforcement in the PFC. These sequences become strategies for error avoidance and explorative search. Over time, they learn the prediction of reward and the prediction of errors Schultz et al. [1997], Schultz [2000].

We perform some functional analysis on the PFC network in Figure 12. The connectivity circle in Fig. 4.22 A can permit to visualize the functional organization of the network at the neurons' level. We subdivide the PFC network into two submaps corresponding to the task dynamics in blue and red. We draw the strong intra-map connections between the neurons in the same color to their corresponding sub-maps as well as the strong inter-map connections between neurons of each map. Each neuron has a different connectivity in the network and the more it has connection the more it is central in the network. These neurons propagate information within

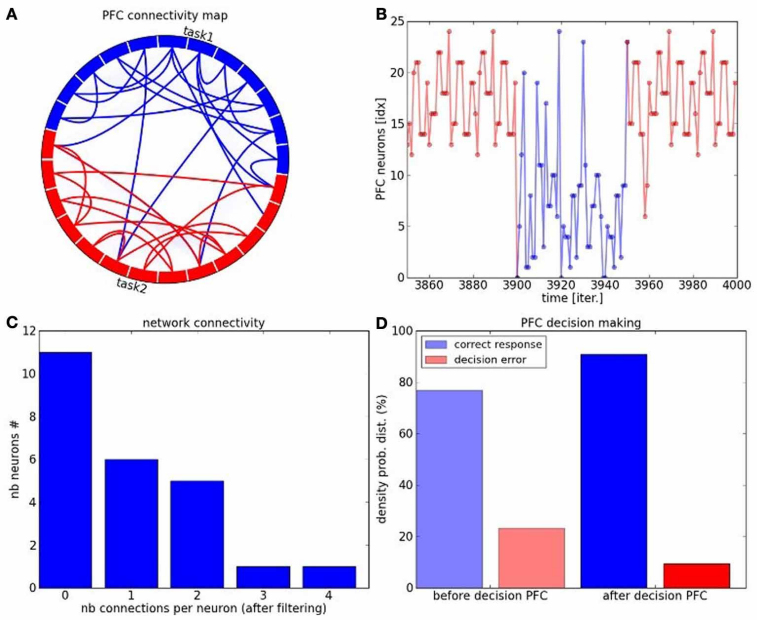

FIGURE 4.22 – PFC network analysis. (A) Connectivity circle for the neurons of the PFC map. In blue are displayed the neurons belonging to cluster 1 and in red are displayed the neurons belonging to cluster 2. The number of links within each cluster (intra-map connectivity) is higher than the number of links between them (inter-map connectivity). Moreover, the number of highly connected neurons is also weak. these charateristic replicate the ones of complex systems and of small-world networks in particular. (B) Task switch is done through these hub-like neurons which can direct the trajectory from one or the other task. (C) The connectivity level per neurons within the network follows a logarithmic curve typical of complex networks, where the mostly connected neurons are also the fewer and the most critical with 4 distant connections. (D) The PFC network contributes to enhance the decision-making process in comparison to the PPC-ACC system due to the learning of the temporal sequence and to its better organization.

and between the sub-maps, see Fig. 4.22 B. In complex systems terms, they are hub-like neurons from which different trajectories can be elicited. In decision-making, they are critical points for changing task. The density probability distribution plotted in Fig. 4.22 C shows that the maximum number of connections per neuron with strong synaptic weights reaches the number of four connections.

Their number drastically diminishes with respect to the number of connections and their trend follows a logarithmic curve. These characteristics correspond the properties of small-world and scale-free networks. In Fig. 4.22 D, we analyze the performance of the overall system when the PFC is added. The decision-making done in the PFC permits to decrease the error by a factor two : ten percents error in comparison to experiment 2. The prediction done in the recurrent map shows that the PFC is well organized to anticipate rewards and also task switch.

Discussion

The ability to learn the structure of actions and to select on the fly the proper one given the current task is one great leap in infants cognition. During development, infants learn to differentiate their motor behaviors relative to various contexts by exploring and identifying the correct struc-

tures of causes and effects that they can perform by trial and errors. This behavior corresponds to an intrinsic motivation, a mechanism that is argued to drive cognitive development. Besides, Karen Adolph emphasizes the idea of "learning-to-learn" in motor development, an expression akin to Harlow that appears in line with the one of intrinsic motivation. She proposes that two learning mechanisms embody this concept during the development of the motor system—, respectively an associative memory and a category-based memory,– and that the combination of these two learning systems is involved in this capacity of learning-to-learn. Braun et al. [2010] foster a similar concept and suggest that motor categorization requires 1) a critic for learning the structure, i.e., an error-based system, and 2) a learning system that will learn the conditional relationships between the incoming variables ; which means, the parameters of the task. They argue that once these parameters are found, it is easier to transfer knowledge from one initial task to many others. All-in-all, we believe that these different concepts on structural learning are important to scaffold motor development and to have intrinsic motivation in one system. Thus the question arises what are the neural mechanisms involved in structural learning and in flexible behaviors ?

To investigate this question, we have modeled an architecture that attempts to replicate the functional organization of the fronto-parietal structures, namely, a sensorimotor mapping system, an error-processing system and a reward predictor Platt and Glimcher [1999], Westendorff et al. [2010]. The fronto-parietal cortices are involved in activities related to observations of alternatives and to action planning, and the anterior cyngulate cortex is a part of this decision-making network. Each of these neural systems contribute to one functional part of it. The ACC system is processing the error-negativity reward to the PPC maps for specialization and to the PFC network for reward prediction. The PPC network organizes the sensorimotor mapping for different tasks whereas the PFC learns the spatio-temporal patterns during the act. In particular, the PPC is organized around the mechanism of gain-modulation where the gain-fields neurons combine the sensory inputs from each other. We suggest that the mechanism of gain-modulation can implement the idea of structural learning in motor tasks proposed by Braun and Wolpert Braun et al. [2009], Braun et al. [2010]. In their framework, the gain-field neurons can be seen as basis functions and as the parameters of the learning problem. It is interesting to note that Braun and al. make a parallel with the bayesian framework, which has been also proposed to describe the gain-field mechanism. For instance, Deneve explains the computational capabilities of gain-fields in the context of the bayesian framework to efficiently represent the joint distribution of a set of random variables Deneve and Pouget [2004].

Parallely, we used three specific intrinsic mechanisms for enhancing structural learning : the rank-order coding algorithm, the cortical plasticity and an error-based reward. For instance, the rank-order coding algorithm was used to emulate efficiently the so-called spike timing-dependent plasticity to learn spatio-temporal sequences in a recurrent network Bi and Poo [1998], Abbott and Nelson [2000]. The PFC system exploits their properties for self-organizing itself by learning the sequences of each task as well as the switch points. PFC neurons learn specific trajectories and at each iteration, a competition process is at work to promote the new steps of the ongoing sequence. Besides, cortical plasticity was modeled in PPC maps with an activity-dependent learning mechanism that promotes the rapid learning of novel (experienced-based) tasks and the stabilization of the old ones. An advantageous side-effect of this mechanism is that PPC neurons become context-dependent, which is a behavior observed also in the reaching neurons of the parieto-motor system, the so-called mirror neurons Gallese et al. [1996], Bro-

zovic et al. [2007]. The results found on cortical plasticity are in line with observations on the rapid adaptation of the body image and of the motor control. Wolpert observed that the motor system incorporates a slow learning mechanism along a fast one for the rapid formation of task sets Wolpert and Flanagan [2010]. The cortical plasticity is also influenced by an error-based system in ACC that reshape the PPC dynamics with respect to the task. The negative reward permits to inhibit the wrong dynamics but not to elicite the correct ones. Those ones are gradually found by trial and errors, which replicate an exploration process.

We believe that these different mechanisms are important for incremental learning and intrinsic motivation. However, many gaps remain. For instance, a truly adaptive system should show more flexibility during familiar situations than during unfamiliar ones. Retranscribed from Adolph and Joh [2005], a key to flexibility is (1) to refrain from forming automatic responses and (2) to identify the critical features that allow online problem solving to occur. This ability is still missing in current robots. In the context of problem solving in tool-use, Fagard and O'Regan emphasizes the similar difficulty for infants to use a stick for reaching a toy. They also observe that below a certain age, attention is limited to one object only as they just cannot "hold in mind" the main goal in order to perform one subgoal Fagard et al. [2012], Rat-Fischer et al. [ress]. Above this period, however, Fagard and O'Regan observe an abrupt transition in their behaviors when they became capable to relate two actions at a time, to plan consecutive actions and to use recursion. They hypothesize that after 16 months, infants are able to enlarge their focus of attention to two objects simultaneously and to "bufferize" the main goal. We make a parallel with the works of Koechlin and colleagues Koechlin et al. [2003], Collins and Koechlin [2012] who attribute a monitoring role to the frontal cortex for maintaining the working memory relative to the current tasks and for prospecting the different action sequences or episodic memories Koechlin and Summerfield [2007], which will be our next steps.

Free-Energy Optimization for Generating and Retrieving Long-Range Spatio-Temporal Patterns in Recurrent Networks

Introduction

In the motor domain, Wolpert and colleagues propose that the brain learns the causal structure in sensorimotor circuits (e.g., the hidden parameters of a sensorimotor task) to perform then action sequences assembled online based on contextual signals from the environment e.g. for coordinate transform or embodied simulation Kording and Wolpert [2006]; Orban and Wolpert [2011]. For these examples, it is argued that the causal structure is encoded directly within the neural representations of cognitive chunks or motor primitives that a working memory can access further to explore and construct off-the-shelf satisfying neuronal chains with respect to the context. This adaptivity in the adult brain and human behavior is hypothesized to be constructed slowly during infant development as Piaget and the tenants of the embodied approach of cognition proposed it Thelen and Smith [1995]. This rises difficult questions on how to learn low-level sensorimotor neuronal rules with causal reasoning capabilities ? How to explore the different alternatives in the perceptuo-motor space given a specific context ? How to initiate flexible yet goal-directed chains of causation (active causation) van Hateren [2015] ?

One candidate mechanism for flexible neural coordination is synchrony. At the neural level, experimental and modelling studies have shown that spiking recurrent neural networks (RNN) can encode temporal relationships by strengthening the synaptic connections between neurons. However, the control of the neurons' spikes at the millisecond order to propagate information is non-trivial : the spontaneous activity within the network rapidly perturbs the neural dynamics and it is rather difficult then to maintain any stability for controlling long-range synchrony. As a novel idea, we envision the coordination of the spikes' trains as an optimization problem and instead of controlling directly the firing time of the neurons (i.e., the probability of the neuron to fire or not at a specific timing), we propose to control rather the neurons' sub-threshold activity (i.e., to find which input value can generate a spike at a specified time). Making an analogy with the butterfly effect in chaos theory, we propose that the tiny control of the neurons' sub-threshold activity can permit to drive at the mesoscopic scale the spikes' synchrony ; Tsuda et al. [2004]; Kelso [1995]; Rabinovich et al. [2006].

For this, we propose to use an optimization technique (a reinforcement signal) to drive the neurons' sub-threshold activity toward a targeting goal ; by looping this process several time, we expect the emergence of long-range neural sequences from largely unstructured spiking recurrent neural networks ; see Fig 4.23 a). This idea is in line with recent proposals, Rajan et al. [2016] and Rueckert et al. [2016], that use also semi-structured recurrent network models for planning. In comparison to them, we extend their results by adding a second structure along with the recurrent network, an associative map (AM), that will recursively and timely control it ; see Fig 4.23 b). We will show that our coupled system can generate long temporal sequences of spikes in a dynamic and robust way recursively. We introduce our model as a neural mechanism based on *Iterative Free-Energy Optimization for Recurrent Neural Networks*, which is the anagram of INFERNO. Moreover, this architecture is supported by several proposals and observations that consider the functional organization between the cortex with the sub-cortical regions (the basal ganglia) ; c.f. Seger and Miller [2010]; Guthrie et al. [2013]; Topalidou and Rougier [2015]; Miller [2015]; Benedek et al. [2016]; Koechlin [2016].

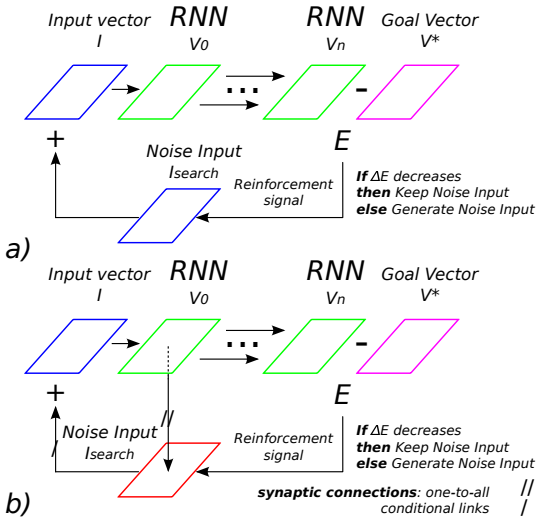

FIGURE 4.23 – Optimization technique used to control a recurrent spiking neural network. a) Model-free reinforcement signal controls the input vector I_{search} of RNN by comparing its output vector V_n at time $t = n$ with respect to a goal vector V^* : as E is diminishing, the descent gradient stochastically converges to the optimal input vector $I_{search} = I^*$ that generates V^*. b) Model-based reinforcement signal, $I_{search} = I^*$ is learned by an associative map and reinjected for any specific V_0.

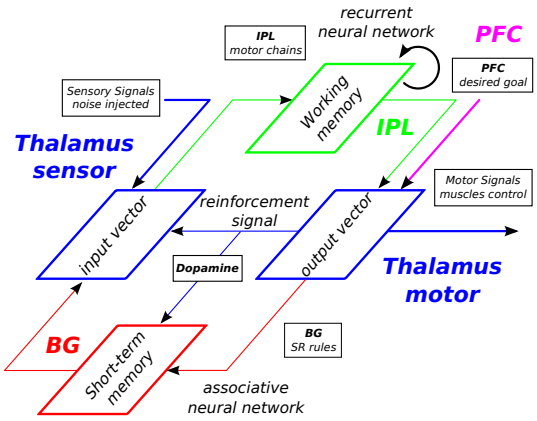

FIGURE 4.24 – Neural architecture INFERNO for Iterative Free-Energy Optimization of Recurrent Neural Networks. This architecture is a model-free reinforcement learning for exploratory behaviors in a recurrent working memory (WM) of spiking neurons and model-based reinforcement learning in a short-term memory (STM) with reward signal. The former memory model corresponds to the Inferior Parietal Lobe (IPL) where motor chains are assembled dynamically. The later memory model corresponds to the Basal Ganglia (BG) where simple signal-responser rules are learned by an associative map (AM) to trigger one spatio-temporal sequence into the working memory. The frontal cortex (PFC) provides the targeting signal to the IPL and BG. The dopaminergic signal supervises both the exploratory search in the WM and the learning in the STM when the goal has been retrieved. RNNs, once unfolded in time, can be seen as a virtually deep feedforward network in which all the layers share the same weights LeCun et al. [2015]. The reinforcement signal on the output dynamics can serve to control the input dynamics with noise to search stochastically the inputs that diminish the error to the output dynamics.

For instance, Miller [2015] proposes that the flexible processing of contextual situation done in the neo-cortex (CX) is driven by a sub-cortical controller, the basal gangial (BG), toward a targeting goal provided by the prefrontal cortex (PFC). We will discuss about the revelance of our model based on neurobiological considerations in the next section.

In order to demonstrate the capabilities of our model for recursivity and boot-strapping capabilities, we will design several experimental setups for habit learning (top-down control) and retrieval phases (bottom-up self-organization) of spiking neurons sequences, and its application to sequential planning of arm movements. We will discuss then the relevance of our model with respect to neurobiological data, its computational power for robotics and AI, neuromorphic hardware implementations, and its affiliation to certain computational principles of the brain proposed by Friston et al. [2009]; Eliasmith et al. [2012]; Graves et al. [2014]; LeCun et al. [2015].

Neurocomputational considerations and other models

The computational architecture that we have briefly described in Figs 4.23 and 4.24 has some neurobiological fundations. At the brain level, one cortical area found important for processing neural chains is the Parietal cortex that includes the Post-Parietal Cortex (PPC) and the Intra-Parietal Lobe (IPL). These structures are hypothesized to form a working memory of action-perception rules Pezzulo and Cisek [2016]. For instance, some experiments show that they serve for embodied simulation like mental rotation or coordinate transformation Andersen and Buneo [2002]; Cohen and Andersen [2002] and for retrieving/generating spatio-temporal sequences Chang et al. [2009]; Cui and Andersen [2009]. Recently, they have been identified to serve for sequence generation Rajan et al. [2016] and for self-generated thought Benedek et al. [2016].

In line with these proposals, we see the spiking RNN in our framework to play the role of the IPL working memory, the associative map to play the role of BG, the PFC to provide the goal task and the reinforcement signal to correspond to a dopaminergic signal ; see Fig 4.24. Following this, the IPL cortical neuronal chains can be assembled dynamically and recursively toward higher-level actions and functions depending on the targeting goal furnished by other brain structures, supposedly the Pre-Frontal Cortex (PFC) and the Basal Ganglia (BG). This architecture appears important for reaching and grasping Andersen and Cui [2009]; Chersi et al. [2011], arithmetic operations Miller [2015]; Buschman and Miller [2014] as well as language formation. For instance, in the language domain, lexical chains are hypothesized to be constructed dynamically based on a global context and a set of grammatical rules.

Our computational model of IPL-PFC-BG loop captures some of the features of Daw's model for the representation of complex tasks Daw et al. [2005]; Miller [2015], which embeds in turn some ideas found in classical symbolic AI about tree-search algorithms. As explained by Miller [2015], *"at each state, one can choose between one of many different responses, each of which leads to a new state : In this view, behaviour can be modelled as starting at the top-most 'node' in the tree, choosing a response 'branch', entering a new state, choosing another response, and so on until one has completed the task (hopefully resulting in a reward)"*. Here, branching is done by BG, entering a new state in the cortical working memory until completion of the task given by PFC using a Dopaminergic reinforcement signal.

Moreover, our model is greatly in line with recurrent spiking neural network models using reinforcement signals for sequential planning Rueckert et al. [2016] and Rajan et al. [2016]. Its

capabilities to boot-strap clusters recursively and to retrieve ordinal sequences make it compatible also with reservoir computing methods Verstraeten et al. [2007]; Mannella and Baldassare [2015] such as the echo-state networks Hinaut et al. [2013], RNNPB Tani et al. [2004] or the dynamical neural fields Sandamirskaya and Schoner [2010]. Its properties to assemble dynamically neural chunks remind further Genetic Programming optimization of neural networks like NEAT and others Stanley and Miikkulainen [2009].

Interestingly, once unfolded in time, its structure can be seen also as a virtually deep feed-forward network in which all the layers share the same weights LeCun et al. [2015]. Rolfe and LeCun proposed an architecture similar called DrSAE, in which auto-encoders evaluate and minimize the function given by the recurrent map Rolfe and LeCun [2013]. The INFERNO architecture combines a self-organized structure (IPL) with a supervised one (BG) as the DrSAE architecture. Here, the reinforcement signal on the output dynamics can serve to control the input dynamics to search stochastically the inputs that diminish the error.

This stochastic descent gradient that we employed in RNN can remind the accumulation of evidences process sampled continuously over time of the LIP neurons Gold and Shadlen [2001, 2007]; Rorie et al. [1997]. These neurons show ramping responses infering latent decision making so that the better the evidence, the larger the amplitude. The decision making can be seen as a random fluctuation Wiener process pressured by time constraints and decision thresholds Diederich and Oswald [2014].

Methods

Neural Units and STDP-like Algorithm

We used in the recurrent neural network a variant of the Hebbian equations, the Rank-Order Coding (ROC) algorithm, which grasps well the structure of the Spike Timing-Dependent Plasticity algorithm and of the classical Delta rule in the spatio-temporal domain Thorpe et al. [2001].

STDP has been discovered to modulate the neural activity of temporally related neurons in many brain regions by reinforcing their links. The Rank-Order Coding algorithm has been proposed by Thorpe and colleagues as a discrete and faster model of the derivative integrate-and-fire neuron and of the standard STDP reinforcement learning algorithm Van Rullen and Thorpe [2002]. The rationale is that ROC neurons are sensitive to the sequential order of the incoming signals ; that is, their *rank code*. The distance similarity to this code, say $rank(x)$ –, which corresponds to the *argsort* function in Matlab,– is transformed into an amplitude value by the function $f(x) = \frac{1}{rank(x)}$.

A scalar product between the input's rank code with the synaptic weights furnishes then a distance measure and the activity level of the neuron. If the rank code of the input signal matches perfectly the one of the synaptic weights, then the neuron fully integrates this activity over time and fires. At contrary, if the rank coding of the signal vector does not match properly the ordinal sequence of the synaptic weights, then integration is weak and the neuron discharges proportionally to it. To this respect, this mechanism captures the intrinsic property of cortical spiking neurons.

The neurons' output V is computed by multiplying the rank order of the sensory signal vector x, $f(x) = \frac{1}{rank(x)}$, by the synaptic weights w ; $w \in [0, 1]$. For an input vector signal I of dimension M and for a population of N neurons (M afferent synapses), we have :

$$V_{n \in N} = \sum_{m \in M} \frac{1}{rank(I_m)} w_{m,n} \tag{4.28}$$

The updating rule of the neurons' weights is similar to the winner-takes-all learning algorithm of Kohonen's self-organizing maps Kohonen [1982]. For the best neuron win and for each element m of the current input signal I with $m \in M$, we have :

$$\begin{aligned} w_{m,win}(t+1) &= w_{m,win}(t) + \epsilon \Delta w_{m,win}, \\ \Delta w_{m,win} &= \frac{1}{rank(I_m)} - w_{m,win}. \end{aligned} \tag{4.29}$$

with ϵ the learning rate equals to 0.01 in our experiments.

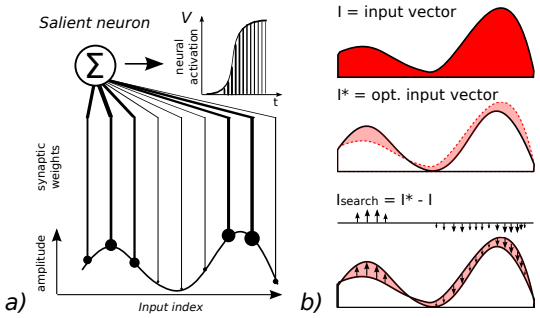

FIGURE 4.25 – Spike optimization. We can consider the control of the amplitude level V of one neuron as an optimization problem. a) For one input vector I for which a neuron is the most responsive, we have $I = I^*$ and $V = V^*$. b) Controlling the amplitude level V of that neuron requires to find for any input I, the input error vector I_{search} that satisfies $I_{search} = I^* - I$. The exploration of I_{search} can be done by stochastic gradient descent and meta-heuristics methods. This optimization technique can be applied and extended at a neural population-level.

Free-Energy Optimization Mechanism

Viewed as an optimization problem, the control of the RNN dynamics consists on retrieving the most salient inputs that will trigger the neural units to specific amplitude values. This is an inverse problem and can be solved with a gradient descent. In order to explain better the mechanism behind, we can reduce the control of the RNN dynamics to its simplest case with the controlling of one neuron solely, see Fig 4.23 a) and Fig 4.25 a-b).

If we consider I^* to be the optimal input signal from which one neuron will fire the most at $V = V^*$ using eq. 4.28, one heuristic will consist on searching the term I_{search} to be added to the current input dynamics I so that we can have $I + I_{search} = I^*$ and the neuron will reach $V = V^*$, see Fig 4.25 b) with I_{search} shaded in light red. As a meta-heuristic method, retrieving I_{search} can be done with a stochastic gradient descent (greedy search) by injecting some noise to I while using V as a metric distance : any intrinsic noise that diminishes the error E to the desired goal V^* is reinforced and kept (exploitation), or otherwise forgotten to select another random vector Ie (exploration). This optimization technique can be extended to a population of neurons and applied to distant rewards, in these cases the terms I, I_{search}, E and V are vectors.

The number of iterations necessary for the WM to converge is not taken into account, therefore the recurrent map will explore several solutions in an unlimited amount of time till convergence. One common solution is to use a threshold value to stop the search. This problem is known in neuroscience as the credit assignement problem Izhikevich [2007] : to which particular past event shall we assign credit for the current reward received ?

In its present form, the reinforcement signal algorithm corresponds in AI to a classical metaheuristic method with random walks, which does no prevent from local minima. It may correspond in neurocomputational theory to dopaminergic modulation and to model-free reinforcement learning Barto and Sutton [1997]. However, it does not take into account more sophisticated types of signals, which could be given further by other types of neuromodulators Doya [2002].

TABLE 4.1 – Free-energy optimization based on stochastic gradient descent to minimize prediction error.

Code Lines	Stochastic optimization as Accumulation Evidences Process	
#01	At time $t = 0$, initialize V, V^*, I	
#02	choose randomly I_{search}	
#03	compute $V_{search}(t)$ from $V(t)$, $I + I_{search}$	
#04	**While** $t \leq$ *horizon_time*, repeat :	Prediction error E on the output vector
#05	compute $V_{search}(t+1)$ from $V_{search}(t)$	
#06	**If** $V^* - V \geq V^* - V_{search}(t+1)$:	
#07	$I = I + I_{search}$	
#08	$V = V_{search}$	
#09	**break**	
#10	$t = t + 1$	
#11	**Goto** #02	

V is used as a reinforcement signal to control the level of noise I_{search} to inject in the input dynamics I in order to explore local or global minima toward V^*.

Recurrent Network Model

The neural architecture consists of one recurrent neural network arranged as in Fig 4.23 a). The neurons in the recurrent map ($N = 25$ neurons) encode a temporal sequence directly from their feeded back activity. The temporal horizon H for each synaptic link is defined to be of $H = 20$ iterations max ($1\,ms$ corresponds to 1 cycle), which is therefore the maximum possible time length to be encoded by any synaptic link. Its value is chosen with respect to the average synaptic time found in the neurons of the cortical maps, about $50\,ms$ Abbott and Nelson [2000]. The network is implemented as a buffer of dimension $[H \times N] = [20 \times 25]$ so that each neuron n integrates with the synaptic weights $w_{m,n}$ and the function $f(BUFFER[m])$ with $m \in M$ and $M = [HN]$ to generate the output value V_n. To force the network to be recursive, we update at each iteration the buffer by shifting at each iteration the rows to have $h(x+1) \leftarrow h(x)$ and by adding to the first row of the buffer at $h = 0$, the latest update of the neural activity V_n. Now, in order to inject external inputs I to the recurrent network, the neural population V_n receives

an input vector of same dimension I_n added to the first row of the buffer and *only* at $h = 0$ and weighted by 0.5 ; $V_n = \sum f(BUFFER)w_{m,n} + 0.5 * I_n$. The function f is the inverse function as explained in section 4.3.2.

TABLE 4.2 – Description of the buffer algorithm used to simulate integration over a temporal horizon.

Code Lines	Recurrent Map Buffer to compute temporal horizon
#01	**Compute** V_n, $V_n = \sum_m f(BUFFER)w_{m,n} + 0.5 * I_n$
#02	**Shift** the buffer with $h \in [0, H-1]$, $BUFFER[h+1, n] := BUFFER[h, n]$
#03	**Add** to the first row $h = 0$, $BUFFER[0, n] := V$

The buffer is used to model the recurrent activity of the neural network over time. After each iteration, the buffer that retranscribes the neural activity over time is shifted and presented again to the neural population.

Associative Network Model

The previous section explains how our optimization technique serves to retrieve the optimal I^*_{search} to be added to the current input vector I using the reinforcement signal E, the error signal, in order to reach the desired amplitude value V^*. The optimal signal I^*_{search} found can be learned by an associative layer with perceptrons with all-to-one and one-to-all connections that link the input value I to the associative neurons V_a and these to the output value I^*_{search}, see Fig **??** b). The neurons' equation is similar to the equation of Kohonen neurons with $V_{a \in A} = \sum_{m \in M} g(I_m, w_{m,a})$ (all-to-one connectivity) and $I^*_{search} = \sum_{m \in M} g(V_a, w_{m,a})$ (one-to-all connectivity), where

$$g(x, y) = \frac{1}{1 + RMS(x, y)}, \qquad RMS(x, y) = \sqrt{\sum (x - y)^2}. \tag{4.30}$$

The weights of the associative neurons are updated with respect to the reinforcement signal ΔE in RNN, similar to eq. 4.30 :

$$\begin{aligned} w(t+1) &= w(t) + \epsilon \Delta E \Delta w, \\ \Delta w &= I(t) - w(t), \\ \Delta E &= E(t) - E(t-1). \end{aligned} \tag{4.31}$$

Results

We resume in the table below the different experiments that we have done to present our model. The first experiment corresponds to the study of the RNN optimization along with the stochastic

descent gradient toward goal-driven control. The second experiment presents its application to a 3 degrees-of-freedom robotic arm control. The third experiment shows the AM-RNN coupled system and its capabilities for habit learning ; e.g., for arm postures. The fourth and fifth experiments describe the ability of AM-RNN working memory to generate long-range spatio-temporal learnt sequences, in a flexible way (resp. experiment 4) or in forced fashion (resp. experiment 5).

TABLE 4.3 – Table of the different experimental setups.

Section	Exp.	Architectures	Description of the different experiments done on their corresponding section.
4.3.3 3.1	1	RNN, Optimization control	
4.3.3 3.2	2	RNN, Arm control	
4.3.3 3.4.1	3	AM $\leftrightarrow$ RNN, Habit learning	
4.3.3 3.4.2	4	AM $\leftrightarrow$ RNN, Bottom-up	
4.3.3 3.4.3	5	PFC$\rightarrow$AM$\leftrightarrow$RNN, Top-down	

RNN goal-driven control

In this section, we study solely the RNN, decoupled from the associative map, in order to study its behavior during goal-driven control. We make the recurrent map to learn at first some spatio-temporal rules till convergence of its dynamics for several iterations using the reinforcement mechanism presented in last section. When the neurons' synaptic weights become stable enough after one thousand iterations, the network is ready to be used for testing.

For this, we define a desired output V^* as goal vector and we let the reinforcement signal to drive the search of the input vector I_e from a fixed input vector I chosen arbitrarily and only for the first iteration. We plot in Fig 4.26 the euclidean distance of RNN's output V to the desired output vector V^* for one hundred trials starting with different initial conditions. This first graph shows how well all trajectories of the network are converging to a global minima. This convergence is also rapid as it requires at most 20 iterations to reach to it. We display in Fig 4.27 the raster plot of the neurons' dynamics for the input vector in the top chart and for the output vector. After initial conditions, the input and output vectors converge both rapidly to a stable pattern, for which the neuron 24 is the most active neuron (indicated arrow).

The goal-directed behavior of the working memory is also exemplified in Fig 4.29 a) and b) in which the neurons dynamics at several time step is plotted for the input and output vectors respectively. The super-imposed activity level in black for the input and output vectors corresponds to small variation of the input vector controlled by the reinforcement signal in a) (red line) that induce the convergence of the output dynamics to the desired vector in b) (plain line). We observe that *small* amplitude variation in the input dynamics are well sufficient to make *big* amplitude variation in RNN as the output dynamics in blue gradually converges to the desired goal. This shows that the working memory can be controlled as a dynamical system or a chaotic system and its sensitivity to initial conditions can be used to retrieve any spatio-temporal pattern as it would be for an attractor Tsuda [1991].

In Fig 4.29 we present four raster plots taken from the recurrent map, which all converge to the same neuron spiking, neuron $\#14$ in red at time $t = 20$ iterations, and for a different goal

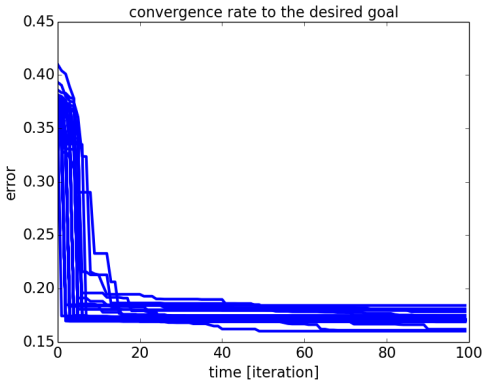

FIGURE 4.26 – RMS convergence to one targeted goal by the RNN for one hundred trials. The amplitude level of the neurons in the RNN converges rapidly to the desired output vector rapidly in dozen iterations ; some solutions found are more precise than others due to local minima.

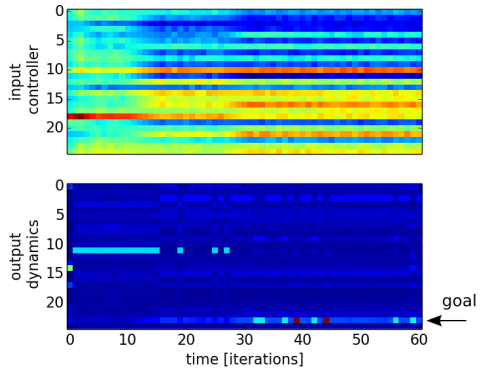

FIGURE 4.27 – Raster plots of the input vectors injected to the RNN and its respective output vector for the first 60 iterations toward a target solution. Following a hill-climbing random walk, we obverse the rapid retrieving by the input controller of the desired RNN's spatio-temporal pattern (a different example of such desired pattern is presented in Fig 4.29).

than in the previous figure. The amplitude level of the recurrent map dynamics for the four maps are different yet they converge all to the triggering of the same neuron. We make the note that the neural activity at the population level is sub-threshold till the activation of the desired neuron at the end. Although the network and the learning process is based on spikes, the inter-dependency among the neurons is enough to produce parallely weak coordinated dynamics, which can have a strong effect.

The causal chaining in the neural network is not straightfoward to observe. We propose therefore to plot the spatio-temporal trajectory within the working memory for ten solutions found ; see Fig4.30. We plot the neural trajectory till reaching the goal vector by selecting at each iteraction the most active neuron. In our example, the goal to reach is the neuron $\#25$ ordered from the time-to-trigger$= 0$ at the most-right of the plot. We make the note that the most active neuron at each iteration is also the most influential for driving the neural activity for the next steps. We can observe from the graph that all trajectories have different lengths, although in average they converge after ten iterations. At the same time, the spatio-temporal trajectories

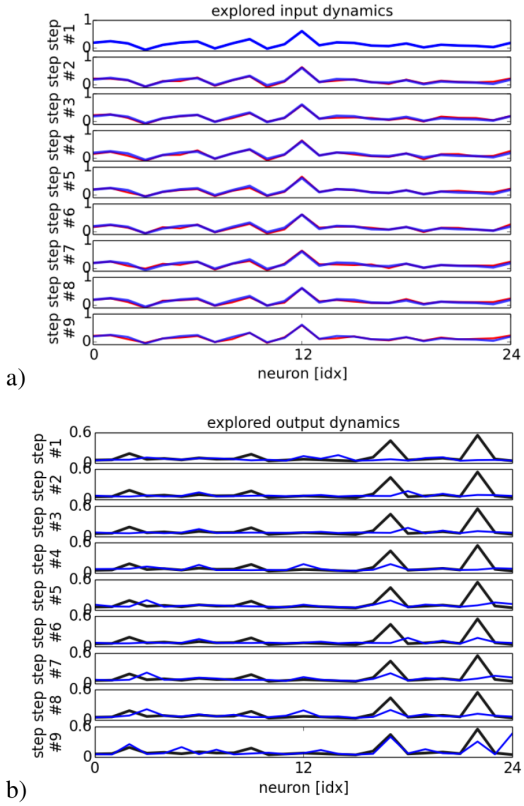

FIGURE 4.28 – Snapshot of the explored input and output's RNN dynamics for the first 10th iterations and their convergence to the desired output values (in black) ; resp. a) and b). The small amplitude variations added in the input dynamics (red line) achieve to induce big output changes in RNN with the triggering of the desired spikes (plain black line).

present some similar patterns within their dynamics placed coherently at the beginning, middle and end of the sequence that we retrieve in different trials. These patterns come from the short-range synaptic rules learned and represent one chunk or one unit that is combined with others to constitute a longer chain, up to sixteen elements in our case. We make the note that these chunks are dynamically assembled and not predefinedly learned, although they present one stable shape.

RNN Arm Control

We use the RNN as a working memory for controlling the motion of a three joint robotic arm in a 2D space, see Fig 4.31 a). We exploit the goal-directed behavior of the recurrent network for sequential planning and for the reaching of five positions in space. The three angles of the robotic arm are coupled to the dynamics of three neurons of the recurrent network with same properties than the one presented in the previous section and the reinforcement signal is simply the euclidean distance of the end-effector to the goal. The neural activity between $[0; 0.1]$ for the three neurons (sub-threshold activity) were renormalized between $[0; 2\pi]$ in radians for each joint angle. The result of the arm trajectory is presented in Fig 4.31 a) and the output dynamics of the neural network is shown respectively in Fig 4.31 b). The network easily retrieves the

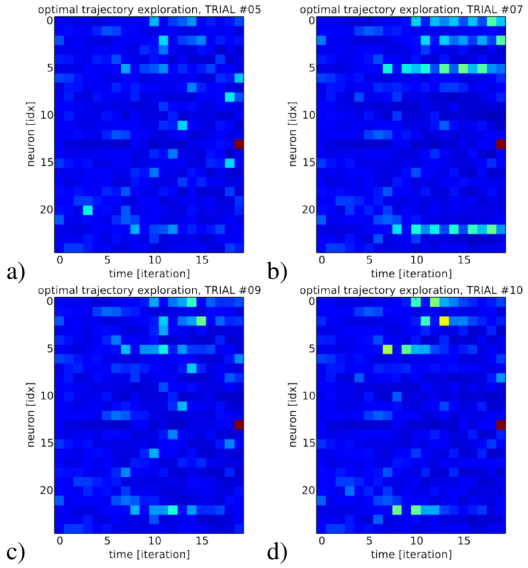

FIGURE 4.29 – Raster plots of four strategies found by the RNN to trigger the firing of neuron $\#14$ in twenty iterations. The four trajectories show some similar sub-threshold patterns although they exhbit also high variabilities, in the temporal delays as well as in the amplitude level.

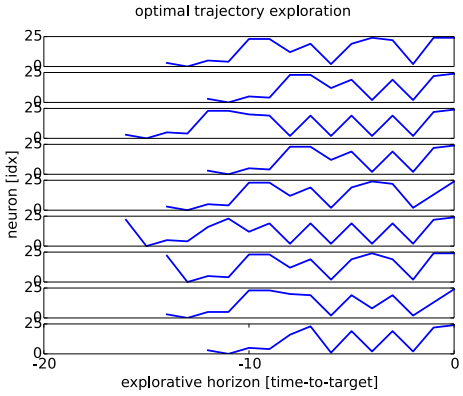

FIGURE 4.30 – Ten trajectories found till triggering of neuron #25. The trajectories are created by picking up at each iteration the most active neuron. The ten trajectories present a mix of neural chunks found in all of them and of novel patterns found solely in them. Each trajectory is retrieved dynamically (novelty) although the solutions appear similar (redundancy) due to the constraint dynamics in RNN.

different positions in several iterations and updates its dynamics exploiting the reinforcement signal.

Spiking Recurrent Network analysis

In order to understand better the organization of the spiking recurrent network, we analyze its functional properties at the population level and its dynamics at the neuron level. First, we analyze the redundant clusters found within the optimal sequences and the processing time neces-

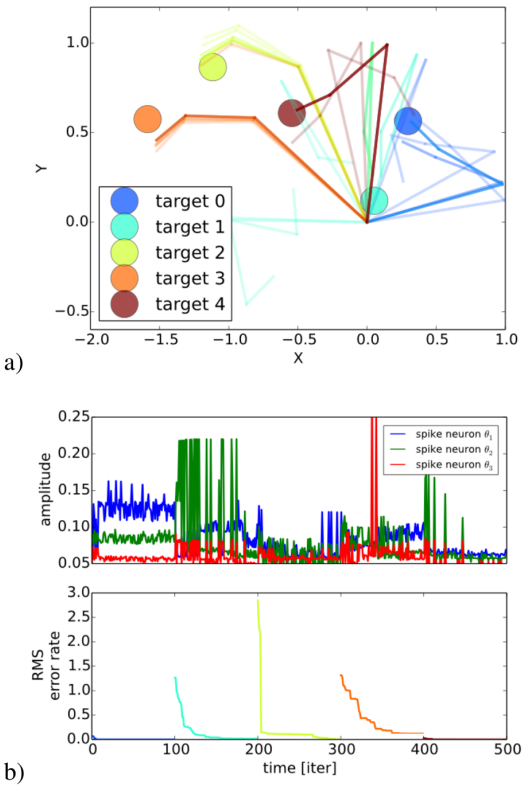

FIGURE 4.31 – Arm control by the recurrent network with a reinforcement signal. a) The three d.o.f. planar robot is controlled by the spiking recurrent neural network for which the amplitude level of three neurons control the three joint angles. b) The euclidian distance to the goal location furnishes a reward to the motor neurons.

sary to discover them as those presented in the previous section, resp. Figs 4.32 a) and b). In Fig 4.32 a), we have counted the occurrence of clusters (neural pairs, triplets, etc...) retrieved for a long period of time during spontaneous activity with respect to their size. These clusters are not orthogonal from each other but are combined into longer-range patterns so that their frequency is inversely proportional to their length ; ordinal neural pairs and triplets are proportionally easier to be triggered and retrieved than longer clusters. Meanwhile, the log-curve histogram and cluster coefficients indicate the hierarchical structure of the sequences, which corresponds to scale-free dynamics and small-world properties of the recurrent network Watts and Strogatz [1998]. Thus, the reaction time necessary to retrieve one goal depends on the problem complexity (e.g., the locking into a local minimum or not) and requires around a dizain of iterations in order to converge.

In Fig 4.32 b), the reaction time depends mostly on the initial conditions of the recurrent network and of the explorative search. For solutions difficult to retrieve, the map requires an explorative search above a dizain of iterations. This variance can be compared with the density probability found in the real IPL neurons during visual search, which show similar trends Gold and Shadlen [2007].

At the neurons level, we measure the probability distribution of the neurons' variance till

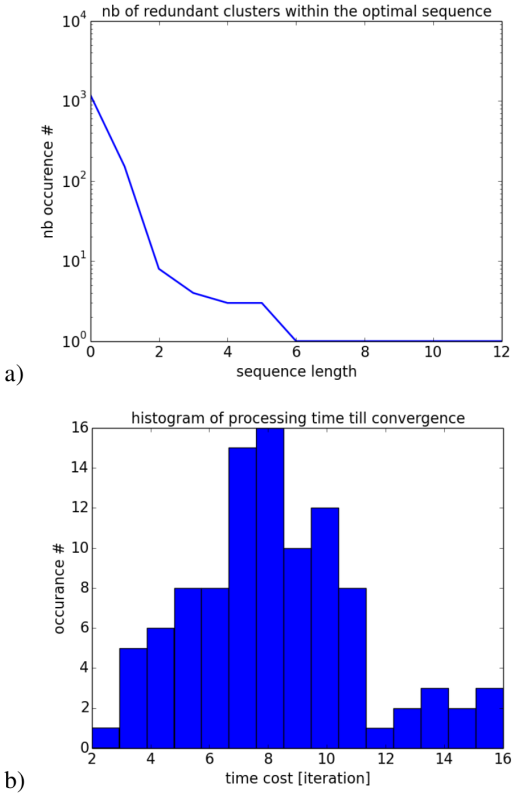

FIGURE 4.32 – Cluster analysis in RNN. In a), number of clusters found within an optimal sequence with respect to their length. This histogram shows that for any optimal sequences, repetitive clusters are found, which are more often present when they are small than big ; this shows some hierarchies within RNN and the property of scale-free dynamics. In b), the average processing time necessary for the RNN to retrieve the goal dynamics. For one hundred trials, it requires in average a dozen of iterations till convergence.

convergence to a desired goal since variance is a hallmark of cognitive activity and of decision maker Gold and Shadlen [2007]. The histogram presents a log-curve distribution with two-third of the neurons with low or weak amplitude variability and one third of the neurons high amplitude variation, see Fig 4.32. This results indicates how exploration is done, having one third of the neurons really effective for the neural map to converge to the output dynamics and to generate a spatio-temporal pattern, whereas the rest of the neurons is not.

It indicates also the neurons' connectivity level within the RNN, or its sparsity. One-third of the neurons interact with each other so that weak amplitude variations in a small set of neurons is enough to interact with another subset and to control its activity. This feature has been emphasized in nonlinear mixed selective neurons Rigotti et al. [2013].

BG-IPL coordination : Recursivity and Bootstrapping

In the previous section, we have investigated the control of a recurrent network by a reinforcement signal mechanism to drive its output dynamics to a desired goal as in Fig 4.23 a). Here, we make to learn this signal by another learning system, an associative memory AM as shown

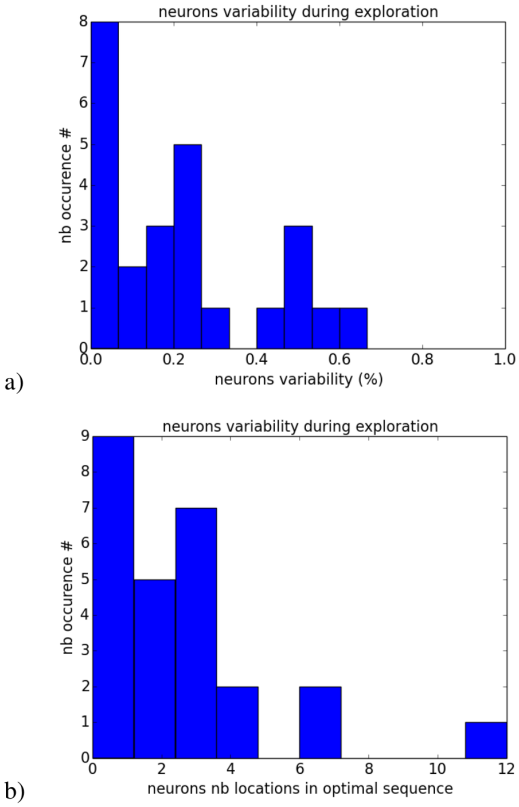

FIGURE 4.33 – Histogram of the neurons variability measured during exploration and their relative position found within the sequence for hundred trials. These graphs attempts to explain how exploration is done. In a) and b), during the solution-search, the two third of the neurons are rapidly placed within the optimal sequence and one third of the neurons are highly variable and can change positions up to twelve locations within the sequence.

in Fig 4.23 b). By learning directly the inputs that produce a high-valued reinfocement signal, we can reduce the exploration phase and boot-strap at the same time the working memory dynamics to the goal trajectory. By doing so, we expect the two interacting learning systems to generate longer spatio-temporal sequences of sub-goals. This schema is assumed to be played by the Basal Ganglia, which learns rapidly simple stimulus-response rules, and the IPL-like RNN, working at a slower temporal rate Daw et al. [2005]. As an analogy with reinforcement learning, it corresponds to learn the rewarding Q-values associated to an action Doya [2002]. In our framework, the Q-values correspond to the activity-level of the AM neurons. This optimization technique in our case can be viewed as model-based reinforcement learning Sutton and Barto [1998].

To resume, we propose here to complete our architecture and to add an associative map AM that learns the RNN's input-output association with respect to the reinforcement signal already used for explorative purpose. The bi-directional coupling between the two systems can be done in two ways to generate longer spatio-temporal sequences : in a self-driven fashion when it is the RNN that controls the AM or in a controlled fashion, when the AM controls tighly the RNN's activity. In our example, this second memory contains twenty neurons so that

each neuron can trigger a specific spatio-temporal sequence of the RNN. These two ways are explained thereinafter.

Habit learning of arm sequence

We propose to re-use the experiment done on arm control in section 4.3.3 but this time for learning the targeting goals with an associative memory during exploration of the IPL-like recurrent network.

We present in Fig 4.34 the averaged learning rate and convergence time when the BG-like associative network is exposed to several presentation of the same goals ; respectively in a) and b). We can observe that the average time interval required by the associative map to make the IPL map to convergence is decreasing for each exposure of the targetting goal : as the BG network is learning, the explorative search done on the IPL dynamics is diminishing over time, see Fig 4.34 a). Sometime however, the error level appears not related to the number of exposure as for the blue curve around iteration 500 for example because we might be in a local minima, which makes the error correction to be slow. Nonetheless, the recurrent network trains the associative network faster and the response time to retrieve any sequence is quicker, see Fig 4.34 b). Without the BG network, the response level would have been slower and similar to the level found at its slowest performance as during the first exposure.

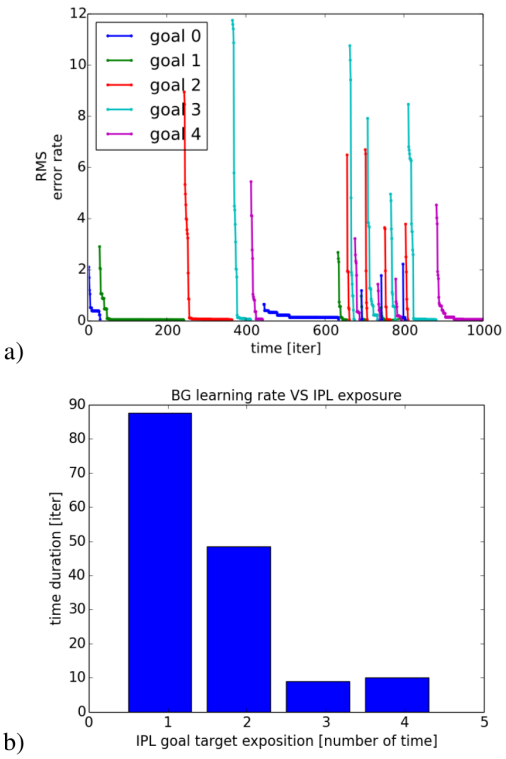

FIGURE 4.34 – BG training by the IPL neural network and convergence rate with respect to the number of exposure of targetting goals. In a), time duration and error rate for the IPL network to reach the assigned goals iteratively (arm posture). In b), as the associative map learns the recurren map inputs, the convergence rate decreases on average with the number of exposure of the goals.

IPL→BG→IPL bottom-up associative recall

When we let the two coupled systems work in an autonomous fashion –, which means that we do not force the activity of one specific BG neuron for example,– the RNN's output activates the most salient neuron in the BG-like network, which recursively controls the RNN's dynamics in return, see Fig 4.35 a). The result is the autonomous recall in a self-organized fashion of spatio-temporal patterns by the BG-like neurons of the exact RNN ordinal sequence –, in our case of thirty steps,– so that when one BG neuron is activated, its corresponding sequence is observed ; e.g., the two same sequences reactivated are super-imposed in red.

As similar to the RNN neurons, the BG-like neurons can form also spatio-temporal sequences to create longer patterns. When the same pair is activated as in Figs 4.35 b) and c) in red and green traces, the slightly same sequences in RNN are reproduced. The activation of these two chunks can be considered as part of one integrated sequence over an interval span of forty steps.

In certain situations, when the two maps have a very stable bi-directional coupling, the coupled systems can generate even longer sequences above 190 iterations, see Fig 4.36. In this figure, the raster plots taken at two different period of time are almost aligned from each other within the black dashed lines. The associative map has generated a sequence over ten neurons.

PFC→BG↔IPL top-down control, forced bootstrapping

Self-driven activity shown in the previous section can generate long range episodes, but can we generate even longer ones by forcing the temporal order of AM neurons activation ? This experiment differs from the previous one in the sense that we externally force the activation of BG-like neurons to fire in a specific order : i.e., we bypass the spontaneous activty of AM neurons and we control the one selected till convergence of RNN to the desired output dynamics, which means till the AM neuron activity is satisfyingly high above a threshold. This role is supposed to be played by the PFC, which can learn the sequential order of the AM BG-like neurons. This feature will not be investigated in this section. At each retrieval of one RNN episodic memory, which can be more or less rapid, the next BG neuron is selected in the sequence when its activity level reaches a threshold value, therefore the temporal interval can fluctuate for each episode. Fig 4.37 presents the forced RNN spatio-temporal sequences at two different temporal intervals for the same serial order activation of the BG neurons. In this figure, the spatio-temporal patterns produced are spaning a very long interval range, over several hundred iterations, which is higher in comparison to the self-driven activity presented previously.

Fig 4.37 presents the activity control of the AM neurons at two different time interval (bottom and top charts). This result shows how the spiking order can be stabilized over long spatio-temporal patterns (200 iterations) even within a recurrent map for the generating of neural chains proper to the configuration of the RNN. The similarity measure computed above is based on a covariation measure to detect the relative temporal displacements between patterns of the two intervals. The BG-like neural system 'replays' or reenacts the neural chains proper to the one learned during action, as described in simulation theory of action representation Gallese [2005].

We can compare the two behaviors of the IPL-BG system by measuring the density probability distribution of the number of clusters found with respect to the clusters' length, when the two maps are bidirectionally coupled and self-driven (section 4.3.3) or when the activity of the BG map is supervised (section 4.3.3).

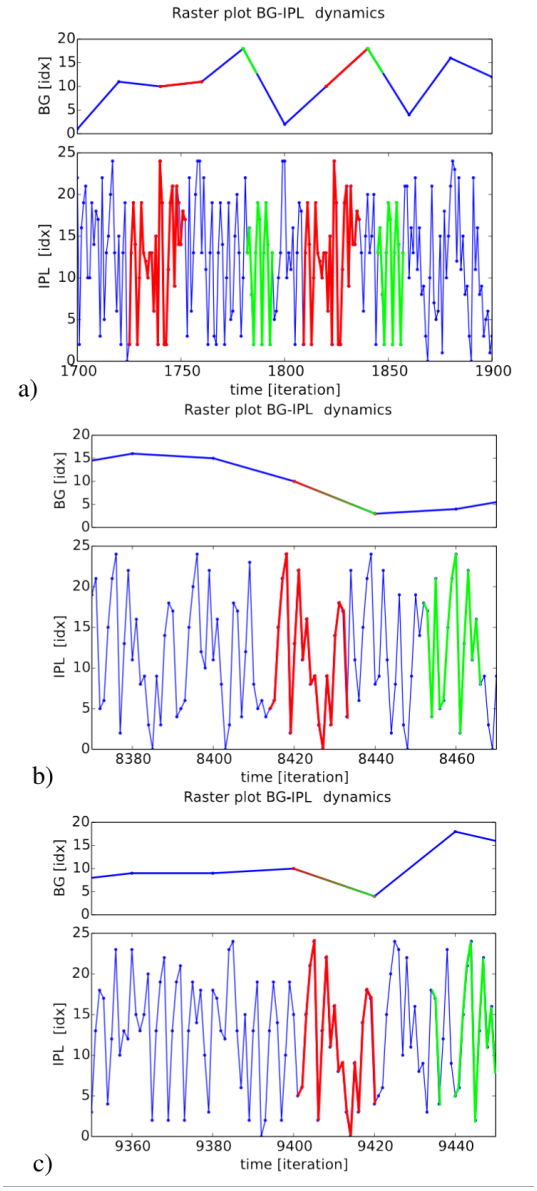

FIGURE 4.35 – Interactive coupling between the recurrent map and the associative map. Each neuron of the BG-like associative memory learns a stimulus-response pattern that triggers a specific spatio-temporal pattern in the IPL-like working memory. In a), we super-imposed in red the RNN dynamics when the AM neuron #10 triggers. Stable spatio-temporal clusters as long as 28 iterations can be retrieved. The BG-like network can bootstrap dynamically the neural population of the IPL-like network. In b) and c), when two consecutive BG pairs are formed –, here the neurons #10 and #3,– the IPL network can form longer sequences although they possess some variability within it ; these longer sequences (40 iterations) are above the temporal horizon of each neuron, which is of 20 iterations.

The Fig 4.38 presents this result with the density probability of the number of clusters found during the self-driven case plotted in blue using the left axis and found during the controlled case plotted in green using the right axis. The two densities present a logarithmic curve of dif-

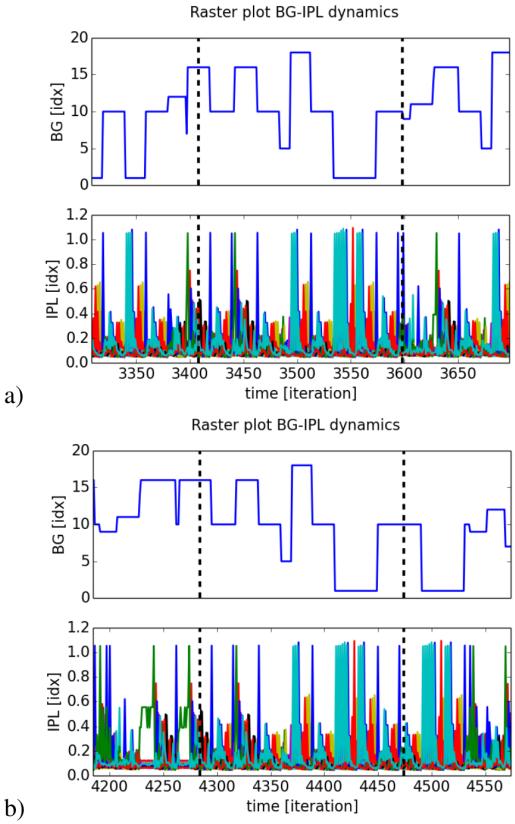

FIGURE 4.36 – Self-driven interaction between RNN and AM. Presentation of the amplitude dynamics of the recurrent map for a sequence length of two hundred iterations between 3420 and 3600 in a), and 4280 and 4460 in b). The amplitude level of the recurrent map is almost similar within the interval of the two dashed lines in black.

ferent magnitude order, the self-organized case in blue can generate long range sequences at most of 180 iterations (below $10^{-2}\%$). In comparison, during the controlled case, for which the order magnitude is ten times higher, the probability of occurrence of one sequence of 180 iterations achieved to be reproduced is below 1%. Although robust, the working memory in the self-driven case present more variability and flexiblity, which is more advantageous in unexpected situations. Besides, the external control of the associative map (green line) limits strongly the variability of RNN dynamics and induces the reproduction of long-range spatio-temporal sequences as noise is reduced.

Discussion

We propose a framework based on a coupled recurrent spiking neuronal system that achieves to perform long sequential planning by controlling the amplitude level of the spiking neurons through reinforcement signals. The coupled system models the cortical and subcortical interaction found between IPL and BG networks for neuronal chaining Chersi et al. [2011] Buschman and Miller [2014]. The control done is weak so that the propagated reinforced signals let the working memory plastic enough to converge to the desired internal states from various trajec-

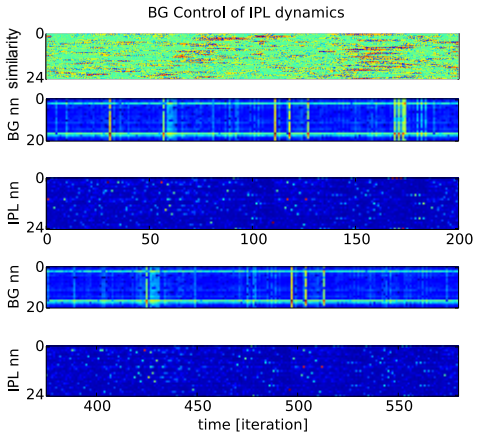

FIGURE 4.37 – Open-loop IPL control by the BG-like neurons following an ordinal sequence. Every twenty iterations corresponding to the temporal horizon of the IPL buffer, the IPL dynamics are bootstrapped from the AM neurons activity. In our example, the same BG sequence is injected to the IPL dynamics for the two raster plots at different period of time. The comparison between the two dynamical systems shows an extreme stability to drive the RNN dynamics over long period of time, even without feedback, see the similarity measure at top.

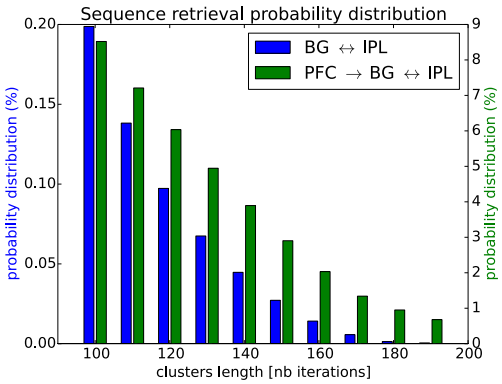

FIGURE 4.38 – Sequence length retrieval during self-driven and forced conditions. We counted the number of temporal sequences found over time and we computed their probability distribution with respect to their length. In the self-driven condition (in blue, left axis) as done in section 4.3.3, the working memory can repeat spatio-temporal sequences of maximum length of 200 iterations, which is already above the limits of a conventional spiking RNN. In the controlled condition (in green, right axis) as done in section 4.3.3, the coupled system can retrieve even longer sequences, ten times more.

tories. Used in a robotic simulation, the neural dynamics can drive a three d.o.f. arm to reach online different locations.

The neural control is done below the neurons' spikes and the sub-threshold amplitude variations injected into the recurrent network can iteratively change its dynamics to make it to converge to attractors or to make it to diverge from repellors. To this respect, our framework embodies some aspects of the free-energy optimization principle proposed by Friston et al. [2009] as an optimization technique and some aspects of chaos control of neural dynamics, like *chaos*

itinerancy Tsuda et al. [2004], in which small feeded back perturbations can give rise to big amplitude variations and permit to go from one memory to another Rabinovich and Varona [2011] Varona and Rabinovich [2016]. At another degree, it conveys also ideas in line with belief propagation and inference in spiking recurrent networks within the Bayesian framework Deneve [2008] in which the iterated computation embedding the exploration/exploitation stages can be seen as an inference process using reinforcement learning. The free energy optimization process has been proposed to drive flexible neural dynamics in a seemingly coherent manner following the Bayesian paradigm Friston [2009]; Pezzulo and Cisek [2016].

The functioning of our architecture is partially similar also to recent proposals for sequence generation by Rajan et al. [2016] and Rueckert et al. [2016], reservoir computing methods by Verstraeten et al. [2007]; Mannella and Baldassare [2015] and to DrSAE model used for classification where auto-encoders iterate a recurrent map using gradient descent Rolfe and LeCun [2013].

The original distinction of our approach with these techniques resides *(1)* on the control of the neurons' amplitude to indirectly control the spikes timing, and *(2)* on the use of an extra memory (BG) that learns to associate the correct input vector to inject to the working memory with respect to its output from a reinforcement signal ; these two features permit to drive the working memory into a desired state. Its computation can be viewed also as a neural 'router' Zylberberg et al. [2011] that makes the recurrent network virtually *deep* : i.e., using the output of the recurrent network as its own entry for processing the next stage LeCun et al. [2015]; Rolfe and LeCun [2013] ; e.g., over 200 iterations of virtual layers in Fig 4.37. For these reasons, the INFERNO compound system has the features of a recurrently deep spiking neural network.

Computational Power. Taking account of the computational power of Rank-Order Coding spiking neurons Thorpe et al. [2001], each neuron can encode 2^N different representations with N their input dimension, in our case $N = M * O$, with $M = 25$ the size of the neurons' population and $O = 20$ the temporal horizon of each neuron (i.e., fixed by the buffer length). Besides, each neuron of the associative memory encodes virtually only one trajectory of the recurrent map as a stimulus-response rule ; in our case the number of neurons in the associative map is $L = 20$. Therefore, the maximum theoretical length for a spatio-temporal pattern possible to retrieve is equal to $L * O$, which is in our case of 400 iterations (or layers). These orders are empirical, however, adding more AM neurons should highly increase the length of RNN sequences produced and the number of possible combinations.

Subsumed and complementary systems. As there is evidence that suggests that although single actions can be selected without basal ganglia involvement, chains of actions seem to require the basal ganglia Jaeger et al. [1993]. The BG with the parietal cortex are found both complementary for action planning Chersi et al. [2011]; Mannella and Baldassare [2015]; Platt and Glimcher [1999], motor simulation Gallese [2005] and thought generation Benedek et al. [2016]. The parietal cortex, involved in implementing complex predictive models as multi-step state-action-state maps (model-based RL), and BG (model-free RL) form a cooperative system driving online behavior Topalidou and Rougier [2015]; Gershman et al. [2014]; Koechlin [2016]. The BG network in our model helps to create long neuronal chains dynamically in the IPL working memory while the IPL working memory trains the BG network.

The numerical limit to subsume new memory maps, one layer at the top of another, is not clear in our model but a third complementary memory, the PFC, can play this role by learning and directing the BG sequences at a higher-level. In our model, we have limited the function

of PFC to provide one goal at a time so that AM sequences can be formed dynamically in a self-organized fashion along with RNN, see section 4.3.3. Learning this temporal sequence by a top layer can permit to generate an even longer plan execution as done in section 4.3.3 for one sequence only and without any learning. Hence, our model can be extended to a more elaborated PFC model as it is known that PFC contributes to sequential planning over seconds Sakai et al. [2002] and to the selection of neural 'programs'.

Multi-Step computation. While the IPL working memory provides, stores, and manipulates representations ; the basal ganglia model map current states to courses of action Alexander et al. [1986]. BG can serve for selection of complex, sequenced actions at the cortical map level Seger and Miller [2010]. Thus, it can be interpreted as a repertoire of *if-then* rules or a set of stimulus-response associations to select appropriate cortical chains. In section 4.3.3, we used our cognitive architecture for iterating a long sequential pattern of 200 steps, a serial WM task, which is a feature that can be used for computational purposes (e.g., arithmetic counter). Here, the BG rules can be seen as *'pointers'* of cortical *'programs'*. This kind of cortical architecture has been emphasized to be used possibly for multi-step computation ; i.e., for implementing neuronal Turing machines Eliasmith [2013]; Zylberberg et al. [2013]; Graves et al. [2014].

Making an analogy with Turing machines, we can see AM as an instruction table, its operations as the injected inputs into RNN, RNN as the infinite tape and their respective neural activity as symbols and states. In our framework, *IF* current activity (symbol) in RNN (tape) is j *AND* current activity (state) in AM (instruction table) is i, *THEN* inject the signal k to j (replacing operation).

Furthermore, the reinforcement signal used here as a heuristic function makes a link with more classical AI algorithms using meta-heuristics like the A^* tree search, as proposed by Daw Daw et al. [2005]. These meta-heuristics are optimization technics that make to converge the recurrent spiking neural network to specific trajectories with some flexibility, see the schema in Fig 4.39, which are directly taken from the trajectories found in Fig 4.30. On the one hand, all the trajectories derive from the spatio-temporal primitives learned by the RNN. On the other hand, they are assembled flexibly to reach one goal. Therefore, for each specific goal, the trajectories found in each structure possess roughly the same structure and prototype (global coherence), see Fig 4.39 a) while the structure within each sub-cluster is however different (internal variability), see Fig 4.39 b).

This shows the capabilities of the RNN to produce hierarchical plans and tree structures, which are found important for human language and cognition Dehaene et al. [2015]. Its structural organization follows also a complex network topology as the log-curve distribution of the clusters' size demonstrate it with scale-free dynamics.

Gain modulatory control. Our optimization technique is based on the control of the sub-threshold activity of the neurons. We propose that this mechanism can be one candidate for flexible neural coordination, along with phase synchrony and spike timing-dependent plasticity.

For instance, sub-threshold activity optimization is similar with the phenomenon known as gain-modulation Salinas and Sejnowski [2001]; Botvinick and Watanabe [2007]. This mechanism describes how the activity level of gain-field neurons can be modulated by the amplitude-level of several neurons sensitive to different variables, which is therefore interesting for neural control Gabbiani et al. [2002]. Gain-modulation is found important for the neural processing in the parieto-motor cortices Blohm and Crawford [2009] and may provide a hint how generative causal chains are formed in a neural population for planning in PFC as proposed by Dehaene

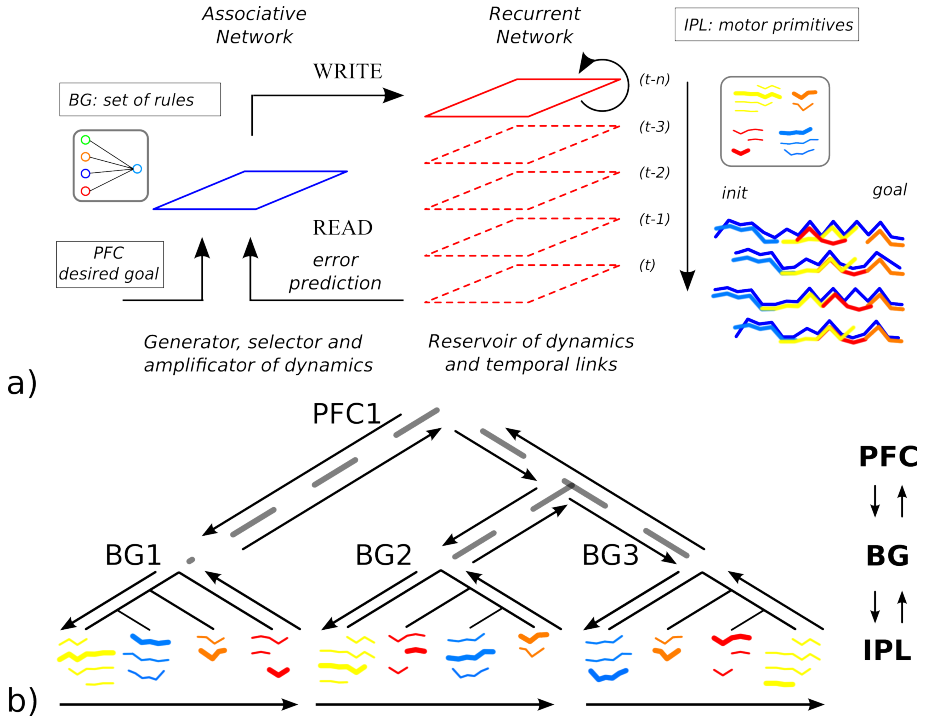

FIGURE 4.39 – Abstract model explaining the IPL working memory. Our model stores a repertoire of motor primitives and assemble them online with respect to a desired goal. a) We super-impose with different colors the clusters of four optimal trajectories found in Fig **??**. b) Each trajectory possesses a hierarchical structure dependent on its higher and lower levels, stable enough to embed same clusters at particular locations (top-down constraints), plastic enough to have slight variations for each cluster (bottom-up).

et al. [2015].

Gain-modulation has been proposed recently to control the amplitude-level of a neural population (its local field potential). It conveys contextual information in a complex form of propagated neural activity ; a mechanism coined as nonlinear mixed selectivity Rigotti et al. [2013]. Furthermore, Botvinick and Watanabe proposed a prefrontal model based on gain-field neurons showing their ability to recall serial order information Botvinick and Watanabe [2007]. Their model assumes that abstract ordinal information is conjoined with item-specific information through a gain-field mechanism.

Dopaminergic optimization. The neurons in the recurrent network have sparse connections from each other so that the system possesses a high number of spatio-temporal patterns and requires several steps to reach the desired configuration ; this behavior corresponds to the characteristics of one working memory. Therefore, in order to retrieve one desired spatio-temporal sequence, a reinforcement signal (presumably dopaminergic neuromodulation) evaluates the exploratory search of the working memory to the desired goal ; depending on the reward value, the sensory input dynamics are strengthened to hill-climb the gradient or elicited to search for another solution. This is similar to model-based reinforcement learning for which the internal primitives of the RNN corresponds to the model. Thus, the neural sequences found in Fig 4.30 are not completely random but depends on the synaptic organization of the RNN so that the later

plastically self-organizes to generate the beginning, middle and end of one complete sequence, see Fig 4.39 on which we super-imposed colours for each stable clusters, as well as cliques and loops found.

Neurocomputation and AI. As proposed by Doya, different concepts of AI can be applied to the modeling and understanding of the functional organization of the brain Doya [2002]. Nonetheless, their use in large scale recurrent spiking neural networks may not be trivial. Our work and others from our lab are attempts to make to converge some distinct concepts found in classic AI and robotics with current computational neuroscience to model the functional organization of different brain areas. For instance, we have shown how self-organization of associate maps can occur in an unsupervised fashion from contingent visuo-tactile signals using the Hebbian Spike Timing-Dependent Plasticity rule Pitti et al. [2009a], we have employed also a novelty-detection mechanism for cumulative learning in a hippocampus model Pitti and Kuniyoshi [2011a,b], and finally how a tabou greedy search may model the anterior cingulate cortex for error-based exploration Pitti et al. [2013a]. The combination of these different AI techniques may reveal with few principles how to model the brain in neuromorphic machines.

CHAPITRE 5

Contribution to Synergistic Models for Soft Robotics

The complex neural dynamics presented in the previous sections allowing body representation from multimodal integration or incremental learning based on error regulation and anticipation in cognitive memories would not been complete without the same investigations done on the motor synergies on a complex body. On the one hand, roboticists still have difficulties to harness the way to control a high-degrees of freedom system or the nonlinearities of soft robots. On the other hand, a bio-inspired control is mostly underactuated and energy-efficient, which requires to design also a complex body following some architectural principles.

Since an adaptive controller is fitted to work with a compliant robot. I have started to develop an extension of my research themes at the material level and at the structural level for rich perception and soft actuation. Pursuing my work on central pattern generators and motor synergies from my PhD, I have started to work on tensegrity structures for the modeling of a soft and compliant vertebral column, some snake-like robots and foot architecture to be compatible with nonlinear controllers replicating central pattern generators, see section 5.2. Not described here, I have started to work on the design of tactile sensors, an artificial skin, to endow robots with the capability to sense their environment through their own actions with the replication of some mechano-receptors.

Morphological Computation based on Tensegrity for Bio-Inspired Robots

In comparison to classical robots that have few degrees of freedom per articulation, biological systems have so many muscles in comparison to their number of bones. Because of this ratio, our body is always in situation of dynamical stress and strain (i.e., pre-stress) which confers to the body its flexibility. One architectural design that resumes well this moprhological computation are tensegrity structures. Tensegrity structures can be seen as physical networks of stress and loads so that they have an inner stress and plasticity in their structure that make them resilient, adaptive and robust to some external loads. In comparison to most robotic designs, tensegrity structures don't follow the newton-law of rigid bodies as they have no joints but the hookean laws of elastic bodies in the sense that they have no momentum or torque since the motors are

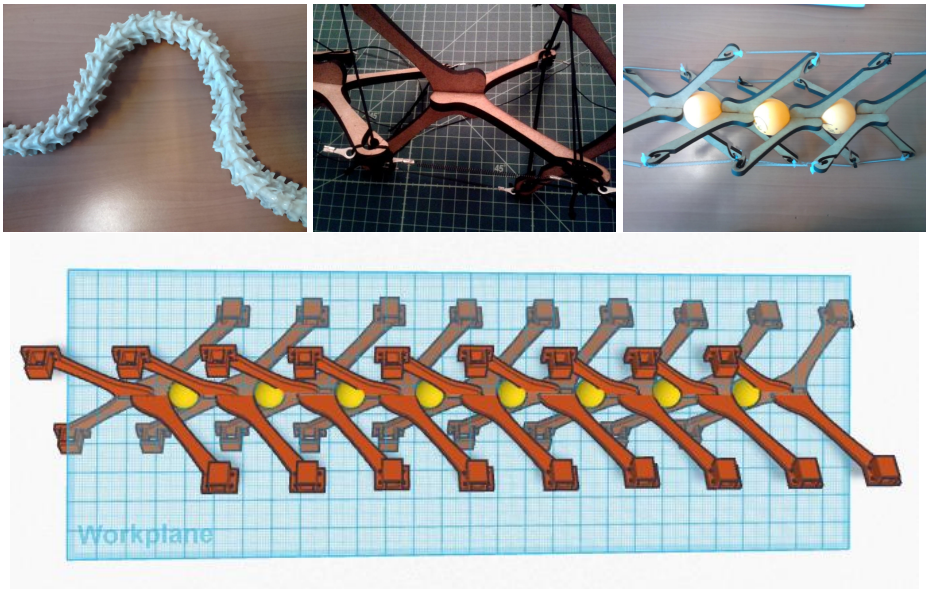

FIGURE 5.1 – Snake inspired architecture based on tensegrity. The compliance of the multi-articulated body and the big number of muscles make such kind of robots difficult to control without bio-inspired models of central pattern generators as nonlinear oscillators for energy-shaping control.

not in the axis of articulation. Tensegrity structures distribute all the mechanical tension on their morphology. This mechanical property confers them to be very light and very robust in theory in comparison with the kinematic chain of joint-manipulators.

In this research, we get inspiration of the human musculo-skeleton system to model a dorsal spine robot based on tensegrity paradigm, see Fig 5.1. We present a tensile self-replicative structure composed of ten 3D printed elements and of eight motors distributed over all the structure to control it. We get feedback from the structure from an accelerometer positioned at its bottom.Its structure shows a large spectrum of behaviors from very soft dynamics that produce rhythmical oscillations to very rigid static postures up to 45 degrees inclination. with co-contraction of the motor activity.

We develop three experiments. In a first experiment, we define the dynamics in open loop control for various modes of coordination by varying the phase and the duration of the PWM control and by analyzing the resonant frequencies of the system and its rhythmical patterns. In a second experiment, we analyze the system statically from a postural viewpoint, in an inverse pendulum configuration, and study its controllability as well as the maximum weight to be put at the end-point to study its robustness. In the third experiment, we propose to explain feedback for close-loop control of the structure in order to model the biological control done by the central pattern generators (CPGs) of the spinal cords and the motor synergies associated with the Kuramoto model.

The scalability of tensegrity structures fulfill the requirements for testing ideas about low-cost platforms for multi-purposes in Research, Art and Education. Tensile robots can be 3D printed and can be highly replicative. Their overall robustness and lightweight can be really put forward in comparison to most robots, which are still fragile and expensive products to design and repair. The ecology of the body morphology changes also the way control in force and in

precision is done and requires to rethink biological control for robots.

Morphological Computation based on Tensegrity for Bio-Inspired Robots

Animal's musculo-squeletal system is based on a complex network of muscles, bones, nerves, tissues and soft-bodies which are hard to replicate accurately in robots Pfeifer et al. [2007b]; McEvoy and Correll [2007]. This dense architecture is however well-ordered so that we can realize soft dynamics, sensorimotor coordination, as well as postural balance at a very low energy cost thanks to the dynamic grouping of the muscles ; a.k.a. motor synergies Todorov [2004]; Bizzi et al. [1995]. The well-distribution of stress and strain throughout the body warranties its ecological control so that when we are exposed to a violent shock, we can still stand or ply and bend our knees or stiffen (or soften) our body and joints, just as a building would absorb an earthquake wave and to balance itself, or as a bridge would lean into the wind. Since the muscles are always in tension, the musculo-squeletal system is always soft and elastic and positioned in a stable or neutral posture. If one effort is made on one particular point and direction, the whole structure complies and takes in charge the exerted tension. When the effort is elicited then, the morphology returns back to its original configuration. This property releases motor control from computing a time costly precise plan and is specific to *tensile structures*, which most biological systems possess as attribute Ingber et al. [2014]; Turvey and Fonseca [2014]; Levin [2002].

In comparison to classical joint articulation robots, biological systems have an impressively high ratio between the number of muscles (joints) with respect to the number of bones (articulations). Because of this ratio, our body is always in situation of dynamical stress and strain (i.e., pre-stressed) which confers it its flexibility. When we are standing upward, groups of muscles are dynamically selected to contribute to our stability Ting [2007]; Allen and Ting [2016]. One architectural design that explains well this type of *morphological computation* Pfeifer et al. [2007b]; Pfeifer and Gomez [2009]; Nakajima et al. [2015] are tensegrity structures Fuller [1975]; Snelson [1965]. Tensegrity structures can be seen as physical networks of stress and loads so that they have an inner stress and plasticity in their structure that make them resilient, adaptive and robust to some external loads. In comparison to most robotic designs, they do not follow the newton-law of rigid bodies as they have no joints and no momentum or torque since the motors are not in the axis of articulation. Instead, they follow the hookean laws of elastic bodies.

Hence, tensegrity structures are mechanical transducers in the sense that they distribute all the mechanical tension on their morphology Ingber et al. [2014]. This mechanical property permits them to be very light and very robust with dynamic gaits in comparison with the kinematic chain of joint-manipulators.

From a robotic viewpoint, tensegrity systems have other advantages in terms of ecology and scalability as their structure and their physics can be replicated at different scales. These features provide them a promising paradigm for integrating structure and control design Paul et al. [2006]; Bliss et al. [2008]; Tietz et al. [2013]. For instance, we can easily formalize a tensegrity system as a network of tension (muscles and soft tissues) and compression (bones), or as a network of springs and masses Hauser et al. [2011, 2012]. Therefore, they can be viewed as complex dynamical systems with many degrees of freedom Caluwaerts et al. [2014]. The redundancy and nonlinearity within such dynamical system might be considered at first as an obstacle to control, however, the symmetries of the overall structure and the many resonant modes generated can serve to decrease the dimensionality of the control problem. For instance,

one way to have an adaptive control is to exploit phase synchronization of these modes pretty much like for coupled chaotic maps Strogatz [2003]; Kelso and Haken [1995].

In previous works, we have showed how we can control such high degrees-of-freedom system with chaotic controllers that *sync* dynamically to the resonant frequencies of several robotic devices Pitti et al. [2005, 2006, 2009b, 2010] and to human partners [Melnyk2016]. We believe that this type of control is simple/archetypal enough to convey the important features of controlling the human musculo-squeletal system control as done in the spinal cords by the central pattern generators Ijspeert et al. [2003]; Ijspeert [2008]; Bizzi et al. [2008] as of controlling tensegrity structures.

Furthermore, the scalability of tensegrity structures fulfills the requirements for testing ideas with low-cost and multi-disciplinary platforms at the community level for exploration and experimentation in robotics for Research, as well as in Art and Education. For instance, tensile structures can be 3D printed and can be highly replicative, which can be interesting for the Do-It-Yourself community. In complement of this paper, we provide a website of the project with links for downloading freely the tensegrity modules for building it and to inspire and iterate on the project to one's own. Their overall robustness and lightweight can be really put forward in comparison to most robots, which are still fragile and expensive products to design and repair. The ecology of the body morphology changes also the way control in force and in precision is done and requires to understand biological control and to rethink it for robots. Furthermore, as educational tool, tensegrity robots convey many principles behind control, matter, cybernetics and complex systems in biological systems.

In this paper, we get inspiration of the human musculo-skeletal system to model a dorsal spine robot Ly et al. [2011] based on tensegrity paradigm Flemons [2012], which is also reminiscent to the functional organization of snakes Liljeback et al. [2009]. We present a tensile self-replicative structure composed of ten 3D printed elements and of several motors distributed over all the structure to control it. We get feedback from the structure from an accelerometer positioned at its extremity. In our experiments, its structure shows a large spectrum of behaviors from very soft dynamics that produce rhythmical oscillations to very rigid static postures up to 45 degrees inclination, with co-contraction of the motor activity. We propose three setups to display the capabilities of our system. In the first setup, we define the dynamics in open-loop control for various modes of coordination by varying the phase and the duration of the PWM control and by analyzing the resonant frequencies of the system and its rhythmical patterns. In the second experiment, we analyze the system statically from a postural viewpoint and study its robustness in the upward postion. In the third experiment, we propose to exploit feedback for closed-loop control of the structure using central pattern generators (CPGs) Taga [1995]. Depending on the values of the internal and external coupling parameters, we can self-synchronize non-linear oscillators modeled with Kuramoto units to the resonant modes of the structure and entrain it freely to specific directions. These privileged modes of synchrony represent the natural motor synergies that are possible to generate and control in the multi-segmented structure Der et al. [2005].

Then, we will employ a top-down mechanism that pre-selects the coupling parameters to the most desired motor synergy based on the magnitude of the external perturbations on the vertebral structure. This indirect control may play the role of neuromodulators in the spinal cords that modulate the gain of the sensory feedback on the alpha-motor neurons activity to generate the desired synergy Bizzi [1999]; Marder and Calabrese [1996]; Calabrese [1995] ;

which means selecting the most expected resonant modes relative to the perturbation. For a strong external shock, the controller will set the oscillators to a certain regime producing big oscillations, which can absorb the perturbation. At reverse, for tiny perturbations, the controller will set the oscillators to a different regime that can dampen the perturbations.

Material & Methods

We present a tensegrity structure based on auto-replicative elements, 3D printed and similar to the ones proposed in Frumar et al. [2009]; Flemons [2012], see Fig. 5.2 a) and b). This particular motif reproduces the very stable structure of the tetrahedron (i.e., the pyramides) which can stand easily upward, see Fig. 5.2 c) and d). When two structures are mounted together (two inverted pyramids), the coupled unit structure can move in two directions and can support small sheer torsions, which is ideal for modeling complex human joints' movements like the ankle, the hip, the spine or the shoulder. In comparison to other types of tensegrity motives, this one has the advantage to require less structures and few jonctions part. Each element is connected to others with springs, which confer to the design some visco-elastic properties of pre-stressed structures that permit them to return back to one stable configuration after any external force pressure applied. The whole structure possesses ten segments connected with springs and omnidirectional joints (ping-pong balls) with eight electrical micro motors distributed over all the structure. We used motors with a gear head and a shaft to reel up a 10 cm tendon-like wire. Theses wires generate the local contraction and displacement of each body segment. Very-lightweight and compliant, it presents interesting dynamical properties of oscillatory patterns when the motors are activated in co-ordination and of postural stability when the motors are in co-contraction. Hence, this structure is ideal to model central pattern generators and motor synergies in robots. When each part is assembled in line, they replicate the spinal vertebres system of human beings. As tensegrity systems possess no joints, the suspension between vertebres garanties stability and compliance. And in order to perceive the motion, an inertial measurement unit (IMU) is placed at the top/bottom of the vertebral column. This module permits to measure the linear acceleration at the extremity of the structure and its angular velocity.

According to how it is mounted on the robot, the IMU coordinate system can provide different orientations. It is therefore important to use an appropriate coordinate system aligned with the robot axes. Fig. 5.3 shows the coordinate system used in this article : (1) The x-axis is opposite to the gravitational field and points upward so that the IMU is aligned along the longitudinal axis of the vertebral column robot, (2) the z-axis is perpendicular to gravity and lies in the horizontal plane of the robot body and (3) the y-axis is aligned in accordance to both the x- and z-axes in order to form a right-hand three axis coordinate system.

The rotations in roll ϕ, yaw ψ, and pitch θ represent changes in orientation about the x, z and y-axes respectively.

$$tan\Theta_{xyz} = \frac{-G_{px}}{\sqrt{G_{py}^2 + G_{pz}^2}} \tag{5.1}$$

where G_{px} , G_{py} and G_{pz} are normalized accelerometer reading corresponding to the coordinate system axis x, y and z, see Fig. 5.3.

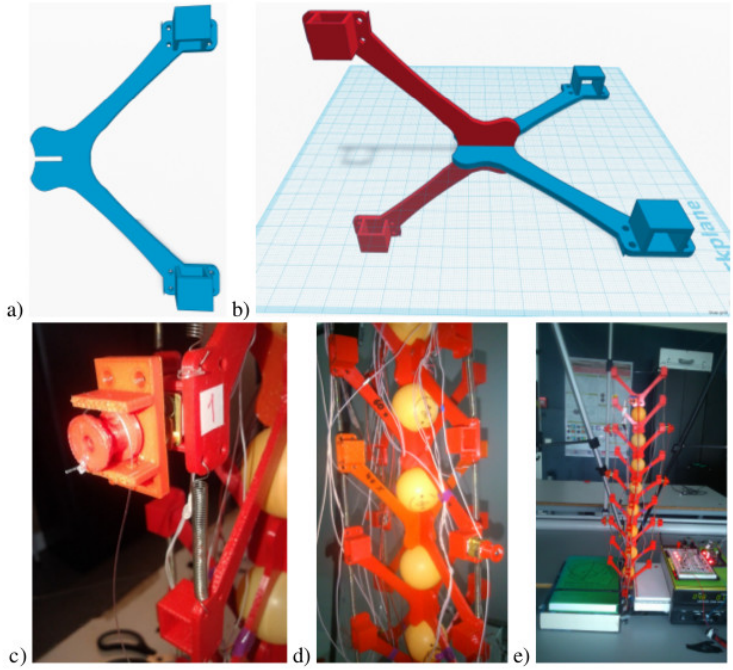

FIGURE 5.2 – Vertebral column robot also viewed as a snake-like robot. This tensegrity-based robot is very compliant and light-weight, mounted with springs in opposition. It possesses 10 segments with motors mounted in pairs to produce co-contractions in phase or in anti-phase for generating discrete and oscillatory patterns. An inertial measurement unit is placed at the end of the structure for position control and acceleration feedback. Each elements are self-replicated and are freely available at https//tinkercad.com/things/6iBMNx721aK.

Dynamic Behavior Analysis in Passive Conditions

We make first a perturbation analysis of the whole structure and present its dynamic behavior when pushed in one plan and when pushed on its own axis of rotation, respectively Fig. 5.3 a) and b). Specifically, we are interested in the passive response under external stresses and the response of the controllers.

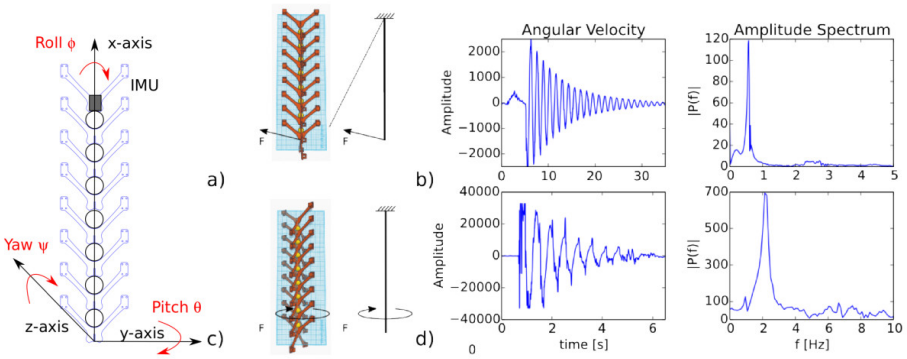

FIGURE 5.3 – Perturbation analysis on the vertical and axial plans of rotation, resp. a) and c). The Fourier transforms in b) and d) show the resonant frequencies of the structure. Two different fundamental resonant frequencies are found for the two axis, respectively 0.5Hz and 2Hz. IMU units at the top or bottom extremity depending on the experiments.

The Fourier diagrams present the resonant frequencies found for the two perturbations. The horizontal perturbation on the structure produces a pseudo-periodic oscillation with a fundamental mode around 0.5Hz, whereas a perturbation around its axis of rotation generates an oscillation around 1Hz.

As one can expect, the length of the structure has a direct impact on the wavelength of the oscillations generated. The more elements are linked together, the more oscillatory patterns are produced, which diminishes at the same time the resonant frequencies of the overall structure below 1Hz for. The structure presents therefore the characteristics of a dissipative system, which is important in order to have resonant modes and to develop motor synergies.

Second, it is extremely easy to produce motion from small perturbations. As the structure is light with no joints, it has few frictions except at its fixation point and reacts as a pendulum. The number of oscillations till stabilization for the two perturbations is very large in one direction, above 10 oscillations in 30 seconds for horizontal perturbations, see Fig. 5.3 b). Therefore, we can expect to generate motor synergies with higher harmonics proportional to this wavelength.

Resonant Mode Analysis in Controlled Conditions

We propose to study in this section the control of the different resonant modes and phase delays of the structure with open-loop controllers using pulse-width modulation controllers (PWM). In order to facilitate the analysis, we group the motors aligned symmetrically in the longitudinal plane forming two clusters of three motors each. We control the phase delay and duration of the PWM between the two motor groups around the fundamental frequency.

If we modulate the duration of the PWM controllers for all the motors as in Fig. 5.4 a-d) respectively from 50 ms ,100ms, 250ms and 500 milliseconds, we can observe a sensitivity on

the oscillatory patterns of the tensegrity structure. As we might expect, large PWM produces large amplitude oscillations whereas small periods of the PWM generate weak perturbations. The resonant mode occurs for 250 milliseconds period square signal with amplitude variation 3 time larger than for PWM of 50 milliseconds. Above this value, for the case of Fig. 5.4 d), new harmonic modes are super-imposed to the speed signal, which corresponds to complex modes of coordination with the apparition also of harmonic waves.

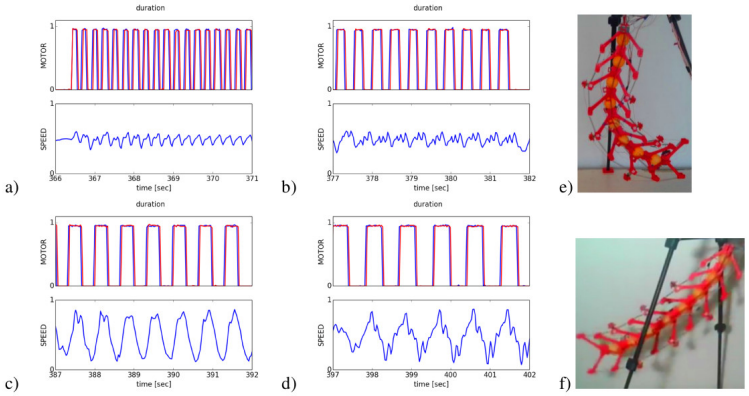

FIGURE 5.4 – Phase duration characterization in controlled condition with PWM. A PWM signal controls the tensegrity structure in the vertical axis with motors aligned along the vertical axis. Modulating the phase duration of the motors, from small durations 50ms (resp a), 100ms (resp b), 250ms (resp c) up to 500ms (resp. d), affects the level of global synchrony and the apparition of complex modes of resonance.

Robustness during Postural Co-contractions

We display the properties of robustness and stability of the spinal vertebrae and of tensegrity structures in general. First, we set its motors in co-contraction and set its neutral postural configuration respectively in the horizontal plane and in upward tension, so that the structure has a maximum momentum and tension on its morphology horizontally and has to exploit fully its physics to stand vertically ; see resp. Fig. 5.5 a) b) and c).

The forces distribution of each motor-driven cables on the whole structure is similar to those of the wires acting on cable-stayed bridges. The distribution and balance of mechanical stresses in the entire structure makes it stabilized in every positions, even for the less energetical ones as the horizontal plane and the vertical planes in order to stand upward, which are also the most difficult to stabilize for humans to support their own weight Turvey and Fonseca [2014]; Allen and Ting [2016].

Results

We explain in this section the experimental setup on the biological models of central pattern generators used and the algorithm employed to control the multi-segments structure for standing upward (multi-d.o.f. inverted pendulum). We will perform one experiment showing the reflexive control of synchronization based on feeded back resonance and the attributes of the coupled system to generate oscillatory patterns and to discover motor synergies. Then, we will perform

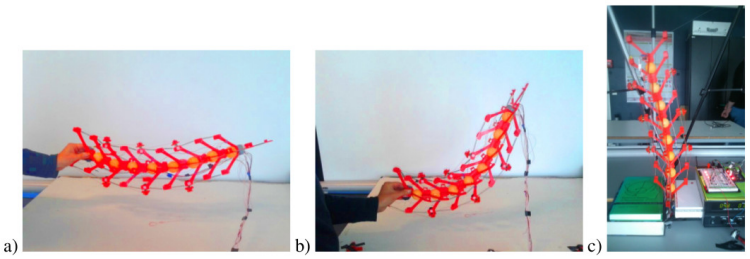

FIGURE 5.5 – Robustness in co-contraction in horizontal and upward postural configuration. Static postures demand to set the contraction of all the motors to specific lengths. In these situations, the motors act as rigid tendons and loads are distributed overall the structure. Maximal efforts are delivered on the structure when set at the horizontal in a), in the vertical plane with different directions in b), and upward at the vertical in c).

one experiment on the active control of the CPG units and motor synergies toward standing balance against external perturbations.

Bio-Inspired CPGs – Kuramoto oscillators

We use as bio-inspired controllers the Kuramoto model, which is a limit-cycle nonlinear oscillator employed in many robotic experiments to model central pattern generators Ijspeert [2008]. Each Kuramoto oscillator ϑ is coupled with each other by the phase so that any weak interactions alter the level of phase synchronization between each pair.

Each oscillator ϑ has its own angular momentum ω, and each one is coupled equally to all other oscillators, see Fig. 5.6 a). We have one oscillator per motor, which corresponds to a population of 6 units. The internal coupling is done by computing the phase difference between the oscillators. The external coupling is done in a similar way by computing the phase difference to the angular momentum of each oscillator. We use as external feedback the position in the Z axis, POS Z, of the top of the structure calculated from where the accelerometer is. By doing so, we provide to the elements the necessary feedback for its embodiment. The tensegrity structure is similar to a spring-like system with damping. In the equations, the feedback signal is viewed as another oscillator by the units. We add three coupling coefficients, $\mathbf{K_i}$, $\mathbf{K_e}$ and $\mathbf{J_e}$ corresponding respectively to the internal coupling among the oscillators, the external coupling of the external signal to the units and the amplitude level of the ouput signal to the motors. In order to take into account the symmetry of the structure, the angular momentum of each co-contracting pair are phase-shifted by π.

$$\frac{d\vartheta_i}{dt} = \omega_i + \mathbf{K_e} sin(I_i - \vartheta_i) + \frac{\mathbf{K_i}}{N} \sum_{j=1}^{N} \sin(\vartheta_j - \vartheta_i) \tag{5.2}$$

$$output_i = \mathbf{J_e} sin(\vartheta_i) \tag{5.3}$$

We draw one diagram of the pre-reflexive control performed by the oscillators on the vertebral column in Fig. 5.6 a) and b), which are the links in blue. In line with biomechanical studies that suggest muscles are not activated independently but are grouped in modular units, the parameters $\{\mathbf{K_i}, \mathbf{K_e}, \mathbf{J_e}\}$ correspond to the neuromodulators driven by the higher units that impose

certain classes of dynamics to the motors ; i.e, the motor synergies Bizzi et al. [1995]. These parameters regulate the synchronization level between the oscillators and the tensegrity column as follows. The internal coupling $\mathbf{K_i}$ synchronizes the oscillators from each others and reduce their variability. The external coupling $\mathbf{K_e}$ influences the coupling to external perturbations. Beside, the control of the amplitude signal to the motors $\mathbf{J_e}$ is used to generate resonant modes and to influence the level of synchronization and of perturbations to the system.

In order to achieve a task, controlling the three parameters $\{\mathbf{K_i}, \mathbf{K_e}, \mathbf{J_e}\}$ dynamically can permit to construct a motion pattern by combining and varying the recruitment of the motor modules, see the green line in Fig. 5.6 b). Therefore, atop of the reflexive control done by the oscillators, we add a higher controller that will supervise the values of the coupling paramaters $\{\mathbf{K_i}, \mathbf{K_e}, \mathbf{J_e}\}$. This controller will drive indirectly the coupling to the structure by changing the coupling parameters toward desired regimes based on feedback and perturbations ; the new circuit is plotted in red in Fig. 5.6 b).

Such controller may be similar to the task-level commands performed by the neuromodulators in the higher centers of decisions to bypass the CPGs' reflexive activity at the spinal cords level Marder and Calabrese [1996]; Todorov [2004]; Ting [2007]. The control task here is reduced to the dynamical control of the three parameters $\{\mathbf{K_i}, \mathbf{K_e}, \mathbf{J_e}\}$ to specific regimes found. We use a K-mean clustering method to categorize the different regimes found in section 5.2.7 with respect to the parameters set and the acceleration ACC. Depending on the most probable regime in which the structure system should be based on acceleration ACC, the top layer will dynamically select the variables $\{\mathbf{K_i}, \mathbf{K_e}, \mathbf{J_e}\}$ so that :

$$argmin_j ||I - \mu_j||^2, \tag{5.4}$$

$$\mu_j = \{K_{i_j}, K_{e_j}, J_{e_j}\} \tag{5.5}$$

where $\mu_\mathbf{j}$ is the mean of the cluster j corresponding to the pair $\{\mathbf{K_{i_j}}, \mathbf{K_{e_j}}, \mathbf{J_{e_j}}\}$.

$$\Delta K_i = \alpha \frac{dE}{dK_i}, \tag{5.6}$$

$$\Delta K_e = \alpha \frac{dE}{dK_e} \tag{5.7}$$

$$\sum x + y = Z \tag{5.8}$$

$$\tag{5.9}$$

with $\alpha = 0.1$ and D represents the speed/position.

Reflexive & Bottom-Up Synchronization

Our first experiment consists on studying the interval range of the external coupling parameter $\mathbf{K_e}$ and see the impact feedback on the internal dynamics of the oscillators when they are coupled to it. We study first the Fourier coefficients of the Kuramoto's units when the control is done in a closed-loop manner without internal coupling, $\mathbf{K_i} = 0$, to which we make to vary $\mathbf{K_e}$ within the interval range $[0; 1]$ $\mathbf{J_e} = 1$; see Fig. 5.7 a).

When $\mathbf{K_e} = 0.0$, the oscillators drive the tensegrity stucture in a completely open-loop fashion with a fundamental frequency centered on the intrinsic mode ω of the oscillators. In this

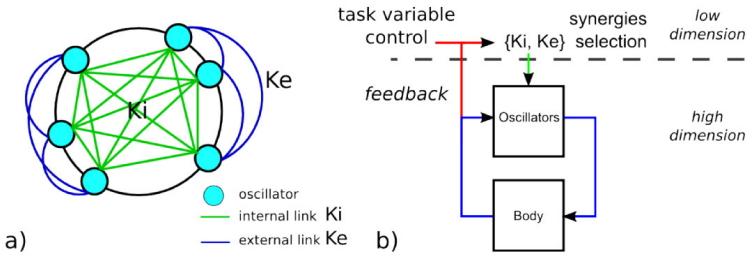

FIGURE 5.6 – CPG-based control of the structure motor synergies based on the indirect coupling parameters $\mathbf{K_{ij}}$ The Kuramoto oscillators are coupled internally to each other based on the parameters $\mathbf{K_i}$. The external coupling is done by the parameter $\mathbf{K_e}$, which sets the influence of the position of the top of the structure with respect to the Z axis on the internal dynamics. The reflexive synergies produced by the oscillators can be controlled by a higher center of decision that selects the global parameters for postural control. This corresponds to a dimensionality reduction of the controller on the robot dynamics, to generate probabilistically stable movement behaviors.

stage, the tensegrity structure performs a strong rhythmic motion without damping and exploitation of the physics of the system. At $\mathbf{K_e} = 0.2$, an interesting behavior occurs in which the oscillators bifurcate to an attractor point, an underdump postural configuration slowly entrained by a slight feedback control till immobilization. This posture is in this plot the upward posture with $Z = 0$. In this situation, the motors remain in this static posture without any feedback and react to small perturbations are reflexes. When the structure is slightly pushed, the oscillators act reflexively to return back to the static posture, where the point attractor is.

Above this value, say for $\mathbf{K_e} \geq 0.4$, the oscillators start to be entrained actively to the dorsal-spine resonant frequencies with a signal per noise ratio that depends on $\mathbf{K_e}$ values. In this stage, the feeded back signal generates stable cyclic motion around the upward position. The higher the coupling ccoefficient, the higher the instabilities of the rhythmical pattern.

To understand in more details what's going on between the point attractor behavior and the limit cycle behavior found, we plot the dynamics of the oscillator in the interval range $\mathbf{K_e} \in [0.15; 0.4]$, see Fig. 5.7 b). We observe a birfucation diagram of the oscillator to the dynamics of the vertebral column. We analyze below the three cases found depending on the coupling parameters $\{\mathbf{K_e}, \mathbf{K_i}, \mathbf{J_e}\}$.

We display three different phase plots for the three behaviors presented earlier with respect to $\mathbf{K_e} \in \{0.0; 0.2; 0.4\}$, see **Figure 5.8** resp. a), b), c). But in order to define more precisely the behavior of the system, we add two new conditions to compare with when $\mathbf{J_e} = \mathbf{0.6}$ and when $\mathbf{J_e} = \mathbf{1.0}$ that modulate more or less strongly the motor output.

These graphs show the plots during 10 seconds of the internal CPGs dynamics and of the position at the tip of the structure oscillating around the Z axis for $\mathbf{J_e} \in [\mathbf{0.6}; \mathbf{1.0}]$. The graphs on the right charts are the phase space plotted between POS Z and CPGs. In Fig. 5.8 a), The tensegrity structure is totally open-loop driven and forced to follow the oscillators cycle without any feedback. At reverse, the situation in Fig. 5.8 b) corresponds to an under-damped case for $\mathbf{K_e} = 0.2$ where the oscillators go to a point attractor centered on the neutral position of the structure. Besides, when the coupling term $\mathbf{K_e}$ augments above 0.2 as it is the case in Fig. 5.8 c), the Kuramoto's oscillators start to be entrained to the phasic regime of the structure. The higher the coefficient $\mathbf{J_e}$, the stronger is the synchronization.

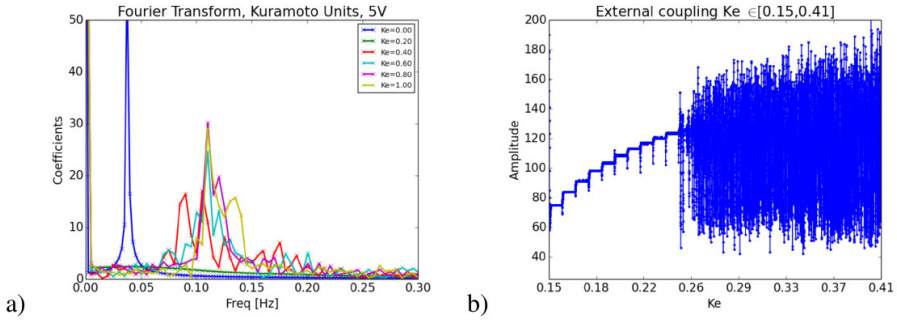

FIGURE 5.7 – Influence of the external coupling parameter $\mathbf{K_e}$ on the resonant modes of the backbone tensegrity structure. In a), we plot the Fourier coefficients with respect to the quantity of feeded back signal injected into the oscillators within the interval range $\mathbf{K_e} \in [\mathbf{0.0}, \mathbf{1.0}]$ from open-loop control to stable closed-loop entrainment. In b), we plot the details of the dynamics of one oscillator with respect to $\mathbf{K_e}$ in the interval range $[\mathbf{0.15}, \mathbf{0.40}]$ when the system bifurcates from an under-damped state to a rhythmical regime with the resonant frequencies of the tensile structure.

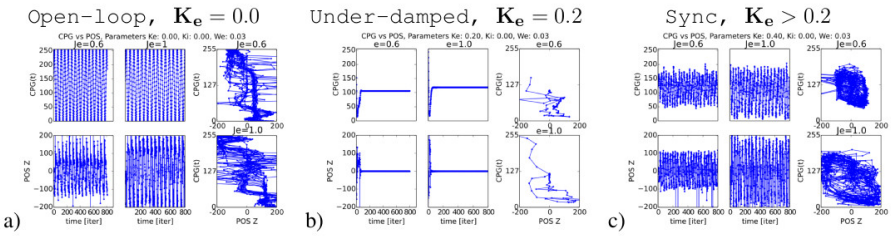

FIGURE 5.8 – Phase plots for external coupling $\mathbf{K_e}$ corresponding to three different behavioral patterns and for different amplitudes $\mathbf{J_e}$. (a) $\mathbf{K_e} = 0.0$, the oscillators control in open-loop vertebral column to their intrinsic regime different from the one of the structure. (b) $\mathbf{K_e} = 0.2$, The oscillators go to a stable point attractor that return back when perturbed. This corresponds to a stable and passive pre-reflexive stage. (c) $\mathbf{K_e} > 0.2$, the general regime of synchronization is stabilized to generate rhythmical patterns around the center, which vary also depending on the motor force $\mathbf{J_e}$.

Active Top-Down Control

Based on the results found from the different coupling parameters, it is possible then to command the vertebral column indirectly depending on the different coupling parameters with respect to external perturbations. We can define some motor strategies that link the coupling parameters $\{\mathbf{K_e}, \mathbf{K_i}, \mathbf{J_e}\}$ to at least three behaviors for postural control, namely the under-damped upward posture when no feedback is furnished, the rhythmical balance during phase synchronization and the forced controlled with strong feedback during co-contraction. The motor strategies are :
Rule 1 : $\{\mathbf{K_e}, \mathbf{J_e}\} = \{\mathbf{1}, \mathbf{0}\}$ when $|ACCZ| < 0.1$
Rule 2 : $\{\mathbf{K_e}, \mathbf{J_e}\} = \{\mathbf{1}, \mathbf{1}\}$ when $|ACCZ| > 0.5$
Rule 3 : $\{\mathbf{K_e}, \mathbf{J_e}\} = f(ACCZ)$ when $0.1 < |ACCZ| < 0.5$

Rule 1 corresponds to the standing posture of the column at the vertical, in its stable position. The tensegrity structure is totally passive when no feedback and deviations are sensed. The coupling parameter $\{\mathbf{J_e}\}$ is set to 0 for the motor output.

Rule 2 corresponds to the case in which a strong perturbation is given to the structure in its axis of rotation. The rule pushes the global parameter $\mathbf{J_e}$ to the value 1, which corresponds to a strong feedback and then reduces it to 0.

Rule 3 corresponds to the case of a soft push on the structure and to its dynamical adaptation to it. This situation is a subcase of the previous rule 2, which synchronizes and adapt the vertebral column robot to a particular cyclic regime and resonant state based on feedback.

We plot in Fig. 5.9 an example of the top-down control strategy used to stabilize the tensegrity robot based on the modulation of $\mathbf{J_e}$ when a strong push has been applied on the structure and for four transitory regimes. The top chart displays the variation of $\{\mathbf{J_e}\}$ over time, the middle chart displays the position of the structure in the Z axis and centered on its vertical axis at 0 and the bottom chart corresponds to the dynamics of one oscillator. When a strong perturbation is applied, the higher controller generates an oscillatory regime to absorb the shock. Depending on the decreasing speed of the parameter $\mathbf{J_e}$, the forced oscillatory regime of the CPGs will be under-damped (long transitory regime) or over-damped (fast transitory regime). The transitory regime varies from an interval length of 20 seconds for the slower decays of $\mathbf{J_e}$, see Fig. 5.9 (a-b), to the shorter interval lengths of $5-7$ seconds for quicker decays of $\mathbf{J_e}$, see Fig. 5.9 (c-d). All the oscillations finish with a small vibratory mode around the vertical axis, till its return to a static posture with the release of the motors from co-contraction. This strategy was efficient in ninety percent of the cases, irrespective to the shock level.

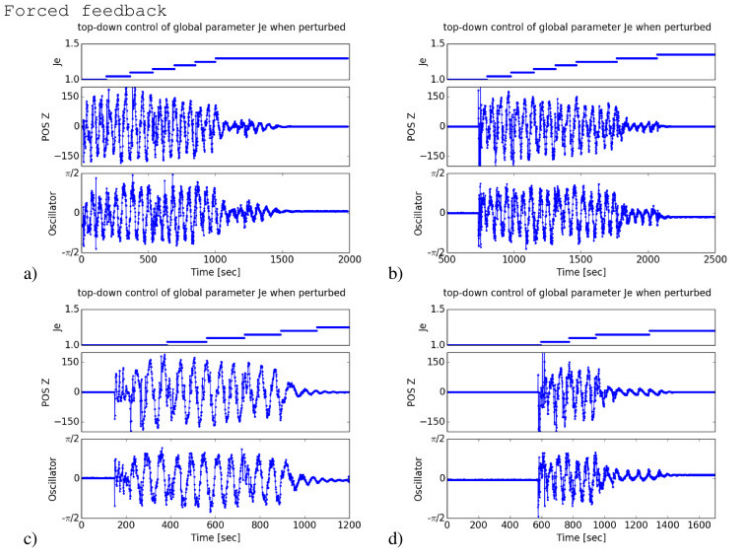

FIGURE 5.9 – Feedback control of the global parameter $\mathbf{J_e}$ on the CPG oscillatory regime for shock absorption. When a strong perturbation is imposed on the structure, an oscillatory regime is established by the top-down controller on the vertebral column to absorb the shock with a high amplitude till their attenuation. This transitory regime depends on the amplitude of the shock and of velocity of the $\mathbf{J_e}$ to steer the oscillators and the motors till their release when the column is stable enough to return back and stand at its upward posture. The more $\mathbf{J_e}$ decays slowly, the longer the transition to a stable regime (under-damped oscillations). The more $\mathbf{J_e}$ decays fastly, the quicker the transition to a stable regime (over-damped oscillations).

Discussion

We presented a tensegrity-based model of a vertebral column controlled actively with nonlinear oscillators and feedback for rhythmical balance and upward posture. We show that tensile structures present interesting properties for the design of soft and bio-inspired robots with the use of replicative elements to insure a redundancy of the global behavior at the macroscale level and a flexibility with the many degrees of freedom of each element. These structures are lightweights and pre-tensed, which make them physically robust to shocks even passively as they distribute their tension on all their elements. Furthermore, their stiffness can be linearly controlled with the co-contraction of the motors to switch from a flexible behavior to a rigid one. The dimensionality of the system makes it a complex system and the way to control it requires to exploit its passive dynamics and to entrain the controllers to its resonant frequencies for upward balance or for rhythmical motion.

Placed in the horizontal, at the vertical or in an undefined posture, the energy distribution of stress and strain is self-sustained. In an inverse pendulum configuration, the tensile structure can be controlled for upward balance. This physical property also observed in animals can be an important feature for the design of energy-efficient humanoid robots for standing, moving and manipulating objects McGeer [1990]; Collins et al. [2005]; Bliss et al. [2008]; Tietz et al. [2013]. As its elements are simple enough to be 3D printed and replicated, they make the entire tensegrity structure easy (and fun) to construct as well as low-cost. The energy-efficiency of the physics has an overall impact on the control design and energy consumption and its autonomy as it makes it lightweight, with less friction and easier to move, which reduces the power consumption of the motors and their necessary torque per Joule, which allows to have smaller, weaker, less precise and at the end very cheap motors.

This eco-logical design makes bio-inspired tensegrity models a competitive choice for the conception of future price- and energy-saving robots. For instance, the autonomy of current robots is still poor as they are often over-dimensionned in term of weight and of force. They often cannot be used for a long period of time, which is critical in situations of rescue tasks, in uneven environments or space Caluwaerts et al. [2014].

From a control viewpoint, the physics of this complex system require to adopt a more bio-inspired type of control with loosely and parallely distributed units for adaptation to the body dynamics. In the end, the elastic properties of the tensegrity-based articulated trunk may ease its control Alexander [2005] ; i.e., its morphological control Pfeifer and Bongard [1999]; Pfeifer and Gomez [2009]; Pfeifer and Pitti [2012]. The central pattern generators in the spinal cords are local neural units that can generate a rhythmical pattern even without any feedback. Their activity however is always under the local feedback control of muscles spindle signals and the global feedback control of neuromodulators at the spinal circuits level or at higher level. These feeback loops make these units embodied to the physics of the structure and contingent to a global co-ordination at the task level. We use Kuramato oscillators to entrain the vertebral column to its own rhythms and to synchronize them dynamically to the structure's resonant frequencies thanks to of the IMU unit. This phenomenon is known as *feedback resonance* and is used as a strategy to control the vertebral column to its resonant frequencies for shock absorption and postural balance. The tensile robot presents interesting damping properties that make it easy to stabilize at the upward configuration, either passively or actively Iida and Pfeifer [2004]. This is in line with observations done on biological systems and humans on the importance of an actuated head and flexible trunk to body balance Turvey and Fonseca [2014] and passive wal-

kers Alexander [2005]; Laumond et al. [2015]. Our adaptive control will be extended in future works with the use of feedback error for dynamical synchronization of the structure to one particular rhythm with the use of more biological models of neurons having reciprocal, inhibitory and oscillatory modes Amrollah and Henaff [2010]; Nassour et al. [2014]; Melnyk and Henaff [2016]; Pitti et al. [2010]. We will design a neural controller of the global parameters for the dynamical entrainment of the resonant frequencies as well as of the phase resetting Nakanishi et al. [2004]. At now, we have employed only one IMU unit at the top vertebral column. In future works, we will employ more IMU units for each segment as it is known that the vestibular system, perceiving rotational velocities and linear accelerations, uses this information to generate a unified inertial reference frame, centered in the head that allows whole-body coordinated movements and head-oriented locomotion Berthoz [2000]; Falotico et al. [2016].

Starting from this tensegrity-based vertebral column robot, it is natural then to think to design other body parts based on tensegrity Flemons [2012]. We will attempt to go further in that direction with a more complex body, possibly for walking Pitti et al. [2009b]. Finally, as an educational tool, and in order to enable experimentation in robot design, we are happy of sharing the 3D model with videos in a website (see Supplemental Data) to make it available for a large audience and reusable for the Do-It Yourself community and the scientific community to expand it to new designs and shapes.

Conclusion and Future Work

Synthèse

I have presented an extended overview of what is constituting my research going from short-time scales of neural dynamics to the longer time scales of body dynamics, learning and development. These five chapters give me the opportunity to overview myself the pros and cons of my research. Ten years after the writing of my Ph.D. thesis and of the research done in between, the writing of this mémoire could permit me to make some scientific critics.

By looking back to my different works done in these areas, in chapter 3 on neural models for body representation, multimodal integration and the study of the mirror neurons system, with many models less successfull based on associative hebbian learning or with spiking timing-dependent plasticity, the better understanding for me on the mechanisms underlying sensorimotor transformation and spatial representation in the Parietal Cortex done by Gain-Field neurons has permitted to construct more robust neural networks for multimodal integration. It served me to understand how amplitude modulation can be an important computational mechanism present over all the brain.

For instance, Gain-Field networks present interesting properties for modeling transformation function, thanks to its multiplicative function and in comparison to radial basis functions and to multilayers networks, its architecture is less complex, which may serve to aggregate efficiently various signals into multiple reference frames. Although the results on multimodal integration were restricted first on bimodal integration, combining visuo- and tactile stimuli, tactile and proprioception, audio- and vision for spatial representation. I started to extend this work to three modalities, like audio- visual and motor, or tactile visual and motor integration.

By augmenting the number of modalities, I realized that new emergent properties could be realized off-the-shelf and more easily than I thought on tasks that were seen complicated at first like self-other differentiation, body image, ego- versus allocentric spatial representation, speech and person recognition, reaching and grasping tasks. This research on multimodal integration constitutes one important aspect of my work, the results are still at their beginning and didn't show all their potential in the modeling of a perceiving robot throughout its senses toward spatial moving in 2D space and toward the understanding of the construction of oneself and of others.

In chapter 4, I have presented different neural architectures that model the construction of working memories during development. The underlying mechanisms are based on the modeling of neuromodulators for reinforcement learning, novelty detection and noise attenuation, which influences in return the functional integration in these structures during the learning stages. The first neural architecture is a model of the hippocampo-cortical complex for novelty retrieving,

and retention of information during the first year. The second model is a neural architecture of the prefrontal and cortical interaction for decision making and sequence selection and learning. The third model is a neural architecture of the cortico-basal loop for memory sequence learning and retrieving. The results found in these networks are emerging properties for information accumulation and retention, the capability to discriminate contextual networks and to learn long-range memory sequences.

These models are to me a good step toward making a developmental cognitive architecture similar to the human working memories with the ability to adapt to novel situations by testing new possibilities and by learning dynamically from them. One of the goal is to make a life-long learning system capable to apprehend new situations. I believe that this work may serve toward the design of a future neurocognitive hardware.

In chapter 5, I have start to think about a novel robotic structure based on tensegrity in order to have a more compliant system and more complex dynamics. I still believe that soft robotics is our future in robotics. The vertebral column robot served me to study a more biologically based control from my previous experiments done during my PhD on central pattern generators and on the emergence of motor synergies. We observed that the system is very dynamic and underactuated but it is still possible to control with nonlinear controllers and oscillators through the exploitation of resonance and of its passive dynamics. My goal will be to expand our results to new robotic models in order to have a theory of motor synergies and central pattern generators for dynamical motion control, something crucially missing in my research otherwise. I would like to adapt this to arm motion, balance and body posture, which puts forward the notions of tensegrity.

Perspectives

All along this document, I gave a detailed overview of the research work I have been involved in for the last 10 years in order to demonstrate my abilities to animate/supervise research activities (including the supervisions of MSc and PhD students, the writing of proposals for project funding, the sustaining of national and international collaborations, publications, etc.).

It is now time to think about the future and give concrete elements about my scientific project for the years to come. In this following section, I give scientific elements as well as details about the funding strategy.

Working Memories for Life Long Learning Machines

It is still difficult for roboticists to make robots capable to learn for a long period of time and to learn complex rules that go beyond simple reinforcement learning. Incremental learning is an important design principle for cognitive robotics but results in our community is still harsh. In order to have adaptive robots, one will have to design a cognitive architecture for what is termed now Life Long Learning. I would like to exploit the different biological mechanisms used for designing working memories based on spiking neurons for novelty discovery and habit learning. Using these ideas from dynamic systems, I hope to make a more complex and robust version of neurocognitive architectures for robots that can deal with the unexpected, and that can serve for a robot to think spatially based on multimodal information and sensorimotor coordination, which is something poorly done yet in the current state of art.

I believe that our work on Predictive Coding and Free-Energy Minimization for sensorimotor integration in multiple recurrent neural networks with the INFERNO model is an important step for me that could embed aspects of Embodied AI (learning sensorimotor primitive, temporal coding) with aspects of Old-fashioned Symbolic AI such as Active Inference and the Bayesian probabilities.

Old fashion AI has succeeded to apply logical and inference rules on discrete and constrained environments, graphs. Although all incoming information is asynchrone, one important step will be for robots to think causally, sequentially and ordinally with their body and to resolve problems dynamically through their actions, through their perceptual experience in the world.

By doing so, a developmental robot can acquire intuitive rules from Physics and the Social environment and employing these rules toward achieving one complex goal, to acquire a biographical memory, which is still a drawback in current robotics. To some points, this should lead to the construction of a Neural Turing Machines as coined by Alex Graves, a working memory capable to learn sequences and solve problems dynamically, to replay them online and to generalize them into 'routines' ; grounded to the body sensorimotor rules. Solving this problem will have perhaps the highest impact in the near future with the development of neuromorphic hardware.

My collaboration with the Laboratory IRCICA, Université de Lille on Neuromorphic Hardware for memory sequences based on Spiking Neurons with an ANR submission is an important step toward it.

Robot Body representation, Thinking Spatially and Socially

Another important design principle that I will consider is the ability for a robot to learn to calibrate its own body representation and to learn to think spatially, causally and physically relative to it by constructing eyes-, arm-, hands- centered representations. This egocentric representation is important in order to reach and grasp objects and to have a dynamic body image that changes with respect to actions toward objects and toward persons. The challenge is to model the so-called Mirror Neurons System. Further researches on neural modeling of the Parietal Cortex will serve to have a multimodal representation, body-centered based on vision, proprioception, tactile information.

Another direction of research will be to extend the egosphere centered on the head in order to incorporate a facial representation, based on facial motion, sound representation, eye gaze and tactile mapping toward joint attention, mentalizing, theory of mind. Having a robot that can express itself through body motion and facial expression as well as speech is an important step in order to reach another functional level of cognitive functions for social interaction.

My collaboration with Sofiane Boucenna from ETIS Laboratory and Rana Eisselly, Bahia Guellai and Maya Gratier of the Baby Lab of Nanterre University on multimodal integration in infants and in robots with whom an ANR project has been submitted. My other collaboration with Philippe Gaussier from ETIS Laboratory and Daniella Corbetta from University of Tenessee on the construction of a body image in infants and robots is an important step toward it.

Tools, Language, Ideomotor and Predictive Coding

The Ideomotor principle describes the idea that our brain exploits some sensorimotor rules, selects some actions beforehands and simulates situations never occured before in order to reach

some desired outcomes. This idea appears highly relevant to overcome recursive and complex tasks such as tool-use and language, although the mechanisms behind and the architectures proposed in the litterature are not clearly exposed and still investigated. It is in line with other concepts such as active perception, or active inference, the ability to infer a desired perception or to infer hidden causes linked to some effects. This principle has some links with Bayesian Inference and the Free-Minimization Principle, or to the Predictive Coding Paradigm, which puts forward the role of action and of embodiment to learn these rules. These properties may serve to construct a cognitive architecture as exposed earlier that may achieve to solve hard cognitive problems such as active perception, motion coordination, action sequence. The working memory that I proposed INFERNO and the modeling of a body representation based on multimodal integration can serve to reach these higher cognitive skills.

My previous works with PhD students and future research with the Neurocybernetic Team from ETIS Lab will help to reach this goal.

Smart Materials and Soft Robotics

Since the design of the body has an impact on its control and on its behaviors, thinking about its hardware and its morphology makes sense if we want to have autonomous and adaptive robots ; it concerns on the hardware part : the design of their artificial muscles, of their artificial skin and of the visco-elasticity of their soft tissues. Besides, it concerns on the morphology part : the geometrical and structural properties of their body. These different aspects cannot be neglected for the ecology of motion and balance.

Truly autonomous robots require thus to rethink the design of robots for low-power consumption and ecological concerns : how passive dynamics and compliance can serve control for so many behaviors such as objects manipulation, postural balance, walking or social interaction.

I have made some slow advances in this part by working on a prototype of an artificial skin and on the design of low-pow, lightweights and compliant robots. On the one hand, softness and compliance of the body has to be incorporated ultimaly into the controller in order to have some optimality in motion control. On the other hand, augmenting the capability to touch and to be touched to are a prerequisite to endow robots of compliant physical and social interactions.

The way to perform one optimal control in a high-degrees of freedom system for flexible and dynamical motion is still unknown. I believe that having an integrative view can help to construct a complementary system between robot body and its controller. Following this, I will pursue new principles for the control of soft robots.

In that perspective, tensegrity structures have interesting design properties, as they are highly distributed to implement mechanically a nonlinear stiffness which is present in biological organisms ; the balance between stress and strain of these structures confers them to be robust and compliant again external shocks. This design may serve to model complex articulations motion like the ankle, the hip, the foot, the hand, the vertebral column or the elbow, which are important for compliant robots. I will work toward the understanding of the mechanical design of the human joints in order to have more biologically-inspired robots to perform energy-efficient postural balance, walking, and grasp with the associated modeling of the motor synergies and central pattern generators.

My collaboration with Olivier Romain from ETIS Laboratory under the french consortium VEDECOM on the future of autonomous vehicles will serve to develop a novel version of our current artificial skin in order to augment its spatial resolution using spectral information.

Bibliographie

Abbott, L. and Nelson, S. (2000). Synaptic plasticity taming the beast. *Nature neuroscience*, 3 :1178–1182. 104, 113, 120

Acerra, F., Burnod, Y., and de Schonen, S. (2002). Modelling aspects of face processing in early infancy. *Developmental Science*, 5(1) :98–117. 45

Adolph, K. (2008). Learning to move. *Curr Dir Psychol Sci*, 17(3) :213–218. 99

Adolph, K. and Joh, A. (2005). *Learning to Learn in the Development of Action*, volume 33. In J. Lockman, J. Reiser, & C. A. Nelson (Eds.), Action as an organizer of perception and cognition during learning and development Minnesota Symposium on Child Development. 98, 99, 114

Adolph, K. and Joh, A. (2009). *Multiple learning mechanisms in the development of action*. New York Oxford University Press. 83, 98, 99

Ajemian, R., Bullock, D., and Grossberg, S. (2001). A model of movement coordinates in the motor cortex posture-dependent changes in the gain and direction of single cell tuning curves. *Cerebral Cortex*, 11(12) :1124–1135. 61, 62

Alexander, G., DeLong, M., and Strick, P. (1986). Parallel organization of functionally segregated circuits linking basal ganglia and cortex. *Annu Rev Neurosci*, 9 :357–381. 135

Alexander, M. (2005). Walking made simple. *Science*, 308(5718) :58–59. 153, 154

Allen, J. and Ting, L. (2016). Why is neuromechanical modeling of balance and locomotion so hard ? *chapter 7. Journal of Motor Behavior*, 7 :197–223. 142, 147

Amrollah, E. and Henaff, P. (2010). On the role of sensory feedbacks in rowat-selverston cpg to improve robot legged locomotion. *Frontiers in neurorobotics*, 4. 154

Andersen, R. and Buneo, C. (2002). Intentional maps in posterior parietal cortex. *Annu. Rev. Neurosci.*, 25 :189–220. 117

Andersen, R. and Cui, H. (2009). Intention, action planning, and decision making in parietal-frontal circuits. *Neuron*, 63 :568–583. 117

Andersen, R., Essick, G., and Siegel, R. (1985). Encoding of spatial location by posterior parietal neurons. *Science*, 230 :450–458. 60

Andersen, R. and Mountcastle, V. (1983). The influence of the angle of gaze upon the excitability of the light-sensitive neurons of the posterior parietal cortex. *J. Neuroscience*, 3 :532–548. 60

A.P., G., Merchant, H., Naselaris, T., and B., A. (2007). Mapping of the preferred direction in the motor cortex. *Proc Natl Acad Sci USA.*, 104(26) :11068–72. 60

Balas, B. (2010). Using innate visual biases to guide face learning in natural scenes a computational investigation. *Developmental Science*, 5(1) :469–478. 46

Baraduc, P., Guigon, E., and Burnod, Y. (2001). Recording arm position to learn visuomotor transformations. *Cerebral Cortex*, 11 :906–917. 62

Barto, A. (1995). Adaptive critics and the basal ganglia. *In J. Houk, J. Davis, D. Beiser (Eds.), Models of information processing in the basal ganglia. Cambridge, MA MIT Press.*, pages 215–232. 103

Barto, A. and Sutton, R. (1997). Reinforcement learning in artificial intelligence. *Advances in Psychology*, 121 :, 358–386. 80, 120

B.E., S., T.R., S., and Rowland, B. (2009). The neural basis of multisensory integration in the midbrain its organization and maturation. *Hearing Research*, 258 :4–15. 45

Bednar, J. and Miikulainen, R. (2003). Learning innate face preferences. *Neural Computation*, 15 :1525–1557. 46

Benedek, M., Jauk, E., Beaty, R., Fink, A., Koschutnig, K., and Neubauer, A. (2016). Brain mechanisms associated with internally directed attention and self-generated though. *Scientific Reports*, 6 :22959. 115, 117, 134

Benedetti, F. (1995). Orienting behaviour and superior colliculus sensory representations in mice with the vibrissae bent into the contralateral hemispace. *European Journal of Neuroscience*, 7 :1512–9. 46

Benedetti, F. (2006). Differential formation of topographic maps in the cerebral cortex and superior colliculus of the mouse by temporally correlated tactile-tactile and tactile-visual inputs. *European Journal of Neuroscience*, 7 :1942–1951. 46, 57

Berthoz, A. (2000). *The Brain's Sense of Movement*. Harvard University Press. 154

Bi, G. and Poo, M. (1998). Activity-induced synaptic modifications in hippocampal culture, dependence of spike timing, synaptic strength and cell type. *J. Neurscience*, 18 :10464–10472. 104, 113

Bizzi, E., Cheung, V., d'Avella, A., Saltiel, P., and Tresch, M. (2008). Combining modules for movement. *Brain Research Reviews*, 57(1) :125–133. 143

Bizzi, E., Giszter, S., Loeb, E., Mussa-Ivaldi, F., and Saltiel, P. (1995). Modular organization of motor behavior in the frog's spinal cord. *Trends in Neurosciences*, 18(442-445). 142, 149

Bizzi, E. Clarac, F. (1999). Motor systems. *Current Opinion in Neurobiology*, 9(6) :659–662. 143

Bliss, T., Werly, J., Iwasaki, T., and Bart-Smith, H. (2008). Experimental validation of robust resonance entrainment for cpg-controlled tensegrity structures. *IEEE Transactions On Control Systems Technology*, 21 :666–678. 142, 153

Blohm, G. and Crawford, J. (2009). Fields of gain in the brain. *Neuron*, 64 :598–600. 135

Blohm, G. and Crawford, J. (2012). Computations for geometrically accurate visually guided reaching in 3-d space. *Journal of Vision, in special issue 'Sensorimotor processing of goal-directed movements'*, 7(5) :4, 1–22. 59

Blohm, G., Khan, A., and Crawford, J. (2008). Spatial transformations for eye–hand coordination. *New Encyclopedia of Neuroscience*, 9 :203–211. 59

Boot, P., Rowden, G., and Walsh, N. (1992). The distribution of merkel cells in human fetal and adult skin. *The American Journal of Dermatopathology*, 14(5) :391–396. 48

Botvinick, M. and Watanabe, T. (2007). From numerosity to ordinal rank a gain-field model of serial order representation in cortical working memory. *The Journal of Neuroscience*, 27(32) :8636–8642. 135, 136

Boucenna, S., Andry, P., Gaussier, P., and Hafemeister, L. (2010). Imitation as a communication tool for online facial expression learning and recognition. In *International Conference on Intelligent Robots and Systems (IROS), 2010*, pages 1–6, Taipei, Taïwan. 44, 47

Brass, M. and Heyes, C. (2005). Imitation is cognitive neuroscience solving the correspondence problem ? *Trends in Cognitive Sciences*, 9 :489–495. 45

Braud, R., Pitti, A., and Gaussier, P. (2017). A modular dynamic sensorimotor model for affordances learning, sequences planning and tool-use. *IEEE TCDS*, page to appear. 77

Braun, D., Aertsen, A., Wolpert, D., and Mehring, C. (2009). Motor task variation induces structural learning. *Current Biology*, 19 :352–357. 102, 113

Braun, D., Mehring, C., and Wolpert, D. (2010). Structure learning in action. *Behavioural Brain Research*, 206 :157–165. 102, 113

Bremner, A., Holmes, N., and Spence, C. (2008). Infants lost in (peripersonal) space ? *Trends in Cognitive Sciences*, 12(8) :298—305. 57, 58

Brozovic, M., Gail, A., and Andersen, R. (2007). Gain mechanisms for contextually guided visuomotor transformations. *The Journal of Neuroscience*, 27(39) :10588–10596. 113

Buschman, T. and Miller, E. (2014). Goal-direction and top-down control. *Phil. Trans. R. Soc. B*, 369 :20130471. 117, 132

Caggiano, V., Fogassi, L., Rizzolatti, G., Thier, P., and Casile, A. (2009). Mirror neurons differentially encode the peripersonal and extrapersonal space of monkeys. *Science*, 324 :403–406. 77

Calabrese, R. (1995). Oscillation in motor pattern-generating networks. *Current Opinion in Neurobiology*, 5 :816–823. 143

Caluwaerts, K., Despraz, J., Sabelhaus, A., Bruce, J., Schrauwen, B., and SunSpiral, V. (2014). Design and control of compliant tensegrity robots through simulation and hardware validation. *J. R. Soc. Interface*, 11 :20140520. 142, 153

Casey, M. and Pavlou, A. (2008). A behavioral model of sensory alignment in the superficial and deep layers of the superior colliculus. *Proceedings of the International Joint Conference on Neural Networks (IJCNN) 2008, Hong Kong IEEE*. 46

Chang, S., Papadimitriou, C., and Snyder, L. (2009). Using a compound gain field to compute a reach plan. *Neuron*, 64 :744–755. 60, 117

Chersi, F., Ferrari, P., and Fogassi, L. (2011). Neuronal chains for actions in the parietal lobe a computational model. *PLoS ONE*, 11(6) :e27652. 117, 132, 134

Chersi, F., Mirolli, M., Pezzulo, G., and Baldassare, G. (2013). A spiking neuron model of the cortico-basal ganglia circuits for goal-directed and habitual action learning. *Neural Networks*, 41(6) :212–224. 80

Churchland, A. and Ditterich, J. (2012). New advances in understanding decisions among multiple alternatives. *Current Opinion in Neurobiology*, 22 :920–926. 107

Clark, A. (2015). *Surfing Uncertainty Prediction, Action, and the Embodied Mind*. Oxford University Press. 80

Cohen, Y. and Andersen, R. (2002). A common reference frame for movement plans in the posterior parietal cortex. *Nature Rev. Neuroscience*, 3 :553–562. 117

Colliaux, D., Molter, C., and Yamaguchi, Y. (2009). Working memory dynamics and spontaneous activity in a flip-flop oscillations network model with a milnor attractor. *Cogn. Neurodyn.*, 3 :141–151. 85

Collins, A. and Koechlin, E. (2012). Reasoning, learning, and creativity frontal lobe function and human decision-making. *PLoS Biology*, 10(3) :e1001293. 98, 114

Collins, S., Ruina, A., Tedrake, R., and Wisse, M. (2005). Efficient bipedal robots based on passive-dynamic walkers. *Science*, 307(5712) :1082. 153

Cothros, N., Wong, J., and Gribble, P. (2006). Are there distinct neural representations of object and limb dynamics ? *Exp. Brain Res.*, 173 :689–697. 98, 99

Court, J. and al. (1997). Nicotinic and muscarinic cholinergic receptor binding in the human hippocampal formation during development and aging. *Developmental Brain Research*, 101 :93–105. 82, 83, 88

Court, J., Perry, E., Johnson, M., Piggott, M., Kerwin, J., Perry, R., and Ince, P. (1993). Regional patterns of cholinergic and glutamate activity in the developing and aging human brain. *Developmental Brain Research*, 74 :73–82. 82, 88

Crish, S., Dengler-Crish, C., and Comer, C. (2006). Population coding strategies and involvement of the superior colliculus in the tactile orienting behavior of naked mole-rats. *Neuroscience*, 139 :1461–1466. 45

Cuevas, K. and Bell, M. (2011). Eeg and ecg from 5 to 10 months of age developmental changes in baseline activation and cognitive processing during working memory task. *Int. J. of Psy.*, 80(2) :119–128. 84

Cui, H. and Andersen, R. (2009). Posterior parietal cortex encodes autonomously selected motor plans. *Neuron*, 56 :552–559. 60, 117

d'Arcy, T. (1917). *On Growth and Form*. Cambridge University Press. 80

Daw, N., Niv, Y., and Dayan, P. (2005). Uncertainty-based competition between prefrontal and dorsolateral striatal systems for behavioral control. *Nat. Neurosci.*, 8 :1704–1711. 117, 128, 135

de Haan, M., Pascalis, O., and Johnson, M. (2002). Specialization of neural mechanisms underlying face recognition in human infants. *Journal of Cognitive Neuroscience*, 14 :199–209. 44

de Schonen, S. and Mathivet, E. (1989). First come first served a scenario about the development of hemispheric specialization in face processing in infancy. *European Bulletin of Cognitive Psychology*, 9 :3–44. 45

Dehaene, S., Meyniel, F., Wacongne, C., Wang, L., and Pallier, C. (2015). The neural representation of sequences from transition probabilities to algebraic patterns and linguistic trees. *Neuron*, 88 :2–19. 135

Del Giudice, M., Manera, V., and Keysers, C. (2009). Programmed to learn ? the ontogeny of mirror neurons. *Developmental Science*, 12(2) :350–363. 58

Deneve, S. (2008). Bayesian spiking neurons i inference. *Neural Computation*, 20 :91–117. 134

Deneve, S. and Pouget, A. (2004). Bayesian multisensory integration and cross-modal spatial links. *J. of Phys.–Paris*, 98 :249–258. 60, 113

Deneve, S., Pouget, A., and Duhamel, J. (2002). A computational perspective on the neural basis of multisensory spatial representations. *Nature Rev. Neurosciences*, 98 :741–747. 60

Der, R., Hesse, F., and Martius, G. (2005). Learning to feel the physics of a body. *Proc. Intl. Conf. on Computational Intelligence for Modelling, Control and Automation (CIMCA 06). Washington, DC, USA IEEE Computer Society*, page 252–257. 143

Descarries, L., Mechawar, N., Aznavour, N., and Watkins, K. (2004). Structural determinants of the roles of acetylcholine in cerebral cortex. *Progress in Brain Research*, 145 :45—58. 82, 91

Diamond, A. (1985). Development of the ability to use recall to guide action, as indicated by infants' performance on a-not-b. *Child Development*, 74 :24–40. 84, 99

Diamond, A. (1990). Rate of maturation of the hippocampus and the developmental progression of children's performance on the delayed non-matching to sample and visual paired comparison tasks. *Ann. N. Y. Acad. Sci.*, 608 :394–426 ; discussion 426–33. 100

Diederich, A. and Oswald, P. (2014). Sequential sampling model for multiattribute choice alternatives with random attention time and processing order. *Frontiers in Human Neuroscience*, 8(697). 118

Dominey, P., Arbib, M., and Joseph, J. (1995). A model of corticostriatal plasticity for learning oculomotor associations and sequences. *J. Cogn. Neurosci.*, 7(25). 45

Doya, K. (2002). Metalearning and neuromodulation. *Neural Networks*, 15 :495–506. 83, 84, 86, 87, 120, 128, 137

Dräger, U. and Hubel, D. (1976). Topography of visual and somatosensory projections to mouse superior colliculus. *J Neurophysiol.*, 39(1) :91–101. 45

Dwyer, J., McQuown, S., and Leslie, F. (2009). The dynamic effects of nicotine on the developing brain. *Pharmacology & Therapeutics*, 122 :125—139. 82, 83

Eliasmith, C. (2013). *How to build a brain A neural architecture for biological cognition*. Oxford University Press, New York, NY. 135

Eliasmith, C., Stewart, T., Choo, X., Bekolay, T., DeWolf, T., Tang, Y., and Rasmussen, D. (2012). A large-scale model of the functioning brain. *Science*, 338(6111) :1202–1205. 117

Fagard, J., Rat-Fischer, L., and O'Regan, J. (2012). Comment le bébé accède-t-il à la notion d'outil ? *Enfance*, 64(1) :73–84. 114

Falotico, E., Cauli, N., Kryczka, P., Hashimoto, K., Berthoz, A., Takanishi, A., Dario, P., and Laschi, C. (2016). Head stabilization based on a feedback error learning in a humanoid robot. *Autonomous Robots*, pages 1–17. 154

Farroni, T., Johnson, M., Menon, E., Zulian, L., Faraguna, D., and et al. (2005). Newborns preference for face-relevant stimuli : Effects of contrast polarity. *Proceeding of The National Academy of Sciences of the USA*, 02 :17245–17250. 57

Ferrari, P., Paukner, A., Ruggiero, A., Darcey, L., Unbehagen, S., and Suomi, S. (2009). Interindividual differences in neonatal imitation and the development of action chains in rhesus macaques. *Child Development*, 80(4) :1057–1068. 44

Ferrell, C. (1996). Orientation behavior using registered topographic maps. *Proceedings of the Fourth International Conference on Simulation of Adaptive Behavior*, pages 94–103. 45

Flemons, T. (2012). The bones of tensegrity. *"http//www.intensiondesigns.com/bones_of_tensegrity"*. 143, 144, 154

Fluet, M., Baumann, M., and Scherberger, H. (2010). Context-specific grasp movement representation in macaque ventral premotor cortex. *Journal of Neuroscience*, 30(45) :15175–1518. 60

Friston, K. (2009). The free-energy principle a rough guide to the brain ? *Trends in Cognitive Science*, 4(7) :293–301. 80, 134

Friston, K., Daunizeau, J., and Kiebel, S. (2009). Reinforcement learning or active inference ? *PLoS ONE*, 4(7) :e6421. 80, 117, 133

Fruchterman, T. and Reingold, E. (1991). Graph drawing by force-directed placement. *Software Practice and Experience*, 21 :1129–1164. 49

Frumar, A., Zhou, Y., Xie, Y., and Burry, M. (2009). Tensegrity structures with 3d compressed components development, assembly and design. *Journal of the Intenational Association for Shell and Spatial Structures*, 161(2) :99–110. 144

Fuller, R. B. (1975). Synergetics explorations in the geometry of thinking. *Scribner*. 142

Gabbiani, F., Krapp, H., Koch, C., and Laurent, G. (2002). Multiplicative computation in a visual neuron sensitive to looming. *Nature*, 420 :320–324. 135

Gail, A., Klaes, C., and Westendorff, S. (2009). Implementation of spatial transformation rules for goal-directed reaching via gain modulation in monkey parietal and premotor cortex. *Journal of Neuroscience*, 29(30) :9490–9499. 60

Gallese, V. (2005). Embodied simulation from neurons to phenomenal experience. *Phenomenology and the Cognitive Sciences*, 4 :23–48. 130, 134

Gallese, V., Fadiga, L., Fogassi, L., and Rizzolatti, G. (1996). Action recognition in the premotor cortex. *Brain*, pages 593–609. 113

Gaussier, P., Banquet, J., Sargolini, F., Giovannangeli, C., Save, E., and Poucet, B. (2007). A model of grid cells involving extra hippocampal path integration, and the hippocampal loop. *Journal of Integrative Neuroscience*, 6(3) :447–476. 59

Georgopoulos, A., Kalaska, J., Caminiti, R., and Massey, J. (1982). On the relations between the direction of two-dimensional arm movements and cell discharge in primate motor cortex. *J. Neurosci.*, 2 :1527–1537. 60, 62

Georgopoulos, A., Taira, M., and A., L. (1993). Cognitive neurophysiology of the motor cortex. *Science*, 260(5104) :47–52. 61

Gershman, S., Markman, A., and Otto, A. (2014). Retrospective revaluation in sequential decision making a tale of two systems. *J Exp Psychol Gen*, 143 :182–194. 134

Glasër, C. and Joublin, F. (2010). Firing rate homeostasis for dynamic neural field formation. *IEEE Transactions on Autonomous Mental Development*, 99(99) :1. 46

Gold, J. and Shadlen, M. (2001). Neural computations that underlie decisions about sensory stimuli. *Trends in Cognitive Sciences*, 5 :10–16. 118

Gold, J. and Shadlen, M. (2007). The neural basis of decision making. *Ann Rev Neurosci*, 30 :535–574. 118, 126, 127

Gold, P. (2003). Acetylcholine modulation of neural systems involved in learning and memory. *Neurobiology of Learning and Memory*, 80 :194–210. 82

Gopnik, A., Glymour, C., Sobel, D., Schulz, L., Kushnir, T., and Danks, D. (2004). A theory of causal learning in children causal maps and bayes nets. *Psychological Review*, 111 :1–31. 81

Gopnik, A., Meltzoff, A., and Kuhl, P. (2000). The scientist in the crib what early learning tells us about the mind. *Publisher William Morrow Paperbacks*. 81

Graves, A., Wayne, G., and Danihelka, I. (2014). Neural Turing Machines. *arXiv*, 1410.541v2 :1–26. 117, 135

Graves, A. e. a. (2016). Hybrid Computing Using a Neural Network with Dynamic External Memory. *Nature*, 538 :471–476. 80

Graziano, M. and Cooke, D. (2006). Parieto-frontal interactions, personal space, and defensive behavior. *Neuropsychologia*, 44 :845–859. 59, 77

Graziano, M., Hu, X., and Cooke, D. (1997). Visuospatial properties of ventral premotor cortex. *Journal of Neurophysiology*, 77 :2268–2292. 77

Groh, J. and Sparks, D. (1996). Saccades to somatosensory targets. iii. eye-position-dependent somatosensory activity in primate superior colliculus. *Journal of Neurophysiology*, 75(1) :439–453. 45, 49

Guthrie, M., Leblois, A., Garenne, A., and Boraud, T. (2013). Interaction between cognitive and motor cortico-basal ganglia loops during decision making a computational study. *Journal of Neurophysiology*, 109 :3025–3040. 115

Harlow, H. (1949). The formation of learning sets. *Psychological Review*, 56(1) :51–65. 98, 99

Hasselmo, M. (2006). The role of acetylcholine in learning and memory. *Current Opinion in Neurobiology*, 16 :710–715. 82, 83, 84, 91

Hasselmo, M. and McGaughy, J. (2004). High acetylcholine levels set circuit dynamics for attention and encoding and low acetylcholine levels set dynamics for consolidation. *Progress in Brain Research*, 145 :207–231. 83, 89

Hasselmo, M. and Stern, C. (2006). Mechanisms underlying working memory for novel information. *Trends in Cognitive Sciences*, 10(11) :487–493. 82, 83

Hauser, H., Ijspeert, A., Fuchslin, R., Pfeifer, R., and Maass, W. (2012). The role of feedback in morphological computation with compliant bodies. *Biological Cybernetics*, 106(10) :595–613. 142

Hauser, H., Ijspeert, A., Füchslin, R., Pfeifer, R., and Maass, W. (2011). Towards a theoretical foundation for morphological computation with compliant bodies. *Biological Cybernetics*, 105(xx) :355–370. 142

Heed, T., Buchholz, V., Engel, A., and Roder, B. (2015). Tactile remapping from coordinate transformation to integration in sensorimotor processing. *Trends in Cogn. Sci.*, 19(5) :251–258. 58

Heyes, C. (2003). Four routes of cognitive evolution. *Psychological Reviews*, 110(4) :713–727. 45

Heyes, C. (2010). Where do mirror neurons come from ? *Neuroscience and Biobehavioral Reviews*, 30 :575–583. 58

Hinaut, X., Petit, M., Pointeau, G., and Dominey, P. (2013). Real-time parallel processing of grammatical structure in the fronto-striatal system a recurrent network simulation study using reservoir computing. *PLoS ONE*, 8(2) :e52946. 118

Hwang, E.J. Donchin, O., Smith, M., and Shadmehr, R. (2003). A gain-field encoding of limb position and velocity in the internal model of arm dynamics. *Public Library of Science Biology*, 1. 62

Iida, F. and Pfeifer, R. (2004). Self-stabilization and behavioral diversity of embodied adaptive locomotion. *Embodied artificial intelligence, Iida et al. (Eds), LNCS/AI*, 3139 :119–128. 153

Ijspeert, A. (2008). Central pattern generators for locomotion control in animals and robots a review. *Neural Networks*, 21(4) :642–53. 143, 148

Ijspeert, A., Nakanishi, J., and Schaal, S. (2003). learning attractor landscapes for learning motor primitives. *advances in neural information processing systems 15*, pages 1547–1554. 143

Ingber, D., Wang, N., and Stamenovi, D. (2014). Tensegrity, cellular biophysics, and the mechanics of living systems. *Rep. Prog. Phys.*, 046603(77) :48–57. 142

Izhikevich, E. (2003). Simple model of spiking neurons. *IEEE Transactions on Neural Networks*, 14 :1569– 1572. 84, 89, 91

Izhikevich, E. (2006). Polychronization computation with spikes. *Neural Computation*, 18 :245–282. 90

Izhikevich, E. (2007). Solving the distal reward problem through linkage of stdp and dopamine signaling. *Cerebral Cortex*, 17 :2443–2452. 84, 120

Izhikevich, E. M., Gally A., J., and Edelman, G., M. (2004). Spike-timing dynamics of neuronal groups. *Cerebral Cortex*, 14 :933–944. 104

Jaeger, D., Gilman, S., and Aldridge, J. (1993). Primate basal ganglia activity in a precued reaching task preparation for movement. *Exp. Brain Res.*, 95(1) :51–64. 134

James, D. (2010). Fetal learning a critical review. *Infant and Child Development*, 19 :45–54. 45

Johnson, M. (2005). Subcortical face processing. *Nature Reviews Neuroscience*, 6 :766–774. 44, 45, 46, 52

Johnson, M. (2007). Developing a social brain. *Acta Pædiatrica/Acta Pædiatrica*, 96 :3–5. 44

Johnson, M. (2012). Executive function and developmental disorders the flip side of the coin. *Trends in Cognitive Sciences*, 16(9) :454–457. 100

Johnson, M., Dziurawiec, S., Ellis, H., and J., M. (1991). Newborns' preferential tracking of face-like stimuli and its subsequent decline. *Cognition*, 40 :1–19. 45, 55

Joseph, R. (2000). Fetal brain behavior and cognitive development. *Developmental Review*, 20 :81–98. 45

Kakei, S., Hoffman, D., and Strick, P. (2001). Direction of action is represented in the ventral premotor cortex. *Nature Neuroscience*, 4(10) :1020–1025. 67

Kakei, S., Hoffman, D., and Strick, P. (2003). Sensorimotor transformations in cortical motor areas. *Neuroscience Research*, 46 :1–10. 59, 60, 61

Kalesnykas, R. and Sparks, D. (1996). The primate superior colliculus and the control of saccadic eye movements of saccadic eye movements. *Neuroscientist*, 2(5) :284–292. 45

Kaplan, F. and Oudeyer, P.-Y. (2007). In search of the neural circuits of intrinsic motivation. *Frontiers in Neuroscience*, 1(1) :225–236. 80, 98

Kelso, J. S. (1995). *Dynamic Patterns The Self-Organization of Brain and Behavior*. Cambridge, MA MIT Press. 115

Kelso, J. S. and Haken, H. (1995). Synergetics of brain and behavior. *in What is Life ? The next fifty years*, pages 137–160. 143

Keysers, C. (2004). Demystifying social cognition a hebbian perspective. *Trends in Cognitive Sciences*, 8 :501–507. 77

Keysers, C., Kaas, J., and Gazzola, V. (2010). Somatosensation in social perception. *Nature Reviews Neuroscience*, (11) :427–428. 77

Keysers, C., Perrett, D., and Gazzola, V. (2014). Hebbian learning is about contingency, not contiguity, and explains the emergence of predictive mirror neurons. *Behavioral and Brain Sciences*, 37 :205–206. 58, 77

Khamassi, M., Lallée, S., Enel, P., Procyk, E., and Dominey, P. (2011). Robot cognitive control with a neurophysiologically inspired reinforcement learning model. *Frontiers in NeuroRobotics*, 5(1) :1–14. 101, 104

King, A. (2004). The superior colliculus. *Current Biology*, 14(9) :R335–R338. 45

Kinjo, K., Nabeshima, C., Sangawa, S., and Kuniyoshi, Y. (2008). A neural model for exploration and learning of embodied movement patterns. *J. of Rob. and Mecha.*, 20(3) :358–366. 44

Klink, R. and Alonso, A. (1997). Muscarinic modulation of the oscillatory and repetitive firing properties of entorhinal cortex layer ii neurons. *J. Neurophysiol.*, 77 :1813—1828. 83, 87

Knight, R. (1996). Contribution of human hippocampal region to novelty detection. *Nature*, 383 :256—-259. 83

Koechlin, E. (2016). Prefrontal executive function and adaptive behavior in complex environments. *Current Opinion in Neurobiology*, 37 :1–6. 115, 134

Koechlin, E., Ody, C., and Kouneilher, F. (2003). The architecture of cognitive control in the human prefrontal cortex. *Science*, 302(14) :1181–1185. 99, 114

Koechlin, E. and Summerfield, C. (2007). An information theoretical approach to prefrontal executive function. *Trends in Cognitive Sciences*, 11(6) :229–235. 114

Kohonen, T. (1982). Self-organized formation of topologically correct feature maps. *Biological Cybernetics*, 43 :59–69. 46, 102, 119

Kording, K. and Wolpert, D. (2006). Bayesian decision theory in sensorimotor control. *Trends Cogn. Sci.*, 10 :319–326. 115

Kumaran, D. and Maguire, E. (2009). Novelty signals a window into hippocampal information processing. *Trends in Cognitive Sciences*, 13(2) :47–54. 83, 84

Kuniyoshi, Y. and Sangawa, S. (2006). A neural model for exploration and learning of embodied movement patterns. *Bio. Cyb.*, 95 :589–605. 44

Kuniyoshi, Y., Yorozu, Y., Inaba, M., and Inoue, H. (2003). From visuo-motor self learning to early imitation - a neural architecture for humanoid learning. *International conference on robotics and Automation*, pages 3132–3139. 44

Kurjak, A., Azumendi, G., Vecek, N., Kupeic, S., Solak, M., and et al. (2005). Fetal hand and facial expression in normal pregnancy studied by four-dimensional sonography. *J Perinat Med*, 31 :496–508. 57

Lauder, J. and Schambra, U. (1999). Morphogenetic roles of acetylcholine. *Environmental Health Perspectives*, 107 :65—69. 82, 91

Laumond, J.-P., Benallegue, M., Carpentier, J., and Berthoz, A. (2015). The Yoyo-Man. In *International Symposium on Robotics Research (ISRR)*, Sestri Levante, Italy. 154

LeCun, Y., Bengio, Y., and Hinton, G. (2015). Deep learning. *Nature*, 512 :436–444. 116, 117, 118, 134

Lepage, J. and Théoret, H. (2007). The mirror neurons system grasping others' action from birth ? *Developmental Science*, 10 :513–523. 44

Levin, S. (2002). The tensegrity-truss as a model for spine mechanics biotensegrity. *Journal of Mechanics in Medicine and Biology*, 2 :375–388. 142

Lewkowicz, D. and Turkewitz, G. (1980). Cross-modal equivalence in early infancy : auditory-visual intensity matching. *Dev. Psychol.*, 16 :597–607. 58

Liljeback, P., Pettersen, K., Stavdahl, , and Gravdahl, J. (2009). Review on modelling, implementation, and control of snake robots. *J. IASS*, 2(161) :99–110. 143

Lungarella, M. and Sporns, O. (2005). Information self-structuring : Key principle for learning and development. *Proc of the 4th Int Conf on Development and Learning*, 11 :25–30. 57

Lungarella, M. and Sporns, O. (2006). Mapping information flow in sensorimotor networks. *Plos Computational Biology*, 2(10) :1301–1312. 57

Ly, O., Lapeyre, M., and Oudeyer, P. (2011). Bio-inspired vertebral column, compliance and semi-passive dynamics in a lightweight robot. *International Conference on Robots and Systems San Francisco, United States*, page 1–8. 143

Mahe, S., Braud, R. Gaussier, P., Quoy, M., and Pitti, A. (2015). Exploiting the gain-modulation mechanism in parieto-motor neurons application to visuomotor transformations and embodied simulation. *Neural Networks*, 62 :102–111. 61

Mannella, F. and Baldassare, G. (2015). Selection of cortical dynamics for motor behaviour by the basal ganglia. *Biological Cybernetics*, 109 :575–595. 118, 134

Maravita, A. and Iriki, A. (2004). Tools for the body (schema). *Trends in Cognitive Sciences*, 8(2) :79–96. 77

Maravita, A., Spence, C., and Driver, J. (2003). Multisensory integration and the body schema close to hand and within reach. *Current Biology*, 13(2) :R531–R539. 77

Marder, E. and Calabrese, R. (1996). Principles of rhythmic motor pattern production. *Physiological Reviews*, 76 :687–717. 143, 149

Matsukawa, M., Ogawa, M., Nakadate, K. Maeshima, T., Ichitani, Y., Kawai, N., and Okado, N. (1997). Serotonin and acetylcholine are crucial to maintain hippocampal synapses and memory acquisition in rats. *Neuroscience Letters*, 230 :13–16. 82

McEvoy, M. and Correll, N. (2007). Materials that couple sensing, actuation, computation, and communication. *Science*, 318 :1088–1093. 142

McGeer, T. (1990). Passive dynamic walking. *International Journal of Robotics Research*, 9 :62–82. 153

Meck, W., Smith, R., and Williams, C. (1989). Organizational changes in cholinergic activity and enhanced visuospatial memory as a function of choline administered prenatally or postnatally or both. *Behav. Neurosci.*, 103 :1234–1241. 82

Melnyk, A. and Henaff, P. (2016). Bio-inspired plastic controller for a robot arm to shake hand with human. *Proc. of IEEE Int. Conf. on Electronics and Nanotechnology, Kiev, Ukraine*, pages 163–168. 154

Meltzoff, A. (1997). Explaining facial imitation a theoretical model. *Early Development and Parenting*, 6 :179–192. 44

Meltzoff, A. (2007a). *Infants' causal learning Intervention, observation, imitation*. In A. Gopnik & L. Schulz (Eds.), Causal learning Psychology, philosophy, and computation. Oxford Oxford University Press. 81

Meltzoff, A. (2007b). 'like me' a foundation for social cognition. *Developmental Science*, 10(1) :126–134. 44

Meltzoff, A. and Borton, R. (1979). Intermodal matching by human neonates. *Nature*, 282 :403–404. 58

Meltzoff, A. and Moore, K. (1977). Imitation of facial and manual gestures by human neonates. *Science*, 198 :75–78. 44

Miller, E. (2015). The "working" of working memory. *Dialogues Clin Neurosci.*, 15(4) :411–418. 115, 117

Mori, H. and Kuniyoshi, K. (2007). A cognitive developmental scenario of transitional motor primitives acquisition. In *7th international Conference on Epigenetic Robotics*, pages 93–100. 44

Mori, H. and Kuniyoshi, Y. (2010). A human fetus development simulation self-organization of behaviors through tactile sensation. *IEEE 9th International Conference on Development and Learning*, pages pp.82–97. 44

Morton, J. and Johnson, M. (1991). Conspec and conlern a two-process theory of infant face recognition. *Psychological Review*, 98 :164–181. 45

Moschovakis, A. (1996). The superior colliculus and eye movement control. *Current Biology*, 6 :811–816. 45

Munakata, Y. (1998). Infant perseveration and implications for object permanence theories a pdp model of the a-not-b task. *Developmental Science*, 1(2) :161–211. 84

Nagy, E. (2010). The newborn infant a missing stage in developmental psychology. *Inf. Child. Dev.*, page 10.1002/icd.683. 44, 57

Nakajima, K., Hauser, H., Li, T., and Pfeifer, R. (2015). Information processing via physical soft body. *Scientific Reports*, 5 :10487. 142

Nakanishi, J., Morimoto, J., Endo, G., Cheng, G., Schaal, S., and Kawato, M. (2004). An empirical exploratiom of phase resetting for robust biped locomotion with dynamical movement primitives. *International Conference on Intelligent Robots and Systems*, pages 919–924. 154

Nassour, J., Hénaff, P., Benouezdou, F., and Cheng, G. (2014). Multi-layered multi-pattern cpg for adaptive locomotion of humanoid robots. *Biological Cybernetics*, 108 :291–303. 154

Neil, P. A., Chee-Ruiter, C., Scheier, C., Lewkowicz, D. J., and Shimojo, S. (2006). Development of multisensory spatial integration and perception in humans. *Developmental Science*, 9(5) :454–464. 57

Nelson, C. (2001). The development and neural bases of face recognition. *Infant and Child Development*, 10 :3–18. 45

Newcombe, N. and Huttenlocher, J. (2006). Development of spatial cognition. *Handbook of Child Psychology*, 5(2) :734—776. 83, 91

Nicolis, G. and Prigogine, I. (1977). *Self-organization in Nonequilibrium Systems*. New York Wiley. 80

Orban, H. and Wolpert, D. (2011). Representations of uncertainty in sensorimotor control. *Current Opinion in Neurobiology*, 21 :1–7. 98, 101, 115

Pascalis, O., de Haan, M., and Nelson, C. (2002). Is face processing species-specific during the first year of life ? *Science*, 296 :1321–1323. 46

Paul, C., Valero-Cuevas, F., and Lipson, H. (2006). Design and control of tensegrity robots for locomotion. *IEEE Transactions on Robotics*, 22(5) :878980. 142

Pavlou, A. and Casey, M. (2010). Simulating the effects of cortical feedback in the superior colliculus with topographic maps. *Proceedings of the International Joint Conference on Neural Networks (IJCNN) 2010, Barcelona IEEE*, pages 1–8. 46

Pellegrini, G., de Arcangelis, L. Herrmannand, H., and Perrone-Capano, C. (2007). Activity-dependent neural network model on scale-free networks. *Physical Review E*, 76 :016107. 56

Perrault Jr, T., Vaughan, J., Stein, B., and Wallace, M. (2005). Superior colliculus neurons use distinct operational modes in the integration of multisensory stimuli. *J Neurophysiol*, 93(46) :2575–2586. 46

Pezzulo, G. and Cisek, P. (2016). Navigating the affordance landscape feedback control as a process model of behavior and cognition. *Trends in Cognitive Science*, 20(6) :414–424. 80, 117, 134

Pezzulo, G., van der Meer, M., Lansink, C., and Pennartz, C. (2014). Internally generated sequences in learning and executing goal-directed behavior. *Trends in Cognitive Sciences*, 18 :647–657. 80

Pfeifer, R. and Bongard, J. (1999). *How the Body Shapes the Way We Think, A New View of Intelligence*. Bradford Books. 153

Pfeifer, R. and Gomez, G. (2009). Morphological computation – connecting brain, body, and environment - creating brain-like intelligence from basic principles to complex intelligent systems. *LNAI ; Creating Brain-Like Intelligence*, 5436 :66–83. 142, 153

Pfeifer, R., Iida, F., and Lungarella, M. (2007a). Self-organization, embodiment, and biologically inspired robotics. *Science*, 318(5853) :1088–1093. 29

Pfeifer, R., Lungarella, M., and Iida, M. (2007b). Self-organization, embodiment, and biologically inspired robotics. *Science*, 318 :1088–1093. 142

Pfeifer, R. and Pitti, A. (2012). *La Révolution de L'Intelligence du Corps (french)*. Manuella Editions. 29, 153

Piaget, J. (1954). *The construction of reality in the child.* New York Basic Books. 44, 57, 83, 89

Pitti, A., Alirezaei, H., and Kuniyoshi, Y. (2008). Mirroring maps and action representation through embodied interactions. *Connectionist Models of Behaviour and Cognition II, World Scientific*, pages 27–37. 51, 77

Pitti, A., Alirezaei, H., and Kuniyoshi, Y. (2009a). Cross-modal and scale-free action representations through enaction. *Neural Networks*, 22 :144–154. 77, 137

Pitti, A., Blanchard, A., Cardinaux, M., and Gaussier, P. (2012). Gain-field modulation mechanism in multimodal networks for spatial perception. *12th IEEE-RAS International Conference on Humanoid Robots Nov.29-Dec.1, 2012. Business Innovation Center Osaka, Japan*, pages 297–302. 60, 101

Pitti, A., Braud, R., Mahé, S., Quoy, M., and Gaussier, P. (2013a). Neural model for learning-to-learn of novel task sets in the motor domain. *Frontiers in Psychology*, 4(771). 137

Pitti, A. and Kuniyoshi, Y. (2011a). Contribution of the cholinergic innervation to early memory development in the neonate para-hippocampal system. *Proc. of the 3rd International Conference on Cognitive Neurodynamics (ICCN11)*, pages 1 – 4. 137

Pitti, A. and Kuniyoshi, Y. (2011b). Modeling the cholinergic innervation in the infant cortico-hippocampal system and its contribution to early memory development and attention. *Proc. of the International Joint Conference on Neural Networks (IJCNN11)*, pages 1 – 8. 99, 137

Pitti, A., Kuniyoshi, Y., Quoy, M., and Gaussier, P. (2013b). Modeling the minimal newborn's intersubjective mind the visuotopic-somatotopic alignment hypothesis in the superior colliculus. *PLoS ONE*, 8(7) :e69474. 77

Pitti, A., Lungarella, M., and Kuniyoshi, Y. (2005). Quantification of emergent behaviors induced by feedback resonance of chaos. *Recent Advances in Artificial Life Advances in Natural Computation*, 3(15) :199–213. 143

Pitti, A., Lungarella, M., and Kuniyoshi, Y. (2006). Exploration of natural dynamics through resonance and chaos. *Proc. of 9th Conf. on Intelligent Autonomous Systems*, pages 558–565. 143

Pitti, A., Lungarella, R., and Kuniyoshi, Y. (2009b). Generating spatiotemporal joint torque patterns from dynamical synchronization of distributed pattern generators. *Frontiers in Neuro-Robotics*, 3(2) :10.3389/neuro.12.002.2009. 143, 154

Pitti, A., Mori, H., Kozuma, S., and Kuniyoshi, Y. (2009c). Contingency perception and agency measure in visuo-motor spiking neural networks. *IEEE Trans. on Autonomous Mental Development*, 1 :86–97. 68

Pitti, A., Mori, H., Yamada, Y., and Kuniyoshi, Y. (2010). A model of spatial development from parieto-hippocampal learning of body-place associations. *10th International Conference on Epigenetic Robotics*, pages 89–96. 44, 143, 154

Pitti, A., Pugach, G., Gaussier, P., and Shimada, S. (2017). Spatio-temporal tolerance of visuo-tactile illusions in artificial skin by recurrent neural network with spike-timing-dependent plasticity. *Scientific Reports*, 7 :41056. 77

Platt, M. and Glimcher, P. (1999). Neural correlates of decision variables in parietal cortex. *Nature*, 400 :233–238. 113, 134

Porges, S. and Furman, S. (2010). The early development of the autonomic nervous system provides a neural platform for social behaviour a polyvagal perspective. *Inf. Child. Dev.*, page 10.1002/icd.688. 44

Pouget, A. and Snyder, L. (1997). Spatial transformations in the parietal cortex using basis functions. *J. of Cog. Neuro.*, 3 :1192–1198. 60

Pouget, A. and Snyder, L. (2000). Computational approaches to sensorimotor transformations. *Nature Neuroscience*, 3 :1192–1198. 60, 101

Quinn, P., Westerlund, A., and Nelson, C. (2006). Neural markers of categorization in 6-month-old infants. *Psychological Science*, 17 :59–66. 83, 91

Rabinovich, M. and Varona, P. (2011). Robust transient dynamics and brain functions. *Front. Comput. Neurosci.*, 5(24). 134

Rabinovich, M., Varona, P., Selverston, A., and Abarbanel, H. (2006). Dynamical principles in neuroscience. *Reviews of Modern Physics*, 78 :4. 115

Rajan, K., Harvey, C., and Tank, D. (2016). Recurrent network models of sequence generation and memory. *Neuron*, 90 :1–15. 115, 117, 134

Rat-Fischer, L., O'Regan, J., and Fagard, J. (in press). The emergence of tool use during the second year of life. *Journal of Experimental Child Psychology*. 114

Ray, E. and Heyes, C. (2011). Imitation in infancy the wealth of the stimulus. *Developmental Science*, 14(1) :92–105. 45, 46

Reddy, V. (2008). *How Infants Know Minds*. Harvard University Press. 44

Rigato, S., Menon, E., Johnson, M., Faraguna, D., and Farroni, T. (2010). Direct gaze may modulate face recognition in newborns. *Inf. Child. Dev.*, page 10.1002/icd.684. 44, 52

Rigotti, M., Barak, O., Warden, M., Wang, X., Daw, N., Miller, E., and Fusi, S. (2013). The importance of mixed selectivity in complex cognitive tasks. *Nature*, 497(7451) :585–590. 127, 136

Rizzolatti, G. and Arbib, A. (1998). Language within our grasp. *Trends in Neuroscience*, 21 :188–194. 77

Rizzolatti, G. and Craighero, L. (2004). The mirror-neuron system. *Annu. Rev. Neuroscience*, 27 :169–192. 77

Rizzolatti, G. Fadiga, L. F. L. and Gallese, V. (1997). The space around us. *Science*, 277 :190–191. 77

Rochat, P. (1998). Self-perception and action in infancy. *Exp. Brain Res.*, 123 :102–109. 58

Rochat, P. (2011). The self as phenotype. *Consciousness and Cognition*, 20(1) :109–119. 44

Roelfsema, P. and van Ooyen, A. (2005). Attention-gated reinforcement learning of internal representations for classification. *Neural Computation*, 17 :2176–2214. 69

Rolfe, J. and LeCun, Y. (2013). Discriminative recurrent sparse auto-encoders. *arXiv*, page 1301.3775v4. 118, 134

Rorie, A., Gao, J., McClelland, J., and Newsome, W. (1997). Integration of sensory and reward information during perceptual decision-making in lateral intraparietal cortex (lip) of the macaque monkey. *PLoS ONE*, 5(2) :e9308. 118

Rougier, N. and Boniface, Y. (2011). Dynamic self-organising map. *Neurocomputing*, 74 :1840–1847. 104

Rueckert, E., Kappel, D., Tanneberg, D., Pecevski, D., and Peters, J. (2016). Recurrent spiking networks solve planning tasks. *Scientific Reports*, 6 :21142. 115, 117, 134

Sakai, K., Rowe, J., and Passingham, R. (2002). Active maintenance in prefrontal area 46 creates distractor-resistant memory. *Nature Neuroscience*, 5(5) :479–484. 135

Salihagic Kadic, A., Predojevic, M., and Kurjak, A. (2008). Do human fetuses anticipate self-directed actions ? a study by four-dimensional (4d) ultrasonography. *Advances in fetal neurophysiology. Journal of Ultrasound in Obstetrics and Gynecology*, 2 :19–34. 57

Salinas, E. and Sejnowski, T. J. (2001). Gain modulation in the central nervous system where behavior, neurophysiology and computation meet. *The Neuroscientist*, 7 :430–440. 60, 135

Salinas, E. and Thier, P. (2000). Gain modulation a major computational principle of the central nervous system. *Neuron*, 27 :15—-21. 60, 101

Sandamirskaya, Y. and Schoner, G. (2010). An embodied account of serial order how instabilities drive sequence generation. *Neural Networks*, 23 :1164–1179. 118

Schultz, W. Dickinson, A. (2000). Neuronal coding of prediction errors. *Annu. Rev. Neurosci.*, 23 :473–500. 80, 111

Schultz, W., Dayan, P., and Montague, P. (1997). A neural substrate of prediction and reward. *Annu. Rev. Neurosci.*, 275 :1593–1599. 80, 111

Seger, C. and Miller, E. (2010). Category learning in the brain. *Annu. Rev. Neurosci.*, 33 :203–19. 115, 135

Senju, A. and Johnson, M. (2009). The eye contact effect mechanisms and development. *Trends in Cognitive Sciences*, 13(3) :127–134. 44

Shimada, S., Hiraki, K., and Oda, I. (2005). The parietal role in the sense of self-ownership with temporal discrepancy between visual and proprioceptive feedbacks. *NeuroImage*, 24 :1225–1232. 58

Simion, F., Valenza, E., Umilta, C., and DallaBarba, B. (1998). Preferential orienting to faces in newborns a temporal-nasal asymmetry. *J Exp Psychol Hum Percept Perform*, 24 :1399–1405. 44

Singh, S., Lewis, R., Barto, A., and Sorg, J. (2010). Intrinsically motivated reinforcement learning an evolutionary perspective. *IEEE Transactions on Autonomous Mental Development*, 2(2) :, 70–82. 99

Sirosh, J. and Miikulainen, I. (1994). Cooperative self-organization of afferetn and lateral connections in cortical maps. *Biological Cybernetics*, 71 :65–78. 46

Smith, L. and Samuelson, L. (1997). Perceiving and remembering category stability, variability and development. *In K. Lamberts & D. Shanks (Eds.), Knowledge, Concepts and Categories. Psychology Press, East Sussex, UK*, pages 161–195. 83, 85

Snelson, K. (1965). Continuous tension, discontinuous compression structures. *United States patent 3169611*. 142

Sporns, O. and Honey, C. (2006). Small worlds inside big brains. *PNAS*, 103(51) :19219–19220. 51

Sprague, J. and Meikle, T. (1965). The role of the superior colliculus in visually guided behavior. *Science*, 11 :115–146. 55

Stanley, K. and Miikkulainen, R. (2009). Evolving neural networks through augmenting topologies. *Evolutionary Computation*, 10(2) :99–127. 118

Stanojevic, M. and Kurjak, A. (2008). Continuity between fetal and neonatal neurobehavior. *Journal of Ultrasound in Obstetrics and Gynecology*, 2 :64–75. 45, 57

Stein, B. (1984). Development of the superior colliculus. *Ann. Rev. Neurosci.*, 7(22) :95–125. 45

Stein, B., Burr, D., Constantinidis, C., Laurienti, P., Meredith, M., Perrault Jr, T., Ramachandran, R., Röder, B.nd Rowland, B., Sathian, K., Schroeder, C., Shams, L., Stanford, T., Wallace, M., Yu, L., and Lewkowicz, D. (2010a). Semantic confusion regarding the development of multisensory integration a practical solution. *European Journal of Neuroscience*, 31 :1713–1720. 46

Stein, B., Magalhães Castro, B., and Kruger, L. (1975). Superior colliculus visuotopic-somatotopic overlap. *Science*, 189 :224–226. 45

Stein, B. and Meredith, M. (1993). *The Merging of the Senses*. A Bradford Book, cambridge, MA. 45

Stein, B., Perrault Jr., T., Stanford, T., and Rowland, B. (2010b). Postnatal experiences influence how the brain integrates information from different senses. *Frontiers in Integrative Neuroscience*, 30(14) :4904–4913. 45, 49

Strogatz, S. (2003). *Sync The Emerging Science of Spontaneous Order*. New York Hyperion. 80, 143

Sutton, R. S. and Barto, A. G. (1998). *Reinforcement Learning An Introduction*. Cambridge, MA MIT Press. A Bradford Book. 128

Taga, G. (1995). A model of the neuro-musculo-skeletal system for human locomotion. i. emergence of basic gait. *Biological Cybernetics*, 73(2) :97–111. 143

Tani, J., Ito, M., and Sugita, Y. (2004). Self-organization of distributedly represented multiple behavior schemata in a mirror system reviews of robot experiments using rnnpb. *Neural Networks*, 17 :1273–1289. 118

Tenenbaum, J., Kemp, C., Griffiths, T., and Goodman, N. (2011). How to grow a mind statistics, structure, and abstraction. *Science*, 331(6022) :1279–1285. 81, 98, 99

Thelen, E. and Smith, L. (1995). *A Dynamic Systems Approach to the Development of Cognition and Action*. Cambridge, MA MIT Press. 115

Thorpe, S., Delorme, A., and Van Rullen, R. (2001). Spike-based strategies for rapid processing. *Neural Networks*, 14 :715–725. 46, 57, 103, 118, 134

Tietz, B., Carnahan, R., Bachmann, R., D., R., Quinn, D., and SunSpiral, V. (2013). Tetraspine robust terrain handling on a tensegrity robot using central pattern generators. *IEEE/ASME International Conference on Advanced Intelligent Mechatronics (AIM)*, pages 261–267. 142, 153

Ting, L. (2007). Dimensional reduction in sensorimotor systems a framework for understanding muscle coordination of posture. *Prog Brain Res.*, 165 :299–321. 142, 149

Todorov, E. (2004). Optimality principles in sensorimotor control. *Nat. Neurosci.*, 7(9) :907–915. 142, 149

Topalidou, M. and Rougier, N. (2015). [re] interaction between cognitive and motor cortico-basal ganglia loops during decision making a computational study. *ReScience*. 115, 134

Trevarthen, C. (2010). What is it like to be a person who knows nothing ? defining the active intersubjective mind of a newborn human being. *Inf. Child. Dev.*, page 10.1002/icd.689. 44

Triplett, J., Phan, A., Yamada, J., and Feldheim, D. (2012). Alignment of multimodal sensory input in the superior colliculus through a gradient-matching mechanism. *The Journal of Neuroscience*, 32 :5264–5271. 46

Tsuda, I. (1991). Chaotic itinerancy as a dynamical basis of hermeneutics in brain and mind. *World Futures*, 31 :105–122. 122

Tsuda, I. (2015). Chaotic itinerancy and its roles in cognitive neurodynamics. *Current Opinion in Neurobiology*, 31 :67–71. 80

Tsuda, I., Fujii, H., Tadokoro, S., Yasuoka, T., and Yamaguti, Y. (2004). Chaotic itinerancy as a mechanism of irregular changes between synchronization and desynchronization in a neural network. *J. of Integr. Neurosc.*, 3 :159–182. 115, 134

Tsunozaki, M. and Bautista, D. (2009). Mammalian somatosensory mechanotransduction. *The American Journal of Dermatopathology*, 19 :1–8. 47

Turati, C. (2004). Why faces are not special to newborns. *Current Directions in Psychological Science*, 13(1) :5–8. 45

Turvey, M. and Fonseca, S. (2014). The medium of haptic perception a tensegrity hypothesis. *Journal of Motor Behavior*, 46(3) :143–187. 142, 147, 153

Valenza, E., Simion, F., Macchi, F., Cassia, V., and Umilta, C. (1996). Face preference at birth. *J Exp Psychol Hum Percept Perform*, 22 :892–903. 44

van Hateren, J. (2015). Active causation and the origin of meaning. *Biological Cybernetics*, 109 :33–46. 115

Van Rullen, R., Gautrais, J., Delorme, A., and Thorpe, S. (1998). Face processing using one spike per neurone. *BioSystems*, 48 :229–239. 46, 102

Van Rullen, R. and Thorpe, S. (2002). Surfing a spike wave down the ventral stream. *Vision Research*, 42 :2593–2615. 102, 118

Varona, P. and Rabinovich, M. (2016). Hierarchical dynamics of informational patterns and decision-making. *Proc. R. Soc. B*, 283 :20160475. 134

Verstraeten, D., Schrauwen, B., D'Haene, M., and Stroobandt, D. (2007). An experimental unification of reservoir computing methods. *Neural Network*, 20 :391–403. 118, 134

Victor, J. and Purpura, K. (1997). Metric-space analysis of spike trains theory, algorithms and application. *Network*, 8 :127–164. 90, 95

Wallace, M. (2004). The development of multisensory processes. *Cogn Process*, 5 :69–83. 45

Wallace, M. and Stein, B. (2000). Onset of cross-modal synthesis in the neonatal superior colliculus is gated by the development of cortical inuences. *J Neurophysiol*, 83 :3578–3582. 46, 57

Wallace, M. and Stein, B. (2001). Sensory and multisensory responses in the newborn monkey superior colliculus. *The Journal of Neuroscience*, 21(22) :8886–8894. 45

Wallace, M. and Stein, B. (2007). Early experience determines how the senses will interact. *J Neurophysiol*, 97 :921–926. 46, 57

Watts, D. and Strogatz, S. (1998). Collective dynamics of 'small-world' networks. *Nature*, 393 :440–442. 126

Westendorff, S., Klaes, C., and Gail, A. (2010). The cortical timeline for deciding on reach motor goals. *J. Neurosci.*, 30 :5426–5436. 113

Wolpert, D. and Flanagan, J. (2010). Motor learning. *Current Biology*, 20(11) :R467–R472. 100, 114

Wolpert, D., Goodbody, S., and Husain, M. (1998). Maintaining internal representations the role of the human superior parietal lobe. *Nature Neuroscience*, 1(6) :529–533. 67

Wolpert, D. and Kawato, M. (1998). Multiple paired forward and inverse models for motor control. *Neural Networks*, 11(6) :1317–1329. 67

Yamada, Y., Mori, H., and Kuniyoshi, Y. (2010). A fetus and infant developmental scenario self-organization of goal-directed behaviors based on sensory constraints. *10th International Conference on Epigenetic Robotics*, pages pp.145–152. 44

Yokoyama, C., Tsukada, H., Watanabe, Y., and Onoe, H. (2005). A dynamic shift of neural network activity before and after learning-set formation. *Cerebral Cortex*, 15 :796–801. 98

Yu, A. and Dayan, P. (2002). Acetylcholine in cortical inference. *Neural Networks*, 15(4-6) :719–730. 83

Zylberberg, A., Dehaene, S., Roelfsema, P., and Sigman, M. (2011). The human turing machine a neural framework for mental programs. *Trends in Cognitive Science*, 15(7) :293–300. 134

Zylberberg, A., Paz, L., Roelfsema, P., Dehaene, S., and Sigman, M. (2013). A neuronal device for the control of multi-step computations. *Papers in Physics*, 5 :050006. 135